Hydrogen Production From Catalytic Ethanol Reforming In Supercritical Water

by

Tuan Amran Tuan Abdullah

A thesis
presented to the University of Waterloo
in fulfillment of the
thesis requirement for the degree of
Doctor of Philosophy
in
Chemical Engineering

Waterloo, Ontario, Canada, 2009

AUTHOR'S DECLARATION

I hereby declare that I am the sole author of this thesis. This is a true copy of the thesis, including any required final revisions, as accepted by my examiners.

I understand that my thesis may be made electronically available to the public.

Abstract

As a means to produce high pressure hydrogen in order to reduce compression penalty, we propose to reform liquid fuel (e.g., bio-ethanol) in supercritical water (pressure above 221 bar and temperature greater than 374°C).

Catalytic ethanol reforming in supercritical water for hydrogen production has been carried out in a high pressure packed bed reactor made of Inconel-625. Since Inconel-625 contains mainly nickel, it is expected that the reactor itself can be active toward ethanol reforming. Therefore, a series of tests were first performed in the empty reactor, whose results are a benchmark when studying reforming in the presence of a catalyst. Ethanol reforming in the empty reactor was studied in the temperature range of 450 to 600°C and showed coking/plugging problem at 575°C and above. The ethanol conversion with the empty reactor could be as high as 25% at 550°C and residence time of about one minute. The main reaction products with the empty reactor were H_2, CO and CH_4.

A catalyst screening study was performed to investigate the performance of nickel and cobalt as active metals, supported on γ-Al_2O_3, α-Al_2O_3, ZrO_2 and YSZ for temperatures between 475°C and 550°C. The presence of the catalyst did increase the activity of ethanol reforming, especially at higher temperatures. All experiments in the catalyst screening study were carried out with non-reduced catalysts. Nickel catalysts were found more active than cobalt, likely because of higher reducibility. Indeed, the higher amount of oxygen in Co_3O_4 compared to NiO requires more hydrogen to fully reduce the metal oxides. Both Ni/γ-Al_2O_3 and Co/γ-Al_2O_3 showed little activity below 500°C, and led to failed experiments due to coking/plugging at temperatures of 525°C and above. The strong acid sites on γ-Al_2O_3 are responsible for high selectivity toward ethylene, a known coke precursor. The support α-Al_2O_3 in combination with Ni was active, but yielded lower H_2 selectivity and higher CH_4 selectivity than the zirconia-based catalysts. The Co/α-Al_2O_3 shows low activity. The ZrO_2-based catalysts were active and yielded high H_2 selectivity, but were found very fragile. Finally, the YSZ support was strong and yielded good conversion. Below 550°C the activity of Ni/YSZ is higher than that of Co/YSZ, but at 550°C both catalysts yield nearly complete conversion. The advantage of Co/YSZ is then higher H_2 selectivity and lower CH_4 selectivity compared to Ni/YSZ.

Therefore, Co/YSZ was selected for a more detailed study. The effect of temperature, flowrate, residence time, catalyst weight, Co loading, concentration, and pretreatment with H_2 were considered. Two methods for catalyst reduction were applied: ex-situ reduction where the catalyst is

reduced in a different reactor and in-situ reduction where the catalyst is reduced in the SCW reactor prior to ethanol reforming. At 550°C, Co/YSZ converts all ethanol for residence times as low as 2 s, even with non-reduced catalyst. At 500°C the activity of the in-situ and ex-situ reduced catalysts were similar and greater than for the non-reduced catalyst. At 475°C the ex-situ reduced catalyst showed low activity, comparable to that of the non-reduced catalyst, but the in-situ reduced catalyst yielded much higher conversion. The better performance of the in-situ reduced catalyst was attributed to active metal sites on the reactor's wall after pre-treatment in H_2. The low activity of the ex-situ reduced catalyst is due to the fact that, when exposed to supercritical water for less than 30 minutes, it re-oxidized to CoO. The temperature of 475°C is then too low to generate sufficient hydrogen that will start reducing the catalyst.

Finally, analysis of reaction pathways for ethanol reforming over Co/YSZ showed that the reaction proceeds mostly via ethanol dehydrogenation to form acetaldehyde, the latter species reacting with lattice oxygen on the catalyst to produce acetone and CO_2. Acetone is then reformed by water into CO and H_2. Finally, H_2 and CO react via the methanation reaction to form CH_4. Over Co/YSZ it was found that the water-gas shift reaction is fast (CO selectivity most of the time is less than 0.5%), but the methanation reaction is kinetically controlled. Stopping the methanation reaction before equilibrium allowed for H_2 selectivity higher than what is expected at equilibrium (likewise, CH_4 selectivity is smaller than equilibrium value).

For well-controlled reaction Co/YSZ is a promising catalyst that can be highly selective toward hydrogen during ethanol reforming in supercritical water.

Acknowledgements

I would like to express my sincere gratitude and appreciation to the following persons:

- My supervisor, Professor Eric Croiset, as well Professor Robert R. Hudgins who closely followed my work, for their guidance, advice, ideas and encouragement. I consider myself fortunate to have had the chance to learn from such excellent mentors. Not to forget, another member of the Chemical Reaction Engineering Group, Professor Peter L. Silverton, who also provided me with valuable guidance and support.
- Committee members, Professor William Epling, Professor Mario Gauthier, and Professor Nicolas Abatzoglou for their constructive and valuable comments.
- Ralph Dickhout, Dennis Herman, Rick Hecktus and Bert Habicher for their technical supports throughout the duration of my research.
- Liz Bevan, Ingrid Sherrer, Rosemarie Guderian, Patricia Anderson, and Lorna Kelly for clerical help.
- Colleagues and friends in the Chemical Reaction Group especially, Ahsraf, Zuhair, Mook, Dr. Luke Coleman, Dr. Petr Chladek, Dr. Nouri, Osama, Rangsima, and many more for help, cheer up, and moral support.
- Co-op student, Kayla, Masaya and Adesola, for their valuable assistance in helping me running the experiments.
- Universiti Teknologi Malaysia and Malaysian Higher Education for the sponsorship of my studies.
- My parents, Tuan Abdullah Salleh, Alimah Mohd, and family members for their love, prayer and constant encouragement.
- My wife, Merlyn Bahiyah Hasshim for her love, patience, support and sacrifice.
- Finally, my son, Ahmad Shukri, who fills my life with joy and happiness.

Table of Contents

List of Figures

List of Tables

Chapter 1

Introduction and Motivation

Hydrogen is an important chemical in many industries such as the chemical industry (production of ammonia, methanol, hydrogenation, etc.), petrochemical industry (hydrotreatment), food processing, semiconductor industry, and in the metallurgical industry. The growth in hydrogen demand is already increasing significantly, especially in Western Canada for oil sand upgrading. Moreover, with hydrogen fuel cells now near commercialization, hydrogen is expected to become one of the major fuels for energy generation in the future (Armor, 1999). Unfortunately, hydrogen does not exist in nature in its elemental form and, therefore, has to be produced from hydrocarbon, water or any other hydrogen-containing compounds, such as alcohol. There are currently four routes for hydrogen production: steam reforming, cracking, gasification and water electrolysis (Jen and Thomas, 2001).

Hydrogen production from ethanol is attracting much attention in various laboratories around the world since it has been identified as a promising source of hydrogen among liquid fuels. The main advantage of ethanol is that it can be produced from renewable sources such as corn, wheat or agricultural wastes. Carbon dioxide produced from ethanol will complete a closed carbon cycle naturally and ethanol can thus be considered as almost carbon neutral. In addition, it is biodegradable, relatively inexpensive, easy to transport, has low toxicity (Freni et al., 2001) and is free from catalyst poisons such as sulphur, chlorine etc.

Hydrogen storage is one of the most important issues and potentially biggest roadblock for the implementation of a hydrogen economy (Ritter et al., 2003). A major loss of hydrogen energy happens during the process of compression from low to storage pressure. For energy analysis, Bossel et al. (2003) emphasize that the heat of formation or higher heating value (HHV) is best to evaluate the true energy content of the fuel, based on energy conservation principles (i.e., the 1st Law of Thermodynamics). Hydrogen possesses a very high mass energy density (142 MJ/kg (HHV)), but its volumetric energy density, 12.7 MJ/m^3 (HHV at STP) is the lowest among other gas fuels, the closest being methane (40.0 MJ/m^3 (HHV at STP). Current hydrogen storage technologies for many fuel cell applications such as Proton Exchange Membrane Fuel Cells (PEM-FC) for automotive application

require high pressure (30-35 MPa), with proposals to operate up to 70 MPa. Obviously, pressurizing hydrogen to such high pressures consumes a significant amount of energy. Since compression of a liquid requires considerably less energy, production of hydrogen from liquid fuels at elevated pressure would give a clear advantage in terms of energy savings. For example, calculation using AspenPlus, shows that compressing 6 mol/s of hydrogen from 0.1 MPa to 25 MPa requires a net work of 278 kW. In comparison 7.4 mol/s of an ethanol-water mixture (which can produce 6 mol/s of hydrogen) from 0.1 MPa to 25 MPa (assuming that ethanol water reforming in SCW with ethanol water molar ratio feed of 1:3, with 90% ethanol conversion) just requires a net work of 21.5 kW, which is 13 times smaller than using a compressor to compress hydrogen from atmospheric pressure to 25 MPa. This is the rationale of the present work: generating hydrogen from renewable liquid fuel (bio-ethanol in the present case) at high pressure (25 MPa) by catalytic steam reforming in supercritical water.

Reactions in supercritical water (SCW) – pressures above 22.1 MPa and temperatures above 374°C - have received a lot of attention, most of the work focusing on supercritical water oxidation (SCWO) for decomposition of waste chemical. Instead of waste destruction, chemical synthesis and the production of chemical in supercritical or sub-critical have also attracted significant interests. The prospect of hydrogen production from organic compounds in SCW has been shown in several laboratories. Hydrogen production under SCW conditions has several advantages due to the properties of SCW as described in Chapter 2.

From the literature, the effect of temperature on ethanol water reforming or ethanol hydrolysis in SCW has been studied from (Schanzenbacher et al., 2002), 450 to 500°C (Arita et al., 2003), 550 to 700°C (Taylor et al., 2003), and 400 to 500°C (Hsiao 2003), 600 to 800°C (Byrd et al., 2007b). Only Byrd et al. (2007b) studied catalytic ethanol reforming specifically, using a commercial 5wt.% Ru/Al_2O_3 catalyst in a packed bed reactor, but at very extreme conditions of 600°C and 800°C.

1.1 Research Objectives

The overall objective of this project is to show the practicability of producing high pressure hydrogen from ethanol via ethanol water reforming (EWR) in supercritical water (SCW) conditions in the presence of a catalyst. Therefore, the goal of this research is to develop an active, selective and stable catalyst for ethanol reforming in SCW and to optimize the reaction conditions of this reaction. In order to achieve this objective, this study was divided into the following tasks;

1. A preliminary study with thermodynamics and experiments with the empty reactor to see the effect of the reactor wall.
2. Catalyst screening to identify promising catalysts that are active, selective toward H_2 and CO_2, and stable for ethanol reforming in SCW. The results of this screening study resulted in the selection of cobalt supported on Yttria Stabilized Zirconia (Co/YSZ).
3. Complete characterization of the Co/YSZ in term of performance and catalyst morphology.

1.2 Thesis description

This manuscript describes the research findings for catalytic ethanol reforming in supercritical water. Chapter 1 highlights the introduction and motivation this work. Chapter 2 presents a literature review on supercritical water systems (with emphasis on the properties of SCW as a reaction medium), as well as on hydrogen production in both supercritical water and in atmospheric reforming systems. More conventional atmospheric processes are of interest because they were the starting point in term of catalyst selection for the screening stage. In that regard, the literature review presents several catalysts used for ethanol steam reforming and reports possible reaction mechanisms at atmospheric conditions and in SCW. Chapter 3 describes the experimental apparatus, the catalyst preparation and characterization techniques and the analytical method used for evaluating catalyst performance. Chapter 4 presents the thermodynamics study for ethanol reforming in supercritical water. The free energy Gibbs model was used with the commercial software, Aspen Plus®. In addition, the separation of gas and liquid at high pressure was also briefly investigated. Chapter 5 provides results obtained for ethanol hydrolysis in the empty reactor (no catalyst). This was necessary to evaluate the effect of the reactor itself on the extent and the limitations of the reaction in the temperature range of 450 to 600°C. Indeed because of the extreme SCW conditions, the reactor is made of alloys known to be catalytically active for reforming reactions. Chapter 6 provides the result of the catalyst screening at four different temperatures (475, 500, 525 and 550°C), 250 bar, 5 wt.% ethanol, 1.88 g/min feed flowrate. Two active metals, nickel and cobalt, supported on four types support (γ-Al_2O_3, α-Al_2O_3, ZrO_2, Yittra Stabilized Zirconia (YSZ)) were selected for the screening study. The chemical and physical properties of each catalyst was also characterized and correlated to the catalyst performance. Chapter 7 presents an in-depth study of Co/YSZ (our most promising catalyst) in terms of chemical/physical characterization and performance. Several effects such as temperature, pressure, concentration, and in-situ/ex-situ reduction were studied. Finally, Chapter 8 summarizes the main conclusions of this work and gives recommendations for additional research activities on high pressure hydrogen production in supercritical water.

Chapter 2

Background and Literature Review

In this chapter, a general overview of supercritical water (SCW) properties, hydrogen production in supercritical water (SCW) and ethanol steam reforming (ESR) is presented. The first section presents a review of supercritical water properties followed by a discussion on the potential problem of corrosion in supercritical water. Next, hydrogen production methods in SCW, such as gasification, reforming and partial oxidation, are presented. Catalyst morphology and characterization studies for reaction in supercritical water are reviewed as well. Finally, a subsequent section reviews the literature findings on catalytic reactions for ethanol reforming at ambient to moderate pressures. As part of this chapter, the type of catalysts (active metals and supports) and the effect of operating parameters such as temperature, pressure, reactant concentration and residence time for hydrogen production are also discussed.

2.1 Supercritical Water (SCW)

2.1.1 Properties of SCW as Reaction Medium

There are three common phases for water: ice (solid), liquid and gas/vapour. However, when pressure and temperature exceed the water critical point of 374°C (647 K) and 221 MPa, water possesses properties that are in between those of liquid and gaseous phases. This phenomenon is not only true for water but also for all substances in their supercritical state, in which case they are referred to as supercritical fluids. To understand what is happening at or near the critical point, we should consider the process of phase transition between liquid and gas. As the pressure increases, a gas becomes denser, while as the temperature increases a liquid becomes less dense. Consequently, as the temperature and pressure increases, the density difference between the gas and liquid decreases and finally reaches zero at the critical point. Beyond the critical point, the supercritical fluid density

varies continuously from liquid-like at high densities to gas-like at low density. In the liquid phase, below the critical temperature, the fluid is referred as sub-critical fluid. All these states are shown in Figure 2-1.

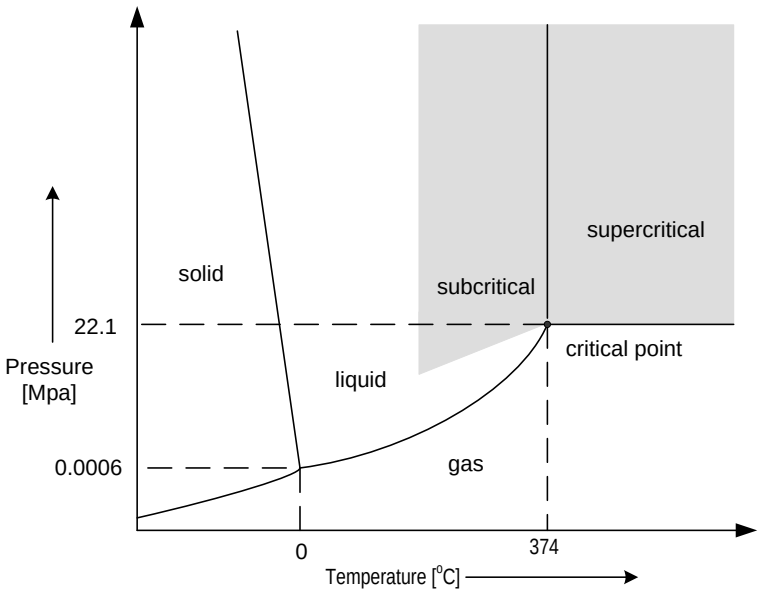

Figure 2-1: Phase diagram of water

The ability to tune its density gives supercritical water (SCW) several advantages, because its properties can be positioned between those of water vapour and those of liquid water. Figure 2-2 shows how several properties of water (density, ionic product and pK_w) change as water undergoes a transition from sub- to supercritical states. This figure it is seen that the water density (ρ) drops swiftly as the temperature goes through the critical temperature, especially when the pressure is near the critical pressure. This observation is valid for the ionic product and the dielectric constant as well. From Figure 2-2, it is clear that several properties of water can change significantly in the vicinity of the critical point. Comparison of several water properties between ambient water, SCW and superheated steam is presented in Table 2-1.

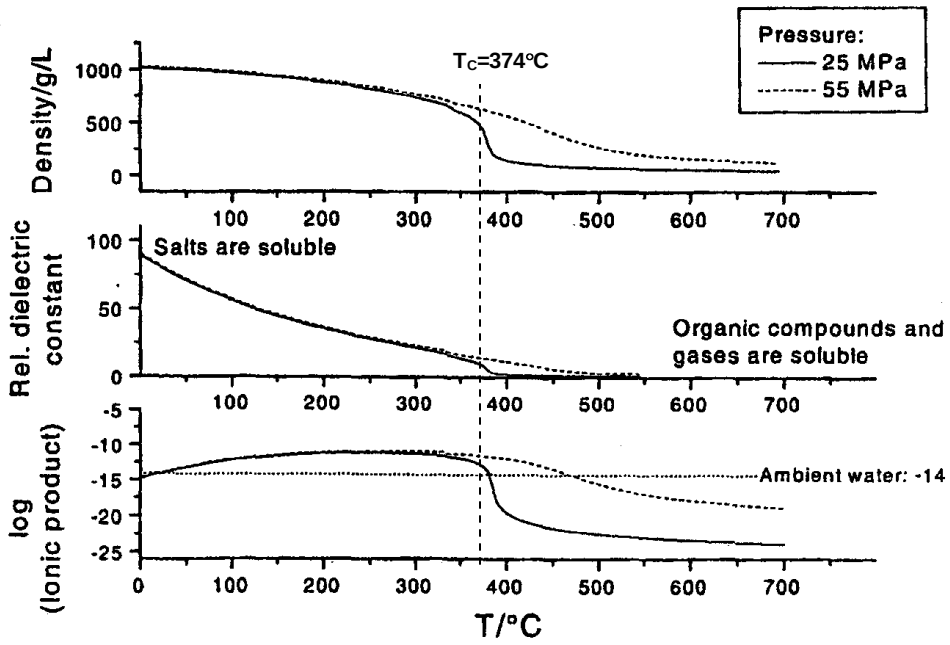

Figure 2-2: Selected properties of water at high temperature (Adapted from Dinjus and Kruse, 2004).

Table 2-1: Summary of physicochemical properties of water (Bröll et al., 1999).

	"Normal" Water	Subcritical Water	Supercritical Water		Superheated Steam
T [°C]	25	250	400	400	400
P [MPa]	0.1	5	25	50	0.1
density [g cm^{-3}]	0.997	0.8	0.17	0.58	0.0003
relative dielectric const.	78.5	27.1	5.9	10.5	1
pK_w	14.0	11.2	19.4	11.9	-
heat capacity [kJ kg^{-1} K^{-1}]	4.22	4.86	13	6.8	2.1
dynamic viscosity [m Pa s]	0.89	0.11	0.03	0.07	0.02

The dielectric constant is one characteristic of the polarity of a solvent and is a function of the fluid density. At ambient conditions (T=25°C, P=1 atm) water is a good solvent for electrolytes, such as KCl, NaOH, Na_2SO_4, because of its high relative dielectric constant of ca. 80, but is poorly miscible with hydrocarbon and gases. Near the critical point, the relative dielectric constant decreases by one order of magnitude and water becomes completely miscible with many organic compounds and gases. In contrast, electrolytes are not miscible at low relative dielectrics constant; thus, SCW can be used to precipitate particles of electrolytes.

The dynamic viscosity (η) in SCW at gas-like is almost similar to superheated steam condition, e.g 0.03 mPa.s at 400°C and 25 MPa. Low value of η presents some advantages for heterogeneous catalytic reactions by improving selectivity and space yield for an overall reaction that is typically limited by mass transfer (Broll et al., 1999). Another important feature when using supercritical condition as a catalytic reaction medium is that all reactants and product can exist in a single homogeneous phase, which eliminates mass-transfer resistances that exist in multiphase systems (Baiker, 1999; Savage, 1995, 1999).

The specific heat capacity (C_P) in SCW is very high, (e.g., 29.2 kJ kg^{-1} K^{-1} at 400°C and 29 MPa), compared to liquid and gases for which C_p only depends on temperature, whereas it is also highly dependent on pressure in SCW. This phenomenon leads to reduce hot spot problems in exothermic reactions such as water gas shift reaction and methanation in SCW. Thermodynamic properties of pure water for a wide range of temperatures and pressures can be easily obtained from steam tables. However, there is still lack of data for binary or multicomponent mixtures. However, at SCW conditions, ethanol (T_c=240.7°C, P_c=6.137 MPa, and ρ_c=276 kg/m^3) is already in its supercritical condition.

2.1.2 Corrosion in sub- and supercritical water

Strongly ionized water with formation of H_3O^+ and OH^- ions in sub- and supercritical regions creates a corrosive environment. Therefore, a good understanding of corrosion mechanisms in sub- and supercritical water is a prerequisite for studying reaction in SCW. Material selection is critical and often, if not always, specialty alloys are necessary (e.g., Hastelloy, Inconel). Corrosion at high pressure and temperature of water has been reported by a few researchers. There is an excellent review paper describing the corrosion phenomena in sub-critical and supercritical water and aqueous solution written by Kritzer (2004). Kritzer reported that the causes for corrosion are solution-dependent (e.g., density, temperature, pH, electrochemical potential and the aggressiveness of the attacking anions) and material-dependent (e.g., alloy composition, surface condition, material purity and treatment).

As seen in the previous section, properties of SCW, such as density, ionic product and dielectric constant, can be tuned by varying the temperature and pressure of the system. High density and high value of dielectric constant favours the solubility and/or the dissociation of ionic species such as salts, acids, and bases and thus favour ionic reactions, in particular those leading to corrosion. In contrast, low-density water suppresses ionic reactions and favour radical reaction pathways, especially at high temperatures (Kritzer, 2004). In addition, at high temperature and lower density, the dissociation of acids and the solubility of salts drop. For example, in supercritical water oxidation (SCWO) process, acid minerals are formed by heteroatoms Cl, P and S, which are frequently components of the organic contaminants (Kritzer and Dinjus, 2001). Formation of acid minerals increases the already corrosive environment of SCW, subsequently stimulating corrosion attack of the SCW construction material. The effect of temperature and pressure on corrosion potential is shown in Figure 2-3. The basis for understanding Figure 2-3 is that generally corrosion is low at densities below about 200–300 kg/m^3. At 300°C, a sub-critical pressure of 10 MPa leads to high corrosion rates, while at 500°C, pressures above ca. 50 MPa are necessary for high corrosion. As seen in Figure 2-3, increasing the pressure at constant temperature increases the rate of electrochemical corrosion. Note that the shift from no corrosion towards strong corrosion is only sharp at temperatures near the critical temperature, while there is no clear dividing line at higher temperatures.

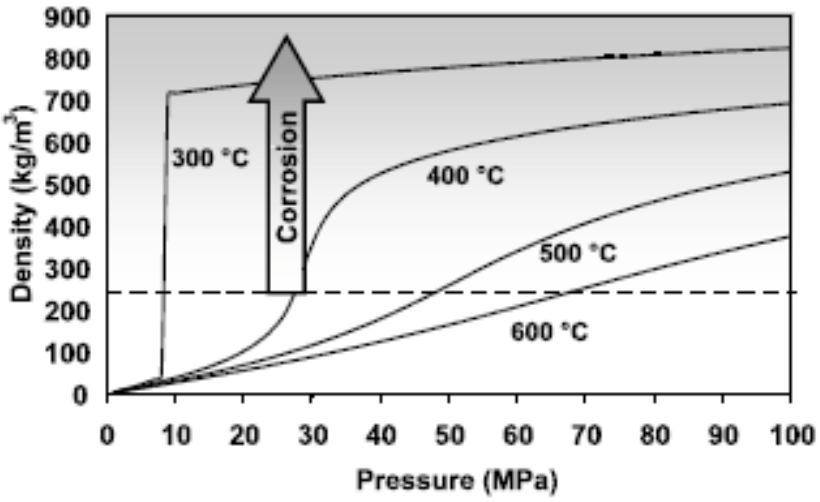

Figure 2-3: Density range of high corrosion at different temperatures. (Adapted from Kitzer, 2004)

Most researchers agree that the presence of inorganic ions plays an important role in corrosion (Kritzer,2004; Kritzer and Dinjus, 2001; Boukis et al., 2003b; Lee et al., 2005). Alumina ceramic dissolved in the presence of high concentration of a base (e.g., NaOH) in low-density SCW leads to the formation of a liquid NaOH phase. Table 2-2 shows the influence of inorganic ions on nickel-base alloys and stainless steels in high temperature water. Some inorganic compounds have a detrimental effect on corrosion resistance, for example chlorine Cl^- and bromide Br^- are highly destructive of the oxide film of nickel-based metals.

Table 2-2: Influence of inorganic ions on the corrosion of nickel-base alloys and stainless steels in high-temperature water (Adapted from Kitzer, 2004)

Ion	Mode of action	Result
F^-	Weak complex former	Homogeneous corrosion possiblea; passivating influence?
Cl^- ; Br^-	Penetrate into & destroy protecting oxide-film	Strong localized corrosion: pitting and SCC[a]
SO_3^{2-} ; SO_4^{2-} ; $S_2O_3^{2-}$	Oxidate in high-temperature water by forming S^{2-} and S^{ob}	Strong homogeneous degradation possible
S^{2-}	Reductive in high-temperature waterb	Release of H_2 possible; SCC possible
NO_3^-	Strongly oxiding; main corrosion products well soluble	Strong general corrosion possible
CO_3^{2-} ; PO_4^{3-} CO_3^{2-} PO_4^{3-}	Low-soluble salts	Corrosion-inhibition possible
OH^-	Low-soluble salts	Strong passivating; corrosion-inhibition possible
H^+	Enhanced solubility of protecting oxides	Strong general corrosion possible[a]

[a] In the presence of oxidizing compounds.

2.1.3 Hydrogen Production in Sub- and Supercritical Water

Table 2-3 summarizes some of the most notable studies on hydrogen production in SCW. Most catalytic reactions were carried out in batch reactors. The formation of methane is favoured at temperatures below <600°C due to methanation and acetaldehyde decomposition, which dominate in liquid-like (high-density) water. The presence of catalysts such as alkali salt (e.g. KOH, NaOH), metal oxide (e.g ZrO_2, NiO), active metal (e.g. reduced nickel) and carbon-derived materials (e.g. charcoal, activated carbon) were able to enhance the production of hydrogen through the water gas shift reaction even at temperatures lower than 600ºC. In contrast, hydrogen formation is favoured at higher temperature (>600°C) even without catalyst, because the gas-like (low density) properties of water seem to promote the water-gas-shift reaction and thus produce more hydrogen. The following discussion focuses on a few selected studies on hydrogen production in SCW.

Table 2-3: Hydrogen production at near and supercritical water

Group	Reference	Feedstock	Reactor	Catalyst	Reaction condition	Conv. (%)	Main Gas
Antal's Group (Hawaii Natural Energy Institute, USA)	Yu et al., 1993	glucose, wet biomas (water hyacinth, alga)	Plug flow (Inconel-625 and Hastelloy C276)	None	600°C, 34.5 MPa	Variable	H_2
	Xu et al., 1996	Glycerol, glucose, cellobiose	Plug flow (Inconel-625)	Charcoal, activate carbon	600°C 34.5 MPa	100	H_2 and CO
	Xu et al., 1998	Corn starch, Wood sawdust, sewage sludge	Packed bed (Hastelloy C276)	Carbon	650°C 22 MPa	100	H_2 and CO_2
Arai's group (Supercritical Fluid Research Centrer, Japan)	Watanabe et al., 2001, 2002, 2003a & 2003b	Formaldehyde Acetic Acid 2-propanol glucose and cellulose	Batch (316 Stainless Steel)	CeO_2, MoO_3, TiO_2 and ZrO_2 H_2SO_4, KOH& NaOH	400°C 25-40 MPa	variable	CH_4 and CO
	Sato et al., 2004	Lignin, Alkylphenol	Batch (Stainless Steel)	Ni/MgO, Ru on γ-Al_2O_3, C Pt on γ-Al_2O_3, C	400°C 24 MPa		CH_4, CO_2 and H_2 (depend on the catalyst)
	Osada et al., 2004	Lignin & Cellulose	Batch Stainless steel	Ru/Al_2O_3 Ru/TiO_2	400°C 30 MPa	10-74	CH_4
	Osada et al., 2006	Lignin, 4-propylphenol	Batch (316 SS)	Ru/ TiO_2, Ru/Al_2O_3, Ru/C, Pt/C, Pt/Al_2O_3, Rh/C, Pd/C, Ni/Al_2O_3	400°C 37.1 Mpa	Not reported	CH_4, CO, H_2

Fraunhofer Institut für Chemische Technologie, Germay	Schmieder et al., 2000	Glucose, vanillin, Lignin	Plug flow (Nimonic 110 & Inconel-625)	KOH, K_2CO_3	600°C 25 MPa	100	H_2 and CO_2
	Boukis et al., 2003, 2006	Methanol	Plug flow (Inconel-625)	None	400-600°C 25-45 MPa	~100%	H_2
	Pinkwart et al., 2004	Diesel	Packed bed (material not mention)	Commercial catalyst $NiO/Al_2O_3/SiO_2/MgO$ $NiO/Al_2O_3/SiO_2/MgO/CaO/K_2O$	550°C 25 MPa	18 – 80	H_2
	Sinag et al., 2004	glucose	Batch (Inconel-625)	K_2CO_3, Ni, Ni-Raney	500°C 30 MPa	Not reported	H_2 and CO_2
Gumpta's Group Department of Chemical Eng. Auburn University, USA	Byrd et al., 2007a, 2007b, 2008	Glucose, Glycerol, ethanol	Packed bed Inconel 600	Commercial catalyst (5% wt. Rh/Al_2O_3)	600-800°C 22.1-27.5 MPa	~100%	H_2, CO, CH_4, CH_4
Various universities	Yoshida and Oshima, 2004	Glucose Glucose/lignin	Packed bad (316 SS)	Ni-5256E ®	400°C 25.7 MPa	~96%	H_2
	Hirth and Franck, 1993	Methane, Ethane, Methanol, CO, Formic Acid	Plug flow (Nickel Alloy)	None	600°C 60 MPa	2.54 - 30.6	H_2 and CO_2
	Elliot et al., 1993	p-cresol	Stirred Batch (Inconel)	Ni, NiO, Co, Cr, W, Mo, Cu. Ni on C, ZrO_2, Y/ZrO_2, SiO_2, γ-Al_2O_3, α-Al_2O_3, η-Al_2O_3, Ru on γ-Al_2O_3, δ-Al_2O_3, α-	(subcritical) 350°C 20 MPa	0.02-93%	H_2, CH_4 and CO_2 (depending on the type

				Al_2O_3, C, ZrO_2, Rh on C, α-Al_2O_3, γ-Al_2O_3. Pt on γ-Al_2O_3, α-Al_2O_3			of catalyst)
	Izumizaki et al., 2005	Cellulose, Pulp, Mixture	Batch (Inconel-625)	RuO_2	450°C 440 MPa	~62%	CH_4 (low T) H_2 (high T)
	Taylor et al., 2003	Methanol, Ethanol, Ethy Glycol	Plug flow (Inconel-625)	None	700°C 27.6 MPa	~99.5%	H_2
	Arita et al., 2003	Ethanol	Batch Quartz	Stainless steel (316 SS) Cu	400-500°C 23 MPa	Not reported	H_2
	Furusawa et al., 2007	Lignin	Batch Stainless steel	Ni(O)/MgO	400°C 30-37 MPa	Not reported	H_2, CH_4, CO_2,C_2H_6

Yu et al. (1993) conducted gasification of glucose in SCW in a tubular reactors made of Inconel-625 and Hastelloy-C276. The formation of H_2, CO_2, CO, and CH_4 at 600°C, 34.5 MPa and 30 s residence time, with nearly no tar or char product, were detected in the product stream using an Inconel reactor. They found that the conversion and yield were highly dependent on the material used for the reactor and on the initial concentration of glucose. Complete gasification was achieved with low glucose concentration. Also the Inconel reactor yielded higher selectivity toward hydrogen due to the enhancement of the water gas shift reaction, producing a gas rich in hydrogen and carbon dioxide, whereas the Hastelloy reactor produced more carbon monoxide. Xu et al. (1996) reported that the use of activated carbon as catalyst did increase the gasification efficiency of several organic compounds such as glucose, glycerol, methanol, etc. They showed that biomass could be completely gasified at temperatures above 600°C in the presence of activated carbon. They found that simple compounds of biomass, such as glycerol, completely gasified in SCW at 600°C and 34.5 MPa even without a catalyst to a hydrogen rich gas with almost no CO formation. Later, Xu et al. (1998) demonstrated that other heavy biomass compounds such as wood sawdust, corn starch gel or digested sewage sludge also could be gasified into a hydrogen rich gas with the presence of activated carbon catalysts, yet the operating temperature was increased to 650°C and the pressure decreased to 28 MPa compared to previous reports. These conditions resulted in no tar detected in the reactor and in improving hydrogen production with only small traces of carbon monoxide in the gas effluent.

The presence of alkali solution such as KOH (Kruse, 2000; Schmieder et al., 2000), K_2CO_3 (Sinag et al., 2004; Schmieder et al., 2000), CaOH (Wang, 2001), NH_3OH, and NaOH (Kruse, 2003) enhances the hydrogen yield and selectivity. For example, Kruse et al. (2003) have shown that adding KOH to the solution in the gasification of pyrocatechol (biomass in a group of lignin) led to nearly complete conversion (~99% conversion). Also, the yield of hydrogen was almost three times greater in the presence of alkali (5 wt.%). They considered that the enhancement of hydrogen yield by adding alkali was due to the enhancement of the water gas shift reaction.

Boukis et al. (2003a) demonstrated methanol steam reforming in SCW for hydrogen production using a reactor made of Inconel-625 in the range 400 – 600°C, at a pressure of 25 MPa, and initial concentrations ranging from 5 to 64 wt%. Methanol conversions up to 99.9 % without adding catalyst resulted in a hydrogen rich gas with small amounts of CO, CO_2 and methane. Depending on the operating conditions gas product containing up to 75 vol% hydrogen (theoretical equilibrium limit) was achieved for residence times of less than a minute. Even though no catalysts

were used, they recognized the significant impact of the catalytic activity of the reactor wall made of Inconel-625 on the conversion. Pre-treatment of the inner reactor with hydrogen peroxide (strong oxidation agent) enhanced the reaction activity toward hydrogen production.

Ethanol water reforming in SCW has been studied as well in a limited way with and without catalyst. Taylor et al. (2003) studied the reforming of several organic compounds such as methanol, ethyl glycol, and ethanol in supercritical water at 550 – 700°C and 27.6 MPa in a tubular Inconel-625 reactor. They mentioned that the conversion of ethanol was close to 100%, and that the main dry product composition is: H_2 (~50%), CH_4 (25%), CO_2 (20%) and a balance of CO and C_2H_4 at 700°C and residence time of 3 to 6 s. For the catalytic ethanol water reforming in SCW, only two papers have been reported. Arita et al. (2003) studied ethanol reforming using a flame-sealed small quartz reactor in order to avoid the catalytic activity of the wall. At temperatures between 400 and 500°C and a density of 0.2 g/cm^3, they showed that hydrogen and acetaldehyde were the major products in SCW without any oxidizing reagent or catalysts. They also observed that the addition of a copper wire resulted in an increase in hydrogen composition in the gas mixture by a factor of two. A recent contribution on catalytic ethanol reforming in SCW was done in a continuous packed bed reactor by Byrd, et al. (2007b). They used a 0.5m × 3mm ID tubing, made of Inconel-600 and loaded with 2 g of 5wt.% Ru/Al_2O_3. They then tested the catalyst in a temperature range from 600°C to 800°C and pressures from 22.1 to 27.5 MPa. They demonstrated that ethanol conversion was complete with and without catalyst at 800°C. The only difference was the product composition. There were no data shown for empty reactor runs at 600°C and 750°C; therefore, it is difficult to compare the significance of the presence of the catalyst at high temperature, since the reactor itself was made of Inconel-600 (Allow Wire International®, 72% min. Ni, 14-17% Cr., and 6-10% Fe).

Other researchers found that adding some oxygen resulted in complete gasification of organic compounds and generated higher hydrogen yields (Holgate, 1995; Lee, 1996; Hirth and Franck 1993; 2002, Hsiao, 2003; Yoshida and Oshima, 2004). For example, Lee (1996) showed that the partial oxidation of methanol is almost complete (~99 % conversion) by adding pure oxygen at temperatures between 400 and 500°C and at a pressure of 25 MPa. Their result showed hydrogen selectivity between 4 and 11. In our laboratory, Hsiao (2003) investigated ethanol partial oxidation in SCW by adding hydrogen peroxide to supply oxygen at 500°C, 25 MPa and 8-50 s residence times. He found that the H_2O_2/ethanol ratio affected the ethanol conversion and hydrogen yield.

2.1.4 The effects of reaction parameters on hydrogen production in SCW

The following section presents the effect of reaction parameters such as temperature, pressure, ethanol-water ratio, and residence time in supercritical water.

Effect of temperature

The effect of temperature on the hydrogen production of organics solution in SCW has been studied with and without catalyst. The reaction temperature has been found to highly affect conversion, yield and by-products formation. Holgate et al. (1995) studied the effect of temperature on the hydrolysis of glucose in a plug flow reactor made of Inconel-625. Figure 2.4 shows the product yield for glucose hydrolysis for temperatures between 400°C and 650°C. Hydrogen and carbon dioxide were the main gaseous species detected, indicating the presence of the water gas shift reaction. Interestingly, acetaldehyde and CO disappeared for temperatures above 575°C, and formation of simple hydrocarbons (such as methane and ethane) and hydrogen were favoured at higher temperatures. These observations are generally consistent with the results reported by Yu et al. (1993) and Lee et al. (2002). The results of Lee et al. (2002) are shown in Figure 2.5, where it is seen that without catalyst, hydrogen yield and yield of other by-products are strongly dependent on temperature. The gasification conversion reached 100% at 700°C and 28 MPa. As the temperature increases, the yield of hydrogen increases sharply, whereas the yield of carbon monoxide decreases above 650°C. For ethanol reforming in SCW, Byrd et al. (2007b) reported that ethanol conversion over commercial Ru/Al_2O_3 was not complete and C_2 species were detected at temperature below 600°C. However, in the temperature range of 700-800°C, the product compositions were mainly H_2, CO, CO_2, and CH_4.

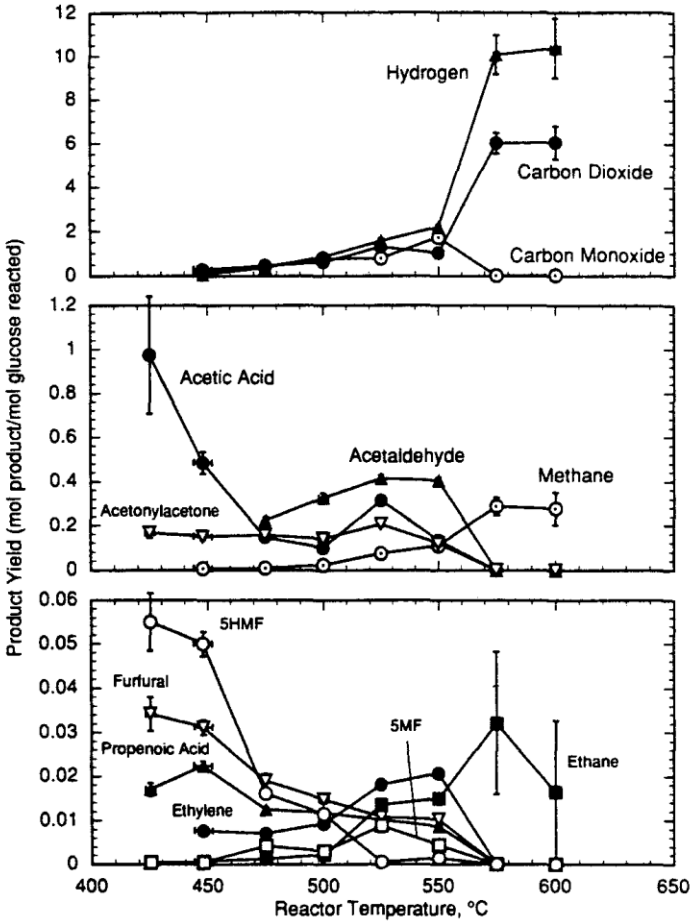

Figure 2-4: Variation of product yields with temperature for glucose hydrolysis at 24.6 MPa. Experimental conditions: $1.02\pm0.02\times10^{-3}$ mol/L glucose, 6.1±0.3 s reactor residence time. No catalyst. (Holgate et al., 1995).

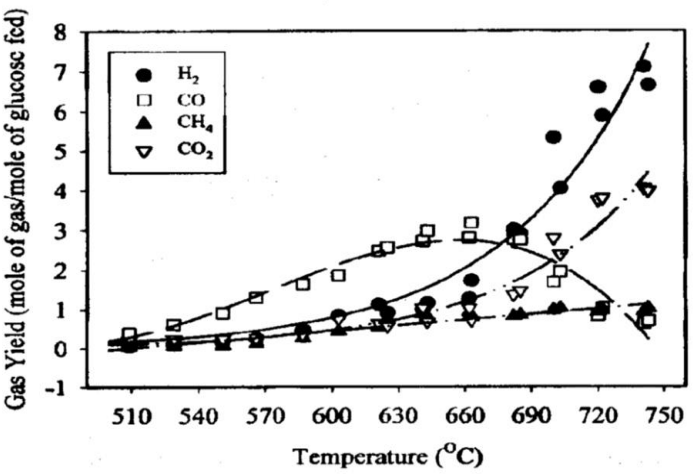

Figure 2-5: Gas product yields as a function of reactor temperature on 0.6 M glucose gasification in SCW at 28 MPa and a 30 s reactor residence time. No catalyst. (Lee et al., 2002).

Effect of pressure

There are only few studies looking at the effect of pressure on hydrogen production in sub- and supercritical water. Gadhe and Gupta (2005) investigated methanol reforming for pressures between 3.4 and 27.6 MPa and at a constant temperature of 700°C. They found that H_2, CO_2 and CO decrease with increasing the pressure in the subcritical region, whereas methane increases significantly until the critical temperature is reached. Sato et al. (2004) observed similar trends. Kruse and co-workers (2000) reported that the hydrogen production from the gasification of pyrocatechol ($C_6H_6O_2$) at 700°C slightly decreases as the pressure increases from 20 MPa to 40 MPa. Their results matched calculated equilibrium data. However, in a small pressure range slightly above the critical point of water, Byrd et al. (2007b) found that there is not much difference in ethanol conversion and product composition in the pressure range from 22.1 to 27.5 MPa, as shown in Figure 2-6.

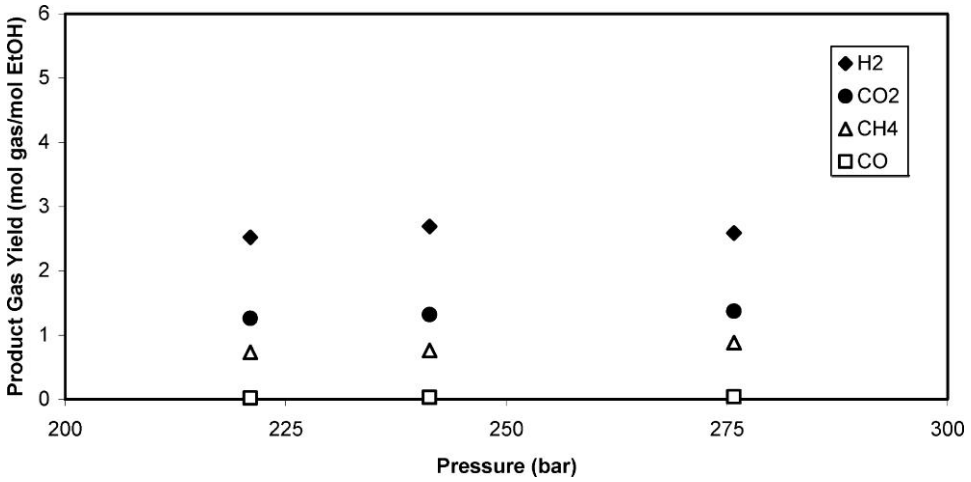

Figure 2-6: Effect of pressure over 5wt. % Ru/Al_2O_3 catalyst with 10 wt % Ethanol, 700°C (Byrd et al., 2007b).

Effect of residence time

Thus far, because most of the studies on ethanol (or other organic materials) reforming in SCW involved non catalytic reactions, the influence of residence time on hydrogen production was reported (Yu et al, 1993; Lee et al, 2002; Hao et al., 2003; Kruse and Dinjus, 2003; Gudhe and Gupta, 2005). They observed that the formation of hydrogen, carbon dioxide and methane increases with longer residence times, while carbon monoxide decreases. For catalytic reactions, Osada et al. (2004) reported their results in terms of reaction time, with methane increasing by increasing the reaction time over all catalytic reactions conducted in a batch reactor. Interestingly,

Arita et al. (2003) showed that the hydrolysis of ethanol in a batch reactor led to higher conversion to hydrogen as the residence time increased, as seen in Figure 2-7.

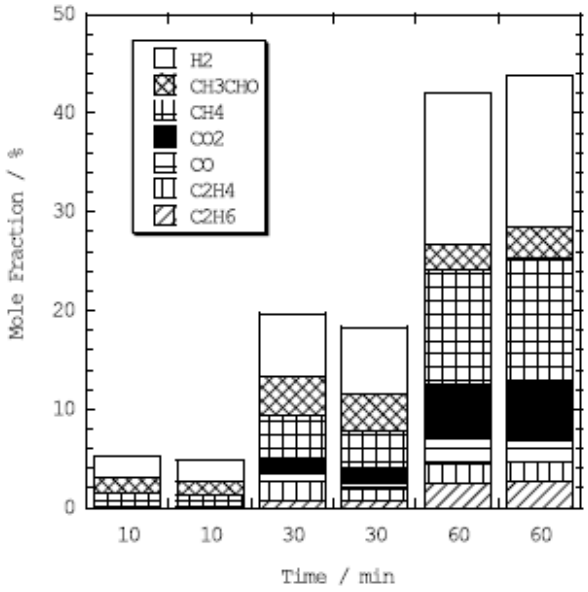

Figure 2-7: Time dependence of the yields of all products for ethanol reaction at a density of 0.20 g/cm^3 at 500°C. Batch reactor (Arita et al., 2003)

Effect of the water to carbon ratio

"The steam to carbon ratio is an important parameter as far as the economics of the process is concerned" (Gudhe and Gupta, 2004). Generally, it was observed that increasing the water to carbon ratios increases the production of hydrogen (Yu et al., 1993; Boukis et al., 2003, Taylor et al., 2003; Lu et al., 2006; Matsumura et al., 2005; and Byrd et al. 2007a, 2007b). For example, Boukis et al. (2003) observed that hydrogen increases rapidly and methane decreases significantly by increasing the water to methanol ratio from 1 to 4 at 600ºC, 25 MPa and a residence time of 15 s as shown in Figure 2-8. A similar pattern was observed for ethanol reforming in SCW. Byrd et al. (2007b) reported that increasing the ethanol concentration from 5 to 20 wt.% decreased the production of H_2 and CO_2 but increased the CH_4 yield as shown in the Figure 2-9.

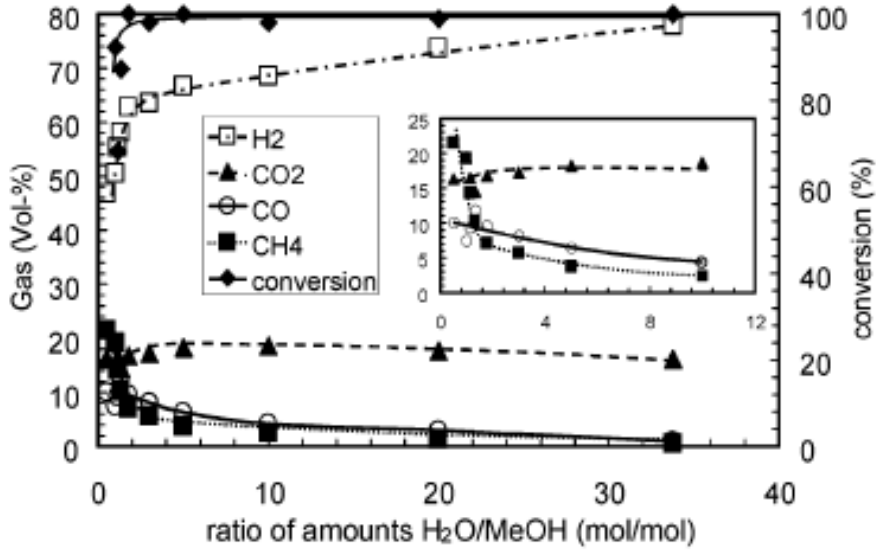

Figure 2-8: Gas composition as a function of the water-to-methanol ratio: P = 25 MPa, T = 600°C, residence time = 15 s. (Boukis et al., 2003a)

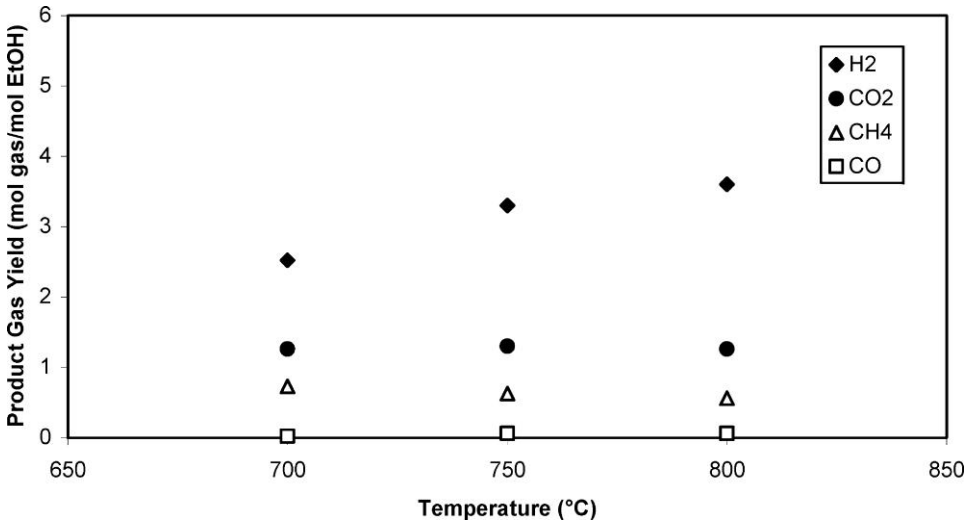

Figure 2-9: Effect of feed concentration of product gas yields at 800°C; 22.1 MPa over 1.9 g of 5% wt. Ru/Al_2O_3 catalyst (Byrd et al., 2007b)

2.1.5 Catalyst Stability in SCW

In SCW environment, an important cause of catalyst deactivation is the transformation of the solid state of the catalyst. Ding et al. (1996) categorized the transformation of solid-state into phase transition (e.g., γ-Al_2O_3 to α-Al_2O_3), solid solution formation (e.g., spinel from Cr_2O_3/Al_2O_3), sintering of metal coated on a support, and migration of active components. These transformations can occur because of the capability of SCW to hydrolyze metal oxide, to promote crystal growth and phase transformations, to reduce solid defects, and to accelerate solid uniformity (Ding et al., 1996). High loss of surface area of catalyst is commonly encountered in SCW reaction. Armbruster et al. (2001a) reported that the Carulite 150® (MnO_2-CuO/Al_2O_3) catalyst tested for hydrolysis and oxidation of ethyl acetate in sub- and supercritical water shows no loss of activity in SCW for at least 200 h at 400°C and 2.4 MPa, but BET -surface area decreased drastically from 264 m^2/g to 15 m^2/g due to sintering. High loss of BET surface area has also been reported by Elliot et al. (1993), Yu and Savage (2001), and Tomita and Oshima (2004).

The presence of oxygen also accelerates the phase transition of the active metal to metal oxide. Yu and Savage (2001), Kruse et al. (2002), Ding et al. (1998) and Tomita and Oshima (2004) reported the transformation of MnO_2 to Mn_2O_3 in SCWO, and the existence of Mn_2O_3 is highly dependent on the concentration of O_2 and temperature. Lin and Wang (2000) found that its copper catalyst exhibits three oxidation states, namely Cu, Cu_2O and CuO on spent catalyst exposed to SCWO. Armbruster et al. (2001b) examined Carrulite 300® (containing 40-60 wt.% MnO_2 and 1-3% CuO) supported on Al_2O_3 and obtained similar observation for phase transition during SCWO oxidation. X-ray amorphous Al_2O_3 also changed to crystalline phase of AlO(OH). Byrd et al. (2007b), who studied ethanol reforming in SCW included a profile of XRD plot, showed that the crystalline structure of Ru/Al_2O_3 catalyst changed after exposure to the reaction, but they did not describe their results in detail.

Even though Elliot et al. (1993) studied reactions in high water density (subcritical region), they are the only ones who conducted an extensive study of catalytic gasification using several active metal catalysts on various supports at conditions close to SCW conditions (20 MPa and 350°C). By experimenting with p-cresol in a batch reactor, they concluded that Ru, Rh, and Ni are active and that catalysts supported on α-Al_2O_3, ZrO_2 and graphite (carbon) were stable in high pressure water at the temperature examined.

2.2 Ethanol Steam Reforming (ESR)

2.2.1 Reaction Schemes for Ethanol Water Reforming

Several reaction schemes have been proposed for ethanol steam reforming depending on the desired products, operating conditions (e.g., temperature), and catalyst used. Ethanol steam reforming and ethanol decomposition are endothermic reaction, so they are thermodynamically favoured at high temperatures. The maximum theoretical product stream (assuming complete conversion into H_2 and CO_2) that can be obtained from 1 mol of ethanol contains 75% mol H_2 and 25% mol CO_2 (see equation (2-1)). However, there are many others reaction pathways that can occur during the ethanol water reforming process. Ethanol water reforming occurs when molecules of ethanol and water react under favourable conditions (see equations (2-1) to (2-3)). Ethanol itself can decompose to other components such as acetaldehyde, acetone and ethylene, when its bond breaks (see equations (2-5) to (2-6).

Ethanol-water reforming to CO_2:

$$C_2H_5OH \rightarrow C_2H_4O + H_2 \qquad \Delta H^{o}_{298K} = 17.3 \frac{kJ}{mol},\ \Delta G^{o}_{298K} = 66.3 \frac{kJ}{mol} \qquad \textbf{(2-1)}$$

Ethanol-water reforming to CO:

$$C_2H_5OH + H_2O \rightarrow 2CO + 4H_2 \qquad \Delta H^{o}_{298K} = 255.7 \frac{kJ}{mol},\ \Delta G^{o}_{298K} = 122.9 \frac{kJ}{mol} \qquad \textbf{(2-2)}$$

Ethanol-water reforming to acetic acid;

$$C_2H_5OH + H_2O \rightarrow CH_3COOH + 2H_2 \qquad \Delta H^{o}_{298K} = 41.8 \frac{kJ}{mol},\ \Delta G^{o}_{298K} = 45.9 \frac{kJ}{mol} \qquad \textbf{(2-3)}$$

Ethanol dehydrogenation to acetaldehyde

$$C_2H_5OH \rightarrow CH_3CHO + H_2 \qquad \Delta H^{o}_{298K} = 68.5 \frac{kJ}{mol},\ \Delta G^{o}_{298K} = 35.1 \frac{kJ}{mol} \qquad (2\text{-}4)$$

Ethanol decomposition to acetone

$$2C_2H_5OH \rightarrow CH_3COCH_3 + CO + 3H_2 \qquad \Delta H^{o}_{298K} = 141.5 \frac{kJ}{mol},\ \Delta G^{o}_{298K} = 46.2 \frac{kJ}{mol} \qquad \textbf{(2-5)}$$

Ethanol dehydration to ethylene

$$C_2H_5OH \rightarrow C_2H_4 + H_2O \qquad \Delta H^{o}_{298K} = 45.3 \ \frac{kJ}{mol}, \ \Delta G^{o}_{298K} = 7.7 \frac{kJ}{mol} \qquad (2\text{-}6)$$

Once ethanol reacts to form components with double bonds (e.g., CO, C_2H_4) or triple bonds (C_2H_2), these products are not thermodynamically favoured at high temperatures and they react to form single bond species (H_2, CO_2, CO, H_2O, CH_4) via mostly exothermic reactions. Coleman (2008) reported, using thermodynamic calculations, that at atmospheric pressure CH_4 and CO_2 are formed significantly below 650K, but H_2, CO, and CO_2 become the main product above 850K. Additional reactions are possible as shown in equation (2-7) to (2-13).

Water gas shift reaction:

$$CO + H_2O \rightleftharpoons CO_2 + H_2 \qquad \Delta H^{o}_{298K} = -41.2 \ \frac{kJ}{mol}, \ \Delta G^{o}_{298K} = -28.3 \frac{kJ}{mol} \qquad (2\text{-}7)$$

Acetaldehyde decomposition or decarbonylation :

$$CH_3CHO \rightarrow CH_4 + CO \qquad \Delta H^{o}_{298K} = -18.9 \ \frac{kJ}{mol}, \ \Delta G^{o}_{298K} = -54.8 \frac{kJ}{mol} \qquad (2\text{-}8)$$

Acetaldehyde water reforming

$$CH_3CHO + H_2O \rightarrow 3H_2 + 2CO \qquad \Delta H^{o}_{298K} = 296.5 \ \frac{kJ}{mol}, \ \Delta G^{o}_{298K} = 369.8 \frac{kJ}{mol} \qquad (2\text{-}9)$$

Acetic acid water reforming;

$$CH_3COOCH_3 + 2H_2O \rightarrow 5H_2 + 3CO \qquad \Delta H^{o}_{298K} = 586.9 \ \frac{kJ}{mol}, \ \Delta G^{o}_{298K} = 396.3 \frac{kJ}{mol} \qquad (2\text{-}10)$$

Hydrogenation of ethylene:

$$C_2H_4 + H_2 \rightarrow C_2H_6 \qquad \Delta H^{o}_{298K} = -137.0 \ \frac{kJ}{mol}, \ \Delta G^{o}_{298K} = -101.1 \frac{kJ}{mol} \qquad (2\text{-}11)$$

Methanation of CO:

$$CO + H_2 \rightleftharpoons CH_4 + H_2O \qquad \Delta H^{o}_{298K} = -206.2 \ \frac{kJ}{mol}, \quad \Delta G^{o}_{298K} = -142.6 \frac{kJ}{mol} \qquad (2\text{-}12)$$

Methanation of CO_2:

$$CO_2 + 4H_2 \rightarrow CH_4 + 2H_2O \qquad \Delta H^{o}_{298K} = -252.9 \frac{kJ}{mol}, \quad \Delta G^{o}_{298K} = -113.6 \frac{kJ}{mol} \qquad (2\text{-}13)$$

Temperatures below 300°C, favour reactions leading to C_2 species (and higher), such as acetone, diethyl ether, ethylene, acetic acid, acetal or methyl ethyl ketone (MEK). For example, acetic acid was found as a product for ethanol reforming over $Cu/K/\gamma\text{-}Al_2O_3$ at 300°C (Marino et al., 2001). Acetone was reported in the case of catalyst supports capable of oxygen storage such CeO_2, ZrO_2 and ZnO (Nakajima et al., 1989; Kugai et al., 2005; Nishiguchi et al., 2005), according to the following reaction scheme (Nishiguchi et al., 2005):

$$2CH_3CHO \rightarrow CH_3CH(OH)CH_2CHO \qquad (2\text{-}14)$$

$$CH_3CH(OH)CH_2CHO + O(s) \rightarrow CH_3COCH_3 + CO_2 + H_2 \qquad (2\text{-}15)$$

Most of the studies on catalytic steam reforming of ethanol at atmospheric pressure report deactivation of catalyst due to coking and tar formation. There are five possible routes for coke formation that have been proposed: 1) polymerization of ethylene under steam cracking conditions (Dybkjaer, 1995), where ethylene is converted into olefin, which polymerizes and finally forms coke on acidic catalytic sites, such as $\gamma\text{-}Al_2O_3$ (Eqn. (2-16)); 2) decomposition of methane into hydrogen and carbon filament (Eqn. (2-17)); 3) Boudouard reaction (Eqn. (2-18)): 4) hydrogenation of carbon monoxide into carbon and water (Eq. (2-19)), and 5) hydrogenation of carbon monoxide into carbon and water (Eqn. (2-20)). Of the last four routes (Eqn. (2-17) to Eqn. (2-20)), the Boudouard reaction is the most likely to happen on the active metal catalyst, because it has the lowest values of Gibbs free energy (-41 kcal/mol), as mentioned by Garcia and Laborde (1991) and Freni et al., (2003). However, polymerization of ethylene was the most mentioned in ethanol steam reforming over acidic support materials, such as $\gamma\text{-}Al_2O_3$ support (Dybkjaer, 1995, Vizcaíno, et al. 2008, Alberton et al., 2007).

Coking or tar formation:

Polymerization of ethylene: $C_2H_4 \rightarrow \text{olefins} \rightarrow \text{polymers} \rightarrow \text{coke}$ (2-16)

Decomposition of CH_4: $CH_4 \rightarrow 2H_2 + C$ (2-17)

Boudouard reaction: $2CO \rightarrow CO_2 + C$ (2-18)

Hydrogenation of CO_2: $CO_2 + 2H_2 \rightarrow 2H_2O + C$ (2-19)

Hydrogenation of CO: $CO + H_2 \rightarrow H_2O + C$ (2-20)

Since, there are a limited number of reports dealing with ethanol reforming in supercritical water, its reaction mechanism is not well known. Generally, the hydrolysis and reforming of ethanol in SCW lead only to the formation of H_2, CO, CO_2, CH_4, C_2H_4, C_2H_6 and acetaldehyde at temperatures below 500°C (Ramayya, 1987; Arita, 2003; Taylor, 2003; Hsiao, 2003). In addition to these species, small amounts of formaldehyde and acetic acid were also reported by Schanzenbacher et al. (2002). Although all of the above mentioned studies did not involve catalysts, they all recognized the importance of the catalytic effect of the reactor wall. Xu et al. (1991) reported that the absence of sulphuric acid as homogeneous catalyst just produced ethane and diethyl ether from ethanol at 385°C and 34.5 MPa. Figure 2-10 shows two reaction schemes proposed by Arita et al. (2003); one starting with ethanol dehydrogenation and the other starting with ethanol dehydration for ethanol hydrolysis at 500°C and a water density of 0.2 g/cm^3 (i.e., pressure ≈26 MPa). The proposed scheme for ethanol water reforming in SCW described by Arita is actually similar to the reaction mechanism proposed at atmospheric pressure (Arita et al., 2003).

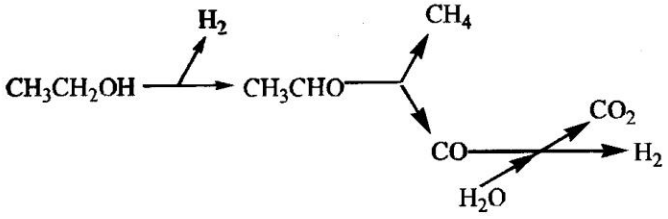

Scheme 1.

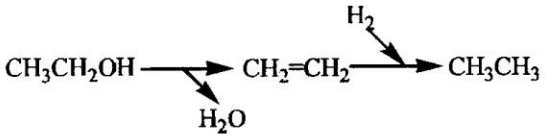

Scheme 2.

Figure 2-10: Proposed reaction route for ethanol hydrolysis (Arita et al., 2003)

Byrd et al. (2007b) suggest that the reaction pathway for ethanol reforming at higher temperatures in SCW, around 700-800°C, in the presence of 5 wt.% Rh/Al_2O_3, begins with dehydrogenation of ethanol to acetaldehyde, then followed by the decomposition of acetaldehyde to CO and CH_4. They stated that the presence of SCW and the involvement of the Rh catalyst helped promote the water gas shift reaction. They proposed that the overall reaction pathway at high temperature (700-800°C) could be written as follow;

(ethanol steam reforming) $C_2H_5OH + H_2O \rightarrow CO_2 + CH_4 + 2H_2$

(water gas shift) $CO + H_2O \rightarrow CO_2 + 2H_2$

(methane steam reforming) $CH_4 + H_2O \rightarrow CO + 3H_2$

2.2.2 Catalytic Ethanol Reforming at Atmospheric and Moderate Pressure

Over the past ten years more than 200 papers have discussed ethanol and bio-ethanol steam reforming at atmospheric pressure. Excellent reviews on this topic can be found in Haryanto et al. (2005), Vaidya et al. (2006) and Frusteri and Freni (2007) and Ni et al. (2007). Catalytic ethanol steam reforming (ESR) at atmospheric pressure has been studied extensively, with focus on various active metals, starting from noble metals to common active metals such as nickel or cobalt, as well as the combination of several active metals. The following discussion will focus in more detail on the behaviour of the active metal and the support material of the catalyst on ethanol steam reforming at atmospheric to moderate pressure.

2.2.2.1 Active Phase

Noble metal

Noble metals such as Ru, Rh, Pd, Pt, Ir, Au, are well known for their high catalytic activity and have been studied extensively in regard to ethanol steam reforming (ESR) at atmospheric pressure (Liguras et al., 2003; Kugai et al., 2005; Erdőhelyi et al., 2006, and Jacobs et al. 2007). Among the noble metals, Rh was found to be the most active, while Ni, Co and Cu showed good activity amongst the non-precious metals. Rh has shown good catalytic activity toward ethanol conversion and hydrogen production due its capability to promote C-C bond dissociation and rupture activity (Sheng et al., 2002, Idriss, 2004; Kugai et al., 2005; Liberatori et al 2007). Liguras et al. (2003) focused on the noble catalysts Rh, Ru, Pt and Pt supported on γ-Al_2O_3, MgO and TiO_2. They also found that among the noble metal catalysts, Rh was the most active, and also

highly selective toward hydrogen production. The activity of Ru was comparable to that of Rh but required 5 times its loading. However, the performance of the noble catalysts tested was highly dependent on catalyst loading and on the support. Liguras et al. (2003) also showed that Rh/MgO was the best catalyst in term of stability and activity at 700°C. However, the drawback for using noble metals is their high cost.

Nickel

Nickel-based catalysts have been studied extensively in relation to ESR. Nickel is relatively low cost, and is widely used in the hydrogenation and steam reforming of hydrocarbons. There are several research groups that focused on just nickel over various supports [e.g., on La_2O_3, γ-Al_2O_3, YSZ, MgO by Fatsikostas et al. (2002); Y_2O_3, La_2O_3, γ-Al_2O_3 by Sun et al. (2005); γ-Al_2O_3, α-Al_2O_3 by Alberton et al. (2007); TiO_2, ZnO, Al_2O_3, Al_2O_3-Fe_2O_3 by Denis et al. (2008); ZrO_2, YSZ and (calcium stabilized zirconia) CaSZ by Bellido and Assaf (2007)]. Generally, the results show that the best nickel catalyst performance is highly dependent on the support and temperature. Fatsikostas et al. (2002) showed that the selectivity of H_2 was in the order of Ni/La_2O_3 ≈ Ni/YSZ > Ni/γ-Al_2O_3 > Ni/Mg, but the selectivity of CO after 20 hour was in the order of Ni/γ-Al_2O_3 ≈ Ni/La_2O_3 > Ni/MgO > Ni/YSZ. Sun et al. (2005) showed that the overall performance of nickel catalyst on a number of supports was better in the order of Ni/La_2O_3 > Ni/Y_2O_3 > Ni/γ-Al_2O_3. An interesting result about nickel is that it has similar capability as Rh in terms of C-C bond association and C-C bond rupture in ethanol steam reforming, but requires higher temperatures compared to Rh (Kugai et al., 2005; Coleman, 2008). Nickel catalysts are active at high temperatures, above 600°C at which point they become effective for ESR toward the main reaction products H_2, CO, CO_2 and CH_4 (Fatsikostas et al., 2002; Fatsikostas and Verykios, 2004; Benito et al. 2005; Coleman 2008). Liberatori et al. (2007) suggested that nickel (Ni^o) would oxidize to NiO below 480°C, then it would return and sustain its metallic phase of Ni^o in the ESR at temperature above 480°C. Liberatori et al. (2007) also proposed a reaction mechanism toward syngas production over nickel catalyst depending on the temperature as shown in Figure 2-11.

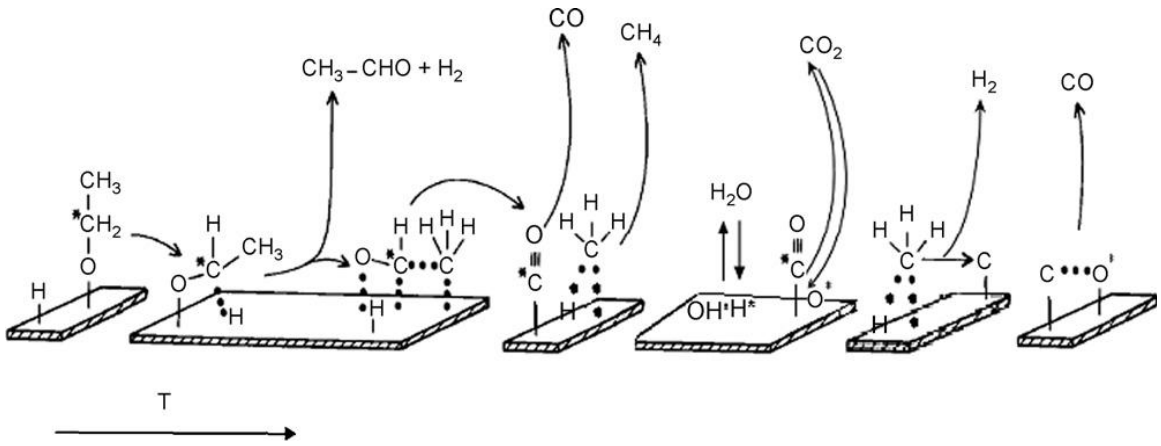

Figure 2-11: Proposed route for ESR on nickel supported metal oxide surface (Adapted from Liberatori et al. (2007)).

Cobalt

Supported cobalt catalysts have also been studied extensively for ESR reactions. Cobalt has the capability to promote C-C bond rupture at temperatures as low as 400°C (Llorca et al., 2002). Haga et al. (1996a) found that cobalt catalyst was the most active catalyst toward H_2 production at 400°C among a number of transition metals (Ti, Zr, Cr, Mn, Fe, Co, Ni, Cu, Zn, Cd, Sb, Ru, Pt, and Rh) supported on γ-Al_2O_3. Haga et al. (1997b) continued their studies with focusing on cobalt on various supports at 400°C (γ-Al_2O_3, SiO_2, ZrO_2, MgO and activated carbon). They found that the role of support was also significant. They suggested that the main reaction pathway for Co/SiO_2, Co/MgO and Co/ZrO was the reaction of ethanol reforming accompanied by the methanation of CO, while on Co/C it was mainly via the decomposition of ethanol toward H_2, CH_4, and CO. They also observed that the formation of hydrogen decreased in the following order: Co/γ-Al_2O_3 > Co/ZrO > Co/MgO > Co/SiO_2 > Co/C. Therefore, it was concluded that the nature of support highly affected the performance of cobalt catalyst. For catalyst stability, Freni et al. (2003) studied Ni, Rh, Pd, Pt and Co supported on MgO. They found that Co/MgO was the second highest in terms of coke formation after Pd/MgO, and that it was active towards the dehydrogenation of ethanol. Freni et al. (2004) also reported that Co on supported MgO catalyst was easily deactivated due to the oxidation of Co in the presence of excess water.

The phase of cobalt under reaction conditions plays an important role in overall catalyst activity, selectivity and product distribution. Bastita et al. (2003) indicated that the phases Co_3O_4 and CoO_x interacting with Al_2O_3 or MgO were not active. Once the cobalt oxide catalysts were reduced to metallic cobalt (Co°), the activity for all the catalysts increased giving ethanol

conversions higher than 90%, and promoting only small amounts (~1%) of acetaldehyde, ethyl ether, acetone and ethyl acetate at 400°C. Llorca et al. (2002) studied cobalt on various supports (MgO, Al_2O_3, SiO_2, TiO, V_2O_5, ZnO, La_2O_3, Ce_2O and Sm_2O_3) for the conditions with and without reduction of the catalyst on the ethanol steam reforming. They found that each catalyst showed phase transformation from CoO to Co° or vice versa. Interesting studies of the cobalt phase transformation during the ESR reaction was carried out in-situ by De La Peña O'Shea et al. (2006) using a XRD. They found the phase Co_3O_4 to be stable up to 275°C, and that it promoted the dehydrogenation of ethanol to acetaldehyde. Co_3O_4 then transformed to a mix of Co_3O_4-CoO in the range of 300-375°C, and formed CoO-Co° under a flowing ethanol/water (1:6 ratio) vapour mixture. At a temperature above 375°C, the catalyst became active and selective for the ESR with only CH_4 as a by-product.

The active phase metal dispersion on the support is important in determining the catalyst activity. Song et al. (2007) conducted H_2 chemisorptions over 10 wt.% cobalt on supported γ-Al_2O_3, TiO_2 and ZrO_2. They found that the ethanol conversion and H_2 yield were parallel with cobalt dispersion. The cobalt dispersion was highest on ZrO_2, followed by γ-Al_2O_3, and TiO_2.

Other active metals

At low temperatures, copper has received attention as a good candidate by several groups. The activity of copper catalysts on the ESR is reported for temperatures as low as 200°C (Marino et al., 1998, 2001; Nishiguchi et al., 2005; Chladek 2007). Copper is good for dehydrogenation of ethanol because of its high ability to maintain the C-C bond (Chang et al., 2006, Chladek, 2007). Also, it is a catalyst for the WGS (water gas shift reaction) reaction (Mariňo et al., 2001). Since the dehydrogenation and reforming of ethanol are endothermic reactions, and thus are favoured at high temperatures, low ethanol conversions were mostly observed at low temperatures with copper. Over copper catalysts, the main reaction products that are usually reported at temperatures below 300°C are H_2, acetaldehyde, acetone and CO_2 (Mariňo et al. 1998; Nishiguchi et al. 2005). Nishiguchi et al. (2005) also reported that another reaction pathway proceeds to produce a significant amount of C_2 species such as diethyl ether, ethylene, acetic acid, acetal, methyl ethyl ketone (MEK). In addition, the activity of copper catalysts easily deteriorate due to sintering at high temperatures because it has a low Hüttig temperature or empirical temperature of 177-400°C, at which copper particles begin to move and aggregate on the support (Tu and Chen, 1998;

Chlaldek, 2007). Therefore, most of the copper catalysts reported in the ESR are combined with another metal such as nickel.

Combinations of Active Metals

Combining two or more active phase metals has shown an improvement on the activity in the ESR at atmospheric pressure. Lately, there has been a significant growth of research on complex catalysts for ESR. Each individual catalyst can promote certain reaction pathways, and becomes active at certain reaction conditions. Therefore, the advantage of having only individual catalysts has been challenged. For the bimetallic Ni/Cu catalyst, Mariňo et al. (2001) reported ethanol reforming at 300°C over Ni/Cu/K/γ-Al_2O_3. The presence of copper increased dehydrogenation to acetaldehyde and subsequently nickel played a role in the C-C bond rupture of acetaldehyde. Vizcaíno et al. (2008) who studied Cu-Ni supported on SiO_2 and γ-Al_2O_3 reported that nickel was the key for ESR toward hydrogen, while the presence of copper reduced the formation of CO and coke. Resini et al. (2008) studied bimetallic Ni-Co supported on YSZ for bio-ethanol steam reforming. They found that ethanol conversion was complete at 400°C with an H_2 selectivty of 65%. The addition of Co suppressed the reaction of dehydration and methanation. Galetti et al. (2007) reported the activity of CuCoZnAl oxide for ethanol reforming in the temperature range between 400 and 600^{o}C. The catalyst was very active with complete conversion, leading to high hydrogen selectivity (87%) and remaining stable even though sintering of the metallic particles of Cu^0 and Co^0 did occur. Other catalysts that have been studied for ethanol reforming are metal oxide forms. Detailed discussion about their activity for ethanol steam reforming is described in the support material section (section 2.2.2.2).

2.2.2.2 Support materials

In principle, the selection of a support for ESR should have several characteristics such as 1) high surface area; 2) high physical and chemical stability (e.g., resistance to attrition and sintering); 3) good selectivity, and 4) low cost. The natural properties of support materials have been found to notably contribute to activity and selectivity on the ESR. Various supports have been tested for ESR at atmospheric pressure. Haga et al. (1997) demonstrated that ethanol conversion was highly influenced by the nature of the support for cobalt supported on Al_2O_3, SiO_2, MgO, ZrO_2 or C (carbon). Not only conversion, but also product composition was also affected by the support. For example, Haga et al. (1997) found that the formation of CH_4 was high on supported carbon

mainly due to the reaction via decomposition of ethanol. However, the formation of CH_4 on the metal oxide supports was mainly by methanation.

ESR is a highly endothermic reaction. Therefore, good thermal stability in a catalyst is mandatory to adapt the reaction at high temperatures. Most of the catalyst supports that have been studied for ESR are from metal oxide groups such as Al_2O_3, ZrO_2, MgO, SiO, La_2O_3, ZnO, TiO_2, CeO_2, etc. Duprez (1992) proposed that the bifunctionality effect on the metal oxide support of the metal-support catalyst system for the steam reforming of hydrocarbons is such that the hydrocarbon (C-C, C-H bond) activates on the active metal and water (the hydroxyl (OH)) activates on the metal oxide support. Aupretre et al. (2002) also suggested that the activity of the ESR would increase as the hydroxyl (OH) mobility on the catalyst surface increases. To support their hypothesis, they studied the activity of Rh and Ni on different metal oxide supports. They observed that the activity was in the order of $1\%Rh/Ce_{0.63}Zr_{0.37}$ > $1\%Rh/12\%CeO_2$-γ-Al_2O_3 > $1\%Rh/CeO_2$ > $1\%Rh/\gamma$-Al_2O_3 and $9.7\%Rh/Ce_{0.63}Zr_{0.37}$ > $1\%Rh/CeO_2$ > $1\%Rh/12\%CeO_2$-γ-Al_2O_3> $1\%Rh/\gamma$-Al_2O_3. Meanwhile, Llorca et al. (2001) who studied the ESR over various metal oxides (MgO, Al_2O_3, V_2O_5, ZnO, La_2O_3, CeO_2 and Sm_2O_3), described the dependence of the activity of ethanol reforming on the acid, basic and redox properties of metal oxides.

γ-Al_2O_3, and V_2O_5 possess acidic properties. γ-Al_2O_3 has been extensively studied for the ESR due to its high surface area as well as its high thermal and chemical stability. The acidic properties of γ-Al_2O_3 highly promote dehydration of ethanol to ethylene. In the presence of steam, ethylene is favoured to polymerize to form coke over the catalyst as has been discussed by Dybkjaer, (1995). The low loading of active metal on the γ-Al_2O_3 leads to rapid catalyst deactivation due to the formation of coke (Bastita et al., 2003; Alberton et al., 2007). Therefore, several researchers have modified the acidic properties of γ-Al_2O_3 by adding alkali (such as K, Li, Na, Mg and etc.) to neutralize the acid sites or by combination with other metal oxides to form Al oxide alloys (Mariño et al., 2001; Navaro et al., 2005; Aupretre et al., 2005; Sánchez-Sánchez et al., 2006; Coleman, 2008, Denis et al., 2008). They reported that by modifying the chemical properties of γ-Al_2O_3 such as adding K, MgO and so on, they were capable of reducing the coke formation.

Compared to γ-Al_2O_3, α-Al_2O_3 has a low surface area, is less acidic, and has a corundum structure. α-Al_2O_3 is the most stable material of the alumina family. However, it is not popular for ESR at atmospheric pressure because of its low surface area. A comparison between γ-Al_2O_3 and

α-Al_2O_3 on the ESR was conducted by Alberton et al. 2007; they found that the activity for H_2 production over nickel on γ-Al_2O_3 was higher than on α-Al_2O_3. This was attributed to the higher dispersion of the nickel particles compared to the type of nickel crystallites deposited on α-Al_2O_3. On α-Al_2O_3, increasing nickel loading did not change the activity notably. However, compared to Ni/α-Al_2O_3, Ni/γ-Al_2O_3 showed faster deactivation due to the formation of coke.

SiO_2 (450 m^2 g^{-1}, 5 micron, Alfa Aesar®) has a higher surface area than γ-Al_2O_3 (80-120 m^2 g^{-1}, 3 micron, Alfa Aesar®) and is known for having inertness properties (Chladek, 2007). SiO_2 is a suitable support for the decomposition and the dehydrogenation of ethanol towards acetone (Nischiguchi et al. 2005) and acetaldehyde (Chladek, 2007). However, for the purpose of hydrogen production, significant coke formation over the SiO_2 catalyst were reported with Cu/Ni/SiO_2 at 600°C by Klouz et al. (2002) and at 650°C by Frusteri et al. (2004). In addition, SiO_2 is not popular at high temperatures due to its low thermal stability, which promotes active metal sintering. Basista et al. (2003) showed that there was almost no interaction of the cobalt species with the SiO_2 support prepared by the incipient wetness impregnation method and analyzed by TPR-H_2.

MgO, ZnO and CeO_2 have basic properties. Llorca (2001) showed that basic properties of MgO and ZnO favoured ethanol dehydrogenation and aldol condensation reactions. Ethanol conversion over ZnO is high because of its redox properties (Llorca et al., 2001). Freni et al. (2003) and Batista et al. (2003) reported less coke formation over Ni/MgO and Co/MgO compared to γ-Al_2O_3 supported catalysts. They concluded that the presence of MgO in the support might reduce the dehydration of ethanol. Another interesting material for acting as a catalyst support is CeO_2, which has the capacity to temporarily store oxygen on its surface. The presence of oxygen is believed to play a role in increasing resistance to coke formation on the catalyst (Vaidya et al., 2006). Also, CeO_2 has the ability to promote CO oxidation and water gas shift reactions (Diagne et al., 2002).

ZrO_2, Y_2O_3 and La_2O_3 all have weak acidic and basic properties; in addition they are also chemically stable. Several reports show that La_2O_3 is suitable for ethanol reforming, even at high temperatures (Fatsikostas et al. 2002; Sun et al., 2004, Sánchez-Sánchez et al., 2007). Fatsikostas et al. (2002) reported that the advantage of La_2O_3 for ESR is due to its capability to react with CO_2 to form lanthanum oxycarbonate ($La_2O_2CO_3$) under the prevalent reaction conditions. Then, $La_2O_3CO_3$ reacts with the adjacent carbon forming over the nickel particles' surface, which leads to cleaning the possible coke off the catalyst. Instead of La_2O_3, Sun et al. (2004), also reported that

Y_2O_3 supported nickel was also a promising catalyst support, which has shown long-term stability without any signs of deactivation at moderate temperature of around 400°C. Several active metals supported on ZrO_2 have been reported for ethanol steam reforming (Breen et al., 2002; Benito et al., 2007; Song et al., 2007). Song et al. (2007) showed that ZrO_2 could provide high metal dispersion for cobalt compared to γ-Al_2O_3 or TiO_2. Instead of high catalytic activity and stability, nickel- and cobalt-supported ZrO_2 did not form any by-products at 700°C (Benito et al, 2007). The addition of certain quantities of additives such as CaO, MgO and Y_2O_3 to ZrO_2 formulate its structure to become highly chemically and thermally stable. There are two group of YSZ. Partially stabilized zirconia containing 3-4 mol% (5.4-7.1 wt%) of Y_2O_3, and fully stabilized zirconia containing 8 mol% (13.75 wt%) of Y_2O_3, respectively. Bellido and Assaf (2007) showed that nickel supported on YSZ is capable of increasing the selectivity of hydrogen and CO_2 due to an increase in oxygen ionic mobility compared to the nickel supported ZrO_2. However, this report is not in agreement with the results on YSZ without active metal, as reported by Resini et al. (2008). They found that ethanol conversion over YSZ began at a temperature above 377°C and was complete at 680°C. The reaction products were quite surprising: even though both of Y_2O_3 and ZrO_2 are weakly acidic, the reaction products were mainly C_2H_4, with significant amounts of CH_4 and CO_2. They concluded that ethanol dehydration was the main reaction promoted by YSZ. However, they also reported that the presence of nickel and cobalt on YSZ had a positive effect on the ethanol conversion and hydrogen production.

2.2.2.3 Effect of catalyst preparation

The catalyst preparation method (precipitation, impregnation, sol gel, etc.), type of precursor, calcination, and reduction also have an impact on the catalyst activity. Haga et al. (1997) suggested that the product composition of ESR were varied due to the crystallite size of Co/γ-Al_2O_3 for ethanol steam reforming. They found that the activity of the catalysts was independent from the starting precursor during preparation. However, Aupretre et al. (2004, 2005) reported that the catalyst activity depended on the type of metal precursor, for example the catalyst prepared from metal chloride solution was more active compared to that from acetate solution for Rh/γ-Al_2O_3 and Mg/Ni/Al_2O_3. The effect of catalyst preparation over product composition was also reported by Kaddouri and Mazzocchia (2004) on Co/SiO_2 and Co/γ-Al_2O_3, which was prepared by incipient wetness, sol-gel and a combination of both. They showed that the combination method provided better catalytic performance toward hydrogen production over Co/SiO_2 catalyst.

However, impregnation was the most popular method that has been used to prepare catalysts for ESR at atmospheric pressure.

2.2.2.4 Effect of reaction conditions

The reaction parameters that are commonly studied in the catalytic ethanol steam reforming are temperature, pressure, ethanol to steam ratio or ethanol concentration, and contact time or residence time.

These reaction parameters were found to have an important effect on conversion, yield and selectivity of hydrogen, and other product compositions. Temperature is the most important parameter that will determine conversion, selectivity, yield and catalytic stability. All of the work on ESR reported in the literature covered the effect of temperature which was in the range starting from as low as 100°C (Nishigushi et al., 2008) to as high as 850°C (Liguras et al., 2003). Increasing temperature typically increases ethanol conversion, hydrogen selectivity, and promotes reactions that converts C_2 species (e.g., ethanol, acetaldehyde) to C_1 species (CO, CO_2, CH_4) as shown in Figure 2-12.

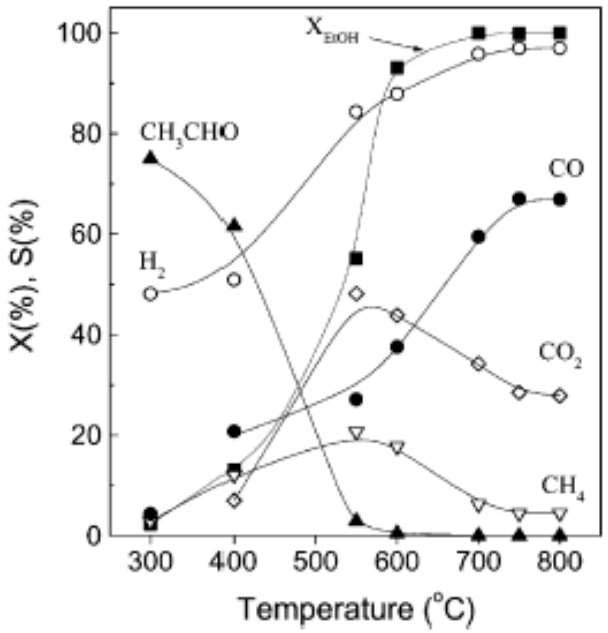

Figure 2-12: Effect of temperature on the ethanol conversion (X (%) and the product selectivity (S (%)) over 17 wt.% Ni/La_2O_3 at atmospheric pressure (Adapted from Fatsikostas et al., 2002).

Thus far, almost all of the reports on ethanol steam reforming were carried out at atmosphere pressure and only a few researchers presented results at moderate pressures. From these few studies, it seems that increasing the pressure up to 11 bar has a negative effect on hydrogen yield, while having a positive effect on ethanol conversion. Aupretre et al. (2005) observed that the catalyst activity of $Rh/Mg_xNi_{1-x}Al_2O_3$ increased with increasing pressure (with the consequence of increasing the residence time) from 1 to 11.1 bar (0.1 MPa to 1.1) at 700°C, but did not have as much of an advantage in terms of product composition, where H_2 yield decreased and CH_4 yield increased. Coleman (2008) also reported a similar pattern for the conversion of ethanol, the yield of H_2 and CH_4 at 400°C and 600°C over Ni/Mg-Al mixed oxide when increasing pressure from 1 to 5 bar (0.1 MPa to 0.5 MPa).

Contact time is usually used for the reporting of space time (GHSV, LHSV, or $W_{catalyst}/F_{inlet}$) for a fixed bed reactor. However, some reports used residence time instead, when considering a reactor volume ($Vol._{reactor}/F_{inlet}$). All studies that considered the effect of contact time agree that increasing contact time increases ethanol conversion (Haga et al., 1997b; Fatsikostas et al., 2002; Vellu et al., 2002;, Cavallaro et al., 2003; Benito et al., 2005). Figure 2-13 shows a typical example of the effect of contact time on the catalytic performance for ESR. Not only has the ethanol conversion been affected, but also the product composition as well. When the reactants or intermediate products are given enough time of contact with the catalyst, the reactions could proceed to consecutive reactions as discussed in the sections 2.2.1 and 2.2.2.1.

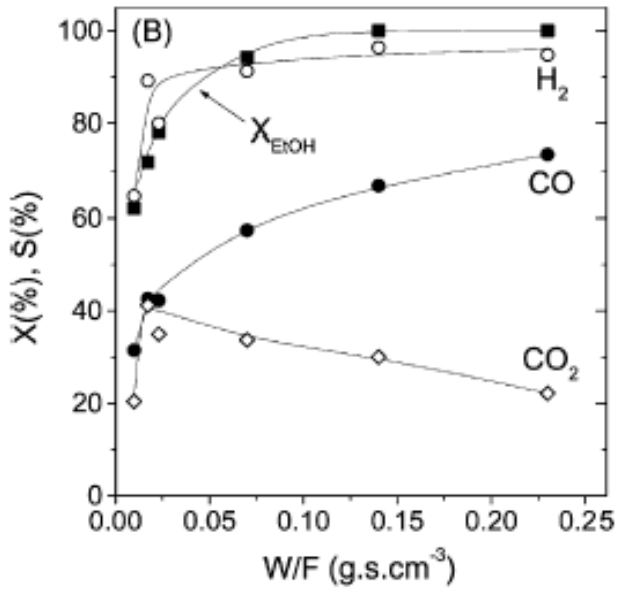

Figure 2-13: Effect of contact time (*W*/*F*) on the ethanol conversion (X(%)) and the product selectivities (S(%)) over the Ni/La_2O_3-Al_2O_3 catalyst at 750 ◦C at atmospheric pressure (Adapted from Fatsiskostas et al., 2002)

Increasing the ratio of water to ethanol resulted in an increase in the selectivity toward the desirable products H_2 and CO_2 and a decrease in the undesirable products such as CH_4, CO and coke (Klouz et al., 2002; Cavallaro et al., 2003a, 2003b; Yang et al., 2006).

Chapter 3

Experimental Section

This chapter presents the catalyst preparation and characterization, the experimental procedure, and the analytical system used to evaluate the catalytic ethanol water reforming reaction in supercritical water. Description of the criteria to determine the catalyst performance is also given at the end of this chapter.

3.1 Catalyst preparation

The wet impregnation method was used to prepare the catalysts. To prepare 10% wt. Co/YSZ, 15.00 g of YSZ was added to 250 mL of heated de-ionized water while being stirred. To obtain a metal loading of 10% wt. cobalt on the support, 8.2307g of $Co.(NO_3).6H_2O$ crystal (Alfa Aesar Co.,) was slowly added to the stirred YSZ solution for 5 hours. The solution was stirred and heated at 90°C until it becomes very thick and paste-like. The paste was then dried overnight at 110°C in an oven. The dry paste was calcined at 550°C for 3 hours, crushed and filtered on two layers of 35 mesh (1.0 mm) and 34 mm (1.4 mm) sieves. Other catalysts such as 10% wt. Ni/γ-Al_2O_3, 10% wt. Co/α-Al_2O_3 and so on, were prepared using a similar procedure as that described for Co/YSZ.

3.2 Catalyst characterization

Catalyst characterization was carried out to identify catalytic properties such as bulk metal loading, total surface area, crystalline phase and oxidation state, and phase transformation. Table 3-1 illustrates the techniques that were used to characterize the catalyst properties. The following sections give more details about the characterizations that were used.

Table 3-1 Characterization techniques

Property	Technique
Surface area and pore volume	Brunauer-Emmett-Teller (BET) Nitrogen physisorption
Bulk metal loading	Inductive Couple Plasma-Atomic Emission spectroscopy (ICP-AES)
Phase transformation	Powder X-ray Diffraction (XRD)
Catalyst Reducibility	Temperature-programmed reduction of H_2
Acid and basic site density	Temperature-programmed desorption (TPD) of NH_3 and CO_2
Surface topography	Scanning electron microscopy (SEM)

3.2.1 Surface area and pore volume analysis

BET nitrogen physisorption method is the most common method of measuring surface area and pore volume in catalysis. The BET method yields the total surface area of support and active metal. A Micromeritics adsorption surface analyzer (Gemini™ V-Series) with ultra pure nitrogen (99.995% N_2, from Praxair) as the adsorbate was used. Prior to analysis, each catalyst sample was evacuated at 300°C in nitrogen for 1 hour to ensure that there was no adsorbed moisture and atmospheric gases such as CO_2 on the catalyst surface. The adsorption and desorption isotherms in the evaluation of BET surface were obtained at the boiling temperature of liquid nitrogen (-195°C). Eleven points were collected in spanning of the pressure ratio (P/Po) from 0.05 to 0.3. Measurement in this range of pressure ratio corresponds to a linear region suitable for the BET equation (see equation (3-1)). This equation assumes monolayer capacity of absorbate on the material surface. Fresh and spent catalysts that had been exposed to ethanol water reforming and to pure water were measured.

$$\frac{P}{(p_o - p)V} = \frac{1}{cV_m} + \frac{(c-1)p}{cV_m p_o} \qquad (3\text{-}1)$$

where,

V = volume of gas adsorbed at pressure p

V_m = volume of gas adsorbed in monolayer

p = gas pressure

p_o = saturation pressure of adsorbed gas

c = a constant related exponentially to the heats of adsorption and liquefaction of the gas

3.2.2 Temperature Programmed (TP) Unit

The reducibility of the catalysts and the acidity/basidity of the catalyst supports were carried out using an in-house built temperature programmed unit, as shown in Figure 3-1.

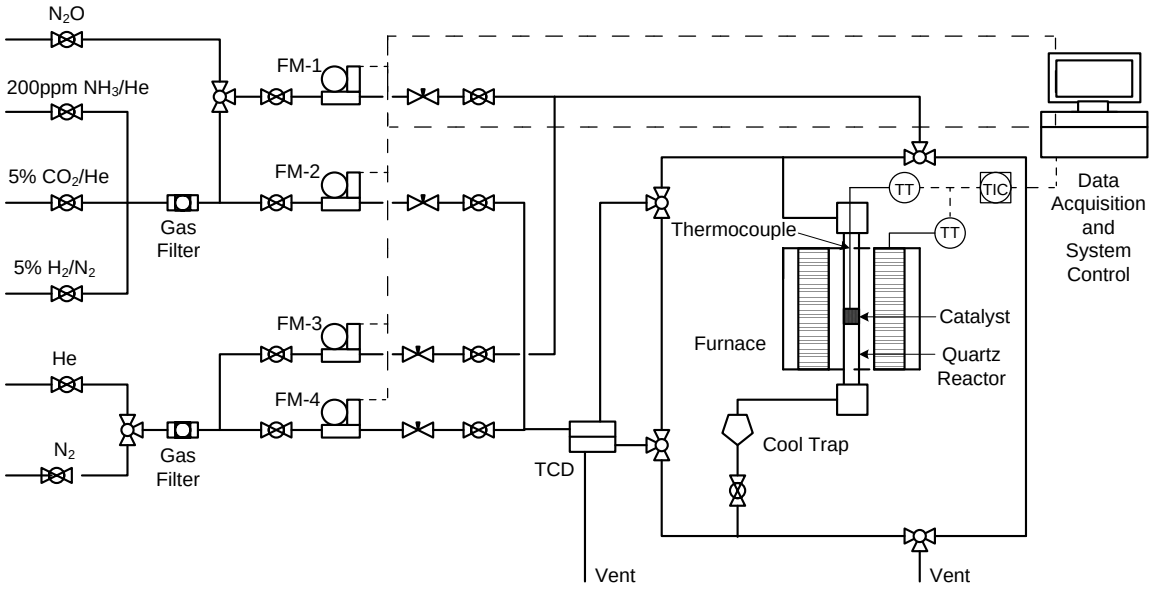

Figure 3-1: Schematic of temperature programmed reduction (TPR) and TPD testing unit.

TPD-H_2:

Temperature programmed reduction (TPR) is used to characterize the reducibility of the catalyst. For TPR-H_2, 50 mg of calcined catalyst (1-1.4 mm of the particles size) at 550°C was used in a quartz fixed-bed microreactor (4 mm I.D., 40 cm length). The sample was purged with N_2 for 30 minutes. Then, the temperature was ramped from 25 to 800°C at a rate of 5°C/min in 5 v/v.% H_2/N_2 mixture. The gas leaving the reactor is cooled down in a cold trap to remove water from the gas stream prior to being analyzed by a thermal conductivity detector (TCD). The rate of hydrogen consumed is measured as the temperature increases. A plot of the rate provides the

reducibility temperature, the amount of hydrogen consumed and the type of the metal-support strength.

TPD-NH_3 and –CO_2:

The acidic and base properties of the catalyst supports were compared using TPD-NH_3 and TPD-CO_2, respectively. These chemisorption characterization techniques are based on the strength of the bond between probe gas, or absorbate, and substrate surface. The strength of the acidic and the basic sites are categorized into weak, moderate and strong site types, which are referred to the desorption rate as a function of temperature. To perform acidity characterization, 0.5 gram of catalyst sample is placed in a 10 mm ID quartz reactor and then pre-treated in flowing 50 mL/min helium at 550°C for 1 hour. The catalyst is then cooled to 100°C while flowing helium. The helium stream is replaced by a stream of 200 ppm NH_3/He for 2 hours at 100°C. Excess of NH_3/He over the surface substrate was purged with 50 mL/min of helium for 1 hour. Then the temperature was ramped from 100°C to 800°C at a rate of 15 °C/min. The rate of desorption of NH_3 from the catalyst is measured by a thermal conductivity detector (TCD). For the basic sites, 5% (vol.) CO_2/He was used in a similar procedure as that with NH_3/He. A plot of the rate the CO_2/NH_3 provide information about the strength of chemisorption on the surface material. To differentiate the sites of different basic/acid strengths, deconvolution using a modified Gaussian method is applied. The strength of the acidic and the basic sites are categorized into weak, moderate and strong site types, depending on the specified temperature range. The built-in Half-Gaussian Modified Gaussian method in Peakfit V4.12® is used, as shown in equation (3-2).

Half-Gaussian Modified Gaussian

$$y = \frac{a_0 \exp\left(\frac{1}{2}\frac{x-a_1}{a_3^2+a_2^2}^2\right)\left(1+erf\left(\frac{a_3\ x-a_1}{\sqrt{2}a_2\sqrt{a_3^2+a_2^2}}\right)\right)}{\sqrt{2\pi}\sqrt{a_3^2+a_2^2}} \qquad (3\text{-}2)$$

where, a_0 is area, a_1 is center, a_2 is width (>0), and a_3 is distortion (≠0) of peaks.

3.2.3 ICP-AES: Active metal catalyst loading

Inductive couple plasma-atomic emission spectroscopy (ICP-AES) was used to confirm the content of cobalt and nickel. Prior to ICP analyzsis, the catalysts must be digested and diluted in a matrix acid. All of the catalyst supports in this study were made of either zirconia or alumina; both are thermally and chemically stable materials. For these materials, microwave acid digestion was preferred in the literature. Acid digestion was done in a 23 mL Parr digestion bomb and placed in a domestic commercial microwave (Panasonic Inverter NN-S533, 1200W®). Prior to the actual digestion in the microwave, the actual microwave power delivered was measured by using a method suggested by Kingston and Jassie (1988). The procedure to measure the power delivered and the data plot of the actual power delivered as a function of setting power level are given Appendix A. For a 23-ml Parr digester bomb, 0.05 g of catalyst (eg. Co/YSZ, Ni/ZrO_2 or etc.) with particles size less than 100 mesh were placed in the microwave for 3 minutes at 400 W. The catalysts were digested in different mixtures of acids, depending on their support, as indicated in Table 3-2. The resulting digestion solution was diluted in 100 mL flask with ultra-high purity deionised water (Milii-Q processing water) to obtain a total metal ion concentration of approximately 500 ppm. For example, to determine the amount of cobalt, the ion of Cobalt in solution was diluted again in 100 mL of dionized water to obtain around 50 ppm and measured using ICP-AES.

Table 3-2: Acid mixtures for ICP digestion as a function of the support

	Alumina support	**ZrO_2 support**	**YSZ support**
85 wt.% Hydrofluoric acid (H_3PO_4)	3 mL	3 mL	3 mL
98 wt.% Sulphuric acid (H_2SO_4)	3 mL	3 mL	2 mL
48 wt.% Tertafluoroboric acid (H_3BF)	2 mL	-	-
40 wt.% Hydrofluoric acid (HBF_4)	-	2 mL	3 mL
37 wt.% Hydrochloric acid (HCl)	0.5 mL	0.5 mL	0.5 mL

3.2.4 XRD: Phase identification and crystal size

Powder X-ray diffraction was used to obtain information about the crystalline phase by means of lattice structural parameters, and to estimate particle size. The X-ray powder diffraction (XRD) measurements were carried out using a Bruker AXS D8 Advance X-ray Diffractometer, with 2.2 kW copper (Cu) X-ray source. Crystal planes were identified by using the Bragg relation (equation (3-3)):

$$n\lambda = 2d\sin\theta; \quad n = 1, 2, 3, ... \tag{3-3}$$

where n is an integer called the reflection, λ is the wavelength of the X-rays, d is the distance between two lattice planes, and θ is the angle between the incoming X-rays and the normal to reflecting lattice plane. In addition, the crystal size of the powder sample was measured from the X-ray broadening by using the Scherrer equation (3-4) (Innes, 1968);

$$d = \frac{0.089\lambda}{B(2\theta)\cos\theta} \tag{3-4}$$

where $B(2\theta)$ is the width of the XRD pattern line at half peak-height (rad), λ the wavelength of the X-ray, θ the angle between the incident and diffracted beams (◦), and d the crystal size of the powder sample (nm).

3.2.5 Scanning Electron Microscopy (SEM)

The SEM is capable of producing very high-resolution images of a sample surface, capable to show details of nanometer in size. Surface topography and morphology were captured by using a SEM, model LEO FESEM 1530 (Zeiss Inc). All images were captured using a Robinson Back Scattering Detector (RBSD).

3.3 Supercritical water reactor setup

Catalytic ethanol water reforming in SCW was performed in a modified process system that was originally designed by Thar Design for supercritical water oxidation. Figure 3-2 presents the diagram of the experimental setup.

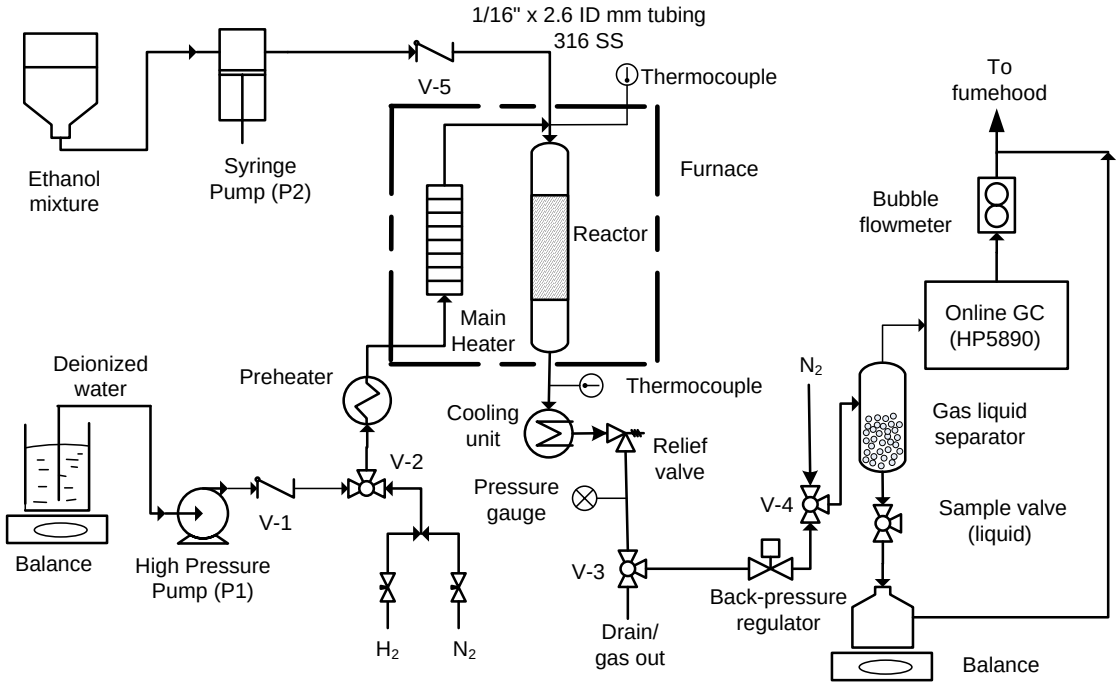

Figure 3-2: **Supercritical water ethanol reforming experimental setup**

The setup is divided into four major sub-sytems: reactant feed/pump, heating coil/reactor/ furnace, cooling system/backpressure regulator/gas liquid product separation, and analysis.

3.3.1 Overall description of the process flow

Water was delivered to a pre-heater at a set flow rate between 1 and 3 g/min by a high-pressure pump. The deionised water feed was placed on a balance in order to monitor the actual mass flow rate. The temperature of the pre-heater was set at 200°C. The water feed was then further heated to the desired reaction temperature in a ¼" coil of 16-ft long ("Main heater" in Figure 3-2) made of Hastelloy tube prior to entering the reactor. The main heater and the reactor are both located in a furnace. Ethanol water mixture with composition of 75% wt. ethanol was injected through a 1/16" 316 SS tubing with 0.26 mm ID by a high precision syringe pump, model

260D ISCO™. The ethanol mixture then mixes with the heated distilled water in a cross above the reactor. The reactant fluid flows downward through the reactor and enters the catalyst bed. The connection between the cross and the reactor is connected by a 1/4" × 1/16" ID with 5 cm long Hastelloy tubing. Figure 3-3 shows the connection and the position of the main heating coil, cross, thermocouple and reactor inside the furnace.

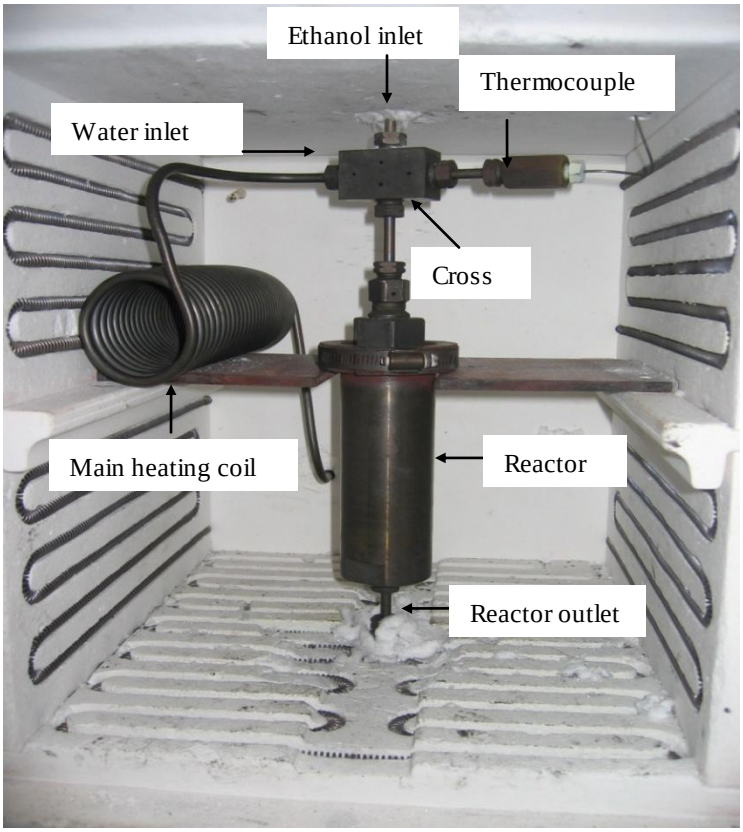

Figure 3-3: Photograph of the reactor/feeding assembly located inside the furnace.

The product stream exiting the reactor and furnace was cooled to 10°C through a heat exchanger before entering the backpressure regulator (BPR) where the pressure was decreased from the reaction pressure (typically 25 MPa) to atmospheric pressure. For safety, a relief valve was located between the cooler and the backpressure regulator. If the pressure exceeds ca. 40 MPa, the relief valve opens automatically. A pressure gauge was also located between the relief valve and the BPR for visual monitoring. The fluid flow exiting the BPR was sometimes unstable because the BPR operates like an on-off valve. The flow instability depends on the stream flowrate and on the amount of gas present. Recall that before the BPR water was in the liquid form and thus the higher the amount of gas present, the better the flow stability. Therefore, 8 mL/min of nitrogen

was supplied at the tri-way valve (V-4 in Figure 3-2), not only to help stabilizing the BPR, but also as an internal standard for the online gas analysis.

The condensable species were separated from the gaseous species in a gas liquid separator. The gaseous product stream exits the separator unit at its top and was directed either to the GC or to a soap bubble flowmeter for composition and flow rate analysis, respectively. At flowrates higher than 200 mL/min, a digital mass flowmeter was used instead of the bubble flowmeter. The liquid collected at the bottom of the separator, was periodically sampled for further analysis. The liquid flowrate was measured by a balance and then was recorded in the computer while the GC was doing its analysis. The pre-heater, and pumps, are controlled using ICM software (Thar Technologies) via a computer. The temperature of the fluid at the outlet of the pre-heater, cooling unit, inlet and outlet of the reactor were also monitored.

Liquid reactant feed delivery system

The water feed was stored in a flask and weighted using a balance model Scout Pro II (Ohous Inc.). The balance was used to measure the water mass flowrate by computing the rate of weight loss versus time. The pump 1 has check valves at the inlet and outlet of the pump head to ensure one-way flow. The pump was able to deliver a flow rate in the range of 1 to 30 g/min. It was frequently observed that the mass flowrate at the setting panel results in a somewhat different flowrate than the actual one (5 to 15% difference). This was why the actual feed flowrate was monitored and recorded using a balance. Meanwhile, ethanol was fed via pump 2, which contain 25% wt. water. Pump 2, ISCO™ model 260D has a high precision delivery value, (correlation coefficient, R^2=0.99) in the range of the required flowrate. Ethanol feed was injected into the cross by a 1/16" 316SS 0.26 mm ID tube. This small inside diameter tubing was designed to maximize its velocity at the injection point in order to minimize possible ethanol cracking before reaching the catalyst bed. For example a 0.153 mL/min feed corresponds to a velocity of 4.8 cm/s. For the experiments that require in-situ reduction, 10 mL/min of hydrogen was mixed with 40 mL/min of nitrogen to yield 20% v/v hydrogen. Note that the reduction was done at atmospheric pressure prior to the actual experiment began. The flow rates of these gases were adjusted by using two digital mass controllers.

Preheater, main heater, reactor and furnace

An electrically heated high pressure preheater model HE designed by Thar Technologies, consisting of 20 ft long and 1/8 inch × 0.02" thickness 316 SS tube was controlled by a six zone

PID temperature controller (CN616 Series, Omega Engineering Inc.). The water was preheated up to 200°C and the temperature was measured at the outlet of the preheater using a J-type thermocouple.

The main heating coiler and the reactor is located in an Isotemp® Muffle furnaces (550 series, Fisher Scientific Inc.,), which has a volume of 2016 in (12" x 14" x 12"). This model features a digital proportional controller and requires setting the temperature at its control panel manually. The furnace can operate at a temperature up to 1125°C. However, the maximum temperature is at 650°C, which is the maximum working temperature of the reactor at 31 MPa. To measure the reactant temperature entering the reactor, a 1/16" type J thermocouple was inserted in the cross above the reactor, where ethanol and water mix up. The temperature difference between the set furnace temperature and the thermocouple reading was typically about 4 ± 1°C below the set value. It was thus concluded that the ethanol injection system was satisfactory and was not affecting significantly the temperature of the mixture before the reactor bed. The main heating coil was made of ¼-inch tube Hastelloy, 19 ft long. Hastelloy-C276 was chosen because of its strength and ability to handle the corrosive environment of the sub- and supercritical water. The coil was obtained from Autoclave Engineers as well. All tubing and fitting outside the furnace are made of stainless steel.

Reactor

A special vessel/reactor was designed to carry out experiments for catalytic reactions in a fixed bed reactor. The reactor (Kuentzel closure pressure vessel), made of Inconel-625 was fabricated by Autoclave Engineers. It has been certified by Autoclave Engineers and the Technical Standards and Safety Authority in Canada (TSSA). Inconel-625 is able to handle extreme conditions such as oxidation reaction in the sub- and supercritical water. The maximum working temperature allowable of the reactor is 650°C at 31 MPa. The catalyst was located in the middle of the reactor supported by a 100 mesh 316 SS wire screen. A 10-mm stainless steel tube with 12.7 mm OD and 2 mm thickness was placed to support the screen. Another 100 mesh SS screen was placed above the catalyst to avoid particle especially from an anti-size lubricant compound that might mix with catalyst bed during opening the reactor. The temperature of the water/reactant entering the reactor was measured by a type J thermocouple at the cross. The catalyst bed was placed in the reactor and consisted of 1.00 g catalyst in the particle range of 1.0 to 1.4 mm Figure 3-4 shows the schematic diagram of the vessel with the catalyst bed.

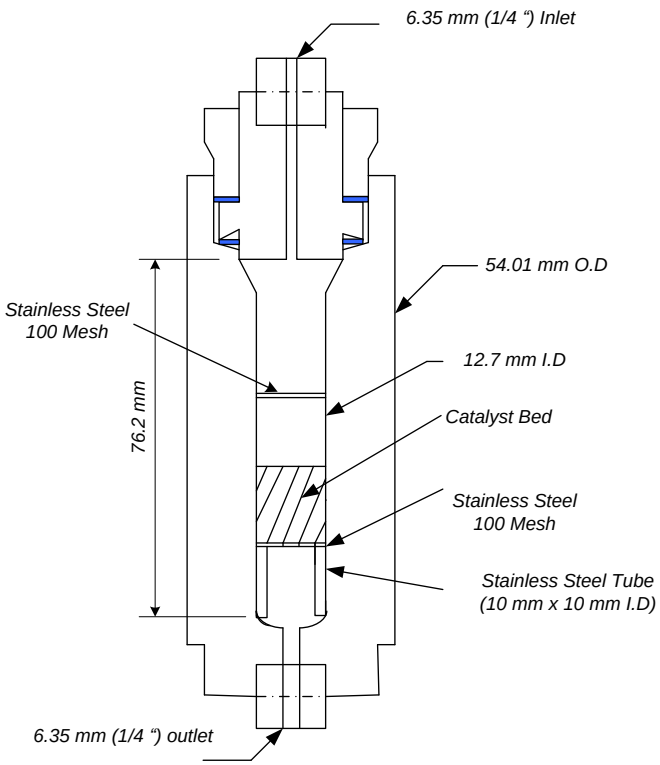

Figure 3-4: Schematic diagram of the reactor.

Cooling system

The product stream exiting the reactor housed in the furnace is cooled down in a heat exchanger designed by Thar Technologies. This system consists of a 20 ft long 1/8 inch 316 stainless steel tube housed in a PVC vessel. The rapid cooling from reaction temperature to 10°C prevents the fluid from remaining in subcritical conditions for a long period. The heat of the product stream is removed by 30% v/v ethylene glycol supplied from a circulating bath model 910-TH type refrigeration/heat (PolyScience Inc). The circulating bath is maintained at 10°C in order to condense all condensable species such as ethanol, acetaldehyde, acetone and water. Note that, another reason is to prevent acetaldehyde form partially vaporizing (its boiling temperature is 21°C) which would render the determination of acetaldehyde composition difficult and inaccurate.

Back-pressure regulator

The pressure of the system was controlled using a back-pressure regulator, model BPR-A 200B (Thar Technologies Inc) via a hand-held controller unit. This back-pressure regulator is able to adjust the pressure by pushing or drawing a needle into a seat during the experiment or even at

the high pressure condition. The back-pressure regulator consists of a motor-driven heated valve assembly controlled by a microcontroller. A strength stainless steel needle resistant to corrosion allow stable pressure control over the range of 1 bar (gauge) to 350 bar (gauge). A built-in pressure sensor provides a closed loop feedback for pressure control. The alarm pressure is set at 350 bar. In case the back-pressure regulator malfunctions, a relief valve with a burst pressure of 420 bar located at the filter entrance will back-up the shut-down system.

Gas-liquid separator

The gas and liquid from the product stream exiting the back-pressure regulator are separated in a flash separator. The separator is made of glass with 25 mm ID × 120 mm height and ¾ filled with glass beads of average 4-mm diameter.

3.4 Analytical System

Gas and liquid were analyzed separately using two gas chromatographs (GC-1(TCD) and GC-2(FID)) model HP5890 series II, which are equipped with a thermal conductivity detector (TCD) and a flame ionization detector (FID), respectively. Chemstation Plus version A.10.02 was used to control both GCs and to analyze the chromatograms.

3.4.1 Gas analysis (GC-1)

The gas product from the separator was continuously fed to the GC equipped with an automatic sampling system and a TCD. The sample was collected in a 100-μL external sample loop positioned at a 6-port switching valve (Model A60, Valco Inc). An air actuator connected with an electrical signal from the GC was used to operate the sampling valve. The collection of the sample occurs every 40 minutes after completing the following two steps: sample analyzing (31 min), and cooling down of the GC (9 min). A 15' × 1/8" stainless steel packed bed column containing 60/80 mesh Carboxen 1000® (carbon molecular sieve particles, Supelco Inc) is used to separate the gas product generally consisting of H_2, N_2, CO, CO_2, CH_4, H_2O and eventually C_2H_4 and C_2H_6 (depending on the reaction temperature and type of catalysts used). Helium is used as a carrier gas and as a reference gas. Detailed operating conditions of the GC are given in Table 3-3. In order to elute the products in a discernable and timely manner, a temperature program was utilized as shown in Table 3-4.

Table 3-3: Operating conditions of GC-1 (TCD)

Carrier gas (Helium)	30 mL/min
Reference gas (Helium)	30 mL/min
Injection port temperature	220°C
Detector Temperature (TCD)	260°C
Detector signal	25 mV – 800 mV

Table 3-4: Temperature program of GC-1

Temperature (^{o}C)	**Rate (^{o}C/min)**	**Hold (min)**	**Total Time (min)**
35		5	5
175	20	2	14
195	10	0	16
225	20	14	31

The TCD response (peak area) of GC-1 was calibrated using custom Praxair certified standard gases, gas #1 and gas #2. Table 3-5 shows the composition of the two certified calibration gases used. In addition to the calibration gases, pure gases mixed with nitrogen were also used to do the calibration of H_2 above 30%, CO_2 and CH_4 above 8%.

Table 3-5: Composition of the custom Praxair certified standard gas

Calibration Gas # 1		**Calibration Gas #2**	
Species	**Concentration (Vol%)**	**Species**	**Concentration (Vol%)**
CO_2	30	C_2H_2	0.499
CO	30	C_2H_4	3.09
CH_4	25	C_2H_6	3.0
C_2H_4	10	N_2	93.0134
C_2H_6	5		

The nitrogen mixed with the stream at the exit of the backpressure regulator for stabilizing and determining the gas effluent flow (i.e., internal standard). The flowrate of nitrogen was set at 8 mL/min for all experiments. Therefore, the total gas product flowrate could be calculated using equation (3-5):

$$F_{Gas} = \frac{F_{N_2}}{y_{N_2}} \tag{3-5}$$

where y_{N2} is the nitrogen composition (vol/vol). Table 3-6 lists the gas calibration result of the known concentration for a specific range of concentration (vol%). The gas calibration plots can be obtained in Appendix B.

Table 3-6: Gas calibration for the gas product species

Species	y_i % (v/v)	r^2	**Range (vol%)**
N_2	$= 5\times10^{-26}PA_i^4 - 4\times10^{-19}PA_i^3 + 1\times10^{2}PA_i$	0.9985	0 - 100
H_2	$= 5\times10^{-4}PA_i$	0.9992	0-100
CO_2	$= 9.2\times10^{-6}PA_i$	0.9996	0-100
CO	$= 1\times10^{-5}PA_i$	0.9988	0-30
CH_4	$= 1\times10^{-5}PA_i$	0.9989	0-70
C_2H_4	$= 1\times10^{-5}PA_i$	0.9981	0-80
C_2H_6	$= 1\times10^{-5}PA_i$	0.9977	0-5

3.4.2 Liquid analysis (GC -2)

Each time the gas sample was automatically injected into GC-1, 2.5 mL of the liquid sample was extracted from the bottom of the separator unit using a syringe and was transferred to a 10 mL sample vial. Then, 1-mL of the liquid sample and 1 mL of 1 vol.% 1-propanol (internal standard) were immediately poured into a 10 mL volumetric flask and diluted with de-ionized water to fill up the 10 mL flask. Subsequently, 1 μL of the prepared sample was injected using a 10-μL Hamilton syringe into GC-2 equipped with FID. The prepared sample was analyzed by a capillary column of 30 m × 0.53 mm ID DB-Wax with 2 mL/min of helium as a carrier gas. Table 3-7 illustrates the operating conditions of GC-2. Even if ethanol and acetaldehyde peak appeared within 3 min, GC-2 was continuously run for an additional 4 min at 230°C to prevent an accumulation of water in the column. Table 3-8 presents the temperature program of GC-2.

Table 3-7: The operating condition of GC-2 (FID)

Carrier gas (Helium)	2 mL/min
Hydrogen	30 mL/min
Air	370 mL/min
Reference gas (Nitrogen)	30 mL/min
Injection port temperature	250 ^{o}C
Detector Temperature (FID)	300 ^{o}C
Split ratio	5
Detector signal	25 mV – 800 mV

Table 3-8: Temperature program of the GC-2

Temperature (^{o}C)	**Rate (^{o}C/min)**	**Hold (min)**	**Total Time (min)**
40		5.0	5.0
230	10.0	5.0	29.0

An internal standard of 1 vol% 1-propanol was added to each liquid sample to obtain a consistent and accurate result. Internal standards were used to compensate for the variation in the injection volume. Therefore, the FID response for each species was normalized with respect to 1-propanol. A relative response factor (RRF) was used as a basic concentration calculation, as seen in equation (3-6),

$$RRF_i = \frac{\text{Peak Area}_i}{\text{Peak Area}_{\text{1-propanol}}} \times \frac{\text{Concentration}_{\text{1-propanol}}}{\text{Concentration}_i} \tag{3-6}$$

and the concentration of species i is calculated using equation (3-7) as follows.

$$\text{Concentration}_i = \frac{\text{Concentration}_{\text{1-propanol}}}{RRF_i} \times \frac{\text{Peak Area}_i}{\text{Peak Area}_{\text{1-propanol}}} \tag{3-7}$$

It is observed from calibration data that the ratio of the peaks does vary linearly with the ratio of the concentrations. RRF can be expressed as a function of the peak area ratios, which is reported in Table 3-9. The value of RRF calculated using equation (3-6) for all species gave a constant value over the range of the liquid species concentration calibrated. Table 3-9 lists the liquid calibration results of the known concentration.

Table 3-9: RRFs for the liquid product species

Species	RRF	r^2	Range (mol/L)
Ethanol	1.9554	0.9966	0.0685-1.7127
Acetaldehyde	4.4039	0.9968	0.0447-0.5537
Acetone	1.3794	0.9981	0.0272-0.2720
Diethyl Ether	0.1103	0.9951	0.0025-0.0102

3.5 Experimental Procedure

In this experiment, especially with catalyst, the ability to control the pressure is critical. Controlling the pressure was the most important and challenging part in the catalytic ethanol water reforming since the reaction product would form two phases, gas and liquid after the cooling unit. Rapid production of gaseous species leads to pressure built up too fast, which may render the back-pressure out of control. Another important step is the heating and pressuring of the fluid to pass through the catalyst bed. There are two main paths to reach the desired reaction conditions, as shown in Figure 3-5: Following "path A", water is first heated and then compressed, whereas in "path B", water is first compressed and then heated. To minimize damage to the catalyst, it was better to avoid high-density water as the temperature increased. Following "path B" would force going through the subcritical region, characterized by high-density water at an elevated temperature. Therefore, "path A" was preferred; that is, the water was heated up slowly and subsequently compressed to be gas-like in SCW at the desired temperature and pressure. From observation, the catalyst would break if the pressure fluctuated too much, which might happen if the back-pressure regulator is not working properly. Therefore, each experiment would begin with only water at a certain pressure which is based on how much pressure would build up from ethanol conversion. Once the pressure was stable (usually approximately 20 to 30 min after pump 1 was turned on), the ethanol mixture was first injected at rate of 1 mL/min until the pressure at pump 2 was half the pressure of pump 1 in order to save time in filling up the line with ethanol. Then, the ethanol flowrate was reduced to the required flowrate. Then, the needle of the back-pressure regulator (BPR) would be adjusted accordingly by pushing or pulling to obtain the desired pressure. The BPR was controlled with a hand-held controller unit. The best way to obtain a desired pressure without problems with the BPR or catalyst breakage was to start at a low pressure and increase the pressure slowly to the desired reaction condition.

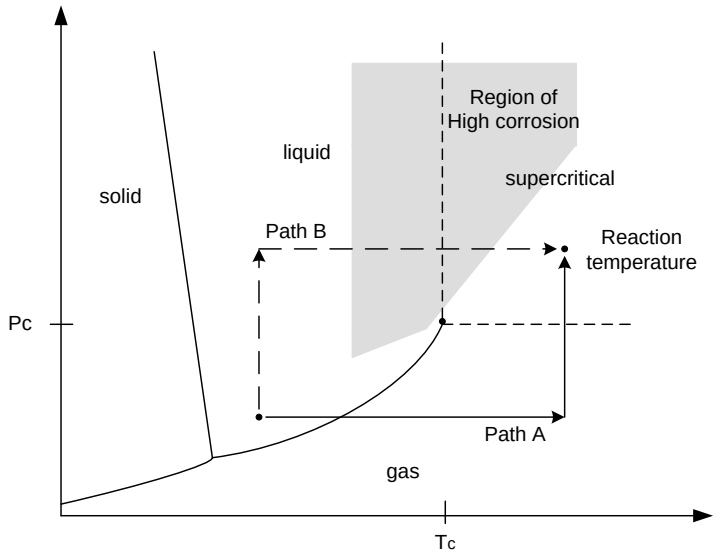

Figure 3-5 Heating up strategy (Adapted from Kritzer and Dinjus, 2001)

Once the ethanol was fed, the pressure rose up slowly. The first sample was collected after 30 min ethanol was fed. During gas analysis, the valve below the separator was closed for 10 min to ensure that the gas product would pass through the GC sample loop. While the valve was closed, the flowrate of the gases was measured using a bubble or digital flowmeter. The liquid product was collected over a defined period of time from the separator by extracting it with a syringe through a rubber septum at the bottom. The liquid flow rate was measured by the rate of weight loss using a balance model Scout Pro II (Ohous Inc.) while the sample was analyzed by the GC. Details of the step by step experimental procedure can be obtained in Appendix C.

3.6 Catalyst performance evaluation

The catalysts were evaluated for their performance based on several criteria such as ethanol conversion, product gas composition, and product selectivity. Some experiments were repeated to check the reproducibility of the results in order to minimize the uncertainty. Ethanol conversion and gas product selectivity are defined according to equations (3-8) and (3-9) respectively. The carbon balance is calculated using equation (3-10).

Ethanol conversion, X_{EtoH}:

$$X_{EtoH} = \frac{F_{EtOH,in} - F_{EtOH,out}}{F_{EtOH,in}} \tag{3-8}$$

where, $F_{EtOH,in}$ and $F_{EtOH,out}$ are the feed and outlet molar flow rate of ethanol with unit of mol/min, respectively.

Product selectivity:

$$S_i(\%) = \frac{F_i}{\sum_{i=n} F_i} \times 100 \tag{3-9}$$

where, F_i is the molar gas flow rate of product i, and $\sum_{i=n} F_i$ is the total molar flowrate of the products.

Carbon balance :

$$C_T = \frac{\sum_i C_{outlet}}{\sum_i C_{inlet}} = \frac{\sum_i C_{outlet(gas)} + \sum_i C_{outlet(liq.)}}{2F_{ethanol(inlet)}} \times 100 \tag{3-10}$$

To estimate the error amongst a set of experimental data, a 95% confidence interval is used to calculate the level of error. A sample calculation can be found in Appendix D.

Chapter 4

Thermodynamic Calculations for Ethanol Reforming in Supercritical Water

In this chapter, thermodynamics calculations for ethanol reforming in supercritical water are presented. This study considers the effect of temperature, pressure and ethanol concentration on conversion and product selectivity. In addition, thermodynamic calculations for gas/liquid separation at different pressures and temperatures are also presented, for preliminary evaluation of potential separation processes for this particular application.

4.1 Process Diagram

The Redlich-Kwong Soave (RKS) model was used to calculate thermodynamic equilibrium properties. This model has been considered adequate to represent supercritical water conditions. For example, this model has been suggested for reforming in supercritical water of biomass by Tang and Kitagawa (2004), and of 2-propanol by Anikeev et al. (2004). However, the heat capacity of each component is assumed to be dependent only on temperature, as given by Aspen. The Gibbs free energy minimization (GFEM) model was used to calculate the mass and energy balances around the reactor. Note that this technique determines the equilibrium composition based on pre-defined product species (all those expected to be present during the reaction) and is independent of reaction pathways. The selection of the species that could be present during the reaction was based on the species detected during the actual experiments carried out in the laboratory with and without catalyst. Those components are hydrogen, methane, carbon monoxide, carbon dioxide, ethylene and ethane, acetaldehyde, acetone and diethyl ether. The thermodynamics equilibrium reaction products are evaluated in term of ethanol conversion and selectivity. Ethanol conversion is defined according to equation 3.8, while product selectivity is defined in equation 3.9. Figure 4-1 shows the process diagram that has been used to simulate the reaction in supercritical water and possible gas product separation process.

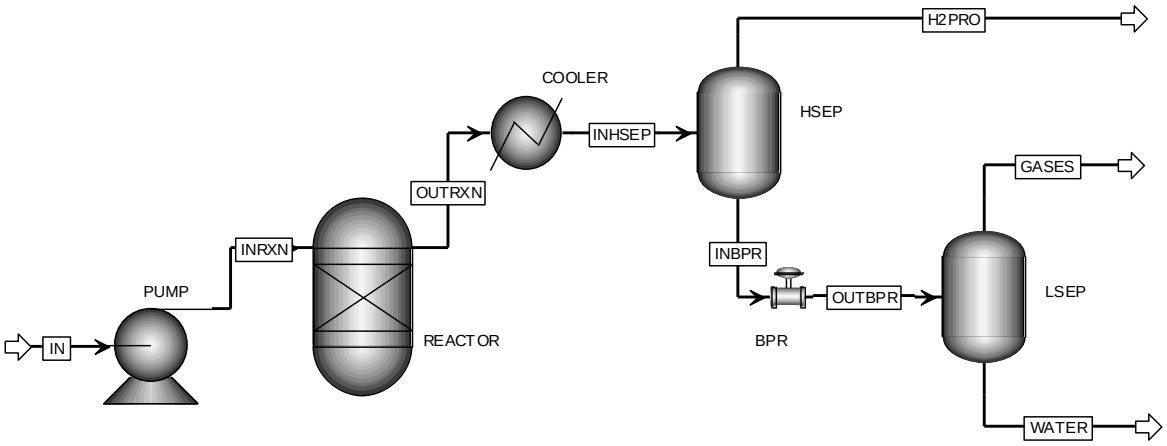

Figure 4-1: Process flow diagram for ethanol water reforming at supercritical water conditions with gas/liquid separation at high pressure.

4.2 Effect of Temperature

Figure 4-2 shows the product selectivities at the supercritical water temperature range, from 400 to 600°C. Only H_2, CH_4, CO_2, CO are shown in Figure 4-2. The other products, such as C_2H_4, C_2H_6, acetaldehyde, acetone and diethyl are not shown in the figure because they are very small, below 0.01 %. The major components have also been reported by those who studied ethanol reforming at atmospheric pressure (Garcia and Laborde, 1991; Fishtik et al., 2002). The ethanol conversion (not shown in the figure) for all temperatures considered here is 100%. From Figure 4-2, the selectivities of H_2 and CO increase with temperature, whereas CH_4 selectivity decreases linearly with temperature. CO_2 selectivity does not vary over the temperature of study and remains around 25%. The H_2 selectivity shows a linear increase from ~10% to ~54% in the temperature range 400 to 600°C. CO selectivity increases non linearly with temperature from 0.02% at 400°C up to 0.6% at 600°C. Therefore, at a temperature of 400°C (close to the water supercritical temperature, 374°C), the reaction product composition is dominated by CO_2 and CH_4, the latter being an undesired product here. At temperature close to our maximum working temperature (600°C), H_2 becomes the main reaction product (~50% at 600°C), but CH_4 would still be present at a level of around 20%. These results shows that H_2 production is favoured at high temperature.

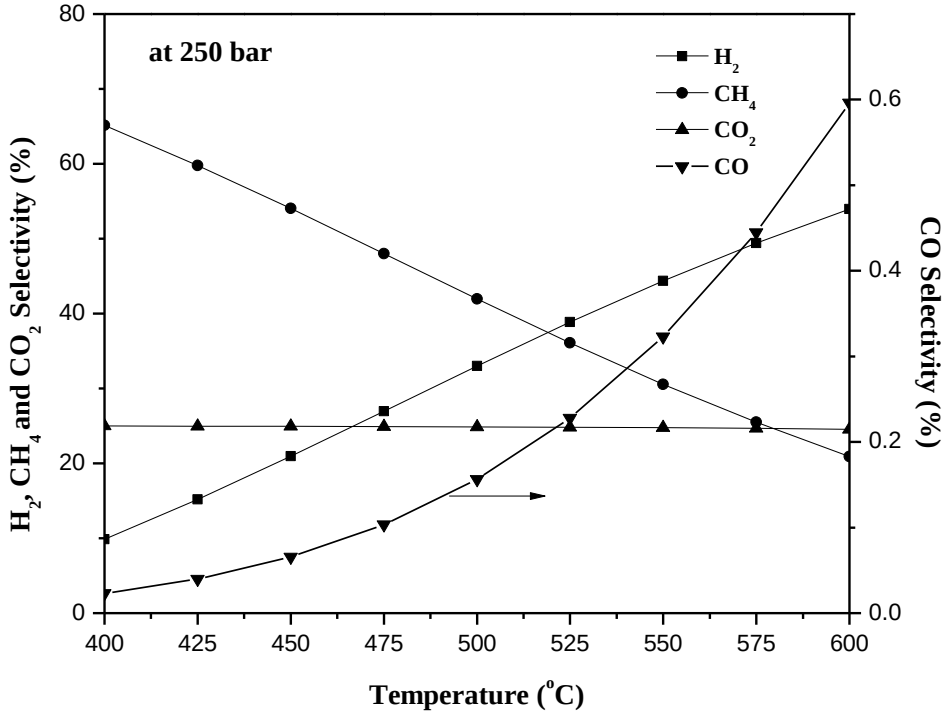

Figure 4-2: Product selectivity as a function of temperature. (Input parameters: 250 bar, 5 wt.% ethanol)

4.3 Effect of Pressure

Figure 4-3 shows the product selectivities of the main species as a function of pressure at 500°C. Increasing pressure does not improve H_2 selectivity. H_2 selectivity decreases from 75% at 1 atm (1.01 bar) to 29% at 300 bar. CO also decreases from from 0.6% at 1 atm to 0.15% at 300 bar. Increasing the pressure also does not have much effect on the CO_2 selectivity, which stays around 25%. The decrease in H_2 selectivity with pressure is counterbalanced by an increase in CH_4 selectivity. CH_4 would be the most favoured species at high pressure; at 300 bar CO selectivity would be 46%.

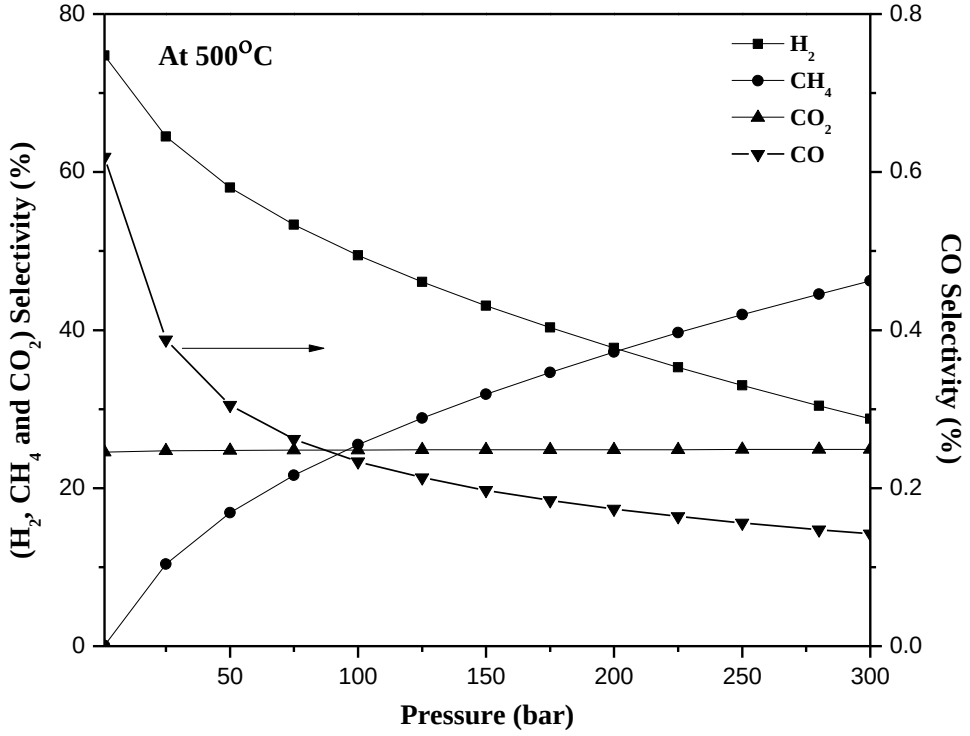

Figure 4-3: Product selectivity as a function of pressure at 500°C. (Input parameters: 500°C, 5 wt.% ethanol)

4.4 Effect of Ethanol Concentration

Figure 4-4 presents the effect of ethanol concentration by weight on product species selectivity. The trends of increasing ethanol concentration on the H_2, CH_4 and CO_2 selectivities are similar to the effect of pressure. H_2 selectivity decreases radically from 47% at 2.5 wt.% to 10% at 25 wt.% ethanol concentration, and then decreases at a lower rate thereafter to be around 6% at 40% wt. ethanol. The rapid decrease in H_2 is accompanied by an equivalent increase in CH_4 selectivity. CO_2 does not vary when changing ethanol concentration. The CO selectivity increases slightly with temperature. This indicates that the reaction change is closely related to the methanation reaction ($CO + 3\ H_2 \rightarrow CH_4 + H_2O$).

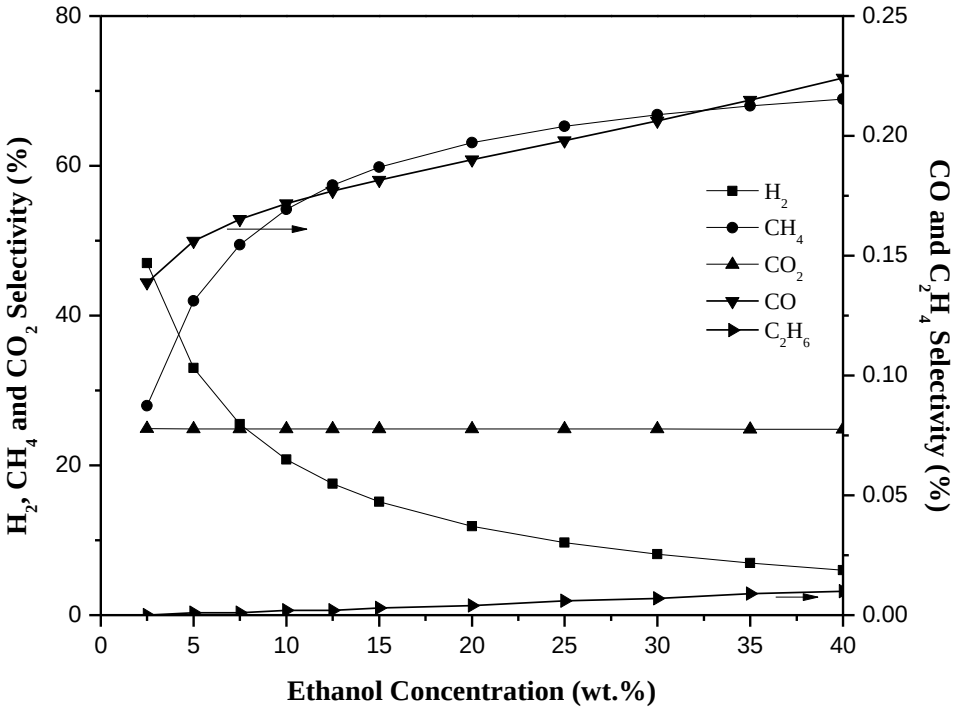

Figure 4-4: Product selectivity as a function of ethanol concentration. (Input parameters: 500°C, 250 bar).

4.5 Gas-Liquid Separation at High Pressure

The rationale of this study is to save compression costs by producing hydrogen directly at high pressure. Obviously, this would work if hydrogen purification could be performed at this high pressure. Although hydrogen separation/purification was not the topic of this thesis, a few calculations were performed to estimate the possibility of separating the bulk of gas product impurities (any gas except H_2) at the reaction pressure or slightly lower than the reaction pressure, by taking advantage of different product solubility in water. Final hydrogen purification was not considered here. Figure 4-5 and 4-6 show the effect of pressure and temperature on the separation of the gas product from water. The thermodynamics model of UNIQUAC, and Redlich Kwong Soave was used to calculate the properties of the liquids (water and ethanol) and gases. The solubilities of gases in liquid are calculated using Henry's Law. In Figure 4-5, at a constant temperature of 10°C, raising the pressure increases the purity of hydrogen. The solubility of carbonaceous species such as CO, CO_2, CH_4, C_2H_4 and C_2H_6 in liquid water increases with

increasing pressure. High solubilities of those carboneous species in water at high pressure left mostly hydrogen in the gas phase. This condition of high pressure gives an advantage for separating gas from liquid. The percentage gas recovery of each species in the gas liquid separator is defined according to equation (4-1).

$$\%\,\text{Gas Recovery} = \frac{\text{Gas Outlet}}{\text{Gas Inlet}} \times 100 \qquad (4\text{-}1)$$

Figure 4-5a shows the results for this gas/liquid separation process when changing the pressure from 1.0125 bar (1 atm) to 300 bar at 10°C. The composition gas inlet is given from the result of the thermodynamic equilibrium reaction at 500 ºC and 250 bar with 10 wt.% ethanol feed concentration. The percentage gas recovery can be seen in the Figure 4-5b. The composition of the gaseous product after gas/liquid separation shows an increase in H_2, and a decrease in CH_4 and CO_2 until 150 bar. Beyond 150 bar, the composition does not vary significantly. Hydrogen recovery achieves about 99.9% which means that H_2 remains in the gas phase, while other gases like carbon dioxide and methane partially dissolve in water at high pressure.

Figure 4-6a shows the results for the gas/liquid separation when changing the separation temperature rises from 0 ºC to 60ºC of a constant pressure of 250 bar. The inlet gas composition is also given from the result of the thermodynamic equilibrium reaction at 500 ºC and 250 bar with 10% wt. ethanol feed concentration. The percentage gas recovery can be seen in Figure 4-6b. Varying the temperature from 0 to 60°C does not change much the gas product composition. In gas recovery, H_2 still remains unchanged with temperature, but other species like CO, CH_2, CO_2 increase. Nonetheless, for separation at 250 bar and 20°C, this simple simulation at least demonstrates that it is possible to remove close to 95% of the CO_2 and about 70% of the methane content in the feed stream.

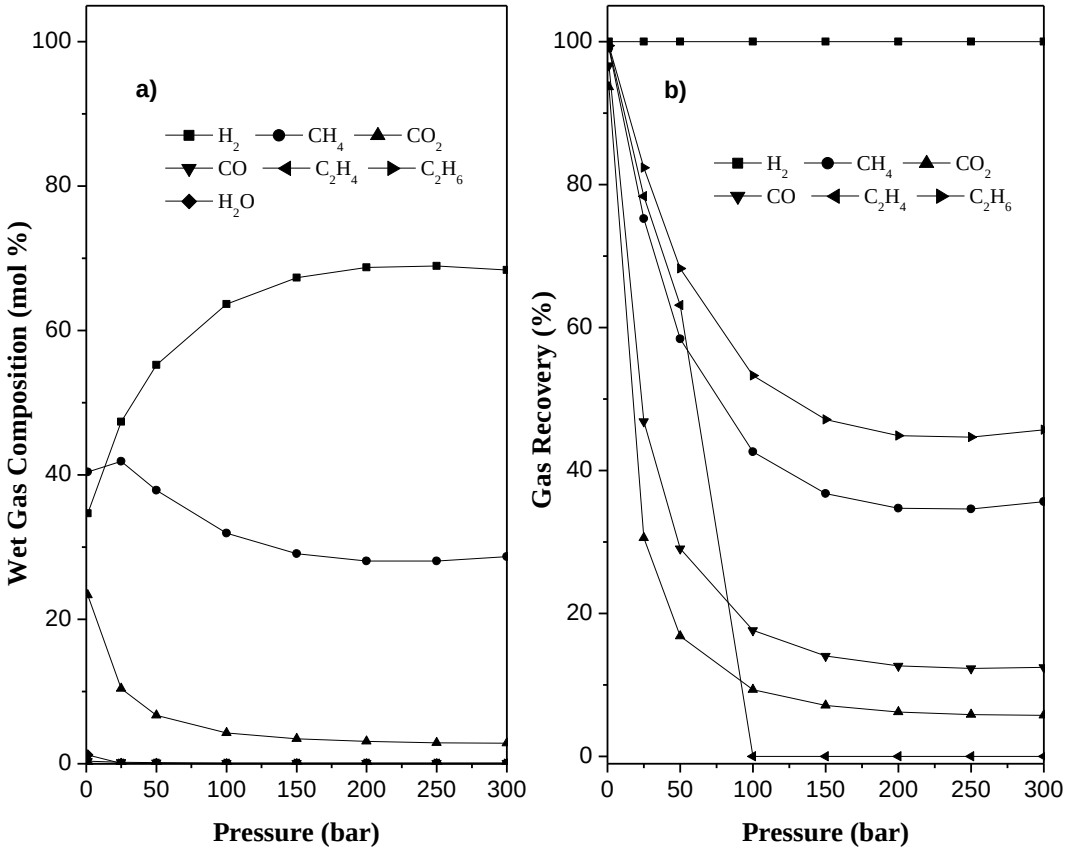

Figure 4-5: Gas/liquid separation with varying flash pressure from 1.01325 bar (1 atm) to 300 bar: a) Percentage wet gas composition and b) Percentage gas recovery.

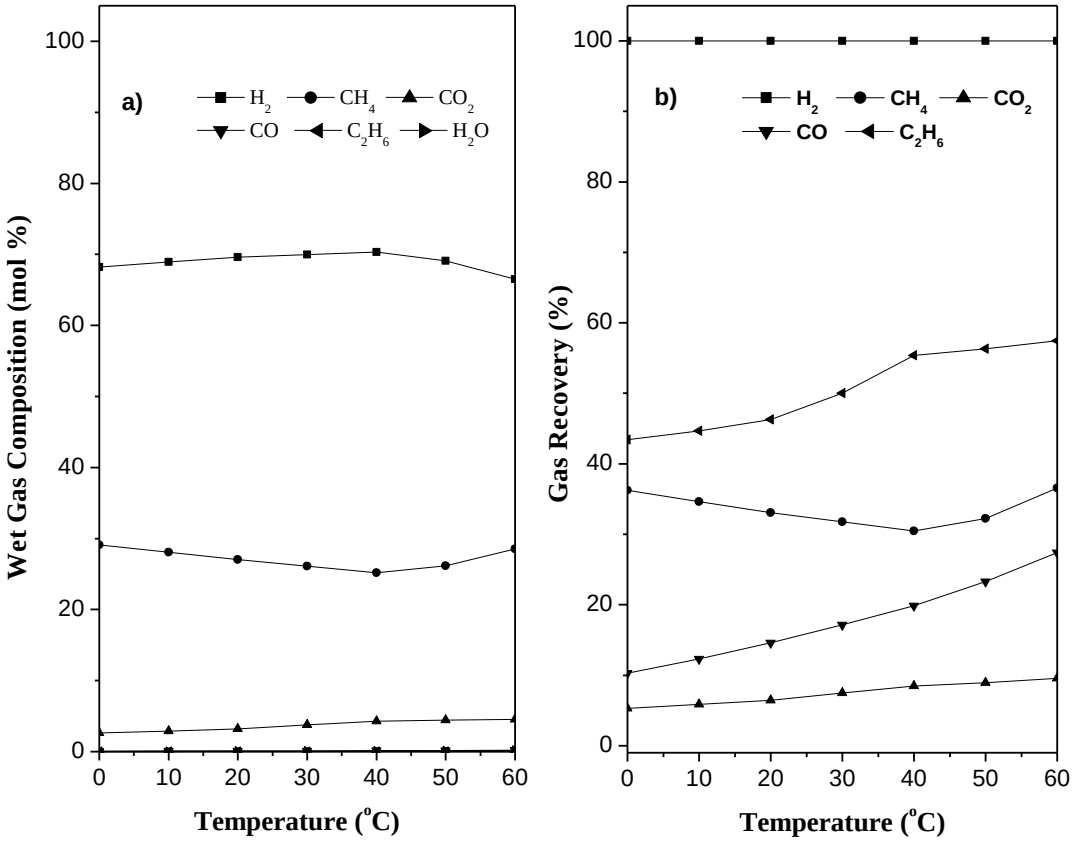

Figure 4-6: Gas-liquid separation as the temperature varies from 0 ºC to 60 ºC: a) Percentage Wet Gas composition and b) Percentage gas recovery.

4.6 Summary

The thermodynamic calculations show that ethanol conversion for the temperatures of study (400 to 600°C) can be complete. H_2 is favoured at higher temperatures, but decreases as pressure and ethanol concentration increase. The disappearance of H_2 is closely correlated to the formation of CH_4. CH_4 is favoured at high pressure and high ethanol concentration. CO_2 remains unchanged when varying temperature, concentration and pressure. Although this thermodynamic calculation indicates a disadvantage of carrying out ethanol reforming at high pressure, especially because of the high level of CH_4 formed, one has to keep in mind that the reaction can be stopped before it achieves equilibrium conditions if this could be advantageous regarding hydrogen selectivity. It will be seen in our experimental results, the methane concentration produced is actually much lower than what is predicted from equilibrium. This chapter also presented a simple flash

simulation that shows that a large fraction of methane and CO_2 (the two most important "impurities") can be removed from the gas stream simply via high flash at high pressure.

Chapter 5

Evaluation of the Catalytic Activity of the Inconel-625 Reactor Toward Ethanol Reforming

This chapter presents an evaluation of the activity of the tubular reactor made of alloy Inconel-625 toward ethanol reforming in SCW. The results presented in this chapter can be used directly if only an empty reactor is to be used, or, more importantly in this thesis, will be used as a baseline in subsequent chapters to distinguish the activity due to the reactor itself and that due to the catalyst. The parameters investigated in this chapter are: effect of temperature, pressure, ethanol concentration, residence time, and pre-treatment with hydrogen. The reaction mechanism of this empty Inconel-625 reactor is also presented in this chapter.

5.1 Description of Operating Conditions

These experiments were carried out to evaluate the catalytic activity of the reactor itself (Inconel-625) and the screen (316 SS) used to support the catalyst bed. The diagram of the reactor design, including the screen, is presented in Figure 3.3. It was necessary to use specialty alloys to accommodate the extreme operating conditions and these alloys are known to be potentially catalytic active toward reforming reactions. The reactor was made of Inconel-625 containing a large amount of nickel, as indicated by its following composition (given by Autoclave™ Engineering Inc.): 61.15% (wt.) Ni, 0.02% C, 0.09% Mn, 0.11% Si, 0.05 % P, 0.001% S, 21.41% Cr, 0.03% Co, 8.85 % Mo, 3.56% (Nb+Ta), 0.32% Ti, 0.26% Al, 4.15% Fe, 3.55% Nb, and 0.007% Ta. Nickel is the most common active metal, which has been studied extensively for ethanol steam reforming at atmospheric pressure. Other components such as Fe, Mo and Cr are also known to be catalytically active. The screen is made of 316-stainless steel wire consisting of 0.08 max. (wt. %) C, 0.75% Si, 2.0% Mn, .045% P, 0.03% S, 16-18% Cr, 2-3% Mo, 10-14% Ni, 0.1% N and the balance is Fe (ASTM 240/A240N).

The volume and the total surface area of the reactor are 9.65 cm^3 and 3.1 cm^2, respectively. Therefore, the ratio of the total volume ($\pi r^2 L$) to the total surface area ($2\pi rL$) of the reactor is 3.14 cm. The Hastelloy tubing connected to the reactor, and through which ethanol is fed, has a length of 5.1 cm (2 inches) and a volume of 0.1 cm^3. The small volume of this Hastelloy tube leads to

small residence times within this tube (for example at 500ºC, 250 bar and 1.88 g/min the residence time is only 0.3 s). Because the residence time in the Inconel reactor for similar conditions is 29 s (two order of magnitude greater), we consider the wall effect of the Hastelloy tubing negligible. The experiments were performed at a pressure of 250 bar, and in the temperature range of 450 to 600°C, with ethanol concentrations varying between 2.5 and 10% wt., and with atotal ethanol/water flowrate ranging from 0.88 g/min to 2.88 g/min. For each experiment, five data points were collected every 40 min.

5.2 Effect of Temperature and Residence Time

For this work the minimum temperature is the water critical temperature (374ºC), but in practice we selected 450ºC as the minimum temperature investigated since below this temperature very low activity was observed. The reactor system was designed for a maximum allowable temperature of 650ºC (at 250 bar). However, at 600ºC, the experiments failed because of plugging, highlighting the importance of decomposition/cracking reactions at higher temperatures. Therefore the highest temperature reported is 575ºC. The results of the effect of temperature and feed flowrate are presented in Figure 5-1. At 575ºC we were able to collect only 1 and 3 data points for feed flowrates of 0.88 g/min and 1.88 g/min, respectively, before plugging. Pressure is monitored at the water feed pump and at the backpressure regulator (BPR). The pressure at the BPR is set constant, usually at 250 bar. The water feed pump pressure is allowed to increase up to a maximum of 350 bar, although it should in principle be close to the BPR pressure. In some experiments (like those at 575 and 600°C), the pump pressure increased, suggesting plugging of the reactor system. Since there were no catalyst particles inside the reactor, it was believed that the plugging was due to the deposition of tar or coke on the screen. This was actually observed visually from looking at the screen at the end of several experiments. A picture of the screen after experiments at 575°C is shown in Figure 5-2. Therefore, the range of temperature that will be considered to study ethanol reforming here is 450 to 550°C.

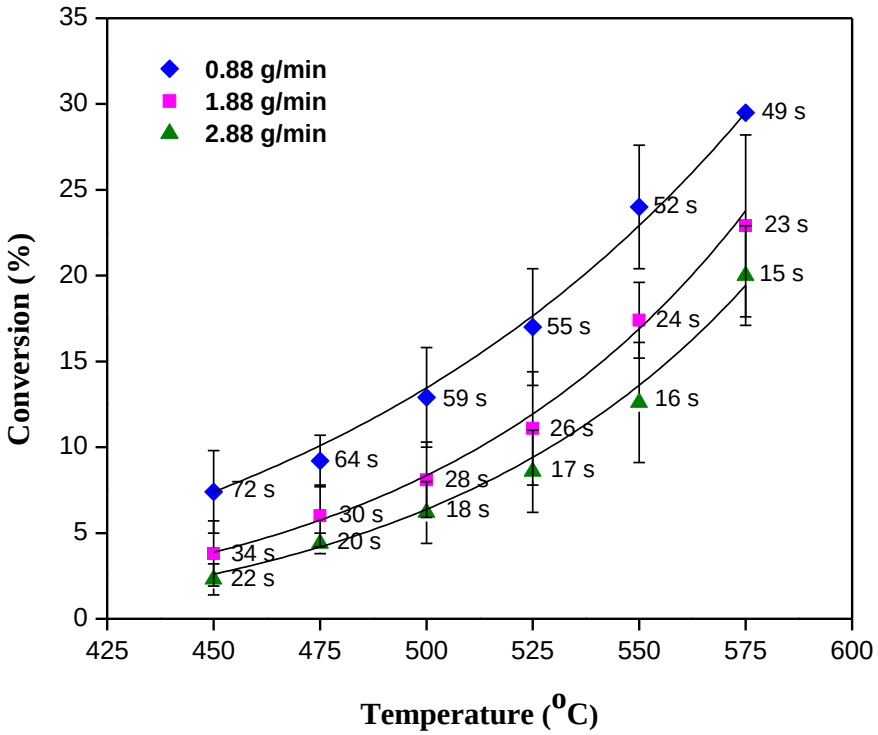

Figure 5-1: Effect of temperature and feed flowrate (corresponding residence time – in seconds - shown at the data point) on the ethanol conversion at 250 bar, 5 wt.% ethanol.

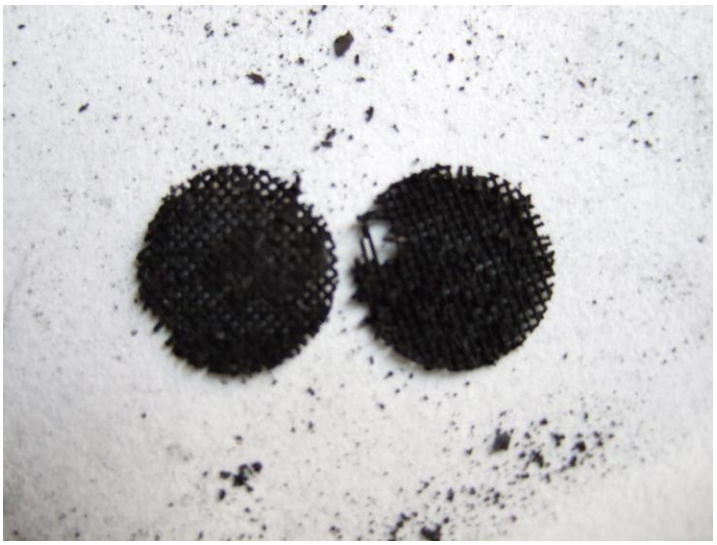

Figure 5-2: The visual of the screen with covering with tar after the experiment failed due to plugging.

The residence time is defined as the ratio of the fluid flowrate at reaction conditions to the reactor volume. To calculate the volumetric flow rate in the reactor at reaction conditions, the density of the fluid is assumed to be similar to that of pure water since the feed liquid mixture contains more than 90 wt.% water. The water density in the temperature range 450ºC to 550ºC at 250 bar decreases linearly from 0.1091 g/cm^3 to 0.0786 g/cm^3. The calculated residence time are shown in Figure 5-1 for all data points. The results indicate that temperature and flow rates (hence residence time) affect noticeably the conversion. At 500ºC, ethanol conversion is comparable to that observed by Hsiao (2003) (at 500ºC and 250 bar) and Schanzenbacher et al. (2002) (496ºC and 246 bar). In this experiment, the ethanol conversion is about 6.2±1.8 % for a residence time of 18 s and 12.9±2.9% for 58 s with initial concentration of 5 wt.%. Hsiao (2003) observed an ethanol conversion of about 10% for a residence time of 10 s and 15% for 50 s with initial feed of 0.46 mol/L (2.128 wt.%). Meanwhile, Schanzenbacher et at., (2002) observed an ethanol conversion of about 7.4% for 6 s residence time and 16.5% for 16 s with an initial concentration of ethanol of 1 mmol/L (0.0046 wt.%). The lower conversion observed here compared to that observed by Hsiao (2003) can be explained by the fact that in the present feed configuration ethanol was injected through a small tube (0.2 mm ID) (low residence time), while in the experiments of Hsiao (2003) and Schanzenbacher (2002) ethanol/water mixtures passed through a long preheating coil. This means that in our case the reaction take place mostly in the reactor, whereas in the case of Hsiao and Schanzenbacher, it is more than likely that a large portion of ethanol already reacted in the preheating tube.

The selectivities for each detected species at various temperatures and flow rates are shown in Figure 5-3. The main reaction products detected in the empty reactor study were hydrogen, methane, CO, CO_2, C_2H_4, and C_2H_6 in the gas phase, and acetaldehyde in the liquid phase. These main products were also reported by Arita et al. (2002) and Hsiao (2003). In the temperature range considered here, the two most important products are acetaldehyde and hydrogen, suggesting that the main reaction is ethanol dehydrogenation. At the lower temperatures of 450 and 475°C the selectivities of acetaldehyde and hydrogen remain constant at approximately 50±5% and 40±5%, respectively. It is also seen that up to 525°C, the selectivities of the major products do not change between feed flowrates of 0.88 and 2.88 g/min. The results show that the selectivity of acetaldehyde is greater than that of hydrogen for temperature below 525°C, whereas it is the opposite for temperature above 525°C. The hydrogen selectivity remains more or less constant at around 40% for the whole temperature range and whole flowrate/residence time considered here. One exception is at 575°C with 2.88 g/min (15 s residence time) where hydrogen

selectivity is closer to 50%, but then decreases down to around 40% for 1.88 g/min (23 s residence time). The acetaldehyde selectivity remains close to 50% for temperatures between 450 and 475/500°C, but decreases as the temperature increases beyond 475/500°C. At 525°C, the acetaldehyde selectivity is around 40% (similar to that of H_2); at 550°C, it is around 30/35% and at 575°C it is around 25/30%. The decrease in acetaldehyde selectivity is accompanied by an increase in both CO and CH_4 selectivities (around 10% at 550 and 575°C). At 550 and 575°C, one should notice that the selectivities of CO and CH_4 are slightly lower for 2.88 g/min than for 1.88 g/min, suggesting that CO and CH_4 are produced via secondary reactions, typically acetaldehyde decomposition, which was not complete at lower residence time. The selectivity of the other species (CO_2, C_2H_4, C_2H_6) remains below 5%, even at higher temperatures.

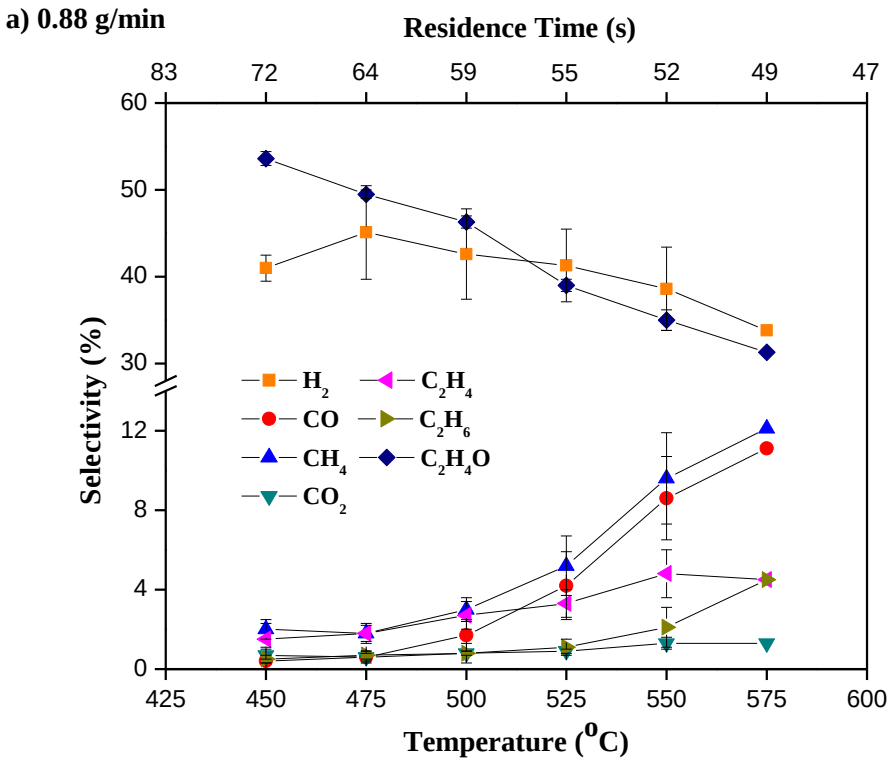

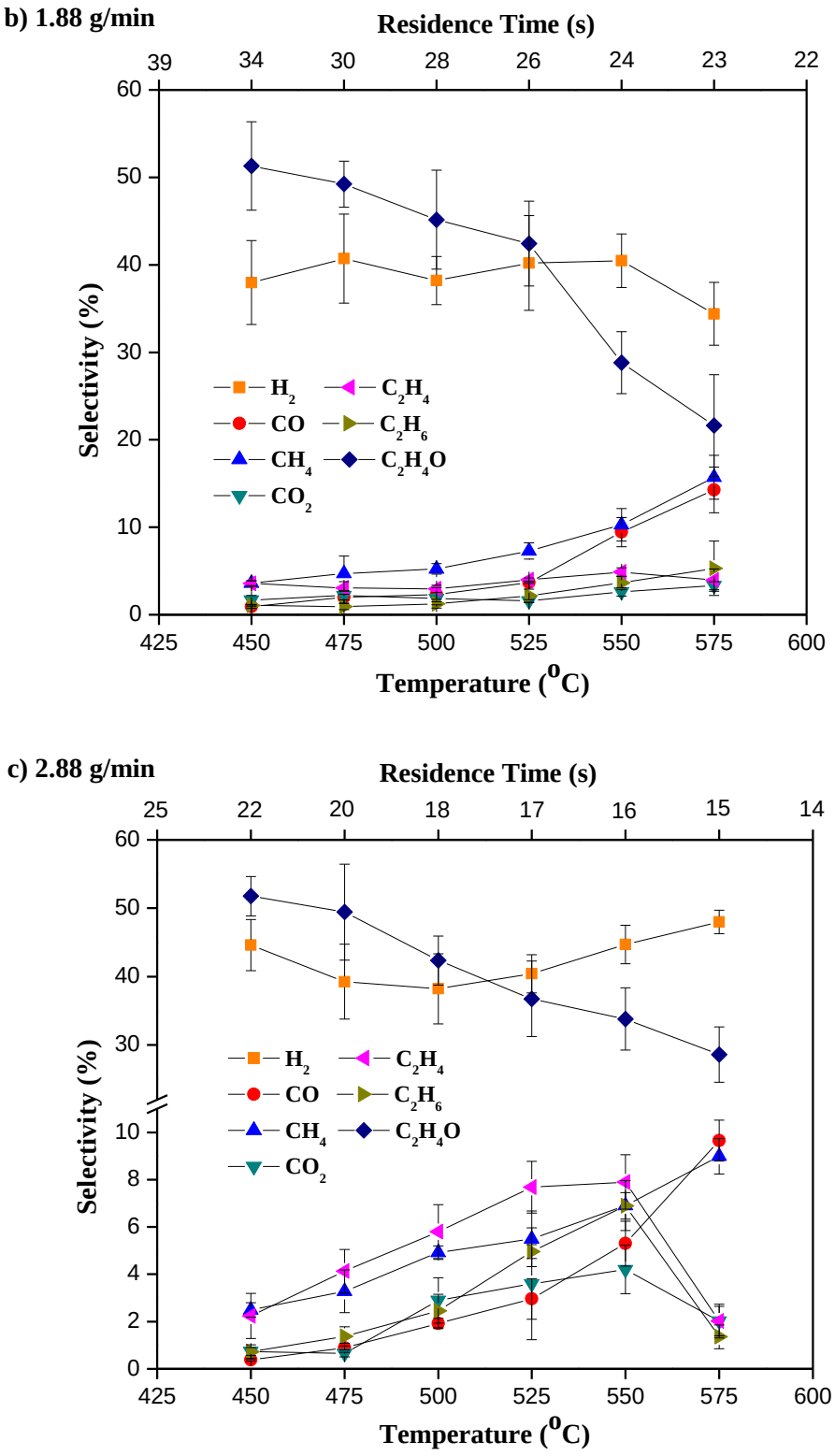

Figure 5-3: Product selectivities of an empty reactor as a function of temperature and flow rates (i.e., residence time) a) 0.88 g/min, b) 1.88 g/min, and c) 2.88g/min. (Pressure of 250 bar, 5 wt % ethanol).

As the temperature increases up to 550°C, Figure 5-3 shows that the C_2H_4 selectivity increases, but decreases at 575°C. The experiments at 575°C and feed flowrate of 0.88 g/min (49 s residence time) and 1.88 g/min (23 s residence time) were characterized by plugging of the reactor. As mentioned previously, at 575°C we could collect only one data point for 0.88 g/min and three data points for 1.88 g/min. Note that we were able to collect 6 data points (normal procedure in those experiments) without problems at 2.88 g/min (shortest residence time of 15 s). The plugging of the reactor at 575°C and lower feed flowrate, combined with the increase in C_2H_4 selectivity with the temperature increase up to 550°C and the abrupt decrease in C_2H_4 selectivity at 575°C, points to coking from the polymerization of ethylene and subsequent plugging of the reactor, as suggested by Dybkjaer, 1995:

Polymerization of ethylene: $C_2H_4 \rightarrow \text{olefins} \rightarrow \text{polymers} \rightarrow \text{coke}$

The result in Figure 5-3 indicates that ethanol is consumed primarily via dehydrogenation, yielding acetaldehyde and hydrogen, followed by acetaldehyde decomposition to form methane and CO. The production of hydrogen, acetaldehyde and other species can be explained by the mechanism proposed by Arita et al. (2003), who conducted ethanol hydrolysis in SCW but in a batch reactor. The initial step of the ethanol water reforming is the dehydrogenation of ethanol to form acetaldehyde and hydrogen:

$$C_2H_5OH \rightarrow C_2H_4O + H_2 \qquad \textbf{(}5\text{-}1\textbf{)}$$

Acetaldehyde is then decomposed to methane and CO as shown in equation **(5-2)**

$$C_2H_4O \rightarrow CH_4 + CO \qquad \textbf{(}5\text{-}2\textbf{)}$$

Ethanol can also decomposed via dehydration yielding ethylene and water, as shown in equation (5-3):

$$C_2H_5OH \rightarrow C_2H_4 + H_2O \qquad \textbf{(}5\text{-}3\textbf{)}$$

Subsequently, this reaction can be followed by hydrogenation of ethylene to produce ethane:

$$C_2H_4 + H_2 \rightarrow C_2H_6 \qquad \textbf{(}5\text{-}4\textbf{)}$$

CO_2 is likely to be formed via the water-gas-shift reaction, equation (5-5):

$$CO + H_2 \rightarrow CO_2 + H_2O \qquad (5\text{-}5)$$

5.3 Effect of Ethanol Concentration

Figure 5-4 illustrates the effect of ethanol concentration (concentrations of 2.5% wt, 5.0% wt., 7.5% wt., and 10%) at 500ºC, 250 bar, 1.70 g/min water. It is important to note that with our current feed water pump (Thar pump P50) it was not possible to vary the ethanol concentration while keeping a constant residence time. Indeed, the flow rate for the Thar pump can be adjusted only in increments of 1g/min. Here, the feed water flow rate was kept constant at 1.70 g/min and the water/ethanol mixture at the ISCO pump was changed to obtain the desired ethanol concentration. Figure 5-4 shows that ethanol conversion decreases as ethanol concentration increases, but at the same time the residence time is also decreasing. It is to be expected that conversion decreases at shorter residence time. Therefore, it is difficult to conclude here whether the change in conversion is due mostly to ethanol concentration, residence time, or a combination or both. We have then plotted in Figure 5-5 the data shown in Figure 5-4 in terms of conversion vs. residence time and compared them with data obtained at constant ethanol concentration. The slope of the effect of residence time at constant ethanol concentration is considerably lower than that at different ethanol concentrations. Therefore, it can be concluded that the effect seen in Figure 5-4 is mostly due to ethanol concentration. The decrease in ethanol conversion at higher ethanol concentration may be due to the saturation of ethanol on the active sites on the reactor's wall. This effect has been suggested by Taylor et al. (2003) who conducted methanol reforming in SCW in a tubular reactor made of Inconel-625. The increase in ethanol concentration from 2.5 to 10% wt. does not change much the hydrogen selectivity, which is around 40% as shown in Figure 5-6. Other gas reaction products such as CO, CH_4, CO_2 and C_2H_4, C_2H_6 increase when increasing ethanol concentration, suggesting that increasing the concentration favours the decomposition of acetaldehyde, hydrogenation of C_2H_4 toward C_2H_6, and water gas shift reaction of CO toward CO_2.

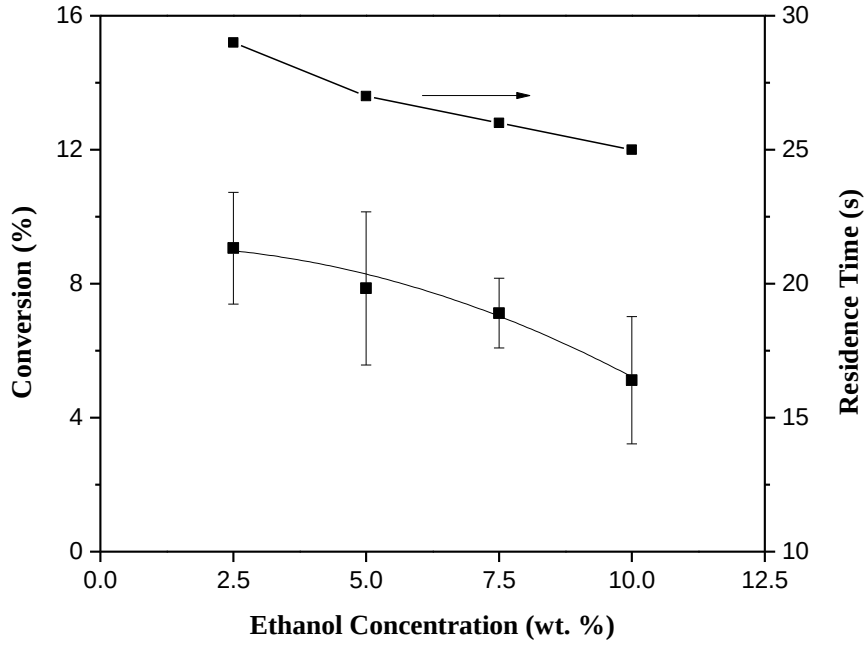

Figure 5-4: Ethanol conversion and residence time as a function of ethanol concentration for the empty reactor at 500ºC, 250 bar, 1.88 g/min

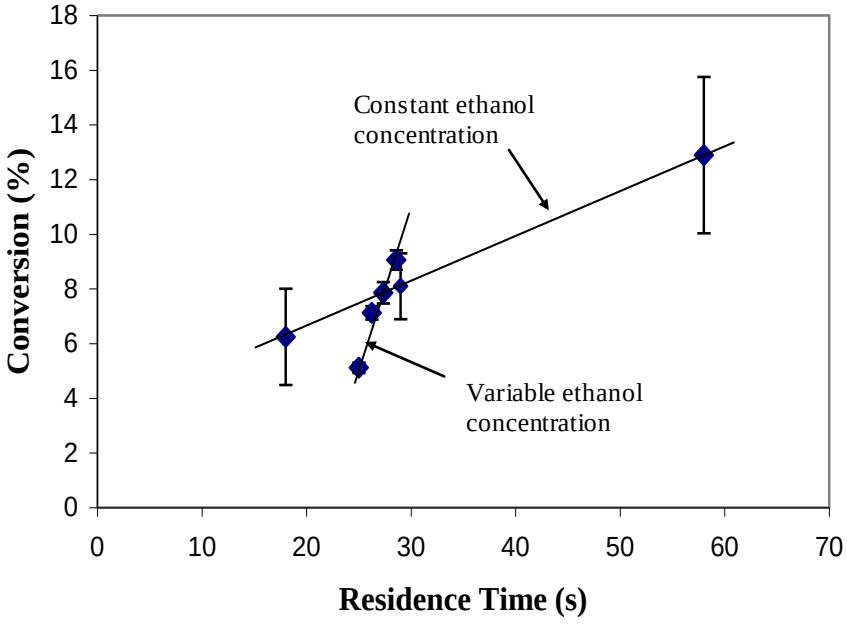

Figure 5-5: Ethanol conversion vs. residence time (500°C, 250 bar)

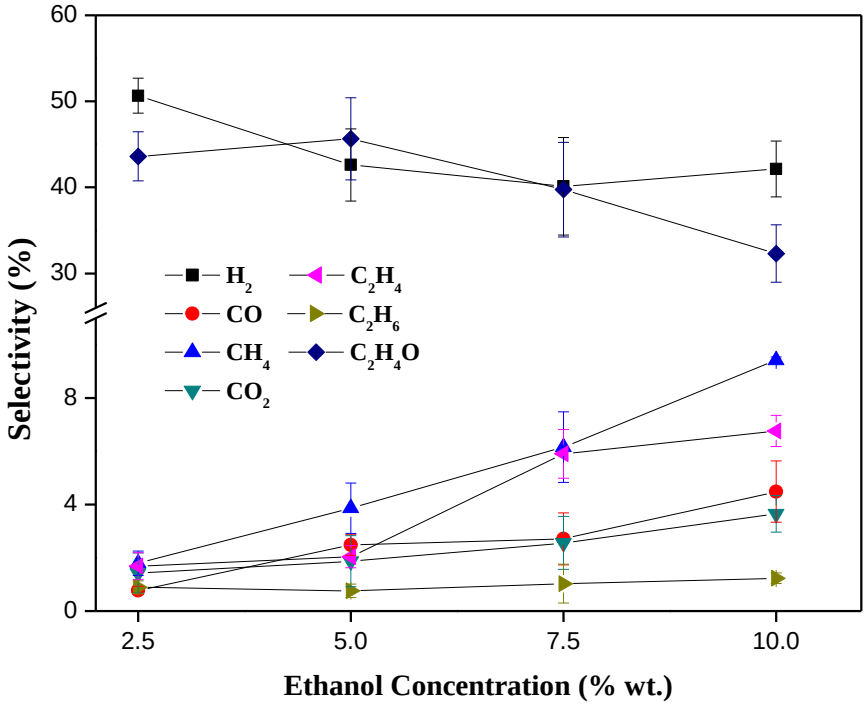

Figure 5-6: Distribution of reaction gas product as a function of ethanol concentration for a tubular reactor at 500ºC, 250 bar, 1.88 g/min feed.

5.4 Effect of Wall Pre-treatment with H_2

Since the reactor's wall is catalytically active, we wanted to see whether this wall activity could be enhanced by reducing it with hydrogen prior to the reforming step. To do so, 20 mL/min with 20% (v/v) hydrogen diluted in nitrogen was fed to treat the reactor wall for 2 h. By means of treatment, the wall covered by metal oxide might reduce to metallic form (in particular reducing nickel oxide to metallic nickel). Figure 5-7 shows the ethanol conversion versus time-on stream. Without pre-treatment, the ethanol conversion remains quite constant during the 200 mins of the experiments (~17% at 550°C, ~8% at 500°C and ~4-5% at 450°C). With pre-treatment, the conversion of the first sample (30 mins after ethanol injection) is higher than without pre-treatment. For higher time-on-stream, the conversion drops to become similar to that obtained without pre-treatment. The ethanol conversions for all three temperatures are about the same for the empty reactor with and without pre-treatment with H_2 after 2 samples (i.e., after ~90 min). This result indicates that SCW likely re-oxidizes the wall's surface. Here, the presence of small amount

of hydrogen formed from ethanol reforming does not seem to be sufficient to maintain the metallic state of nickel on the wall's surface.

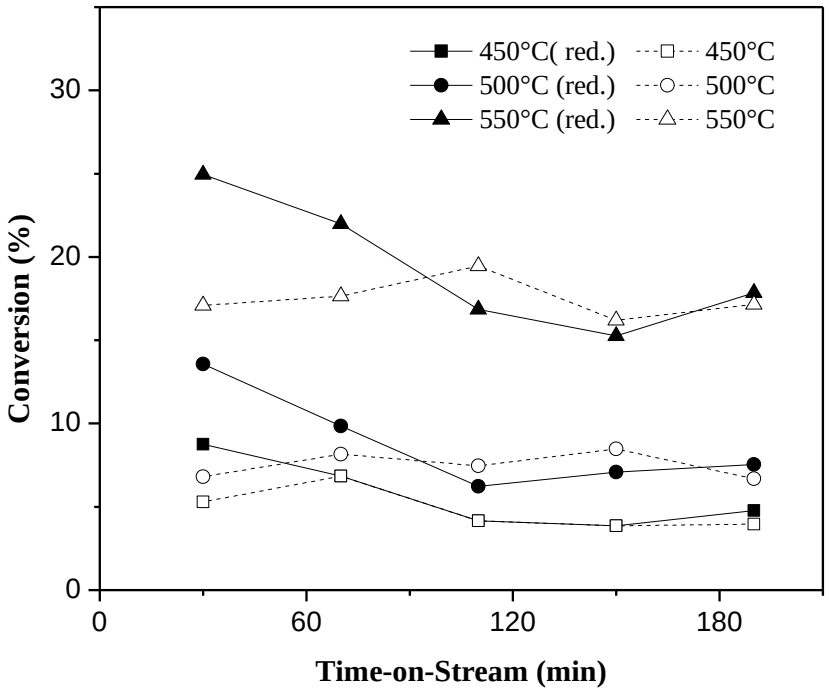

Figure 5-7: Comparison between the ethanol conversion with and without H_2 pre-treatment as a function of time-on-stream (min). Red. in the legend means "reduced" or with pre-treament with H_2 (for closed symbol).

5.5 Effect of pressure

At a constant temperature of 500ºC, increasing the pressure from 225 bar to 280 bar increases the water density from 0.078 g/cm^3 to 0.105 g/cm^3. The effect of increasing the pressure from 225 bar to 280 bar on ethanol conversion and SCW density is presented in Figure 5-8. There is no significant difference of the mean and the variance using a Turkey and Levene test in a statistical analysis of one way ANOVA method (refer to the appendix E). Also, no significant difference in terms of the reaction product yield was observed (results not shown). This denotes that in the pressure range studied here, the corresponding change in density did not affect the conversion.

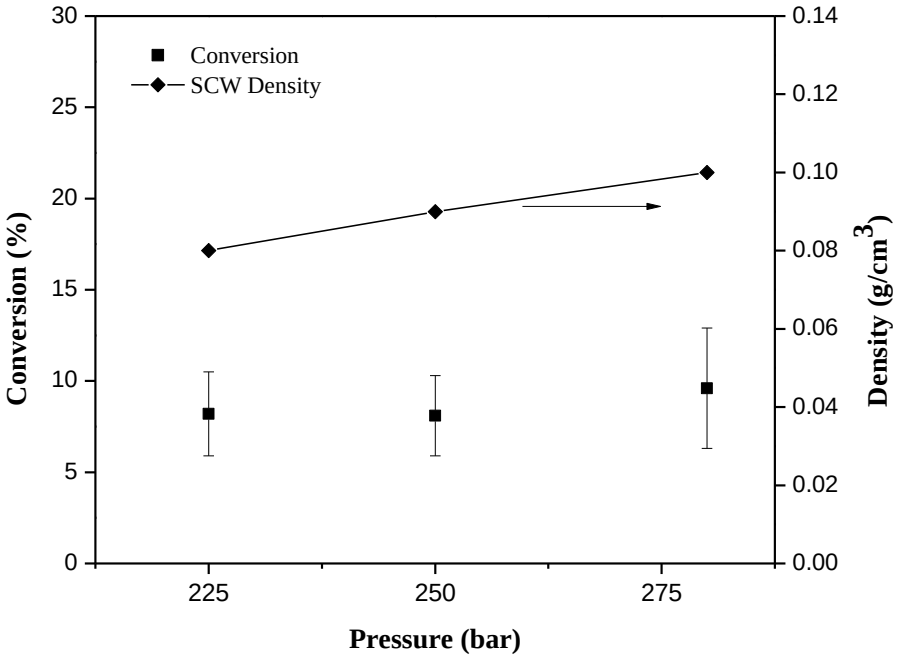

Figure 5-8: Effect of pressure on ethanol conversion at 500ºC, 1.88 g/min and 5% wt. ethanol

5.6 Summary

In this section, ethanol reforming without catalyst has been performed to figure out the extent of the reaction in SCW without catalyst. This study was necessary to analyse the results for the experiments with catalysts in the next chapters. The effects of temperature, flowrate, concentration and pressure have been studied. Ethanol reforming in the empty reactor strongly depends on temperature. This study is important to distinguish the effect of the reactor wall in subsequent chapters. Indeed the reactor is made of Inconel-625, which a high concentration of Ni. Nickel is known to be catalytically active toward ethanol reforming. The experiments show that the reactor would have plugging problem for temperatures beyond 575°C, especially at low feed flowrate. Reactor plugging occurs due to deposition of coke on the screen, the coke particles being eventually formed in the homogeneous phase, or on the reactor's wall. The selectivity results for the empty reactor show that the production of hydrogen is mostly from ethanol dehydrogenation. The decomposition of acetaldehyde is believed to be the main route of CO and CH_4 formation. The small selectivity of CO_2 indicates that the water gas shift reaction is not significant in the empty reactor. The dehydration step is also significant here, as evidenced by the presence of C_2H_4, and by

the formation of tar (ethylene is a known precursor for coke formation). Pre-treatment of the reactor with hydrogen is found to be significant shortly after the ethanol was injected, due to the activity at the reactor wall. However, the conversion returns back to similar value as for the non reduced reactor after some time. Above 575°C, the reactor plugged and thus we decided to limit our experiments to temperatures not exceeding 550°C.

Chapter 6

Catalyst Screening- Reforming over Nickel and Cobalt on Various Supports

6.1 Introduction

This chapter describes the catalyst screening study designed to select a promising catalyst for ethanol reforming in SCW. The performance of the catalyst was evaluated in terms of ethanol conversion, selectivities and stability. The characterization of the physical and chemical properties of the catalysts were studied as well. Stability and high selectivity toward hydrogen are the two main aspects to consider in this screening study before further optimizing the operating conditions of the selected catalyst. Even though rhodium is among the best catalysts found in the literature for ethanol reforming, we disregarded it due to its very high cost. Nickel and cobalt as active metals were selected instead because good activity as reported using them for ethanol steam reforming. The support selected for experiments are γ-Al_2O_3, α-Al_2O_3, ZrO_2 and 8% wt. yttria-stabilized zirconia (YSZ). The selection of the active metal and the support was based on several articles pertaining to ethanol steam reforming at various pressures.

Active metals

Nickel: well-documented fact that it enhances steam reforming reaction with relatively lower cost.

Cobalt: exhibits high activity and selectivity toward H_2 on ESR by suppression of methanation of CO.

Catalyst supports

γ-Al_2O_3 provides high surface area, and is well-documented for ESR at atmospheric pressure.

α-Al_2O_3 reported as the most stable at SCW conditions, but usually has low surface area.

ZrO_2 promotes hydrogen selectivity and is stable in SCW water.

YSZ more stable structure than that of ZrO_2.

6.2 Characterization of the Prepared Catalysts

The catalysts were prepared by an impregnation method as described in section 3.1. The final particles size was in the range 1.0 to 1.4 mm. Recall from section 3.1 that the particles were crushed and sieved from the calcined cake. Physical properties of the virgin catalyst after calcination at 550ºC are given in Table 6-1. The targeted catalysts contain nickel and cobalt in the order of 10 wt%. Nickel and cobalt loadings were checked using ICP-AES (see results in Table 6-1), and it was confirmed that the catalysts achieved the desired content of 10% by weight. As expected, the γ-Al_2O_3 support gives the highest surface area (36-56 m^2/g) among the catalyst selected. In contrast, catalysts supported on ZrO_2 showed the lowest BET surface area (5 m^2/g). Table 6-1 also shows that the presence of cobalt on the γ-Al_2O_3 and α-Al_2O_3 supports leads to a catalyst with lower surface area than that with nickel. XRD analysis shows that, after calcination at 550°C, the nickel is mostly in the NiO form, whereas cobalt is in the Co_3O_4 phase. The higher number of atoms involved for the cobalt catalyst compared to that of the nickel catalyst could be the reason for the lower surface area for cobalt catalysts. Comparison between the zirconia supports indicates that the surface area of the YSZ supported catalyst is higher than that of ZrO_2. This is due to the presence of 8% yittria. Packing bulk density was calculated by dividing the total weight of catalyst by the catalyst volume occupied in a 10-ml cylinder. The catalysts that have high surface area gave the lowest bulk density and the highest catalyst bed height, as shown in

Table 6-1: Physical and bed properties of the nickel and cobalt catalysts

Type of Catalysts	Co or Ni contain[a] (wt.%)	BET surface area (m^2/g)	Packing bulk Density (g/cm^3)	Height of the bed (mm)[b]
Ni/α-Al_2O_3	10.4	16	0.6	1.2
Ni/γ-Al_2O_3	10.4	56	0.7	1.2
Ni/ZrO_2	10.5	5	1.7	0.5
Ni/YSZ	10.3	11	1.1	0.7
Co/α-Al_2O_3	10.4	14	0.6	1.2
Co/γ-Al_2O_3	10.5	36	0.7	1.2
Co/ZrO_2	10.3	5	1.6	0.5
Co/YSZ	9.8	10	1.1	0.7

[a]measured by ICP-AES
[b]calculated from the bulk density and the reactor diameter

6.2.1 Acid Base Properties of the Support

It is well known that the nature of the support affects greatly the activity, product distribution and stability of the catalyst for ethanol reforming (Haga et al., 1997b; Breen et al., 2002; Duan and Senkan, 2005). Of particular importance are the acid and basic strengths of the support. The acid base properties were studied using TPD NH_3 (acidity) and TPD CO_2 (basicity). In this section, only results pertaining to the support are presented.

Prior to analysis, the supports were compressed at 9 MPa and sieved to obtain particles sizes of 1.0-1.4 mm. The adsorption temperature of the probe molecules was set at 100°C to prevent excess adsorbate from forming multiple layers on the surface (Hosseinpour et al., 2009). The physical properties of the support material for BET surface area, average pore volume, and average pore diameter is shown in Table 6-2. The γ-Al_2O_3 powder has a surface area of 240 m^2/g, but after being compressed at 9 MPa, it drops to 80 m^2/g. The α-Al_2O_3 powder surface area is 50 m^2/g and reduces to 10 m^2/g after compression. The BET surface area of YSZ and ZrO_2, after compression, are in the same order as that of α-Al_2O_3. The pore volume and average pore diameter of all four supports are similar; around 0.04 cm^3/g and 2 nm for pore volume and average pore diameter, respectively.

Table 6-2: Physical properties of the catalyst supports (after compression to 9 MPa), as used for TPD analysis.

Support Material	BET surface Area (m^2/g)	Pore Volume (cm^3/g)	Average pore Diameter (nm)
γ-Al_2O_3	82	0.04	1.98
α-Al_2O_3	10	0.05	2.00
ZrO_2	7	0.03	1.99
YSZ	13	0.06	1.99

Figure 6-1 and Figure 6-2 show the results of TPD- CO_2 and NH_3, respectively. These two figures show the desorption rates of CO_2 or NH_3 as a function of temperature, which provides information about the strength of bonding between the adsorbate and the surface of the support. The acid and basic strengths were determined by deconvoluting the density site distribution, that is, fitting the overall distribution using the modified Gaussian method. The fitting was performed using three distributions, representing three categories of strength depending on the temperature

they span. The acidic strength, using TPD-NH_3, are categorized as weak (125 to 260°C), moderate (160 to 360°C) and strong (225°C to the completed temperature of each support). The basic strength, using TPD-CO_2, are weak (130 to 255°C), moderate (170 to 320°C) and strong (220°C to the completed temperature of each support). Because the TPD profiles are dependent on the TPD experiment conditions (Triantafillidis et al., 2000; Hosseinpour et al., 2009), it can be difficult to compare directly TPD results with those published in the literature.

Once the TPD profile is deconvoluted, acid and basic site distribution can be determined by calculating the ratio of the area under each distribution to the total area. The total acid or base density (i.e. moles of NH_3 or CO_2 adsorbed, here at 100°C, per unit mass of support) can also be determined from the TPD curves. The resulting acid and basic site distributions, as well as acid and base densities are shown in Table 6-3 for all four supports considered. Several authors have suggested that the weak strengths have little impact on the catalyst performance and therefore the effect of acidity and basicity are more representative when considering sites of moderate and strong strength. This is why in Table 6-3 the ratio of acid-to-base sites is calculated by considering only the moderate and strong sites.

Table 6-3: TPD results – Acid/Basic Sites distribution and density

	Acid Site				**Base Site**				
	Site distribution (%)			**Total acid Density (µmol/g)**	**Site Distribution**			**Total base Density (µmol/g)**	**Ratio[1] (acid/base)**
	W	**M**	**S**		**W**	**M**	**S**		
γ-Al_2O_3	19	40	41	7.2	29	38	33	6.9	1.19
α-Al_2O_3	24	38	38	3.4	23	47	30	2.3	1.29
ZrO_2	60	40	-	0.6	100	-	-	0.4	-
YSZ	25	30	45	5.7	14	34	52	5.7	0.87

[1] Ratio of acid to base is calculated for the moderate and strong site

Figure 6-1 and Figure 6-2 show very low desorption rates of NH_3 and CO_2, indicating little adsorption of the probe molecules. The small TPD-NH_3 profile covers both the weak and moderate strength sites, whereas the results for TPD-CO_2 reveal only weak sites. The results for TPD-NH_3 are in agreement with the results from Finke et al. (2008) who claimed that the acidity of the

surface hydroxyl group is too weak to adsorb NH_3. Xu et al. (1988) reported also that zirconia has both acid and base sites.

The acid and base site densities for γ-Al_2O_3 are 2 to 3 times higher than for α-Al_2O_3. The desorption of NH_3 for γ-Al_2O_3 is complete at around 560°C, compared to a 520°C for α-Al_2O_3. This difference suggests that γ-Al_2O_3 has stronger acid sites. In addition, the percentage of strong (40%) and moderate (41%) acid sites for γ-Al_2O_3 is slightly higher than moderate (38%) and strong (38%) sites for α-Al_2O_3. Busca (2003) reported that α-Al_2O_3 has weak acid sites due to the presence of more Lewis acid sites, and γ-Al_2O_3 has strong acid sites due to the presence of the Brønsted acid sites. However, the TPD results alone cannot distinguish between Brønsted- and Lewis-acid or -basic sites (Hosseinpour et al., 2009). Even though γ-Al_2O_3 is known as an acidic support, it also strongly adsorbs CO_2 (Busca, 2000), which is also clear from Table 6-3, the acid to base density ratio is a bit higher than one (1.19), but the fraction of strong base sites (33%) is lower than the fraction of strong acid sites (41%). Similar observations can be made for the α-Al_2O_3. Therefore, the γ-Al_2O_3 and α-Al_2O_3 supports both possess more acidic properties.

The profiles of YSZ (see Figure 6-1 and Figure 6-2) show that the adsorption of the probe molecules (NH_3 and CO_2) on the YSZ surface is considerably stronger than for zirconia. Among all supports considered, the temperature at which desorption is complete is the highest for YSZ (~575°C) for both NH_3- and CO_2-TPD) The total acid and base densities for YSZ are similar (5.7 µmol/g). This is consistent with the fact that in most surface science studies, YSZ was considered as an inert material (Zafeiratos and Kennou, 2003). However, from Table 6-3, one can see that the basic site distribution concentrates more toward moderate and strong sites compared to that of the acid sites. This can also be seen from the acid/base ratio lower than unity. It is probably due to the base type material or the effect of the oxygen vacancies.

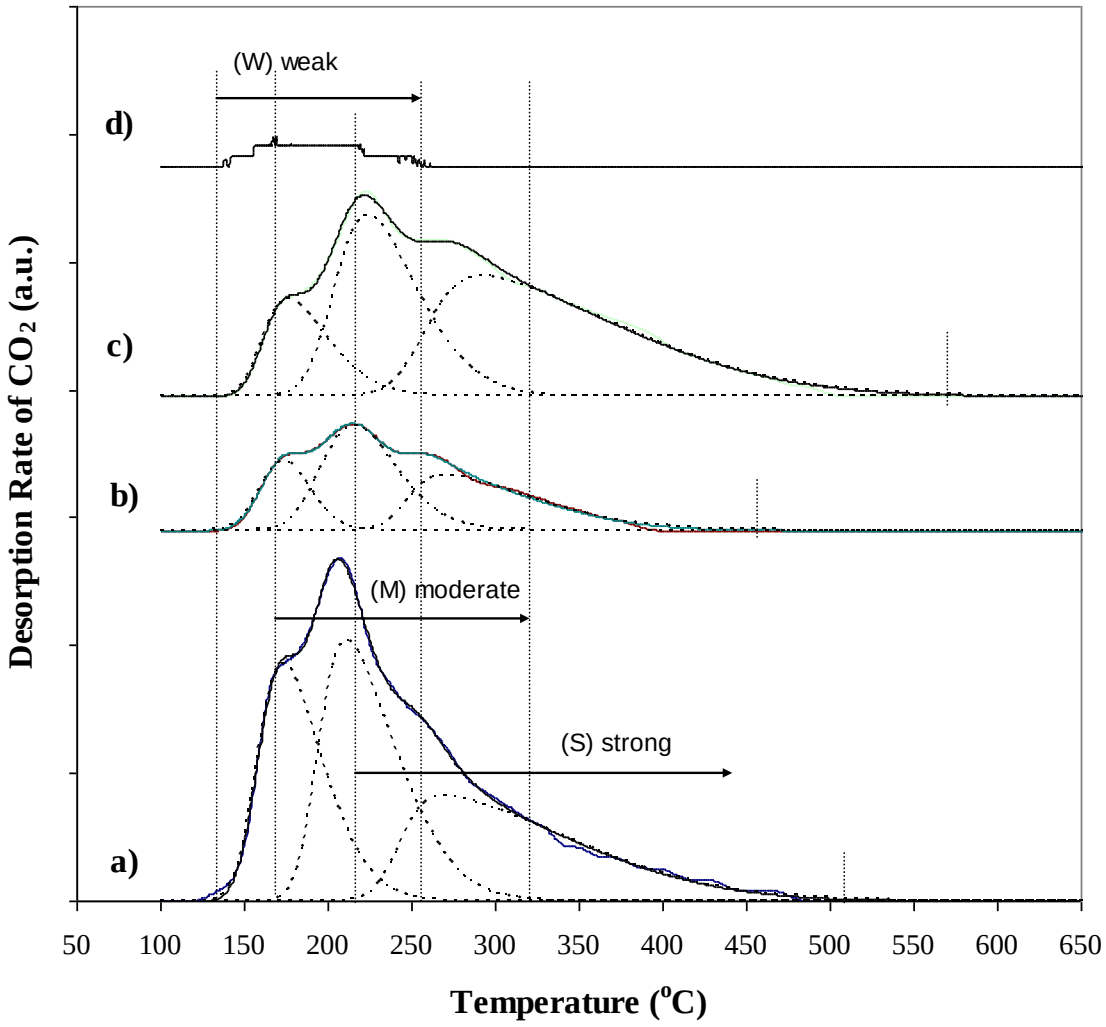

Figure 6-1: The TPD-CO_2 profile for the catalyst support; a) γ-Al_2O_3, b) α-Al_2O_3, c) YSZ and d) ZrO_2.

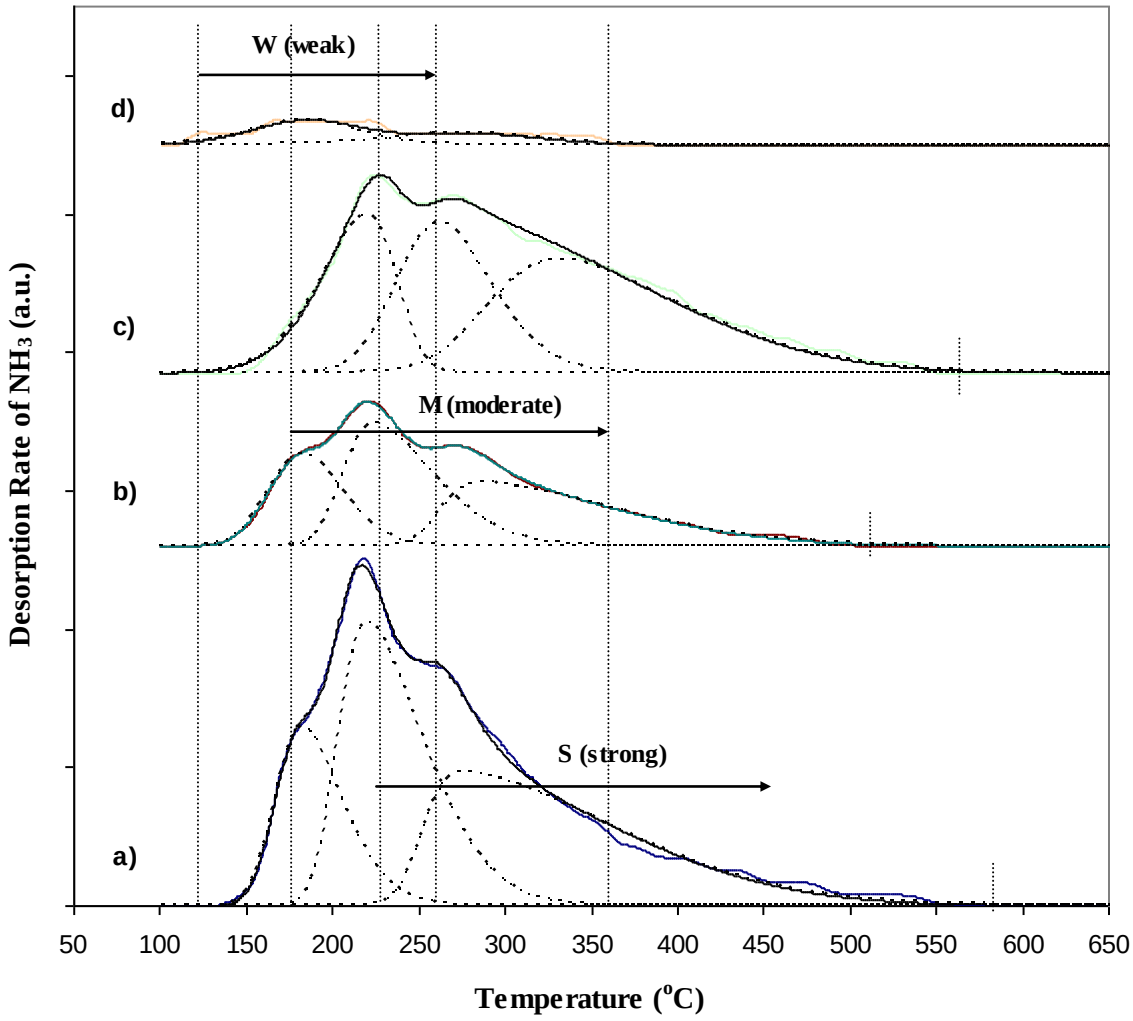

Figure 6-2: The TPD-NH_3 profile for the catalyst support; a) γ-Al_2O_3, b) α-Al_2O_3, c) YSZ, and d) ZrO_2.

6.2.2 Reducibility and Metal-support Interaction

The results of the TPR-H_2 for the calcined catalysts at 550ºC are shown in Figure 6-3 and Figure 6-4 for nickel and cobalt catalysts, respectively. These graphs represent the rate of H_2 consumption over nickel and cobalt catalyst as a function of temperature. They give information about the amount of catalyst being reduced and the interaction of the metal with its support. A summary of the span temperature and the hydrogen consumption is presented in Table 6-4. The span temperature represents the temperature interval between the start and completion of the reduction of metal oxide to metallic phase. The total number of moles of hydrogen consumed per

mass of catalyst or per number of moles of nickel or cobalt characterizes the reducibility of the catalyst.

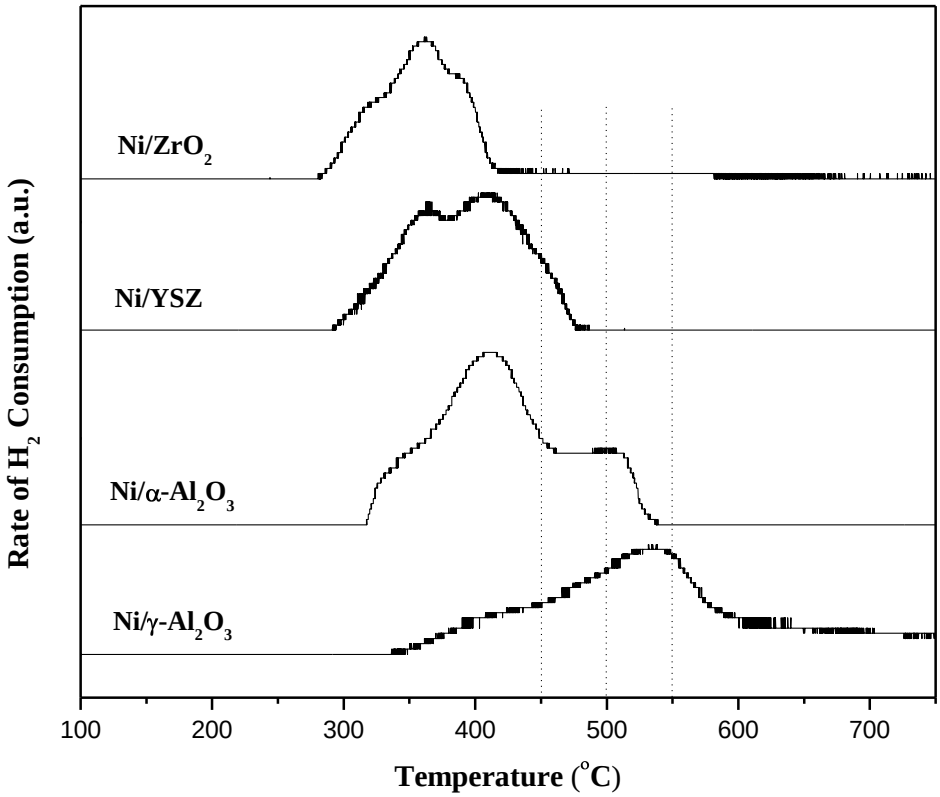

Figure 6-3: TPR-H_2 of 10 wt.% nickel supported on (γ-Al_2O_3, α-Al_2O_3, ZrO_2 and YSZ).

Figure 6-3 shows the TPR-H_2 profile of the nickel catalyst. The span temperature of each nickel catalyst is different. Ni/ZrO_2 reduces over the shortest temperature range, starting around 270ºC and finishing at 420ºC. It is followed by Ni/YSZ, from 280ºC to 480°C and Ni/α-Al_2O_3, from 280 to 540°C. The span temperature of Ni/γ-Al_2O_3 is the widest, from 330°C to 650°C. The maximum peak TPR-H_2 is indicative of the type of interaction between the active metal phase and the support. NiO is a common phase that forms from the hexahydrate precursor used here to make the catalyst (nitrate hexahydrate) for calcinations temperature below 600°C. Parmaliana et al. (1990) demonstrated that the reduction of unsupported NiO with TPR-H_2 arose with a single sharp peak at 370°C with reduction occurring over the 250-425ºC range. This behaviour is somewhat close to the profile observed for Ni/ZrO_2, which indicates that there is a weak interaction between NiO and the ZrO_2 surface. The profile of Ni/ZrO_2 is also in a good agreement with that reported by Diskin et al. (1998), and Molina and Poncelet (1998). Nickel on supported YSZ has two clear

peaks at around 350°C and 400°C, and is completely reduced at 480°C. The profile of YSZ up to 350°C is actually very close to that of ZrO_2, which was similar to unsupported NiO. Thus, we infer that the peak at 350°C with Ni/YSZ represents the reduction of the bulk crystalline NiO, and we ascribe the peak at 400°C to be due to the fraction of NiO that interacts more strongly with YSZ. The TPR of ZrO_2 also shows a peak at 350°C, but the next peak occurs at 370°C, which is at a lower temperature than for Ni/YSZ. This means that the NiO interacts more strongly with YSZ than with ZrO_2, which can be explained by the difference in site strength, as explained in section 6.2.1.

Three peaks can be identified on the Ni/α-Al_2O_3 TPR profile: at 350°C, at 410°C and at 500°C. This Ni/α-Al_2O_3 pattern is in a good agreement with the TPR-H_2 profile given by Molina and Poncelet (1998) for a catalyst calcinated at 500°C. For Ni/ γ-Al_2O_3 the main peak is at 550°C. Nickel on supported γ-Al_2O_3 is reported to have two types of interaction: NiO interacting with the surface γ-Al_2O_3, and metallic nickel bonding with Al_2O_3 to form a nickel aluminate spinel type phase ($NiAl_2O_3$) (Juan-Juan et al., 2006). The formation of $NiAl_2O_3$ phase should occur only for calcination temperatures above 600°C (Molina and Poncelet, 1998). Since our catalyst was calcined at 550°C, we should not expect $NiAl_2O_3$, which was confirmed by the TPR profile. Indeed for TPR-H_2, the peak of the $NiAl_2O_3$ phase only appears at temperatures higher than 700°C (Molina and Poncelet, 1998; Juan-Juan et al., 2006), which was not observed here. This suggests that the catalyst is mainly NiO on γ-Al_2O_3 surface.

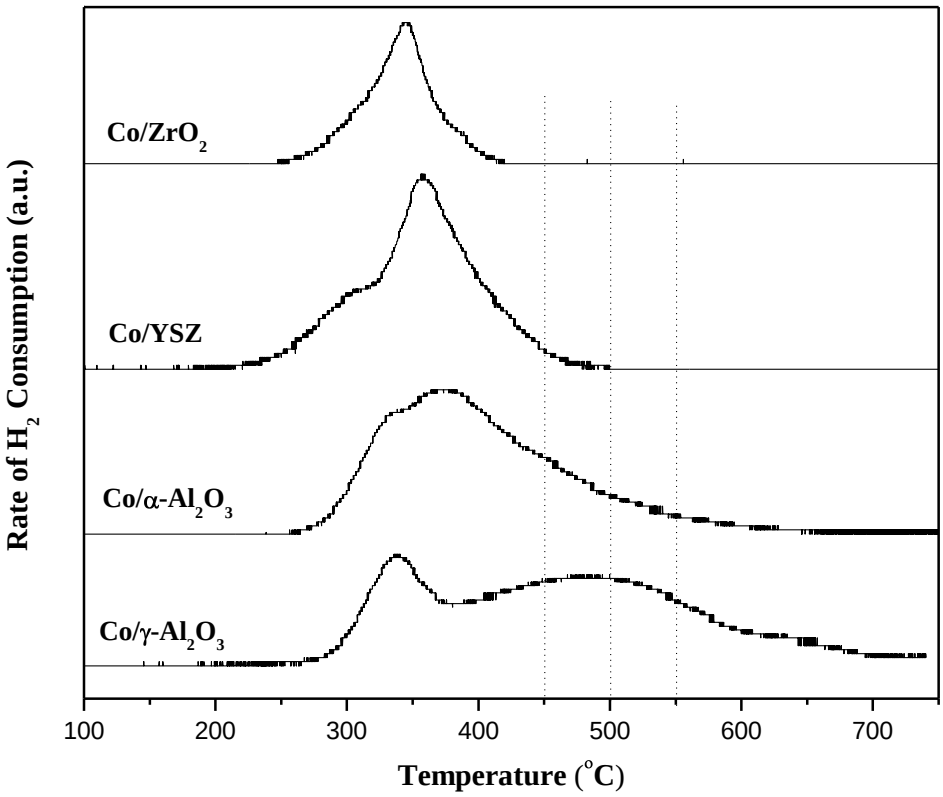

Figure 6-4: TPR-H_2 of 10 wt.% cobalt supported on (γ-Al_2O_3, α-Al_2O_3, ZrO_2 and YSZ)

Table 6-4: Total H_2 consumption over 10 wt. % nickel and cobalt catalyst on various supports.

Catalyst	Temperature span (°C)	Total H_2 Consumption (integration up to 700°C)	
		$\frac{\mu mol\ H_2}{g\ Cat.}$	$\frac{mol\ H_2}{mol\ Ni^o\ or\ Co^o}$
Nickel Catalyst			
N-γAl_2O_3	330 –650	1155	0.68
Ni-αAl_2O_3	360 - 540	1101	0.65
Ni-ZrO_2	280 - 425	614	0.36
Ni-YSZ	280 - 480	852	0.50
Cobalt Catalyst			
Co-γAl_2O_3	250 - 700	1815	1.07
Co-αAl_2O_3	250 - 650	1646	0.97
Co-ZrO_2	250 - 425	861	0.51
Co-YSZ	220 - 500	1332	0.78

Cobalt is known to have two common stable oxidation states: Co^{3+} and Co^{2+}. Co_3O_4 is the common cobalt state present when using cobalt nitrate hexahydrate precursor (Arnoldy and Moulijn (1985); Hilmen et al. (1999); Zhang et al. (2003)). In addition, CoO is not stable in the presence of oxygen at temperatures between 327°C and 727ºC (Arnoldy and Moulin (1985). Therefore, we should expect Co to be only in the Co_3O_4 state for calcined catalyst, which was confirmed through XRD analysis (not shown here). Table 6-4 shows that the cobalt catalysts start reducing at lower temperatures than the nickel one, especially for the alumina supports. For the zirconia-based supports the temperatures at which cobalt and nickel catalysts are completely reduced are close (425°C for ZrO_2 and around 500°C for YSZ).

Table 6-4 also indicates that the amount of hydrogen consumption for the cobalt catalysts is higher than for the nickel catalysts (56% higher for YSZ, 40% higher for ZrO_2 and 49% α-Al_2O_3). This is expected because of the higher oxidation state of the cobalt oxide (Co_3O_4) than the nickel oxide (NiO). Many TPR-H_2 studies (Lin and Chen, 2004; Tuti and Pepe, 2007; and De La Peña O'shea et al. 2007) suggested the reduction of Co_3O_4 goes through CoO before reduction to metallic Co°, which corresponds to the following process:

$$Co_3O_4 \xrightarrow{H_2} CoO \xrightarrow{H_2} Co \qquad (6\text{-}1)$$

Cobalt supported ZrO_2 shows a single peak over the temperature range 250 to 425°C. Meanwhile, Co on YSZ illustrates temperatures spanning from 200 to 500°C, and Co on ZrO_2 temperatures spanning from 225 to 425°C. This shows that Co/YSZ has lower starting reduction temperature and a wider span than Co/ZrO_2. Ni/ZrO_2 and Ni/YSZ have similar starting reduction temperatures of ~ 300°C. Therefore, these results suggest that higher number of oxygens in contact between the support and the metal oxide (Co_3O_4 vs. NiO) could lower the temperature at which reduction starts.

Cobalt on supported α-Al_2O_3 begins to reduce at 300°C and is complete at 650°C. The cobalt supported on γ-Al_2O_3 has a similar starting reduction temperature of 300°C, but complete reduction requires the highest temperature among all cobalt catalyst, as high as 700°C. For Co/γ-Al_2O_3 two peaks were observed at 320°C and 500°C, which is comparable to what is given by Zhang et al. (2003) and Batista et al. (2004). Batista et al. (2004) also reported that Co_3O_4 is the only phase present over Co/γ-Al_2O_3 calcined at around 600°C. Similarly to Ni/γ-Al_2O_3, Co/γ-Al_2O_3

possesses some sites with stronger interactions between Co_3O_4 and γ-Al_2O_3 surface than for the other cobalt catalyst. However, the chance to have cobalt aluminate spinel ($CoAl_2O_3$) in our catalyst is small due to its low calcination temperature, 550°C. Indeed, it was reported that $CoAl_2O_3$ is present only for calcination at 600°C and above (Arnoldy and Moulin, 1985). Also as reported in section 6.2.1, the acidity of γ-Al_2O_3 is stronger than that of α-Al_2O_3 due to the presence of Brønsted acid sites. The difference in acidity between α-Al_2O_3 and γ-Al_2O_3 is suspected to make Co/α-Al_2O_3 easier to reduce than Co/γ-Al_2O_3. Zhang et al. (2003) indeed recognized the significance of the number of acid sites in the reducibility of cobalt. They reported that strong acid sites on γ-Al_2O_3 would result in stronger bonding between cobalt and the γ-Al_2O_3 surface.

6.3 Catalytic Performance

The catalysts considered were either nickel or cobalt, supported on α-Al_2O_3, γ-Al_2O_3, ZrO_2 or YSZ. The catalyst screening study was conducted under the following conditions: 250 bar, 5wt.% ethanol, 1.88 g/min feed, and four levels of temperature (475°C, 500°C, 525°C, and 550°C). For temperatures below 475°C, very little conversion was observed and above 550°C, often the experiments had to be terminated due problems with plugging, likely because of coke particles on the metal screen.

The complete experimental schedule is shown in Table 6-5. Several experiments were repeated to quantify the reproducibility, and the experiments were carried out in a random order. The carbon balances obtained from analysis of both gas and liquid products were around 100±10%. The experiments that failed (usually because of plugging or BPR problems) were repeated several times to confirm whether it failed due to coking, catalyst break-up, or a back-pressure regulator problem. In order to identify the reason for plugging (coking or catalyst break-up), the following test was performed after the reactor plugged: air was fed for 1 hour at reaction temperature to burn out any possible coke on the screen or on the catalyst surface. The pressure was increased back to 250 bar by pumping water in order to see if plugging still occurs. If the system still has a problem, likely it is plugged due to catalyst break-up.

Table 6-5: Experimental schedule

Sample #	Date	Active metal	Support	Temperature (°C)
1	Nov 1, 2007	Ni	γ-Al_2O_3	500
2	July 9, 2008 (rep.)	Ni	γ-Al_2O_3	500
3	Nov 2, 2007	Ni	α-Al_2O_3	500
4	Nov 9, 2007 (rep.)	Ni	α-Al_2O_3	500
5	Dec 1, 2007	Ni	ZrO_2	500
6	May 26, 2008 (rep.)	Ni	ZrO_2	500
7	Jan 7, 2008	Ni	YSZ	500
8	Nov 14, 2007	Co	γ-Al_2O_3	500
9	Nov 18, 2007	Co	α-Al_2O_3	500
10	Nov 29, 2007	Co	ZrO_2	500
11	May 29, 2008 (rep.)	Co	ZrO_2	500
12	Jan 7, 1008	Co	YSZ	500
13	July 15, 2008	Ni	γ-Al_2O_3	475
14	July 16, 2008 (rep.)	Ni	γ-Al_2O_3	475
15	July 24, 2008	Ni	α-Al_2O_3	475
16	July 17, 2008	Ni	ZrO_2	475
17	July 22, 2008	Ni	YSZ	475
18	Aug 4, 2008	Co	γ-Al_2O_3	475
19	Aug 5, 2008	Co	α-Al_2O_3	475
20	Aug 12, 2007	Co	ZrO_2	475
21	Feb 7, 2008	Co	YSZ	475
22	July 14, 2008	Ni	γ-Al_2O_3	525
23	July 16, 2008 (rep.)	Ni	γ-Al_2O_3	525
24	July 25, 2008	Ni	α-Al_2O_3	525
25	May 28, 2008	Ni	ZrO_2	525
26	July 21, 2008	Ni	YSZ	525
27	July 24, 2008	Co	γ-Al_2O_3	525
28	July26, 2008	Co	α-Al_2O_3	525
29	May 29, 2008	Co	ZrO_2	525
30	Feb 11, 2008	Co	YSZ	525
31	May 1, 2008 (rep.)	Co	YSZ	525
32	June 26, 2008	Ni	γ-Al_2O_3	550
33	June 27, 2008	Ni	α-Al_2O_3	550
34	June 25, 2008	Ni	ZrO_2	550
35	June 24, 2008	Ni	YSZ	550
36	Feb 29, 2009 (rep.)	Ni	YSZ	550
37	July 20, 2008	Co	γ-Al_2O_3	550
38	July 19, 2008	Co	α-Al_2O_3	550
39	May 29, 2008	Co	ZrO_2	550
40	Sept. 21, 2008 (rep.)	Co	ZrO_2	550
41	May 9, 2009 (rep.)	Co	ZrO_2	550
42	Feb 12, 2008	Co	YSZ	550
43	May 23 2008	Co	YSZ	550

6.3.1 Ethanol Conversion

Results of the Time-on-Stream

In this section, ethanol conversions as a function of time-on-stream are presented and discussed for all active metal/support combinations considered in the experimental plan. All experiments were carried out for 4.5 hours (unless problems occurred). This was done to not only check for short-term catalyst stability, but also to wait until the catalyst system reaches steady-state. The catalyst was not pre-reduced in H_2/N_2 mixtures prior to injecting ethanol. Figure 6-5 to Figure 6-8 illustrate the ethanol conversion as a function of the time-on-stream over the nickel and cobalt catalysts at four temperatures. Figures 6-5, 6-6, 6-7 and 6-8 are for γ-Al_2O_3, α-Al_2O_3, ZrO_2 and YSZ, respectively.

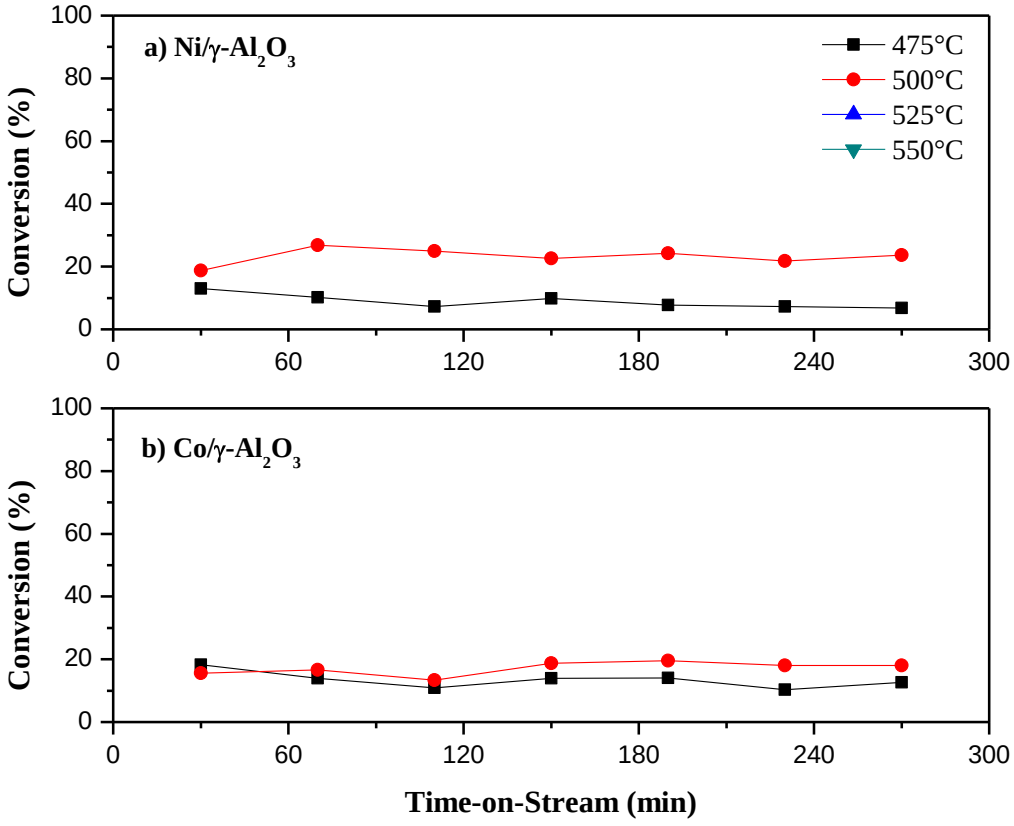

Figure 6-5: Ethanol conversion as a function of time-on-stream over a) 10% wt. Ni/γ-Al_2O_3 and b) 10% wt. Co/γ-Al_2O_3 at 475, 500 and 525, 550ºC. 1 g non-reduced catalyst, 5% wt. ethanol, 1.88 g/min feed and 250 bar.

Figure 6-5 shows the results for the Ni/γ-Al_2O_3 and Co/γ-Al_2O_3 at 475 and 500ºC only. The experiments at 525 and 550ºC over these catalysts failed soon after injecting ethanol, because of coking. The ethanol conversions for both catalysts at 475ºC and 500ºC are stable over 4.5 hours, but are low: at 475°C the conversion for Ni and Co is around 10%, whereas at 500°C it is around 20% for Ni and slightly below 20% for Co (ca. 18%). The conclusion is that the non-reduced nickel and cobalt supported on γ-Al_2O_3 are not promising catalysts for ethanol reforming in SCW: both suffer from coking and very low activity.

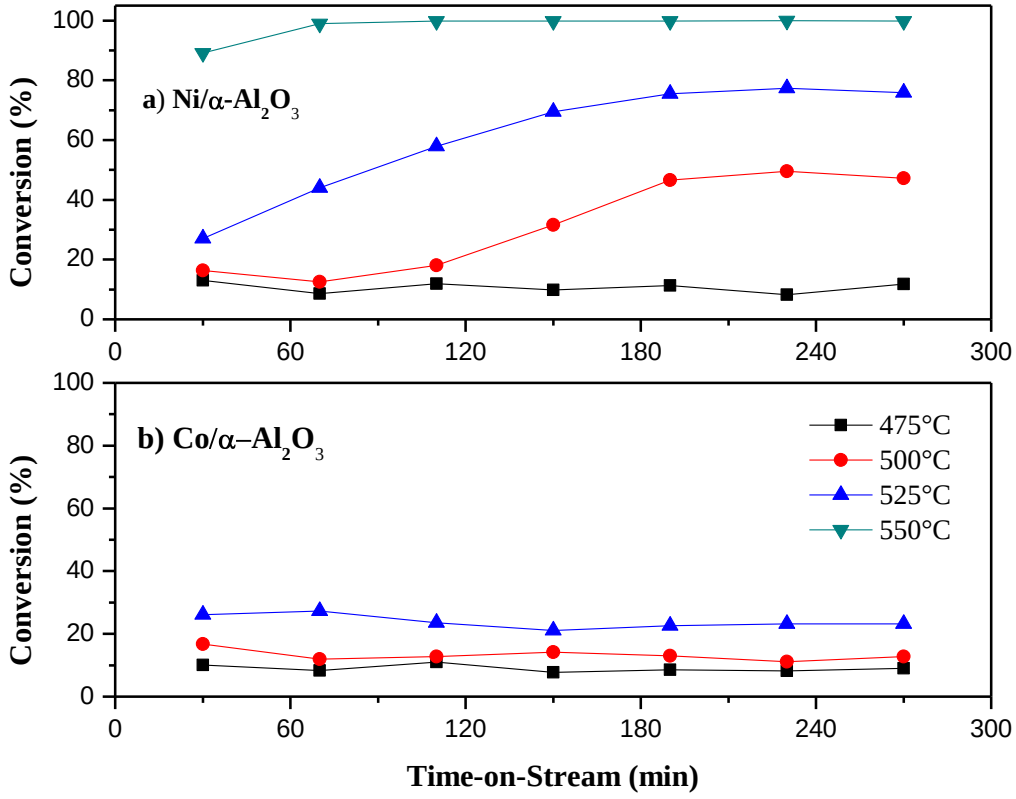

Figure 6-6: Ethanol conversion as a function of time-on-stream over a) 10% wt. Ni/α-Al_2O_3 and b) 10% wt. Co/α-Al_2O_3 at 475, 500 and 525, 550ºC. 1 g non-reduced catalyst, 5% wt. ethanol, 1.88 g/min feed and 250 bar.

Figure 6-6 shows the conversion for nickel and cobalt catalysts supported on α-Al_2O_3. Experiments for nickel supported on α-Al_2O_3 could be done successfully at all temperatures. But for Co/α-Al_2O_3 the experiment at 550°C failed due to coking. This experiment was repeated three times but failed each time, confirming that failure was not due to precedural problems. At 475ºC, the conversions of Ni/α-Al_2O_3 and Co/α-Al_2O_3 are stable for the time of the study at ~10%. At

500°C and above the Ni and Co catalysts behave differently. The activity of the Co/α-Al_2O_3 increases only slightly with temperature (~12% at 500ºC and ~20% at 525ºC), but, as mentioned above, severe coking problems occurred at 550ºC. The behaviour of the Ni/α-Al_2O_3 catalyst is much different from the cobalt one. The results show that, at temperature above 500°C, the conversion first increases with time-on-stream and then plateaus. The conversion values at the plateaus increase with temperature and are much higher than those obtained with Co/α-Al_2O_3: at 500°C, the conversion stabilizes at ~40% after 3 hours (180 mins); at 525°C, the conversion stabilizes at ~75% also after 3 hours; and at 550°C, the conversion reaches a plateau of 100% after one hour. The increase in conversion over time for Ni/α-Al_2O_3 indicates that the catalyst activity is improving over time. We attribute this to reduction of NiO occurring while the reforming reaction proceeds due to hydrogen produced. This behaviour was not observed with Co/α-Al_2O_3, indicating that reduction of Co/α-Al_2O_3, while the reforming reaction proceeds, is much slower than for Ni/α-Al_2O_3.

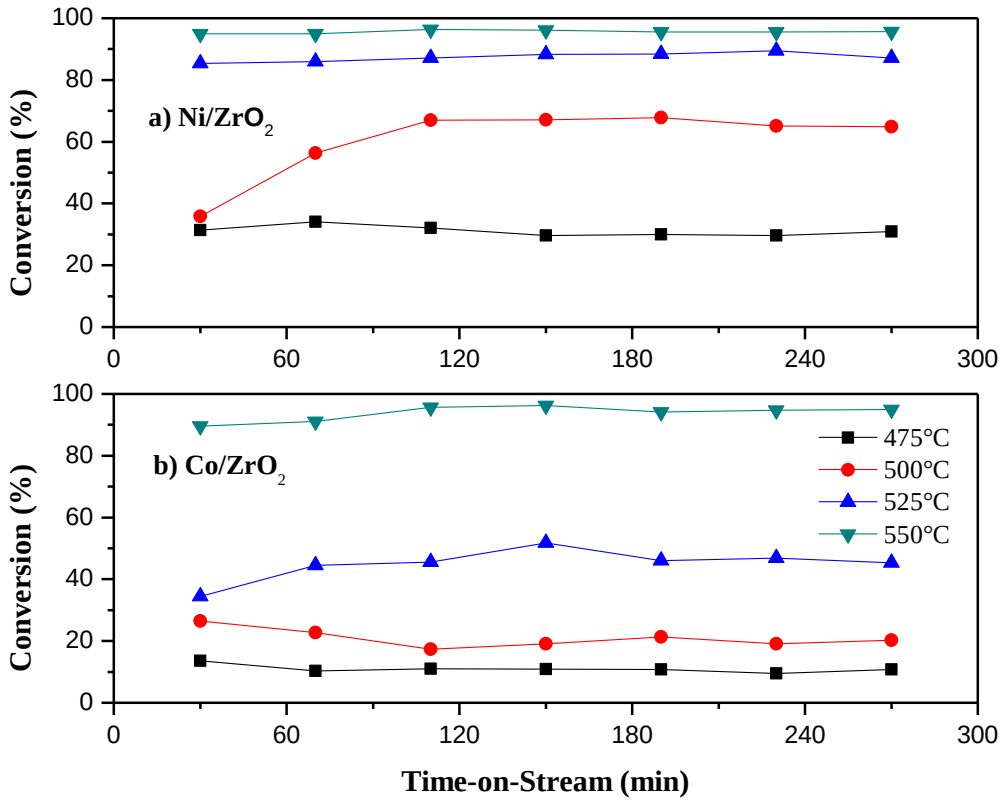

Figure 6-7: Ethanol conversion as a function of time-on-stream over a) 10% wt. Ni/ZrO_2 and b) 10% wt. Co/ZrO_2 at 475, 500 and 525, 550ºC. 1 g non-reduced catalyst, 5% wt. ethanol, 1.88 g/min feed and 250 bar.

Figure 6-7 shows the ethanol conversion for the nickel and cobalt catalysts supported on zirconia. For all conditions studied no coking problem occurred for both Ni/ZrO_2 and Co/ZrO_2. However, for Co/ZrO_2 at 550°C there have been several instances of catalyst break-up followed by problem with the BPR (only one out of four experiments at 550°C was successful). Even at 525°C, although the experiments were all successful, it was visible that the catalyst particles were broken into smaller sizes. A similar observation was made for Ni, but to a lesser extent. Clearly, ZrO_2 appears the most fragile support of all considered here, especially above 500°C.

For Ni/ZrO_2 the steady-state conversion was achieved within 30 mins time-on-stream (first GC injection) at 525 and 550°C. The result at 500°C shows a gradual increase in conversion until it reaches a plateau after about 90 minutes. At 475°C the conversion remained low and constant at ~30%. The steady-state conversion increases in temperature as follows: ~65% at 500°C, ~85% at 525°C and ~95% at 550°C. The activity of Co/ZrO_2 is lower than that of Ni/ZrO_2. The conversion is only 10% at 475°C, 20% at 500°C and 50% at 525°C. However, at 550°C the conversions for both Co/ZrO_2 and Ni/ZrO_2 are the same, reaching 95%. Furthermore, at 525°C, we can observe that the conversion over Co/ZrO_2 increases slightly with time-on-stream for the first 2 hours and then stabilizes. Again, as for the other supports the result indicates that the nickel catalyst is more active than the cobalt one.

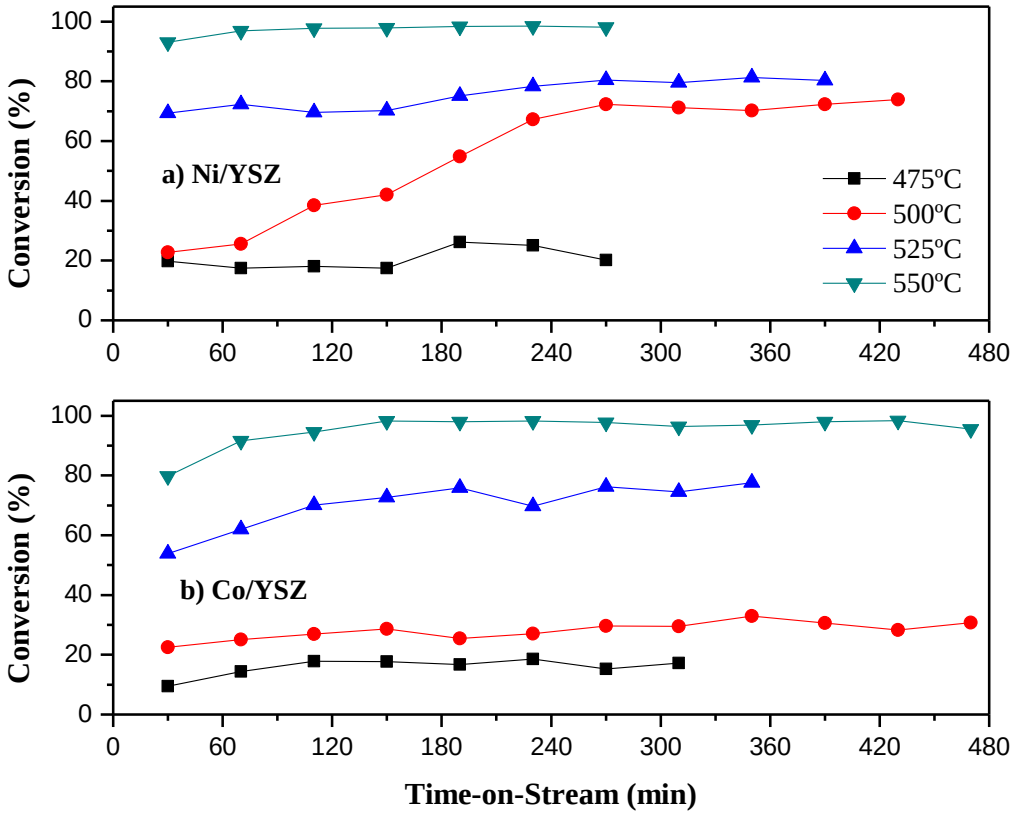

Figure 6-8: Ethanol conversion as a function of time-on-stream over a) 10% wt. Ni/YSZ and b) 10% wt. Co/YSZ at 475, 500 and 525, 550ºC. 1 g non-reduced catalyst, 5% wt. ethanol, 1.88 g/min feed and 250 bar.

Figure 6-8 illustrates the conversion of ethanol over the nickel and cobalt catalysts supported on YSZ. The experiments for all catalysts supported on YSZ were successful at all temperatures, without encountering any coking or catalyst break-up. At 475°C, the conversion over Ni/YSZ is relatively stable around ~20%, higher than that of Co/YSZ at the same temperature (~10%). At 500°C, the conversion over Ni/YSZ increases with time-on-stream from 20% after 30 min up to 65% after 4 hours. Additional data were actually collected beyond 4.5 hours and were around 65%. In contrast to Ni/YSZ, the conversion over Co/YSZ shows a very small increase with time-on-stream at 500°C, reaching ~30% after 4 hours. At 525°C, the conversion over Ni/YSZ increases only slightly with time-on-stream, after 30 min from ~70% (30 minutes) to ~80% after 4.5 hours. For Co/YSZ, the conversion at 525°C is smaller than over Ni/YSZ at the beginning, but increases with time-on-stream to reach a stable conversion of 74% (similar to Ni/YSZ) after 3

hours. At 550°C the conversion is almost 100% after 60 minutes and 90 minutes for Ni/YSZ and Co/YSZ, respectively.

Comparison between Catalysts (Conversion and Selectivity)

Before comparing the catalysts in term of conversion, we briefly report the change in catalyst weight before and after the experiments. This is used to assess whether part of the catalyst is lost during experiment (e.g., via breaking up into small particles or via dissolution). Table 6-6 show the percentages of the weight loss (between fresh loaded catalyst and spent catalyst) and the fraction of catalyst particles whose size is less than 1.0 mm after experiments at 500°C. Recall that the particles size of the fresh catalyst is between 1.0 and 1.4 mm. One should also note that the error in weight loss measured when loading and unloading fresh catalyst (typically 1 g) from the reactor is between 1 and 2%. Cobalt supported on zirconia shows the highest weight loss, followed by nickel supported on zirconia. This is consistent with the observation described before regarding the breakup of ZrO_2 based catalyst in smaller particles. The catalysts supported on YSZ are much stronger than those supported on zirconia.

Table 6-6: Percentages of the weight lose and the particles size less than 1.0 mm after the experiment at 500°C, 250bar, 1 g catalyst, 1.88 g/min feed, and 5% wt. ethanol.

Catalyst	Weight loss (wt%)	particles size (< 1.0 mm) (wt%)
Ni/γ-Al_2O_3	4	4
Ni/α-Al_2O_3	3	5
Ni/ZrO_2	9	10
Ni/YSZ	4	5
Co/γ-Al_2O_3	6	4
Co/α-Al_2O_3	5	3
Co/ZrO_2	19	18
Co/YSZ	4	6

The time-on-stream results presented in the previous section show that, for all successful conditions, the conversion reaches steady-state after at most 3 hours time-on-stream. The catalysts will therefore be compared using average over at least three points after 3 hours time-on-stream,

referred to thereafter as the steady-state condition. The ethanol conversions at steady state over the Ni and Co catalysts, as a function of temperature are presented in Figure 6-9. For comparison purposes, this figure also shows the results with the empty reactor.

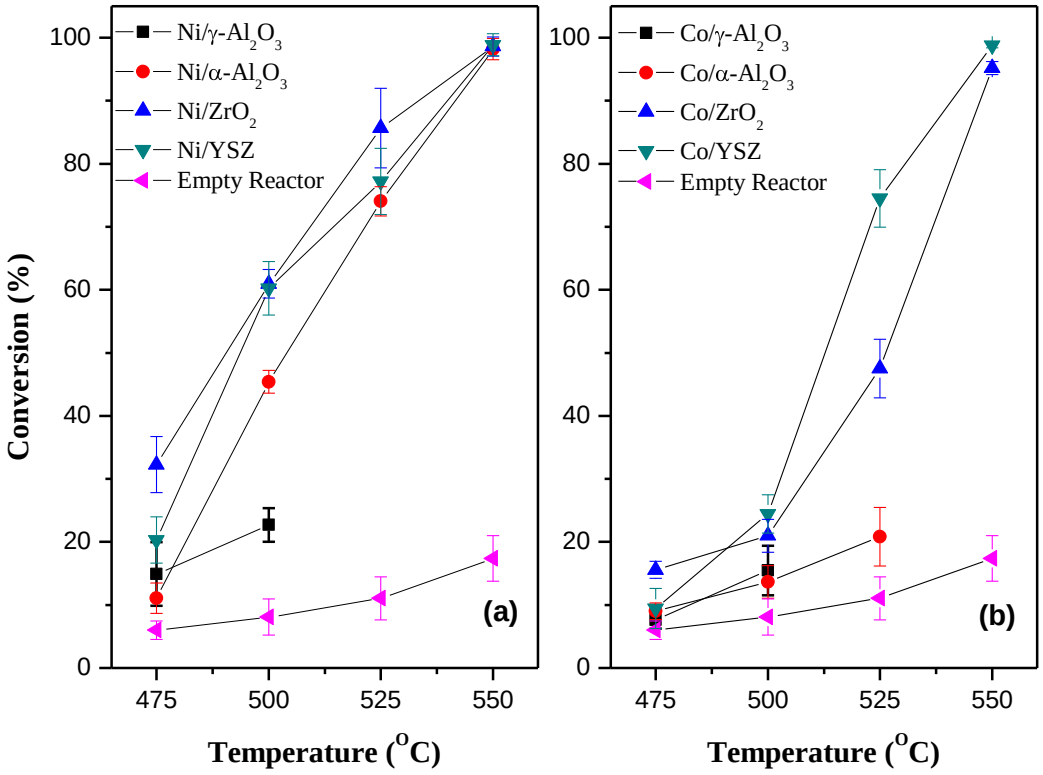

Figure 6-9: Effect of temperature on the ethanol conversion over a) Nickel-based catalyst, and b) Cobalt-based catalyst (250 bar, 1.88 g/min, 5 wt %, 1 g catalyst, no reduction).

The data for Ni and Co on γ-Al_2O_3 are not shown for temperatures above 500°C because of unavoidable coking problems leading to plugging of the reactor. Similarly, data for Co/α-Al_2O_3 are not shown for temperatures above 525°C. Overall, at a given temperature, the ethanol conversion over nickel catalyst is higher than that over cobalt catalyst, with the exception of 550°C where the conversion is close to 100% for both active metals. At 475°C the conversions over the cobalt catalysts are very close to that obtained with the empty reactor (6%), indicating that cobalt has little to no activity at 475°C. Nickel shows increasing activity at 475°C depending on the support according to the following order: α-Al_2O_3,γ-Al_2O_3<YSZ<ZrO_2. Nonetheless, the conversion at 475ºC remains below 30% for Ni/ZrO_2.

At 500°C, the ethanol conversion show significant differences between each nickel catalyst. The conversion of nickel over ZrO_2 and YSZ is quite similar (around 60%), but it is lower over the alumina supports, with the conversion over α-Al_2O_3 (~45%) much greater than over γ-Al_2O_3 (~22%). At 500°C, the conversions over the cobalt catalyst on various supports are still low (between 10 to 25%). Similar to nickel, higher conversion over the cobalt catalyst were obtained with the ZrO_2 and YSZ supports.

At 525°C, the conversions reaches 75 to 85%, with the α-Al_2O_3 still yielding the lower conversion. For nickel the conversion over ZrO_2 is higher than over YSZ. However, for cobalt, the opposite was observed. The conversion over Co/α-Al_2O_3, Co/ZrO_2 and Co/YSZ are 20, 48 and 74%, respectively. Thus, the significance of the support for cobalt catalyst becomes more important at 525ºC. The experiment without catalyst at 525°C is only 12%.

At 550°C, the nickel catalysts achieve 100% the conversion over all supports, except the failed catalyst supported on γ-Al_2O_3. By comparison, the conversion with empty reactor is only about 18%. With cobalt both alumina supports led to failed experiments due to coking and subsequent plugging. A conversion of nearly 100% was obtained at 550°C with the Co/YSZ, whereas with Co/ZrO_2, the conversion was slightly lower at 95%. These results show that all working catalysts are active and able to convert nearly all of the ethanol at 550°C.

6.3.2 Selectivities

In this study the products detected in the gas phase (GC #1, TCD) are: H_2, CH_4, CO, CO_2, C_2H_4 and C_2H_6. The products detected in the liquid phase (GC #2, FID) are ethanol, acetaldehyde and small amounts of acetone and diethyl ether. Refer to Chapter 3 for the definition of selectivity (equation 3.9). The selectivities of each detected species for all catalysts as a function of temperature are shown in Figure 6-10 to Figure 6-17. The selectivities presented here are calculated under the steady-state conditions, as defined in the previous section.

H_2 selectivity:

The results for H_2 selectivity are shown in Figure 6-10. Except for the catalyst supported on γ-Al_2O_3, H_2 selectivity for all other catalysts is above 50%. For Ni/γ-Al_2O_3 and Co/γ-Al_2O_3 the H_2 selectivity is much lower, only 20-25% and 10-12%, respectively in the 475-500°C range. Hydrogen selectivity over Ni/α-Al_2O_3 and Ni/YSZ decreases with temperature; in the temperature range 475-550°C, H_2 selectivity decreases from ~74% to ~48% for Ni/α-Al_2O_3 and from ~78 to ~55% for Ni/YSZ. For Ni/ZrO_2 the selectivity does not vary much with temperature and stays at a value around 55%. Hydrogen selectivity over Co/YSZ decreases with temperature (from 72% at 475°C to 64% at 550°C), which is a similar trend to that for Ni/YSZ. The H_2 selectivity over Co/ZrO_2 decreases with temperature (from 72% at 475°C to 60% at 550°C); in the case of Ni/ZrO_2, the H_2 selectivity was not affected by temperature. In the case of Co/α-Al_2O_3 the observed trend for H_2 selectivity is the opposite to that observed for Ni/α-Al_2O_3. For Co/α-Al_2O_3, the H_2 selectivity increases with temperature (from 39% at 475°C to 56% at 525°C). Overall, above 500°C, the H_2 selectivity with the cobalt catalyst is somewhat higher than that with the nickel catalyst. Comparison between supports shows that the YSZ support is usually better in terms of H_2 selectivity for both Co and Ni, although in the case of nickel, similar H_2 selectivities were obtained with ZrO_2. Bellido and Assaf (2007) showed that H_2 selectivity over nickel supported on YSZ is higher than over nickel supported ZrO_2. Thermodynamic show that in the temperature range considered here, the ethanol should be fully converted. However, our experimental results achieved near 100% conversion only at 550°C. Therefore, we will compare the equilibrium selectivity with the experimental data only at 550°C. The thermodynamic calculation at 550°C gives a H_2 selectivity of 44%, which is lower that was obtained experimentally, especially for the Co catalyst (around 60-65% H_2 selectivity at 550°C). For Ni, the H_2 selectivity is still higher than the thermodynamic calculation, but closer (around 50%). Another observation is that thermodynamically, the H_2 selectivity increases with temperature, whereas in the experiments the opposite was observed (with the exception of Co/α-Al_2O_3). Clearly, at the conditions of experiments presented here, equilibrium was not reached.

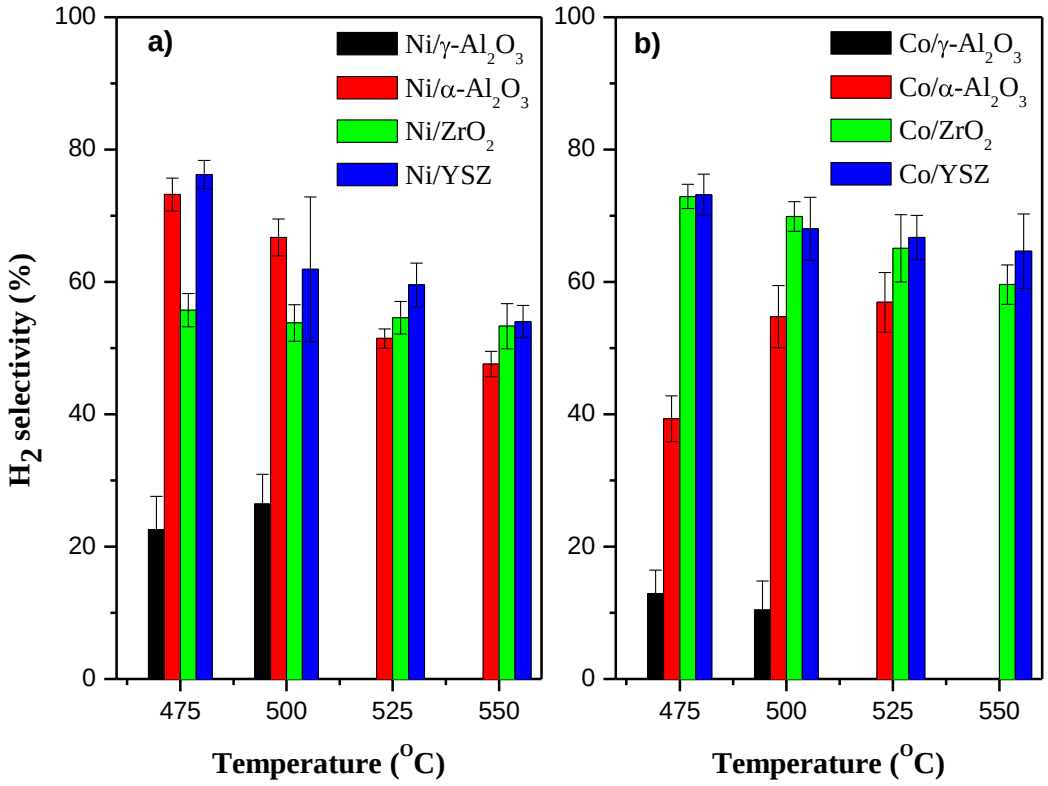

Figure 6-10: Hydrogen selectivity at different temperatures for a) Nickel catalysts and b) Cobalt catalysts (250 bar, 5 wt. % ethanol).

CO_2 Selectivity:

Figure 6-11 shows the CO_2 selectivity. After H_2, CO_2 is the second species in importance produced from ethanol reforming in supercritical water. For all catalysts CO_2 selectivity increases when temperature increases. With γ-Al_2O_3 supports, it was not possible to run the experiments at temperatures higher than 500°C for both nickel and cobalt. The use of Ni or Co on the zirconia-based support leads on similar CO_2 selectivity (maybe slightly higher CO_2 selectivity with Ni). However, for the α-Al_2O_3 support the CO_2 selectivity is significantly higher with Ni than with Co at temperatures higher than 525°C. At 550°, where the conversion is nearly complete, CO_2 selectivity reaches 25% for nickel catalysts and 22% for cobalt catalysts. The CO_2 selectivity obtained at 550°C (for both nickel and cobalt) is actually close to that at equilibrium (25%, see Figure 4-2).

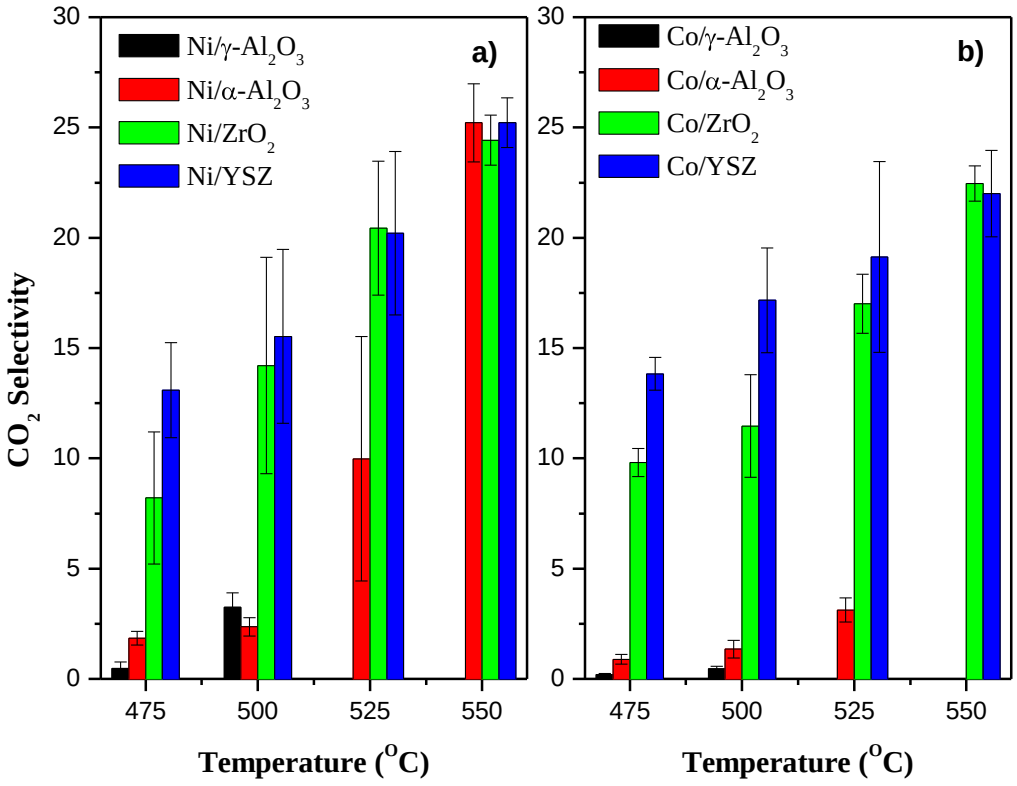

Figure 6-11: CO_2 selectivity at different temperatures for a) nickel catalyst and b) cobalt catalyst (250 bar, 5 wt. % ethanol, 1 g catalyst, 1.88 g/min)

CO selectivity:

Figure 6-12 shows the CO selectivity. At 475°C, except for Ni/ZrO_2, the CO selectivity is low (0.5% and below). For Ni/ZrO_2, the CO selectivity is much higher at 475°C, being greater than 6%. At 500°C, the CO selectivity over Ni/ZrO_2 remains much higher than its Co counterpart, but at 500°C they are equivalent and finally at 550°C, Co/ZrO_2 leads to higher CO selectivity. The selectivity of CO for all nickel catalysts shows first an increase with increasing temperature, followed by a sharp decrease beyond 500°C for Ni/ZrO_2 and Ni/YSZ, and beyond 525°C for Ni/α-Al_2O_3. For the cobalt catalysts the trend is more like a continuous increase in CO selectivity when increasing the temperature up to 500°C. At 550°C, where the conversion is almost complete, the CO selectivity for most catalysts (Ni/α-Al_2O_3, Ni/ZrO_2, Ni/YSZ and Co/YSZ)is near 0.5%, with the notable exception of Co/ZrO_2 for which the CO selectivity is up to 2%. The value of 0.5% is actually similar to that determined from thermodynamic calculation (0.3%).

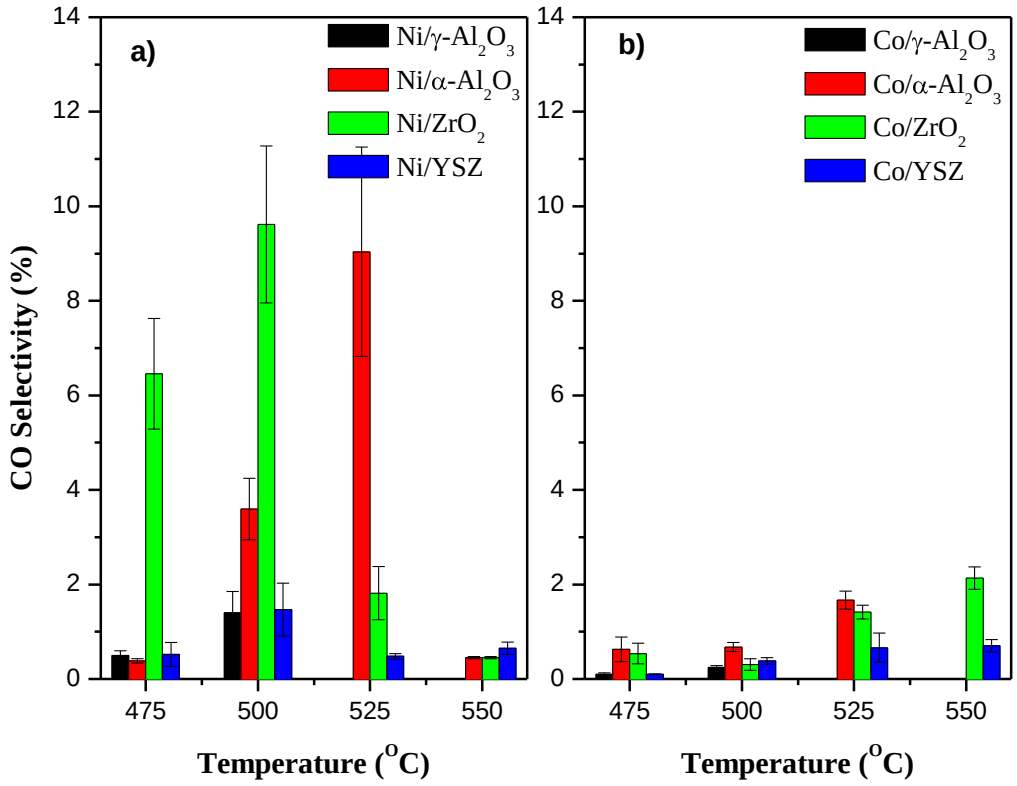

Figure 6-12: CO selectivity at different temperatures for a) nickel catalyst and b) cobalt catalyst (250 bar, 5 wt. % ethanol, 1 g catalyst)

CH_4 selectivity:

The results for CH_4 selectivity are shown in Figure 6-13. Overall, cobalt catalysts demonstrate lower selectivity toward CH_4 than nickel catalyst. For both active metals the CH_4 selectivity increases with increasing temperature. At 550°C (where conversion is nearly complete), nickel on α-Al_2O_3, ZrO_2 and YSZ yield a CH_4 selectivity between 18 and 20%. Both Ni/ZrO_2 and Ni/YSZ provide 18% CH_4 selectivity at 525°C. At 475°C, most Ni catalysts produce low amounts of methane: CH_4 selectivity below 2%, except for Ni/ZrO_2 with CH_4 selectivity around 10%. At 475 and 500°C, the cobalt catalysts CH_4 selectivity is low: around 1% for Co on γ-Al_2O_3, ZrO_2 and YSZ and about 2% for α-Al_2O_3. At 525°C and above the CH_4 selectivity increases notably, especially for the Co/YSZ and Co/ZrO_2, reaching 11% and 14%, respectively, at 550°C (near complete conversion). The trend of increasing CH_4 selectivity with increasing temperature is opposite to what is expected thermodynamically (see Figure 4-2).

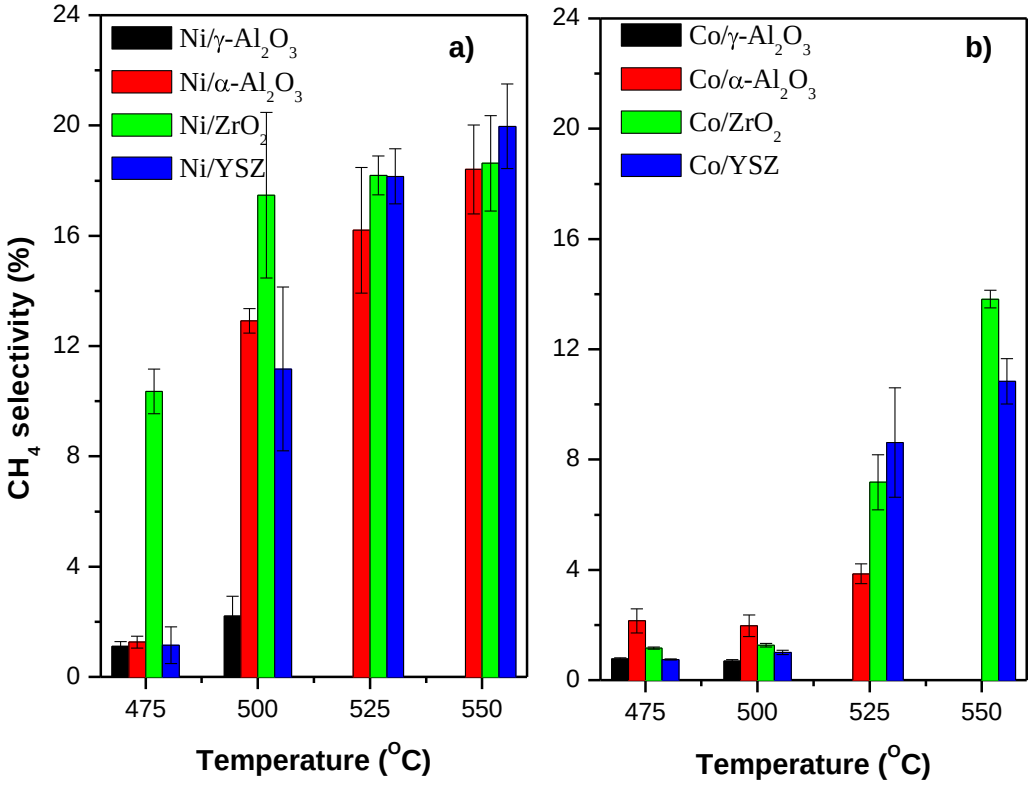

Figure 6-13: CH_4 selectivity at different temperatures for a) nickel catalyst and b) cobalt catalyst (250 bar, 5 wt. % ethanol, 1 g catalyst)

C_2H_4 Selectivity:

Figure 6-14 shows the C_2H_4 selectivity. For 475 and 500°C (at higher temperatures the experiments failed), the γ-Al_2O_3 support shows very high selectivity toward C_2H_4, and this for both Ni and Co active metals: C_2H_4 selectivities are between 35 and 45% for Ni/γ-Al_2O_3 and around 75% for Co/γ-Al_2O_3. For α-Al_2O_3, the C_2H_4 selectivity is significantly lower than for γ-Al_2O_3. For both Ni and Co on α-Al_2O_3, the C_2H_4 selectivity decreases with temperature but the C_2H_4 selectivity over Ni catalyst (from 1.1% at 475°C to 0.2% at 525°C) is much lower than over the Co catalyst (from 8.5% at 475°C to 6% at 525°C). For ZrO_2 and YSZ supports the C_2H_4 selectivity is less than 0.5% at all temperatures and is nearly zero at 550°C. In the case of Co/YSZ and Co/ZrO_2 at 550°C, the data are not shown in Figure 6-14, because the amount of C_2H_4 was below the detection limit. Thermodynamic calculations indicate that the C_2H_4 selectivity at 550°C is close to zero, as well.

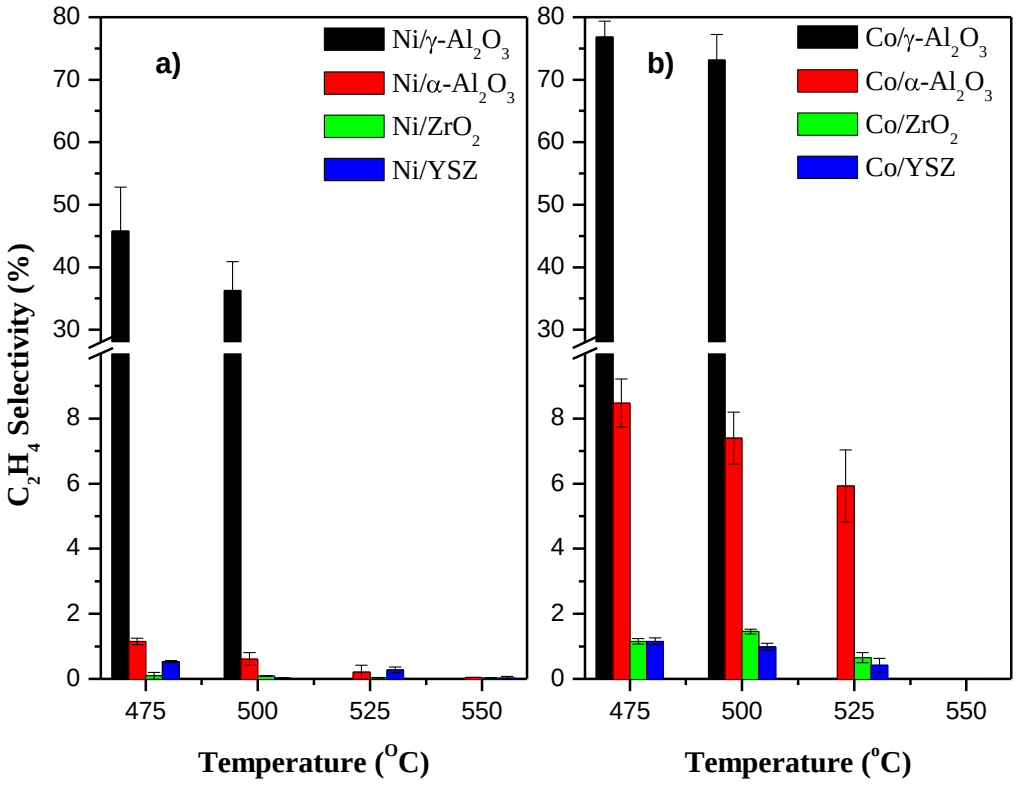

Figure 6-14: C_2H_4 selectivity at different temperatures for a) nickel catalyst, and b) cobalt catalyst (250 bar, 5 wt. % ethanol, 1 g catalyst, 1.88 g/min feed)

C_2H_6 Selectivity:

Figure 6-15 shows the C_2H_6 selectivity. Except for the Ni/γ-Al_2O_3, the selectivity of C_2H_6 is below 1.5%. The highest C_2H_6 selectivity is obtained with Ni/γ-Al_2O_3, with selectivities of 2.5% at 475°C and 4% at 500°C. In contrast, Co/γ-Al_2O_3 yields C_2H_6 selectivities of 1.1 and 1.4% at 475 and 500°C, respectively. For the α-Al_2O_3 support, the C_2H_6 selectivity is greater with Co (around 1-1.5%) than with Ni (lower than 0.5%). For ZrO_2 and YSZ, there is no clear trend for both Ni and Co, but in every case, the C_2H_6 selectivity remains below 0.5%. At the reaction conditions considered here, the C_2H_6 selectivity determined from thermodynamic calculation is near zero.

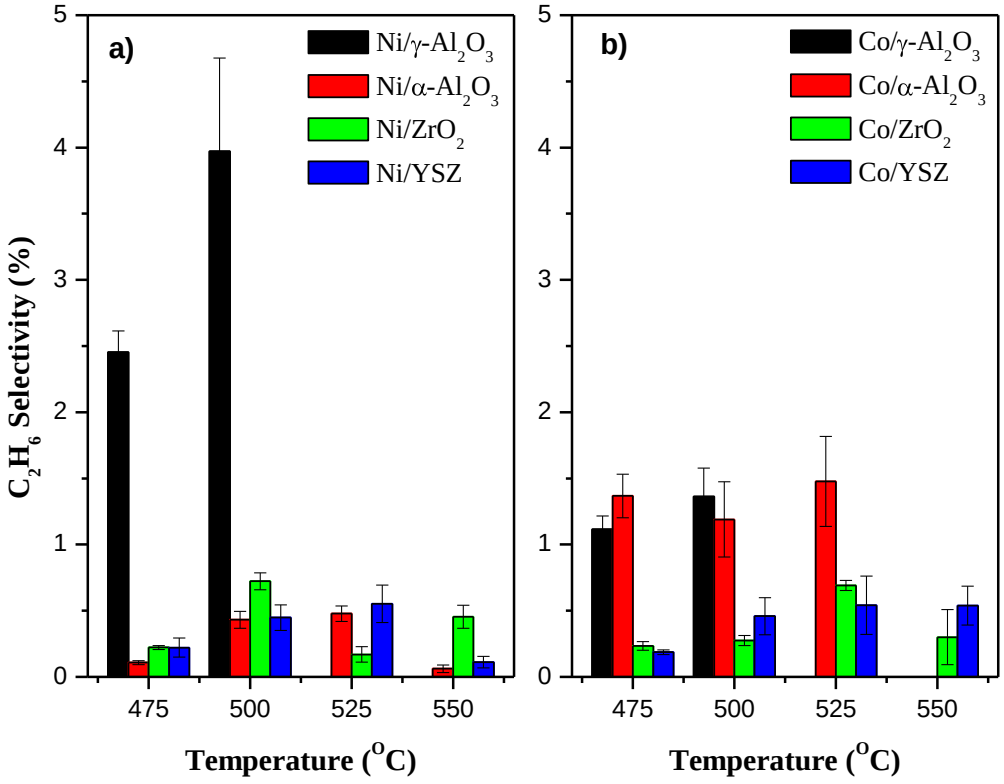

Figure 6-15: C_2H_6 selectivity at different temperatures for a) nickel catalyst and b) cobalt catalyst (250 bar, 5 wt. % ethanol, 1 g catalyst, 1.88 g/min feed)

Acetaldehyde (C_2H_4O) Selectivity:

Acetaldehyde selectivity is shown in Figure 6-16. For the α-Al_2O_3 support, the trend is identical for Ni and Co: acetaldehyde selectivity decreases with increasing temperature. However, in this case, the selectivity is much higher with Co (from 47% at 475°C to 26% at 525°C) than with Ni (from 20% at 475°C to 4% at 525°C). Acetaldehyde selectivity over Ni/γ-Al_2O_3 remains constant at 16% between 475 and 500°C (recall that experiments failed for temperatures above 500°C). In the case of Co/γ-Al_2O_3, the selectivity is 2% at 475°C, but increases up to 13% at 500°C. For the ZrO_2 support, using Co is much more selective toward acetaldehyde than using Ni: the acetaldehyde selectivity for Ni/ZrO_2 is close to zero for temperatures above 500°C, whereas for Co/ZrO_2 it decreases from 7% at 475°C to 4% at 525°C. On the other hand, for YSZ support the acetaldehyde selectivity is slightly greater with Ni than with Co. At 550°C, where the conversion is almost complete, almost no acetaldehyde was detected, which is consistent with thermodynamic calculation that shows no presence of acetaldehyde at 550°C.

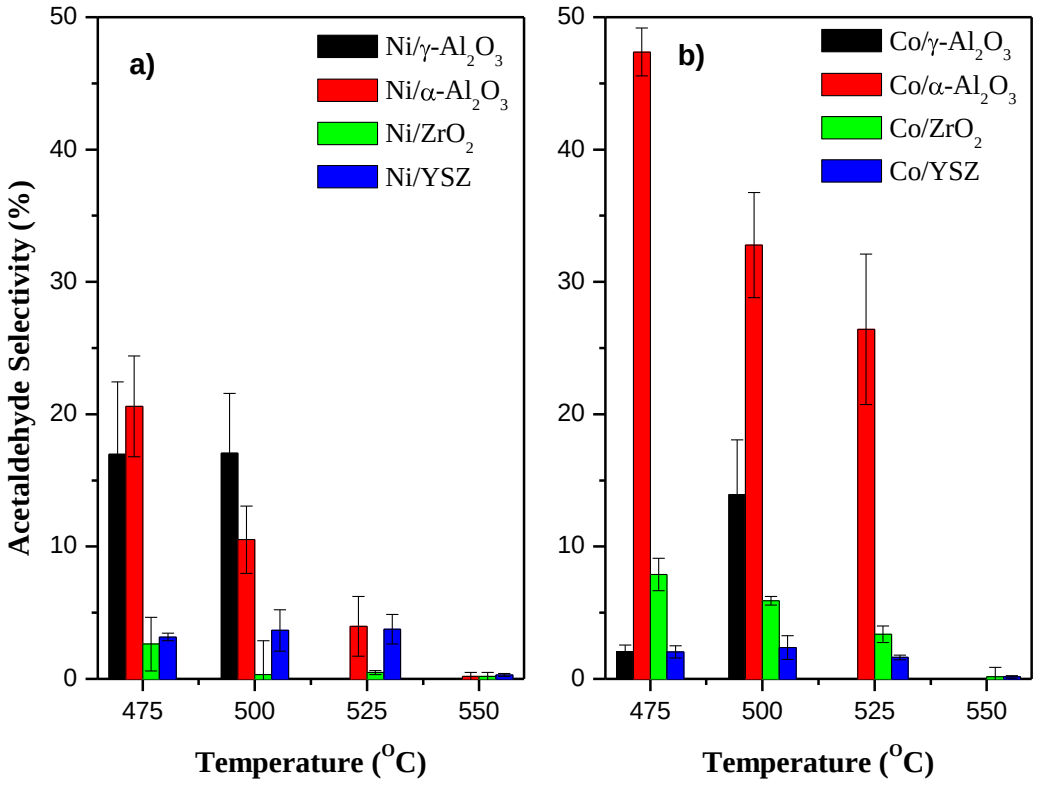

Figure 6-16: Acetaldehyde (C_2H_5O) selectivity at different temperatures for a) nickel catalyst and b) cobalt catalyst (250 bar, 5 wt. % ethanol, 1 g catalyst and 1.88 g/min feed)

Acetone (C_3H_6O) Selectivity:

Acetone selectivity is shown in Figure 6-17. For the alumina supports (α-Al_2O_3 and γ-Al_2O_3), no selectivity toward acetone was detected (or in very little in some cases with α-Al_2O_3). For Ni, ZrO_2 shows some selectivity toward acetone at 500°C, but none above this temperature. On the other hand, Ni/YSZ stands out because of the relatively high acetone selectivity compared to all other supports: the acetone selectivity was 6% at 475°C, then increases up to 12% at 500°C and finally decreases down to 3% at 525°C and almost zero at 550°C. With cobalt catalyst, the trends are clearer for both ZrO_2 and YSZ supports: acetone selectivity decreases when increasing temperature, and the YSZ support is consistently more selective toward acetone. The acetone selectivity for Co/YSZ decreases from around 9% at 475 and 500°C to 3% at 525°C and 2% at 550°C. For Co/ZrO_2, the decrease in acetone selectivity is as follows: 5%, 4%, 1.5% and 0.5% at 475, 500, 525 and 550°C, respectively.

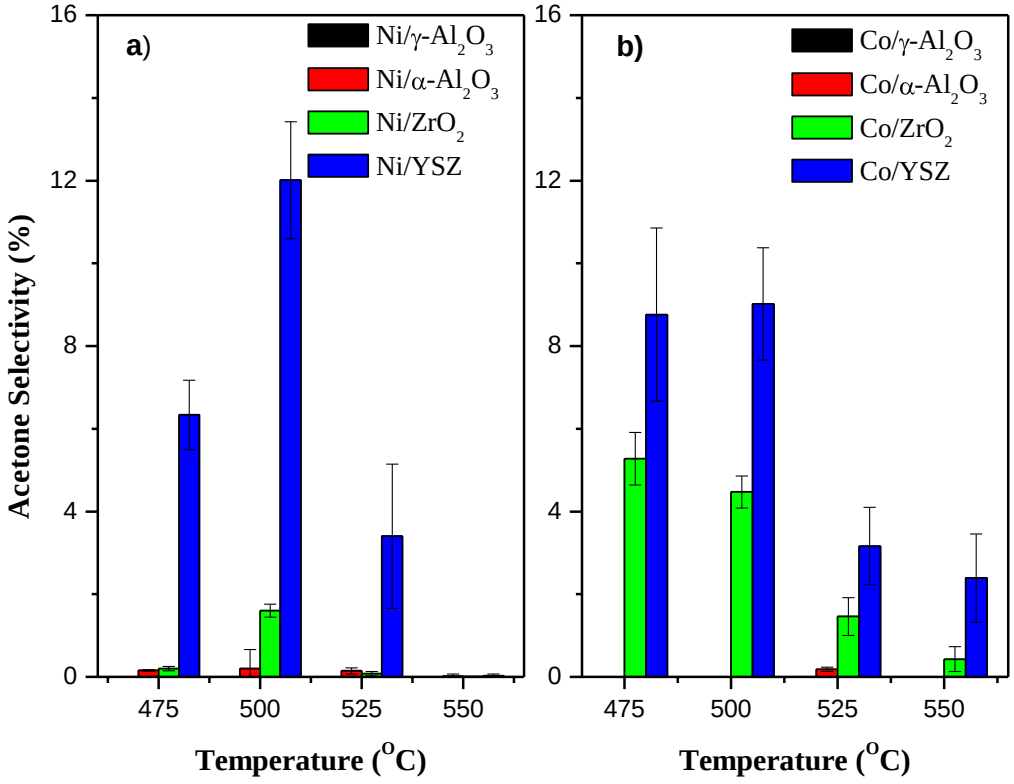

Figure 6-17: Acetone selectivity at different temperatures for a) nickel catalyst and b) cobalt catalyst (250 bar, 5 wt. % ethanol, 1 g catalyst, and 1.88 g/min feed)

6.3.3 Discussion

Activity

Figure 6-9 shows that the γ-Al_2O_3 support yields the lowest activity for both Ni and Co. The difference between the activities over both active metals on various supports can be related to the reducibility of Ni and Co. As seen on the TPR-H_2 in Figures 5.1 and 5.2, both metal oxides (NiO and Co_3O_4) catalysts require higher reduction temperatures when supported on γ-Al_2O_3 than on α-Al_2O_3, YSZ and ZrO_2 (in that order), indicating stronger bonding between NiO/Co_3O_4 and γ-Al_2O_3 than with other supports. Hence, the lower activity observed when using the γ-Al_2O_3 support, in particular with Ni (e.g., see data at 500°C in Figure 5.9). For cobalt at 500°C, the activity remains small, even with the other supports. Recall that the results shown in Figure 5.9 were for non reduced catalysts. The difference between the activity of cobalt and nickel may be attributed the higher demand in hydrogen to reduce Co_3O_4 ($Co_3O_4 + 4H_2 \rightarrow 3Co° + 4H_2O$) than to reduce NiO ($NiO + H_2 \rightarrow Ni° + H_2O$). From the above reaction, the theoretical consumption of H_2 to completely reduce Co_3O_4 should be 33% higher than to completely reduce NiO. The data for total H_2 consumption shown in Table 5-3 indicate that H_2 consumption over Co catalysts is between 42 and 57% higher than over Ni. This is not too far from the expected 33%.

Comparison between the conversions in Figure 6-9 and TPR-H_2 in Figures 5-1 and 5-2 shows a strong correlation between activity (conversion) and reducibility. As seen in Figures 5-1 and 5-2, at 475°C both Ni/ZrO_2 and Co/ZrO_2 are completely reduced, and yield the highest activity among all catalysts studied. The catalysts supported on YSZ are near complete reduction at 475°C, but the activity of Ni/YSZ is about 2/3 that of Ni/ZrO_2. For Co/YSZ the activity at 475°C is very close to that of the empty reactor, indicating very little activity of Co/YSZ at this temperature. The alumina supported catalysts require much higher reduction temperatures (See Figures 5-1 and 5-2). The activities of Ni supported on α and γ alumina are in between those of the empty reactor and Ni/YSZ. Cobalt on alumina catalysts show no to very little activity at 475°C because their conversions are very close to that obtained with the empty reactor. At 500°C, all catalysts supported on ZrO_2 and YSZ are completely reduced and the data on Figure 5-9 indicate that their activities are the highest. Actually, at 500°C, the activity of Ni/ZrO_2 and Ni/YSZ are similar (~60%), whereas the activity of Co/YSZ (~30%) is higher than that of Co/ZrO_2 (~20%). Recall that the Co/ZrO_2 was the catalyst that lost the most weight (through break-up), which may explain the lower activity at 500°C than that of Co/YSZ. Figures 5-1 and 5-2 show that at 500°C, α-Al_2O_3

catalysts are close to complete reduction, but not for γ-Al_2O_3. This correlates well with the activity results at 500°C, in particular for Ni (Figure 6-9a), where the activity of Ni/α-Al_2O_3 (~45%) is much higher than that of Ni/γ-Al_2O_3 (~22%). For the cobalt on alumina catalysts, the activities remain low (~15%), between those of the zirconia based catalyst and that of the empty reactor. At 525°C, Ni/α-Al_2O_3 is almost completely reduced and shows an activity now very close to that of Ni/YSZ. On the other hand, the Co/α-Al_2O_3 still yields a much lower activity than Co/YSZ. The Co/ZrO_2 activity is lower than that of Co/YSZ, which again may be attributed to the loss of catalyst during reaction. At 550°C, except for γ-Al_2O_3, all catalysts are completely reduced (or nearly complete in the case of Co/α-Al_2O_3). All successful catalysts (Ni/YSZ, Ni/ZrO_2, Ni/α-Al_2O_3, Co/YSZ and Co/ZrO_2) yielded conversions above 95% at 550°C.

Selectivity/Reaction Pathway

As seen in Chapter 2 (Literature review), many authors have suggested that the initial step in ESR is either ethanol dehydrogenation with formation of acetaldehyde or ethanol dehydration with formation of ethylene. Acetaldehyde can then decompose into CH_4 and CO or react with lattice oxygen on the catalyst to form acetone. We can then identify three main reaction schemes:

Scheme 1

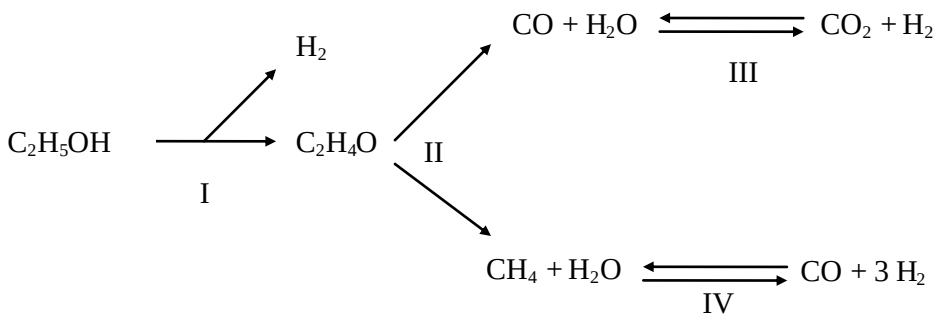

Scheme 2

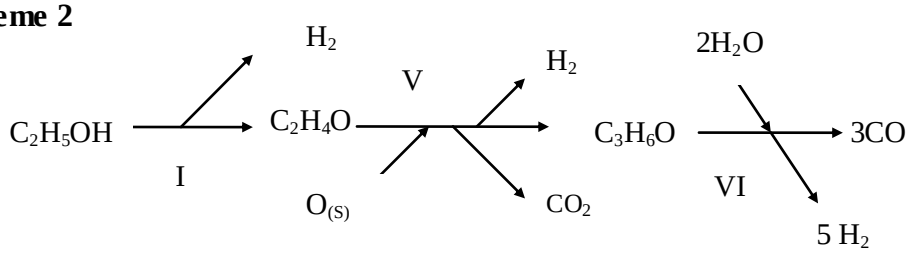

Scheme 3

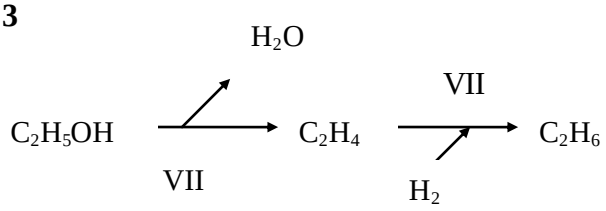

Reactions:
I – Ethanol dehydrogenation
II – Acetaldehyde decomposition
III – Water gas shift
IV – Methane reforming (the reverse being methanation reaction)
V – Acetaldehyde to Acetone
VI – Acetone reforming
VII – Ethanol dehydration
VIII – Ethylene hydrogenation

Figure 6-18: Most Probable Reaction Schemes.

γ-Al_2O_3 Based Catalysts

Figure 6-14 shows, especially for the lower temperatures (up to 500°C) very high selectivity toward C_2H_4 for both Ni and Co supported on γ-Al_2O_3, as well as for Co supported on α-Al_2O_3. For Co supported on ZrO_2 and YSZ some selectivity toward C_2H_4 was observed (but less than 1%). Note that at the lower temperatures, the conversions in several cases are not very high and, actually, are close to the empty reactor. Therefore, it is important to keep the data of the empty reactor in mind when discussing selectivity, especially at lower temperatures. The selectivity toward C_2H_4 in the empty reactor was around 4% for temperatures between 475 and 550°C. Thus, the results observed for Ni or Co/γ-Al_2O_3 and Co/α-Al_2O_3 are clearly due to the catalyst. It can be concluded that γ-Al_2O_3 is very selective toward C_2H_4, which has already been observed by several authors at atmospheric pressure, such as Breen et al. (2002) and Alberton et al. (2007) for Ni/γ-Al_2O_3, and Profeti et al. (2008) for Co/γ-Al_2O_3. Many authors claimed that the high concentration of moderate and strong acidic sites on γ-Al_2O_3 are responsible to promote ethanol dehydration (Djakzer et al., 1998; Alberton et al., 2007). From Scheme 3, the ethylene formed can react with hydrogen to form ethane. This was indeed observed (see Figure 6-15), especially for both Ni and Co on γ-Al_2O_3, but Ni appears more active toward the formation of ethane. The experiments over Ni/γ-Al_2O_3 and Co/γ-Al_2O_3 were characterized by more coking than over the other supports, to the extent that experiments above 500°C failed systematically due to coking/plugging. The high tendency toward coking of these catalysts can be related to their high selectivity toward C_2H_4, whose polymerization is known to lead to coke formation. Indeed, γ-Al_2O_3 has strong acid sites (e.g., refer to section 6.2), which favours the production of ethylene during ethanol reforming (Djakzer, 1998). Although, the γ-Al_2O_3 support favours the dehydration of ethanol (as evidence by the production of C_2H_4), the presence of acetaldehyde shows that ethanol dehydrogenation also takes place. Yet, the acetaldehyde selectivity remains much lower than that obtained with the empty reactor.

α-Al_2O_3 Based Catalysts

The conversion and selectivities obtained at 475°C are similar to that with the empty reactor, indicating the inactivity of the α-Al_2O_3 based catalyst at this low temperature. One experiment with only α-Al_2O_3 was carried out at 525°C and the selectivity of all species (see Appendix F) were actually very close to those of the empty reactor. In addition, the conversion with only α-Al_2O_3 was about 12%, very close to that of the empty reactor (10%). We conclude that the α-Al_2O_3 support is relatively inert (at least up to 525°C). Selectivity toward C_2H_4 was observed

for Co/α-Al_2O_3, but almost none for Ni/α-Al_2O_3 (see Figure 6-14). The C_2H_6 selectivity is also much lower over Ni/α-Al_2O_3 than with the empty reactor. It is likely that the residual C_2H_4 and C_2H_6 selectivities are due to non-catalytic reactions and/or reactions on the reactor's wall (empty reactor). Therefore, also because only a trace amount acetone was detected, we conclude that ethanol reforming over Ni/α-Al_2O_3 follows essentially Scheme 1. The acetaldehyde selectivity decreases with temperature (Figure 6-16a), but this is compensated by an increase in CH_4, CO and CO_2 selectivities, indicating that acetaldehyde decomposes significantly into CH_4 and CO, the later one being then converted into CO_2 via water-gas shift reaction.

Up to 525°C, conversion is no more than 20% with Co/α-Al_2O_3, which is just slightly higher than with the empty reactor. At 550°C, the experiments repeatedly failed because of coking. Recall that this catalyst was not pre-reduced. Non reduced Co/α-Al_2O_3 is therefore not suitable for ethanol reforming in supercritical water.

ZrO_2 Based Catalysts

At 500°C, the conversion of the ZrO_2 supported catalyst only is 12%, which is slightly higher than for the empty reactor (~8%). Therefore, ZrO_2 shows some activity toward ethanol reforming, albeit small. The C_2H_4 and C_2H_6 selectivities of ZrO_2 support (6% and 2%, respectively) are slightly higher than with the empty reactor (4% and 1%, respectively) and thus we can deduct that ZrO_2 based catalyst presents some selectivity toward ethanol dehydration. Also, the selectivities of acetaldehyde, CH_4 and CO are much below the values obtained with the empty reactor (see Figure 6-12, Figure 6-13 and Figure 6-16), whereas the H_2 and CO_2 selectivities are much higher. Then, assuming that the reaction follows mostly Scheme 1 (small amount of acetone, selectivity less than 1%), ZrO_2 appears very active toward CH_4 reforming and CO_2 formation through the WGS reaction.

When combined with Ni, the selectivities toward C_2H_4 and C_2H_6 are nearly zero, indicating that Ni/ZrO_2 does not promote ethanol dehydration, but promotes mostly ethanol dehydrogenation to form acetaldehyde. However, at temperatures above 475°C, the acetaldehyde selectivity is near zero, showing that acetaldehyde decomposes very rapidly into CH_4 and CO or reacts with lattice oxygen to form acetone. This is consistent with the fact that at 500°C the selectivities of CH_4 and CO are high (18% and ~10%, respectively). The high selectivity of CO at 500°C indicates that Ni/ZrO_2 is not very active toward the water-gas shift reaction. Therefore, the high selectivity of

CO_2 (selectivity of 14% at 500°C) may be more due to CO_2 being formed from Scheme 2, than from the WGS reaction. For Ni/ZrO_2 acetone was detected at 500°C, but in small amount. We could therefore assume that acetone reforming takes place rapidly on Ni/ZrO_2.

For Co/ZrO_2 low activity was observed up to 500°C. At 525°C, the conversion reaches ~50% and is complete at 550°C. Above 500°C, the selectivity toward C_2H_4 and C_2H_6 is lower than with the empty reactor. Therefore, the dehydration route is likely to be of minor importance on Co/ZrO_2. However, relatively high acetone selectivity was observed (4% at 500°C and 1.5% at 525°C) indicating the importance of the Scheme 2. The decrease in acetone selectivity with temperature indicates a faster rate of acetone reforming as the temperature increases. At 550°C, where the conversion is complete the methane selectivity is lower than what is expected from thermodynamic calculation and H_2 selectivity is higher. This is a favourable result but we should keep in mind that ZrO_2 had a greater tendency to break up than the other supports.

YSZ Based Catalysts

In many respects, the performance of the YSZ based catalysts is similar to that of the ZrO_2 based ones. Yet, there are two important differences between the YSZ and ZrO_2 based catalysts: 1) the YSZ support yields systematically higher acetone selectivity than ZrO_2 and 2) CO selectivity is lower with YSZ than with ZrO_2, which is particularly obvious in the case of Ni for temperatures of 525°C and below. This would indicate that YSZ favours even more the acetone route than ZrO_2, as well as the water-gas shift reaction.

6.4 Summary

When comparing the performance of Co/YSZ with those of all other catalysts, we see that (for temperatures above 500°C) it:

- involves no coking issues compared to the alumina catalysts, even at 550°C.
- shows YSZ is stronger support than ZrO_2
- offers conversions somewhat lower than Ni/YSZ or Ni/ZrO_2 at 525°C and below, although complete is conversion achieved at 550°C.
- yields the highest hydrogen selectivity, higher than the prediction at equilibrium.
- yields CH_4 selectivity considerably lower than with Ni as active metal. CH_4 selectivity lower than the prediction at equilibrium.
- yields among the lowest ethylene and ethane selectivities.
- yields among the lowest CO selectivity.

We concluded that Co/YSZ was the most promising catalyst of all those investigated. The next chapter will present an in-depth study of the Co/YSZ highlighting the effect of more operating parameters and elucidating reaction pathways.

Chapter 7

Ethanol Supercritical Water Reforming over Co/YSZ: An In-depth Analysis

From the previous chapter on catalyst screening, it was concluded that cobalt supported on YSZ is the most promising catalyst. The present chapter reports the results of a more comprehensive study of ethanol reforming in SCW over Co/YSZ, where the effect of several parameters were considered, such as temperature, flow rate, ethanol concentration, cobalt loading, catalyst weight loading and catalyst reduction. In this chapter, further discussion about the Co/YSZ catalyst characterization is also presented in order to gain insight into its catalytic behaviour.

7.1 Characterization of the Co/YSZ Catalyst

In section 5.1 the characterization of the catalysts covered only limited conditions. In this section, the characterization of the Co/YSZ covers a much broader range of conditions, such as fresh and spent catalysts, catalyst after reduction with H_2, after exposure to supercritical water, and all of these for various operating conditions and cobalt loadings. The Co/YSZ catalysts were characterized using BET-N_2 adsorption, XRD patterns, and SEM.

7.1.1 BET surface area and pore volume- Nitrogen Adsorption

The effect of cobalt loading on the surface area and the average pore size of the calcined catalyst is shown in Table 7-1. The BET surface area first decreases with increasing Co loading, changing from 17 m^2/g at 5% wt. down to 10 m^2/g with 10% wt. Above 10% wt. loading, the BET surface area remains constant. In all cases the BET surface area for this catalyst is not high (less than 20 m^2/g).The average pore volume for all different cobalt loadings is similar, which is about 2 nm.

Table 7-1: BET surface area and pore volume for 5, 10 and 15 % wt. cobalt supported on YSZ (calcined catalyst).

Cobalt loading (% wt.)	BET surface area (m^2/g)	Average pore volume (nm)
5	17	1.99
10	10	1.99
15	10	1.99

The surface area and the average pore volume of the 10% wt. Co/YSZ catalyst for fresh, reduced, after being exposed to SCW, and after 6 hours ethanol water reforming (EWR) at different temperatures is presented in Table 7-2. The BET surface areas measured for the fresh and spent catalysts are similar, in the range of 10 to 13 m^2/g. There is also no difference between the fresh catalyst and reduced catalyst. The BET surface area of the fresh catalyst remains unaffected after being exposed to supercritical water for at least after 2 hours. The reaction temperature (in the range 450-550°C) has no effect on the BET surface area The average pore diameter is also not affected by exposure to SCW or after 6 hours of reforming at all temperatures considered here; it remains around 2 nm.

Table 7-2: BET surface area and pore volume of the fresh and spent catalyst for 10 wt. % Co/YSZ.

	N_2 adsorption	
	BET surface area (m^2/g)	Average pore diameter (nm)
Fresh (calcined)	10	2.0
After reduction with 5% H_2	11	2.0
After 2 hr SCW at 500°C	11	2.0
After 6 hr EWR at 450°C	11	1.9
After 6 hr EWR at 475°C	13	1.9
After 6 hr EWR at 500°C	11	1.9
After 6 hr EWR at 525°C	12	1.9
After 6 hr EWR at 550°C	10	1.9

7.1.2 Temperature Programmed Reduction-H_2

Figure 7-1 shows the TPR-H_2 profile of the 5, 10, and 15 wt. % cobalt loadings. The profiles were deconvoluted based on three characteristic peaks (I, II and III) using the Gaussian method. The results of the deconvolution for the three loadings are presented in Table 7-3. The TPR-H_2 profile for the YSZ support is flat without peaks, illustrating the high thermal stability of YSZ for temperatures up to 900°C. The profiles in Figure 7-1 show that hydrogen consumption increases with the loading of cobalt. This can also be seen in **Table 7-3** for the H_2 consumption per gram of catalyst. All peaks are located at the same temperature and span a similar temperature range, as expected.

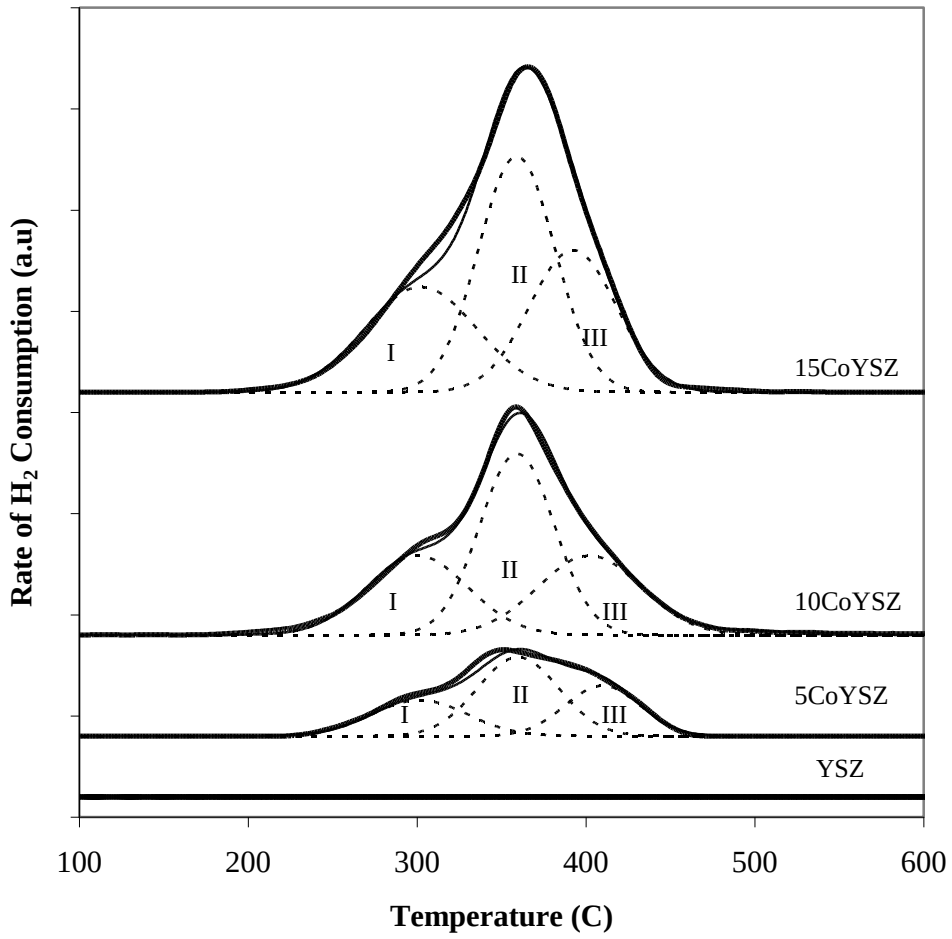

Figure 7-1: TPR patterns of YSZ and CoYSZ : 5% wt., 10 % wt., and 15% wt. cobalt on YSZ.

Table 7-3: Distribution of H_2 consumption peaks for different Co loadings.

Cobalt Loading (wt%)	Relative value of the H_2 consumption						Total H_2 Consumption	
	Peak I		Peak II		Peak III			
	(%)	T(°C)	(%)	T(°C)	(%)	T(°C)	$\frac{\mu mol\, H_2}{g\ Cat.}$	$\frac{mol\, H_2}{mol\, Co}$
5	25	301	47	359	28	409	618	1.45
10	27	301	45	359	28	400	1332	1.55
15	28	302	43	359	29	392	1881	1.47

Table 7-3 shows that the total H_2 consumption (per gram catalyst) is proportional to the cobalt loading: H_2 consumption for 10 wt.% loading is roughly twice the consumption for 5 wt.%, and H_2 consumption for 15 wt.%, three times that for 5 wt.% loading. This also translates in nearly constant H_2 consumption, when expressed per mole of cobalt (around 1.5 mol H_2/mol Co). Theoretically, assuming complete reduction of Co_3O_4, according to:

$$Co_3O_4 + 4H_2 \rightarrow 3Co + 4H_2O \qquad (7\text{-}1)$$

The H_2 consumption should be 1.33 mol H_2/mol Co. The value of 1.5 determined here is in close agreement with the theoretical value.

Bellido et al. (2008) characterized Ni/YSZ catalysts. Although here the active metal is Co, the explanation given by Bellido can be adapted to our catalyst. First, as indicated in the next section on XRD results, only Co_3O_4 phase was present in the calcined catalyst. The low temperature peak (peak I) characterizes the reduction of Co_3O_4 on the oxygen vacancies of the YSZ support; the intermediate temperature peak (peak II) represents the reduction of crystalline Co_3O_4 in the bulk, and the high temperature peak (peak III) characterizes the strong interaction of cobalt with the YSZ support.

7.1.3 X-Ray Powder Diffraction (XRD)

Figure 7-2 shows the XRD patterns over the YSZ support and three different cobalt loadings (5, 10 and 15 wt.%). The XRD patterns were matched with the ICCP-PDF4 (2007) database. For the calcined Co/YSZ catalysts only peak for Co_3O_4 was found (no presence of CoO). The crystallite size using the Scherrer formula was determined and the results are shown in Table 6-4. This table shows that the crystallite size slightly increases when increasing Co loading, from 19.9 nm for 5% loading from 27.5 for 15% loading.

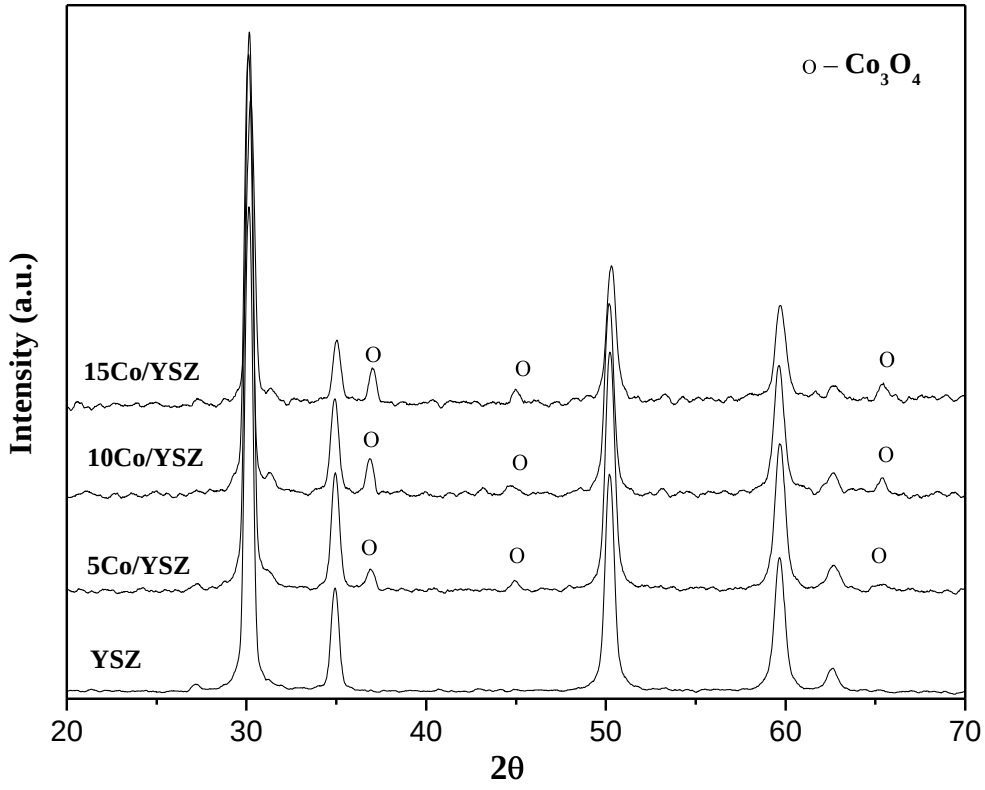

Figure 7-2: XRD Patterns of the YSZ support and the calcined catalyst at different Co loadings (5, 10, and 15 wt.%).

Table 7-4: Crystallite size calculated using Scherrer Formula (Equation (3-4)).

Cobalt Loading (wt.%)	Diameter Particle (nm)
5	19.88
10	24.33
15	27.45

Figure 7-3 shows the XRD patterns of 10 wt.% Co/YSZ for fresh catalyst, reduced catalyst, catalyst exposed to SCW (after 30 minutes) and spent catalysts for various reaction temperatures (after 4.5 hours time-on-stream). Catalysts with and without reduction and exposed to SCW at 500ºC were also analyzed to see the effect of SCW on the oxidation state of cobalt. The results regarding Figure 7-3 can be summarized as follows:

- Comparison between fresh and reduced catalyst [profiles b) and c)] show that Co_3O_4 is completely reduced to a Co^0 phase. Recall that reduced catalyst means the pre-treatment of fresh catalyst in 5% H_2 (balance N_2) for 2 hours at 550°C.
- The fresh catalyst exposed to SCW for 30 minutes (profile d) shows only peaks for the CoO phase. Comparison with the fresh catalyst (profile b), shows that SCW completely reduces Co_3O_4 to CoO after 30 minutes.
- The reduced catalyst exposed to SCW for 30 minutes (profile e) also shows only peaks for the CoO phase (profiles d and e are identical). This indicates that the reduced catalyst is completely oxidized from Co^0 to CoO in SCW after 30 minutes.

The two previous points shows that in SCW, cobalt will end up as CoO, whether the initial catalyst is Co_3O_4 or Co^0.

- Profiles f) to i) represent the XRD profiles of the catalyst after reforming experiments at 450ºC to 550°C. The peaks characterizing CoO diminish as temperature increases and completely disappear at 525°C and above. Simultaneously, a peak at 44.2° characteristic of metallic Co°(1 1 1) plane appears and increases with temperature.

The last point shows self reduction of cobalt during the reforming reaction, likely due to the hydrogen formed in the reaction products. This means that, if the temperature is sufficiently high (e.g., above 500°C), it may be possible to carry out ethanol reforming without having to pre-reduce the catalyst. Of course, this will imply some lag time until the catalyst is fully reduced but, at least at 550°C, we know that the catalyst can be fully reduced after a few hours (the data shown in profile i) were obtained after 4.5 hours time-on-stream).

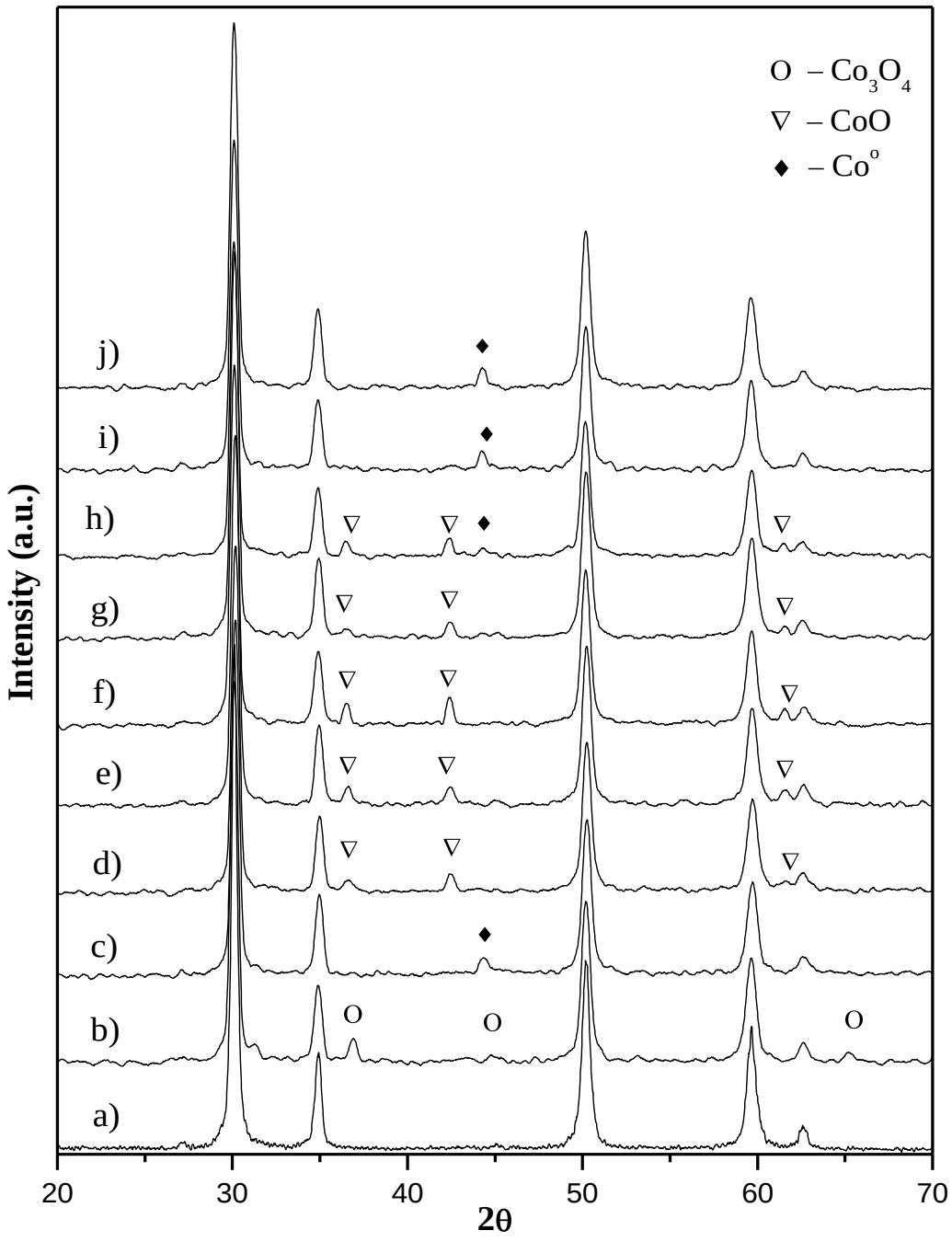

Figure 7-3: XRD profiles of 10 wt.% Co/YSZ for a) YSZ support b) fresh catalyst, c) reduced catalyst, d) fresh catalyst exposed to SCW at 500°C for 30 minutes, e) reduced catalyst exposed to SCW at 500°C for 30 minutes, f) after reaction at 450°C, g) after reaction at 475°C, h) after reaction at 500°C, i) after reaction at 525°C, and j) after reaction at 550°C.

7.1.4 Scanning Electron Microscopy (SEM)

The SEM images of the fresh and reduced catalysts, as well as catalysts exposed to SCW only and to ethanol reforming in supercritical water are presented in Figures 7-4 to 7-8. All images were captured using a Robinson Back Scattering Detector (RBSD). Figure 7-4 shows images of YSZ powder, fresh 10 wt.% Co/YSZ and after reduction of 10 wt.% Co/YSZ. The YSZ support was obtained from YSZ powder with surface area of 16 m^2/g. The image of the powder YSZ shows the agglomerates white particles with spherical shape. The SEM pictures of YSZ powder, fresh and reduced catalyst are almost similar. Even after the fresh or reduced catalysts were exposed to ethanol reforming, the images captured by the SEM are quite similar as shown in Figure 7-5 to 7-8. CoO, Co_3O_4 and YSZ particles were hardly distinguishable by back scattering. Figures 7-7a,b, show the presence of large flat surfaces of cobalt, which was not observed at temperatures below 550°C, and which is representative of cobalt sintering. This flat surface is similar to that reported by Grgicak et al. (2006) for cobalt supported on YSZ. As shown in the next section, small particles were also found in the catalyst bed. An SEM micrograph of these small particles is shown in Figure 7-7c and highlights the presence of filamentous carbon.

From the previous section, it was shown that cobalt oxide species can be self-reduced during the reforming reaction and be totally reduced at 550°C. Some experiments were then carried out, first at 550°C for 200 minutes in order to quickly reduce the catalyst, then at lower temperatures (e.g., 500, 525°C) for the remaining of the experiment. SEM pictures for such situations are shown in Figure 7-8 and are very similar to that of the fresh catalyst.

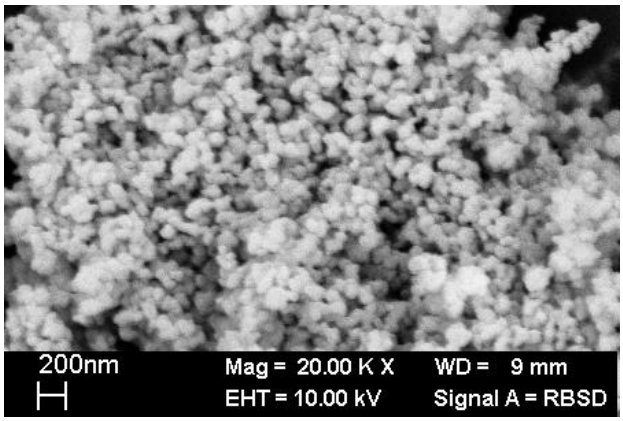

a) YSZ

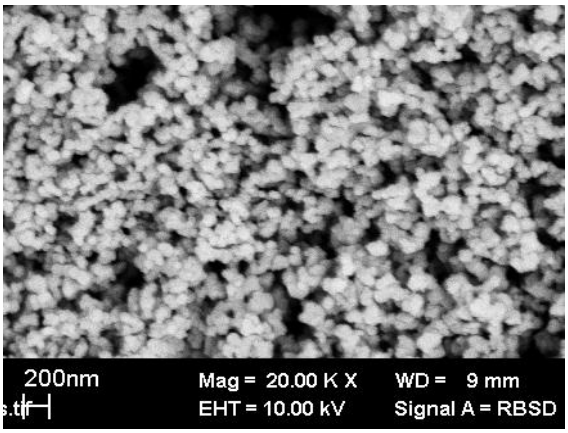

b) Fresh

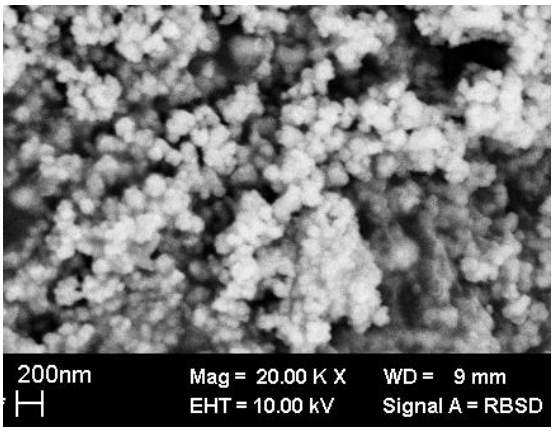

c) Reduced

Figure 7-4: SEM images of a) YSZ, b) Fresh 10 wt%Co/YSZ, and c) Reduced 10wt%Co/YSZ.

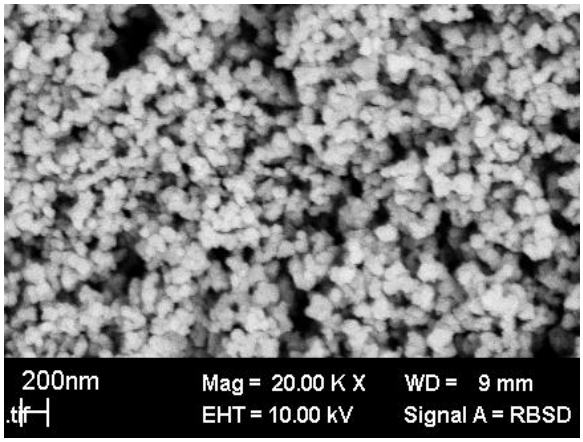

a) Fresh in SCW

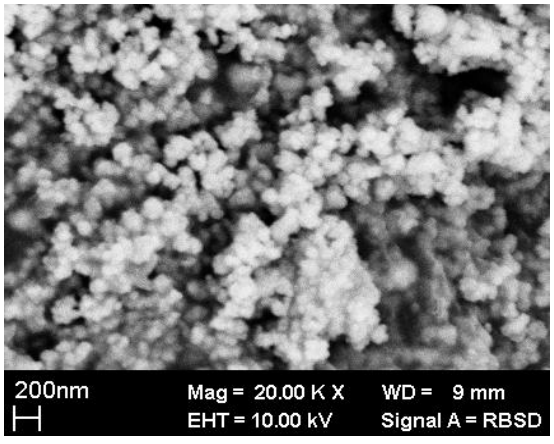

b) Reduced in SCW

Figure 7-5: SEM image of a) Fresh catalyst and b) reduced catalyst both exposed to SCW after 30 minute at 500°C.

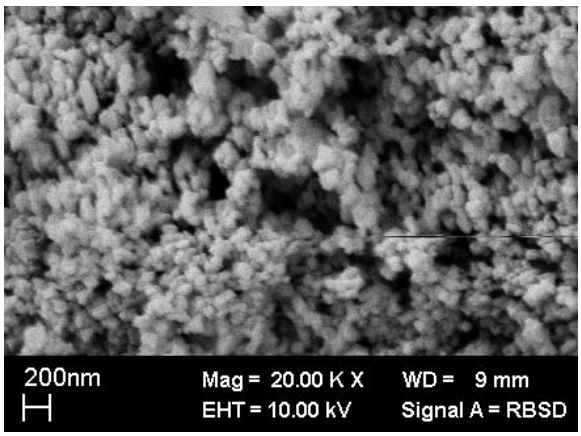

a) ER at 450°C

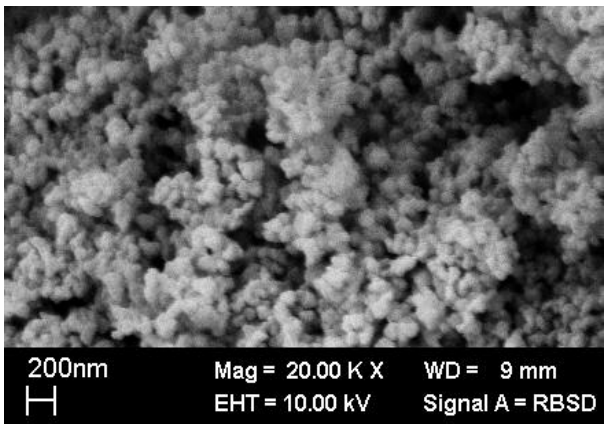

b) ER at 475°C

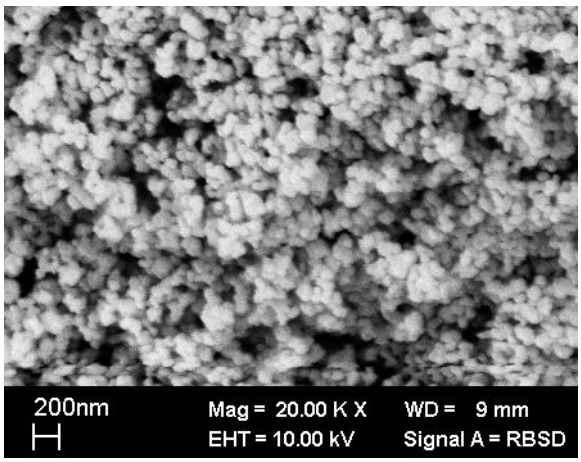

c) ER at 500°C

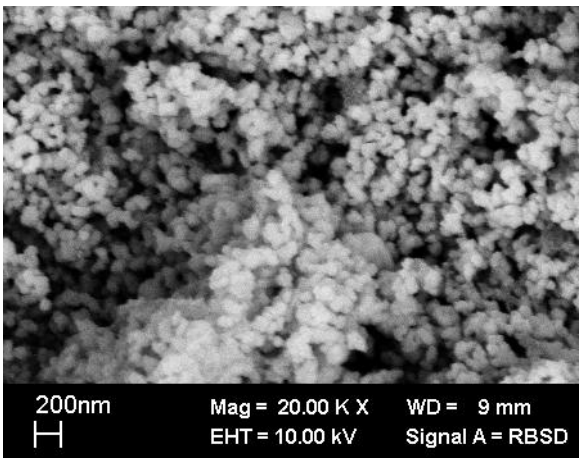

d) ER at 525°C

Figure 7-6: SEM images of unreduced 10 wt.% Co/YSZ after 4.5 hours exposed to ethanol reforming (ER) at different temperatures: a) 450ºC, b) 475ºC, c) 500ºC, and d) 525ºC.

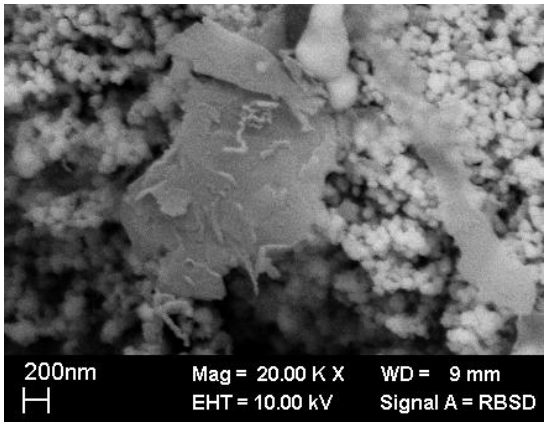

a) ER at 550°C

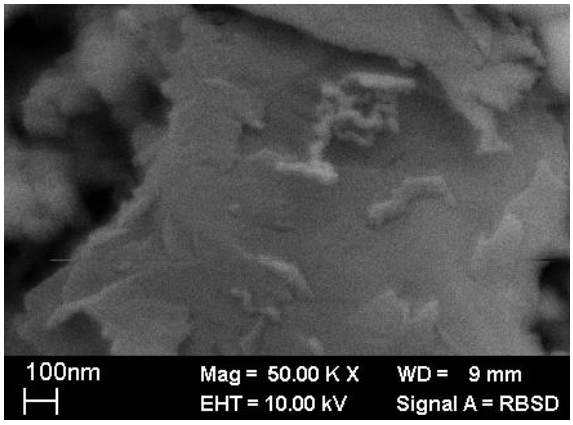

b) ER at 550°C

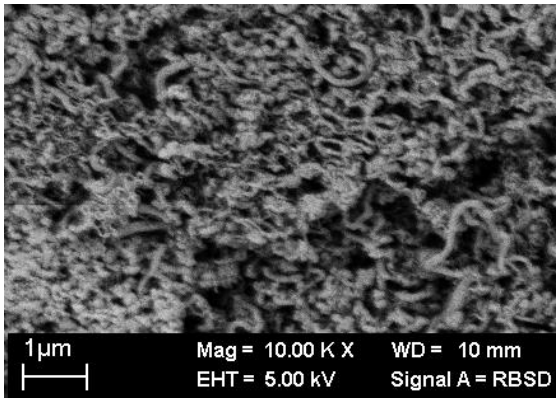

c) SEM of small particles found after reforming reaction at 550°C

Figure 7-7: SEM images of unreduced 10 wt.% Co/YSZ after 4.5 hours exposed to ethanol reforming at 550ºC for different magnifications: a) 20K times and b) 50K times and c) small particles found in the catalyst bed.

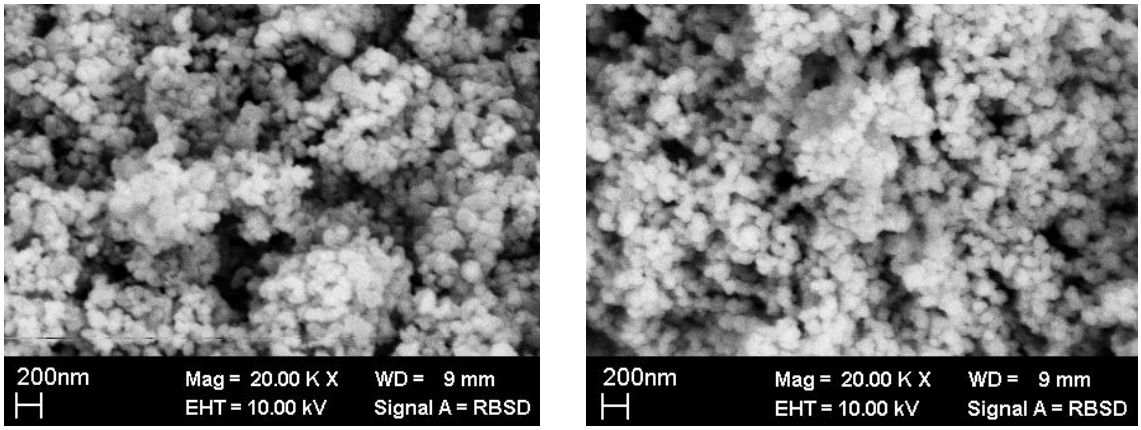

a) b)

Figure 7-8: SEM images of 10 wt.% Co/YSZ after reaction for accelerated "self reduction" a) 550 to 500°C and b) 550 to 525°C.

7.1.5 Images of Catalyst (Macro Photography)

Figure 7-9 shows images of the catalyst from a naked eye perspective captured using a digital single lens reflect (DSLR, Canon model 40D) camera. The image of the fresh catalyst indicates that it is dark grey and without small broken particles. The colour of the catalyst exposed to the reaction at 450°C is also dark grey and is like the fresh catalyst. At 500 and 550°C, parts of the catalyst have broken up, as evidenced by the presence of small black particles (see Figure 7-9c,d). These small particles contain amounts of carbon filament, as seen in the SEM image on Figure 7-7c. Figure 7-9f was obtained after an experiment where the reforming was first carried out at 550°C for 3 hours and then the temperature was lowered to 500°C for the rest of the experiment. This type of experiment aimed at improving catalyst activity without having to pre-treat the catalyst with hydrogen. More details will be provided toward the end of this chapter. Figure 7-9f shows a high fraction of catalyst break up, most likely due to too high pressure fluctuations.

a) Fresh

b) After reaction at 450°C

c) After reaction at 500°C

d) After reaction at 550°C

e) In-situ reduction and reaction at 500°C

f) Accelerated "self reduction" from 550 to 500°C

Figure 7-9: Pictures of 10 wt.% Co/YSZ for: a) fresh catalyst, b) after reaction at 450°C, c) after reaction at 500°C, d) after reaction at 550°C, e) after reaction at 500°C (in-situ reduction catalyst), and f) after accelerated "self reduction" with temperature from 550 to 500°C.

7.2 Catalyst performance

The performance of the Co/YSZ catalyst is discussed in more detail in this section. The experiments were carried out using catalysts with and without pre-treatment/reduction. The reaction parameters of studies over the unreduced catalysts are temperature, feed flowrate, pressure, catalyst weight, cobalt loading and ethanol concentration. Since the unreduced catalysts would experience phase transformation during the reaction, the effects of in-situ/ex-situ pre-treatment with hydrogen (reduction) were also studied.

7.2.1 Effect of Temperature

Figure 7-10 shows the ethanol conversion at three feed flowrates (0.88, 1.88 and 2.88 g/min) and temperature ranges between 450 and 550°C vs. time-on-stream, for unreduced 10 wt.% Co/YSZ catalysts. Referring to Figure 7-10, the conversion at all flowrates are almost complete at 550°C within 2 hours time-on-stream. At 450°C ethanol conversion is low and stable over time, but increases as the flowrate decreases (5%, 10% and 20% at 2.88, 1.88 and 0.88 g/min, respectively). From thermodynamic calculations, the equilibrium conversion should be 100%, even at 450°C. We attribute the low conversion to the small amount of Co° present (almost no presence of Co° after reaction at 450°C as seen in Figure 6-3). At 475°C, for the intermediate flowrate, the conversion is barely 20%, whereas at the lowest flow rate, we observed a clear increase in conversion over time, reaching 55% after 150 minutes. Similarly, at 500°C and 525ºC the ethanol conversion increased over the time. The rate of conversion increase at 525°C is faster than at 500°C, which shows that the increase in activity over time depends on the temperature. We attribute the increase in ethanol conversion over time to the transformation phase of the oxidation state of cobalt.

The pattern of the ethanol conversion with temperature can be related to the TPR-H_2 and XRD results. The TPR – H_2 of Co/YSZ, in the absence of water, shows that cobalt would be completely reduced to Coº at 500ºC. This suggests "self" reduction of cobalt in the presence of product hydrogen, whose extent depends on temperature. Transformation of cobalt oxide to metallic cobalt increases the activity of the catalyst. This explanation can be supported by the XRD result (Figure 7-3) scanned after each experiment with 1.88 g/min. As discussed in section 7.1.3, only CoO exists at temperatures of 450 and 475°C. At 500°C both CoO and Co° phases were detected. At 525°C and 550ºC there is only Co° present. Fully reduced cobalt demonstrates high

activity of the catalyst for the ethanol reforming reaction. Therefore, unreduced catalysts are not active if the reaction temperature is below 500°C.

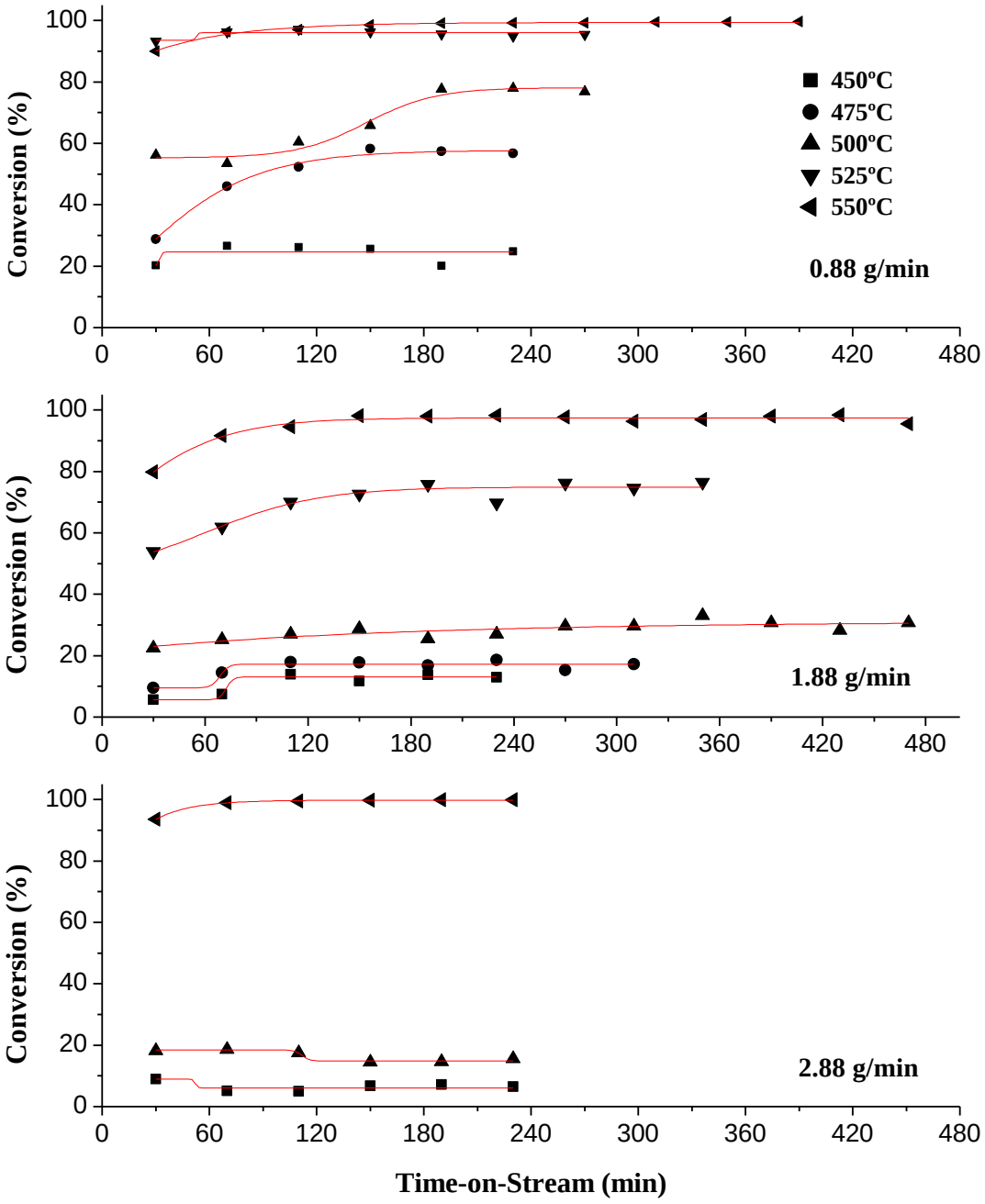

Figure 7-10: Ethanol conversion at different flowrates and temperatures vs. time-on-stream. (250 bar, 5 wt.% ethanol concentration, 1 g non reduced 10 wt.% catalyst).

7.2.2 Effect of Pressure

The effect of pressure on the ethanol conversion and product selectivities over non reduced catalyst at 500°C is presented in Figure 7-11. Three levels of pressure, 225, 250 and 280 bar, were studied, which represent a pressure close to the water supercritical pressure, the most commonly used pressure in this study and maximum allowable working pressure of the reactor, respectively. One-way ANOVA statistical analysis shows no significant difference of the mean and the variance of the ethanol conversion among the three pressures studied. For the selectivities, the main difference is the decrease in hydrogen selectivity as pressure increases, and the simultaneous increase in methane. From the reaction mechanisms shown in Chapter 5, this seems to indicate that out of the methane formed from acetaldehyde decomposition, less is steam reformed with increasing pressure (see Scheme 1). This trend is also consistent with the trend obtained from thermodynamic calculations, although at equilibrium the CH_4 selectivity would be much higher (greater than 40%) and the H_2 selectivity would be much lower (lower than 40%).

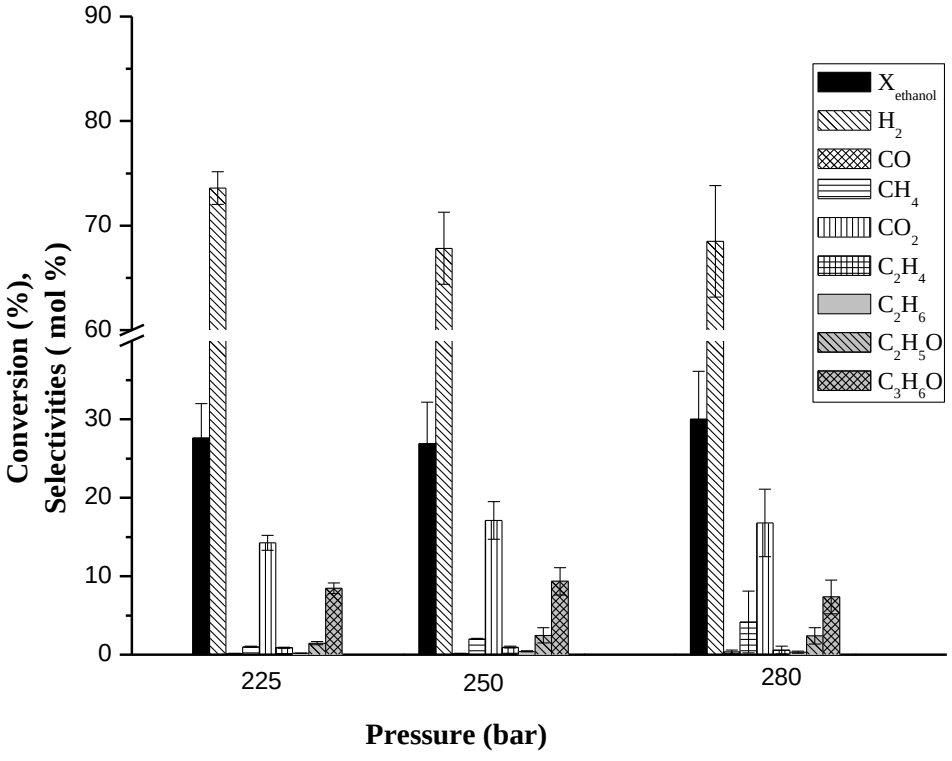

Figure 7-11: Effect of pressure (in the SCW pressure range) on conversion and product selectivities. Reaction conditions: 1 g non-reduced catalyst, 1.88 g/min feed, 5 wt.% ethanol and 500°C.

7.2.3 Effect of Residence time

The residence time is calculated by dividing the volume of the catalyst bed by the actual volumetric flowrate in the reactor. Since the experiments were carried out with mostly around 5 wt.% ethanol, the balance being around 95% water, the supercritical water density at the condtions of the experiments was used for calculating the volumetric flowrate. Two main ways to vary the residence time are changing the flow rate or the volume of catalyst bed (e.g., by changing the mass of catalyst in the bed). Two parametric studies were then performed: one by changing the flow rate with a constant mass of catalyst and one by changing the mass of catalyst while keeping a constant flow rate.

Effect of Flowrate on Conversion

Figure 7-12 presents the experimental data after 230 minutes time-on-stream for different flowrates and temperatures. From Figure 7-10 the conversion reached a plateau after 230 minutes for all operating conditions. For comparison, Figure 7-12 also shows results for the empty reactor (ER) at different flowrates. At temperatures below 500°C, for the highest flowrate (2.88 g/min), the conversions with and without catalyst are the same, showing that under these conditions, the catalyst is inactive. For the empty reactor, decreasing the flow does increase slightly the conversion, this effect being more important as the temperature increases. However, the effect of flowrate on ethanol conversion in the presence of the catalyst (non pre-reduced catalyst) is much more significant, even at the lowest temperature of study 475°C. The effect of flowrate is related to the contact time between the reactant and the catalyst. Referring to Figure 7-12, as expected, the lowest feed flowrate (or the highest contact time) leads to higher ethanol conversion. From temperatures 450 to 525°C, the conversion for 0.88 g/min is higher than 1.88 g/min and 2.88 g/min. The conversion reaches nearly 100% at 525°C with 0.88 g/min (the lowest flowrate here), whereas at 550°C, 100% conversion is reached, even with the highest flow rate of 2.88 g/min.

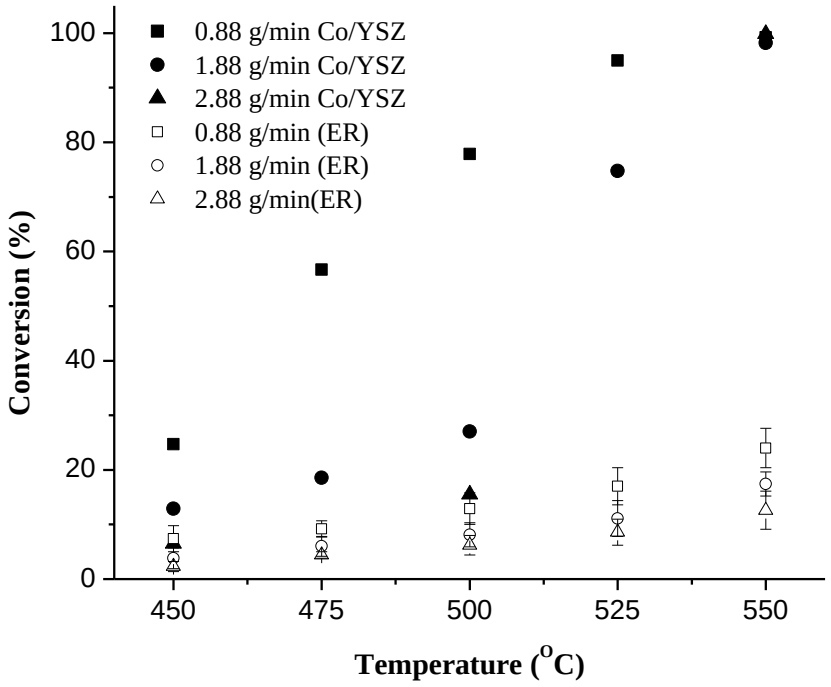

Figure 7-12: Effect of temperature on the conversion at different flowrates.

Effect of Catalyst Mass on Conversion

Figure 7-13 shows the ethanol conversion for three catalyst mass (1, 1.5 and 2 gram) and three temperatures (450, 500 and 550°C) as a function of time-on-stream. The results show that at 450°C, the conversion does not vary between those three catalyst masses and remains low (below 15%). At 550°C, the conversion after 2 hours time-on-stream does not vary and stays at about 100%. In fact, for the experiments with more than 1 g of catalyst in the bed, 100% conversion is achieved within 60 minutes. At 500°C, the behaviour of the catalyst activity is different. Using 2 g of catalyst, the conversion reaches 94% conversion very quickly, after only 30 minutes. The conversion with 1.5 g of catalyst at 500°C shows an increase in conversion over time-on-stream and reaches a plateau of 94% conversion (similar to that achieved with 2 g catalyst) after 6 hours. But, the conversion with 1 g of catalyst shows only a little increment with the time-on-stream, from ~20% (30 minutes) to ~30% (470 minutes). The results show that, by increasing the amount of catalyst, the activity of ethanol reforming increases. The results shown in Figure 7-13 were for non-reduced catalysts. Therefore, we attribute the increase in activity over time (particularly clear with 1.5 g of catalyst at 500°C) to "self" reduction during the early stage of the reaction, from the

hydrogen generated. With larger amount of catalysts, the amount of hydrogen produced is sufficient to "quickly" reduce the catalyst. But, as the mass of catalyst decreases, the amount of hydrogen produced is lower and the reduction of catalyst occurs at a much smaller pace. With 1 g of catalyst, it is not unreasonable to expect that if one would wait much longer, one could see a sharper increase in catalyst activity at some point.

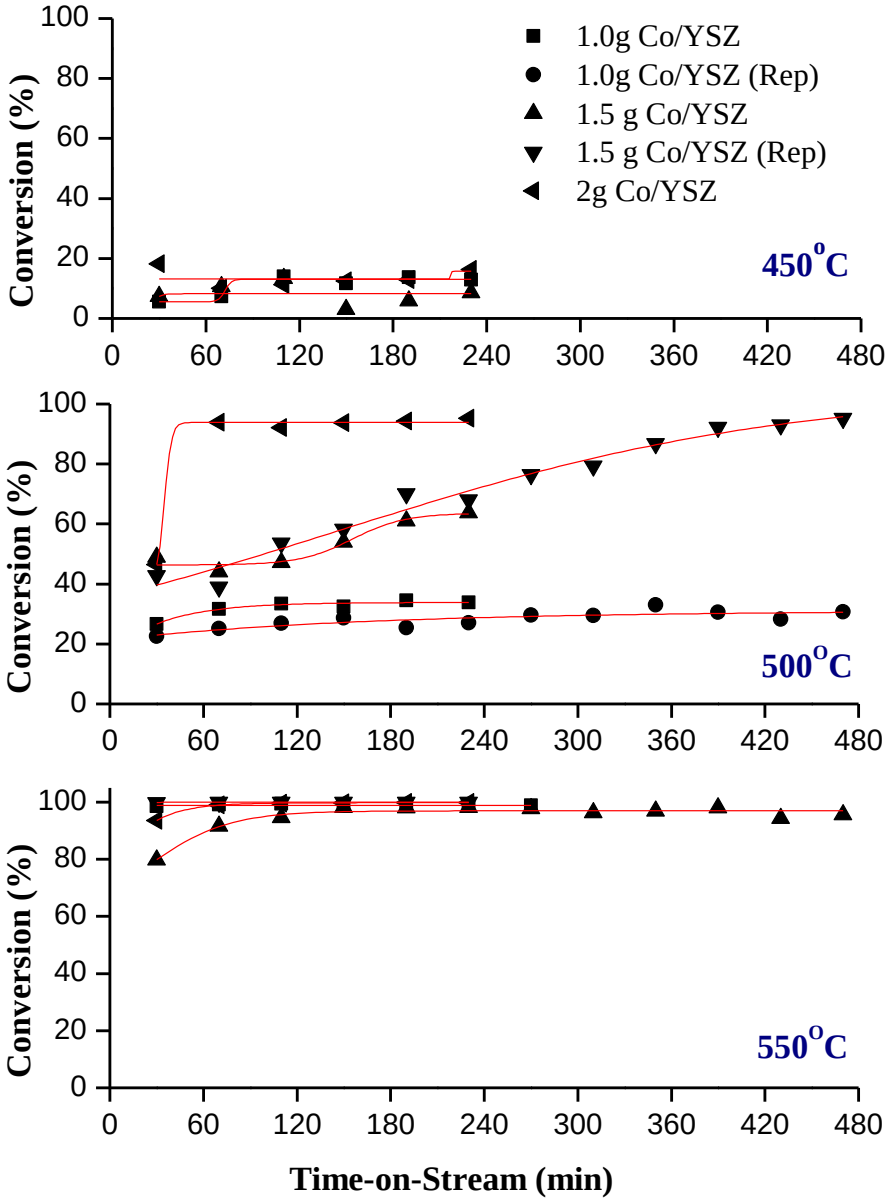

Figure 7-13: Ethanol conversion vs. time-on-stream at different catalyst weights and temperatures. "Rep" in the legend means repeated experiments.

Effect of Residence Time on Conversion

Data from the two previous parametric studies were combined and converted into residence time. The effect of residence time on ethanol conversion at different temperatures is presented in Figure 7-14. The results show that complete conversion can be achieved within 1.5 s at 550°C. At 500°C, the conversion increases significantly with residence time, from about 20% after ~2 s to nearly 100% after 5-6 s. At 450°C, the conversion increases slightly (and linearly) with the residence time from 8% after 2 s to 20% after 7 s.

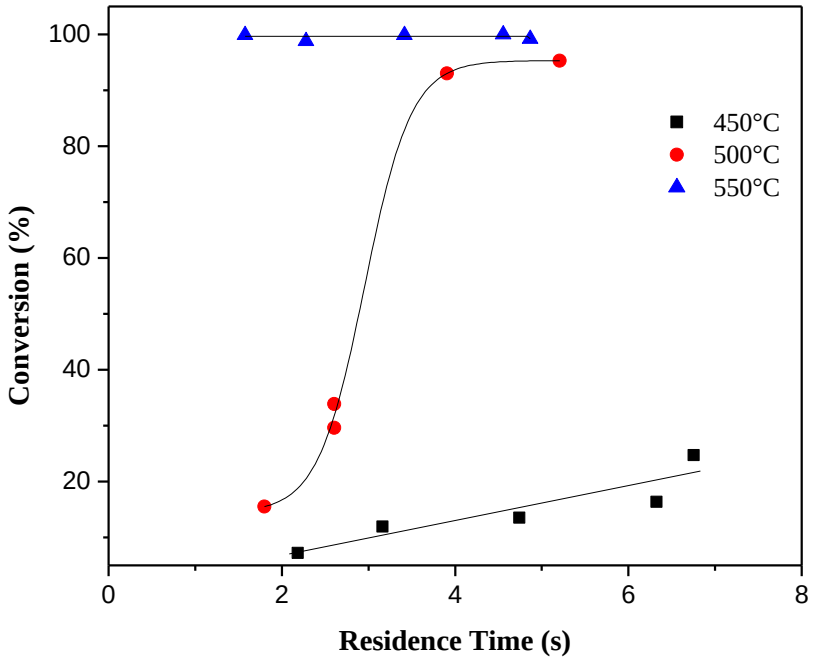

Figure 7-14: Ethanol conversion vs. residence time

The effect of residence time on product selectivity is presented in a subsequent section covering reaction pathway.

7.2.4 Effect of Ethanol Concentration

Three levels of ethanol concentration (2.5, 5 and 7.5) at three different temperatures (450 to 550°C) were considered. The results for conversion vs. time-on-stream are shown in Figure 7-15. At 450ºC, varying the ethanol feed concentration did not affect the ethanol conversion and resulted in conversions between 15 and 18%. Meanwhile, the ethanol conversion at 550ºC was almost complete for all concentrations. At 500°C, the catalyst activity was changing over time especially for ethanol concentration of 7.5% wt. At 2.5% wt., the conversion remains more or less constant over time and at 5.0% wt., the conversion increases very slightly over time. It is worth noting that with 7.5% wt. ethanol the conversion was first flat at a value close to that with 2.5 and 5% wt. ethanol (i.e. 25-30% conversion), before suddenly increasing up to 55%. We attribute this effect again to "self" reduction from the hydrogen formed. With higher ethanol concentration, more hydrogen is produced, which, in turn, can speed up the reduction of the oxidized catalyst.

Figure 7-16 shows the effect of the ethanol concentration on the product selectivity at 550°C. The product selectivity does not vary, except for CH_4 with small increase from 2.5 to 7.5 wt.% ethanol concentration.

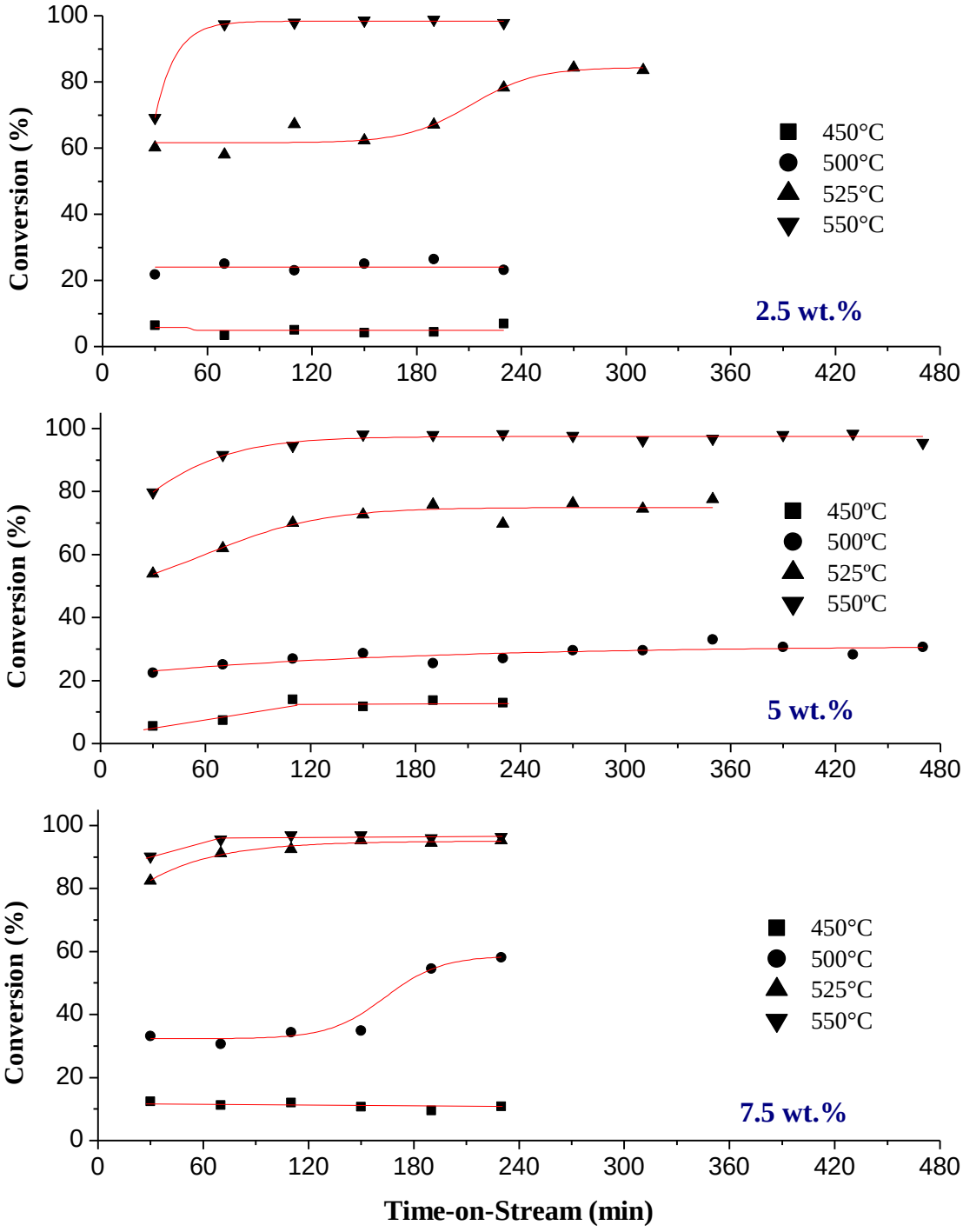

Figure 7-15: Ethanol conversion vs. time-on-stream at different ethanol concentrations. (Reaction conditions: 250 bar, 1 g non reduced catalyst, 1.88 g/min feed flowrate)

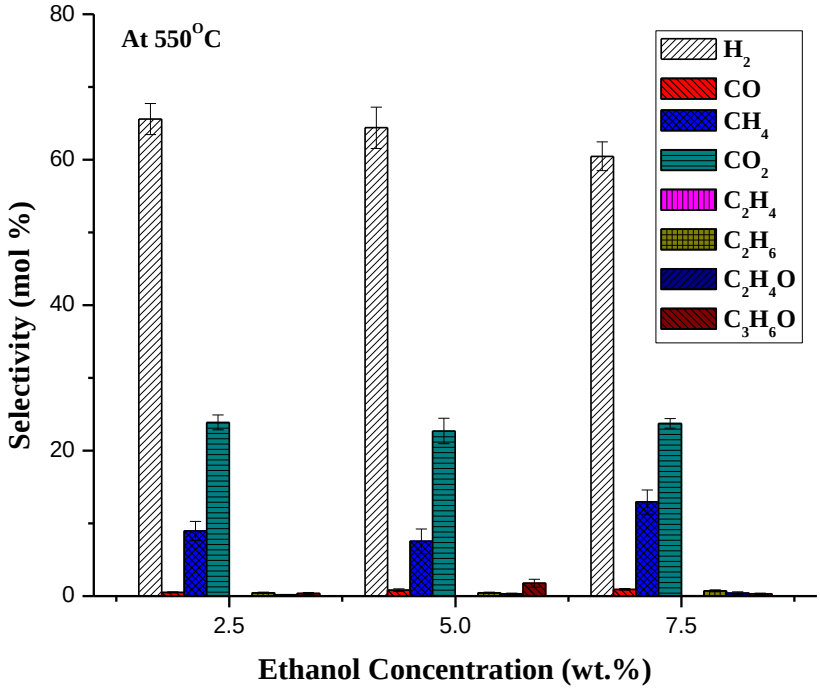

Figure 7-16: Effect of ethanol concentration on product selectivity over 10% wt. Co/YSZ. (250 bar, 550°C, 1 g non reduce catalyst, 1.88 g/min feed).

7.2.5 Effect of Cobalt Loading

Three different cobalt loadings without reduction were studied at 5, 10 and 15% wt. cobalt on supported YSZ. The results for ethanol conversion vs. cobalt loading are presented in Figure 7-17. Unless, the conversion reaches 100%, increasing cobalt loading increases conversion, especially at 500°C and above. At 550°C, the conversion increased between 5 to 10 wt. % loading at which point the conversion reached 100%. Beyond 10 wt. %, the conversion stays at 100%. At 450°C, the conversion is independent of cobalt loading and remains low, at around 10%, which is close to the conversion with the empty reactor indicating the catalyst is not active. Figure 7-18 shows the result for product selectivity for the different cobalt loadings. As seen in Figure 7-17, the conversion increases when increasing Co loading. This is accompanied by a decrease in H_2 selectivity and an increase in methane selectivity.

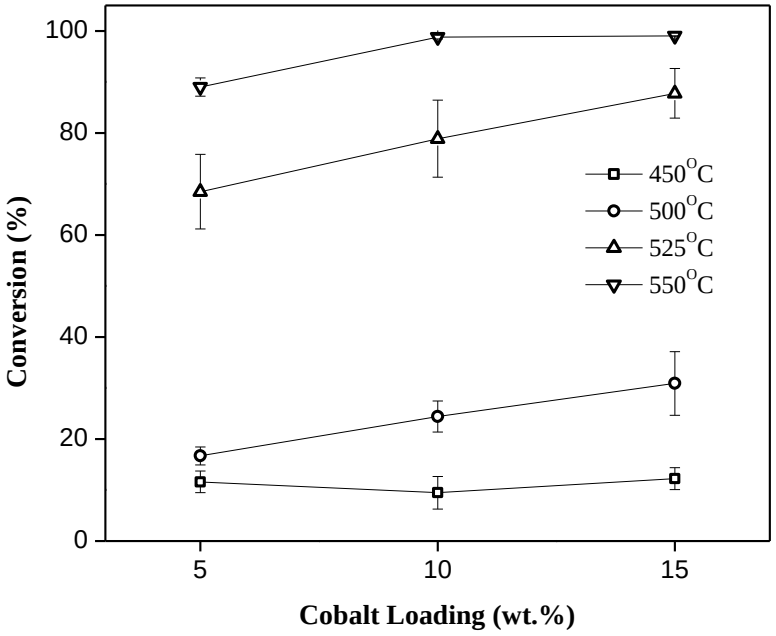

Figure 7-17: Effect of cobalt loading on ethanol conversion at four different temperatures (250 bar, 1 g non-reduced catalyst, 1.88 g/min, 5% wt. ethanol).

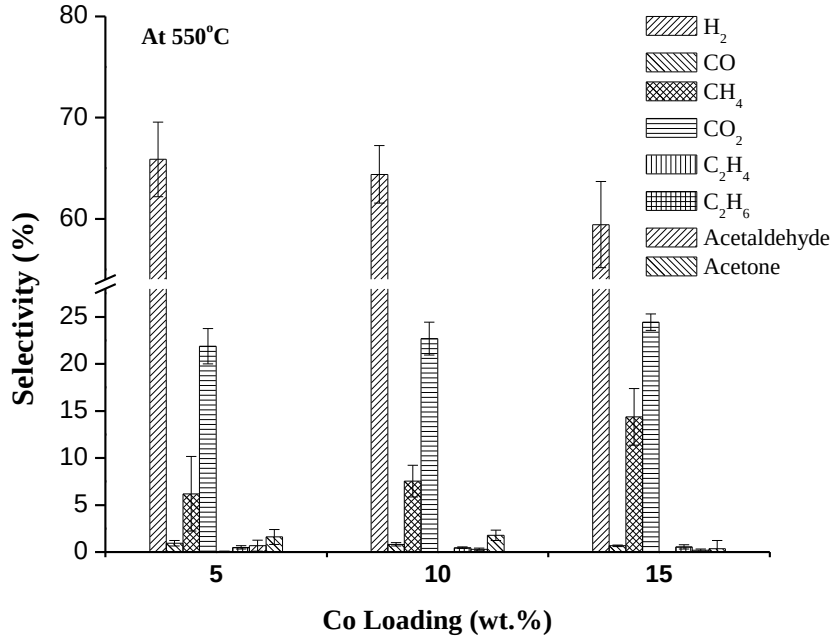

Figure 7-18: Product Selectivity at different Co loadings at 550°C. (550°C, 250 bar, 1 g non-reduced catalyst, 5 wt.% ethanol, 1.88 g/min feed)

7.2.6 Effect of Catalyst Reduction

All results shown so far were for catalysts that were not reduced prior to reaction. Indeed, as mentioned in Section 7.1.3, it was found that a pre-reduced Co/YSZ catalyst would re-oxidized to CoO after 30 minutes exposure to supercritical water. Vice-versa, it was also shown that a calcined Co/YSZ (Cobalt in the form of Co_3O_4) would reduce to CoO in the presence of supercritical water. In addition, the previous results on the performance of the catalysts highlighted the "self" reduction of the catalyst from the hydrogen generated during the reaction. Nonetheless, it was shown in the previous sections that below 550°C, it may be difficult to reach equilibrium conversion (or at least, it may take a very long time) when using a non-prereduced catalyst. It was therefore decided to carry out a set of experiments with reduced catalysts. Two methods were first investigated to determine the effect of the reduced cobalt on catalyst performance: 1) Ex-situ reduction where the catalyst is reduced outside the SCW reactor and 2) in-situ reduction where the catalyst is reduced inside the SCW reactor. The difference between these two methods is the possibility of reducing some metal sites on the reactor's wall in the case of in-situ reforming, as shown in Chapter 5. Both ex-situ and in-situ reductions were carried out at 550°C for 2 hours, which is already higher than the temperature required to completely reduce cobalt oxide to Co°, as shown in Figure 7-3. The ex-situ reduction was carried out in a TPD/TPR experimental setup. The catalyst was loaded in the SCW reactor within 30 minutes after being reduced. The probability of catalyst change during transferring and loading into the SCW reactor is negligible, based on the result of the XRD analysis, which showed that only Co° phase is present even after being exposed to atmospheric conditions for a much longer period of time than that between reduction and loading into the SCW reactor. The in-situ reduction was carried out at atmospheric pressure with 20 v/v % H_2 in nitrogen mixture at 550°C for 2 hours in the SCW reactor.

In-situ and Ex-situ Reduction

Figure 7-19 presents the effect of catalyst reduction (including in-situ vs. ex-situ) at different temperatures over time on-stream. For comparison purpose, conversion in the empty reactor with and without hydrogen pre-treatment is also shown. Recall from Chapter 5 that the main effect of hydrogen pre-treatment of the empty reactor is the higher conversion at low time-on-stream. After about one hour time-on-stream the conversion with hydrogen pre-treatment decreases to the value obtained without pre-treatment. Figure 7-19 shows no noticeable effect of catalyst pre-treatment at 450°C; the catalyst remains unreactive whether the catalyst is reduced or not. At 475°C the surprising result is that ex-situ reduction leads to similar conversion as no reduction, but in-situ reduction yields very high activity: from ~15% conversion with ex-situ

reduction to ~90% conversion with in-situ reduction! The experiments with in-situ and ex-situ reduction have been repeated twice and gave the same surprising result. Although it is still unclear why such a difference is observed, this shows that even at temperatures as low as 475°C, depending on catalyst pre-treatment, it is possible to reach close to equilibrium conversion (i.e. 100% conversion). At 500°C, both ex-situ and in-situ show relatively similar profiles, although with in-situ reduction the conversion reaches its plateau faster than with ex-situ reduction. The transition period to reach the final conversion (close to 100% conversion) is attributed to the time it takes to reduce CoO to Co°. Although not shown in Figure 7-19, the time-on-stream profile at 525°C and 550°C are identical for in-situ and ex-situ reduction, both yielding greater than 98% conversion, even after 30 minutes.

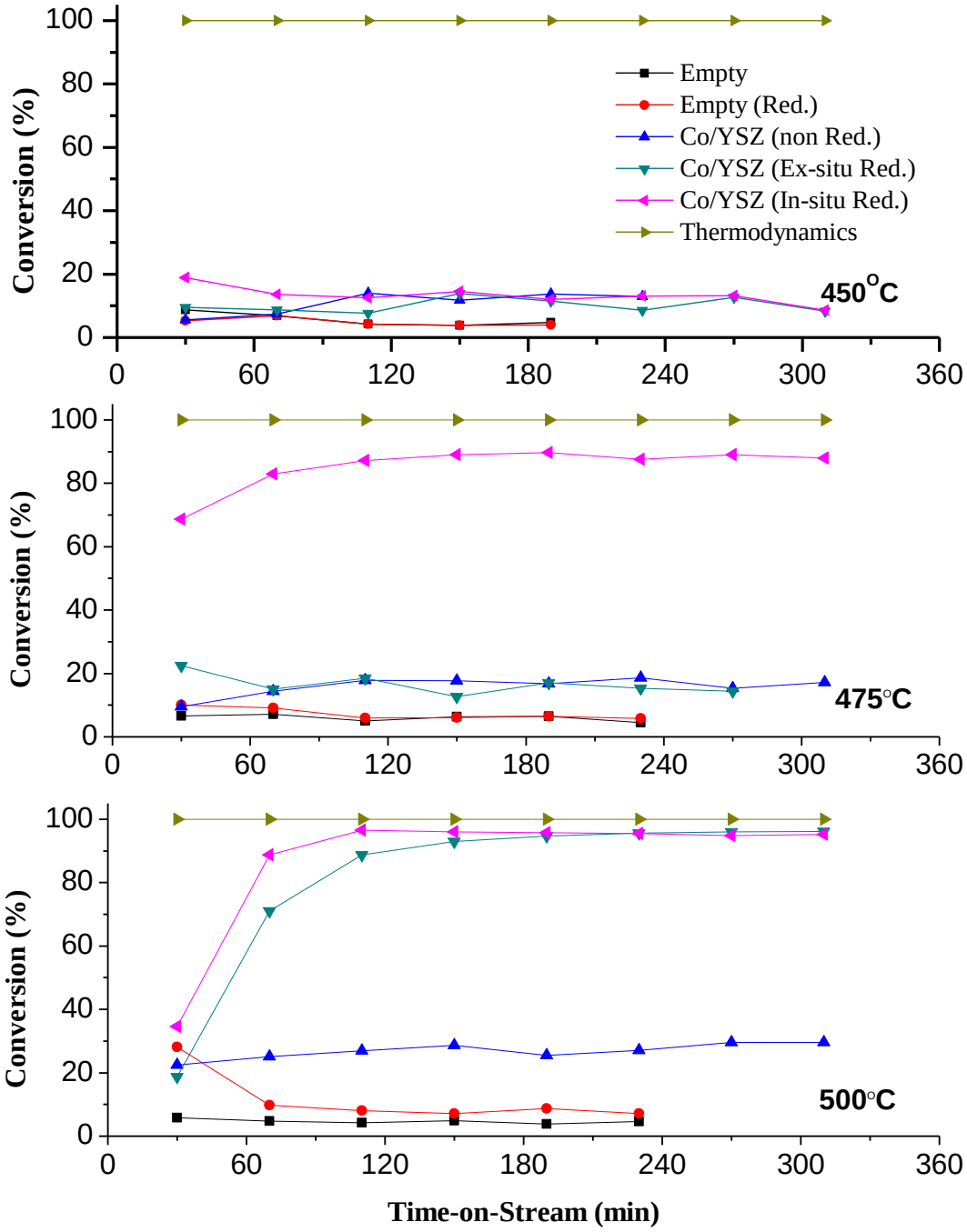

Figure 7-19: Effect of pre-treatment with H_2 (at 450, 475 and 550°C) over 10 wt.% Co/YSZ on ethanol conversion vs. time-on-stream. (250 bar, 5 wt.% ethanol, 1.88 g/min feed, 1 g catalyst).

Reduced Catalyst at Different Temperatures

Figure 7-20 shows the results for ethanol conversion and products selectivities (average of points after 180 minutes time-on-stream) at five temperature levels for the in-situ reduced catalyst. The ethanol conversion increases drastically from 450 to 475°C (~17 to ~84%), but only slightly increases from 475 to 550°C (~84 to ~100%). Note that the experiment at 450°C was repeated twice, and yielded similar results. This means that the reduced catalyst was not active at 450°C and below. Once the reaction achieves nearly 100% conversion, i.e. at 500°C and above, H_2, CO and CH_4 selectivities do not vary much with temperature. CH_4 selectivity decreases slightly when increasing temperature from 500 to 550°C, whereas the opposite trend is observed for H_2. On the other hand, CO_2 selectivity remains constant. Although these trends match the trends from thermodynamics calculations, H_2 selectivity here is much higher than what is expected at equilibrium (e.g., ~60% vs. ~40% equilibrium at 525°C) and vice versa for CH_4 (e.g., ~12% vs. ~35% equilibrium at 525°C).

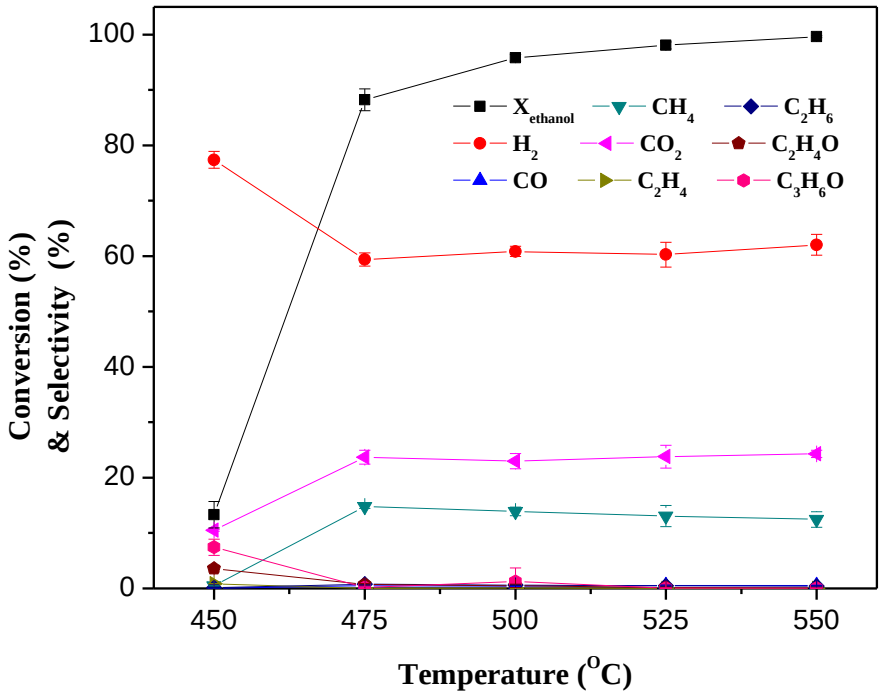

Figure 7-20: Conversion and product selectivity for in-situ reduction of 10 wt.% Co/YSZ. (250 bar, 5 wt.% ethanol, 1.88 g/min feed, 1 g catalyst)

7.2.7 Comparison between Catalyst Performance at Atmospheric and SCW Pressure

Figure 7-21 shows the ethanol conversion at 550°C over non reduced and in-situ reduced 10wt.% Co/YSZ vs. the time-on-stream at atmospheric pressure (1.01 bar) and supercritical water pressure (250 bar). At 250 bars, the conversions for non reduced and reduced catalysts are almost complete (~100%), even after 30 minutes (time for the first data point). At atmospheric pressure, the conversion over in-situ reduced catalyst is around 80%. For the non reduced catalyst at atmospheric pressure, the conversion increases with time-on-stream from ~43% after 30 min to 70% after 240 min. The increase with time-on-stream again shows the change in catalyst activity, due to "self reduction" by hydrogen produced during ethanol reforming, as described previously. At 550°C, reforming in SCW yields higher conversion than at atmospheric pressure. Yet, one should realize that the residence time calculated at atmospheric pressure for the data shown in Figure 7-21 is about 8 ms, which is around 300 times smaller than the residence time at supercritical conditions.

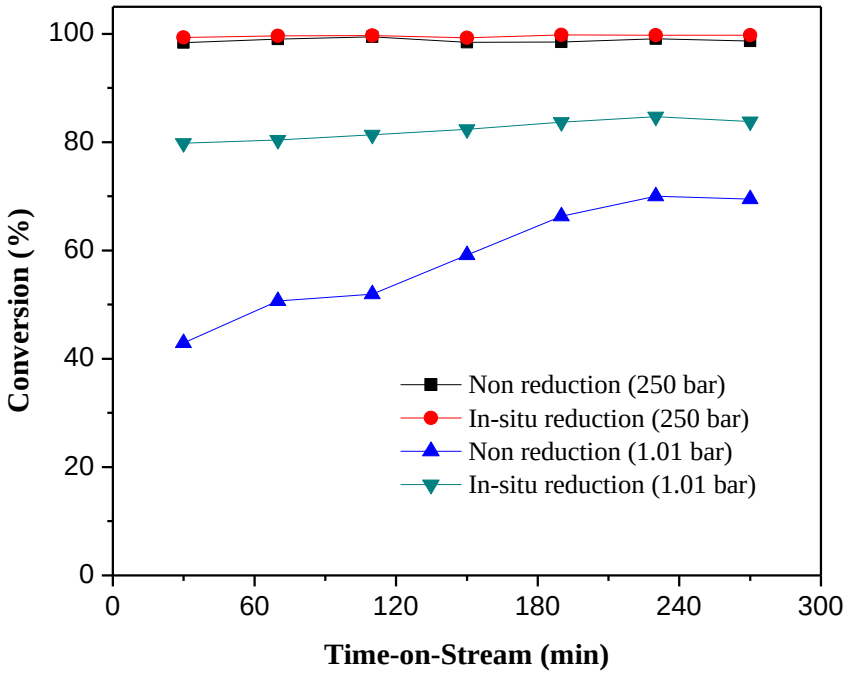

Figure 7-21: Ethanol conversion over 10 wt.% Co/YSZ vs. the time-on-stream at atmospheric pressure 1.01 bar (1 atm) and at supercritical water pressure, 250 bar. (Non reduced and in-situ reduction of the catalyst, 5 wt.% ethanol, 1.88 g/min feed flowrate, 1 g catalyst)

Although the conversion is greater at higher pressure, thermodynamic calculations show that higher pressure would be detrimental to H_2 selectivity, favouring CH_4 formation. Figure 7-22 shows the H_2, CO, CH_4 and CO_2 selectivities at supercritical water and atmospheric pressures at 550ºC. The selectivity of H_2 at atmospheric pressure is ~71% after 240 minutes for the non reduced sample and 75% after 240 minute for the in-situ reduced catalyst. Meanwhile, H_2 selectivity over non reduced and reduced catalysts was ~63%. Increasing the reaction pressure from 1.01 bar to 250 bar decreases the H_2 selectivity by about 16% for the reduced catalyst. CO_2 selectivity at supercritical water and atmospheric pressure are 24%, and 21% (reduced catalyst), respectively, which is close to the equilibrium value of ca. 25%. The decrease in H_2 selectivity is counterbalanced by a net increase in CH_4 selectivity at SCW pressure. The CH_4 selectivity at atmospheric pressure is small, around 0.8% only, whereas it is 11% at 250 bar. On the other hand, CO is favoured at atmospheric pressure, with 2% selectivity compared to 0.7% for reaction in supercritical water.

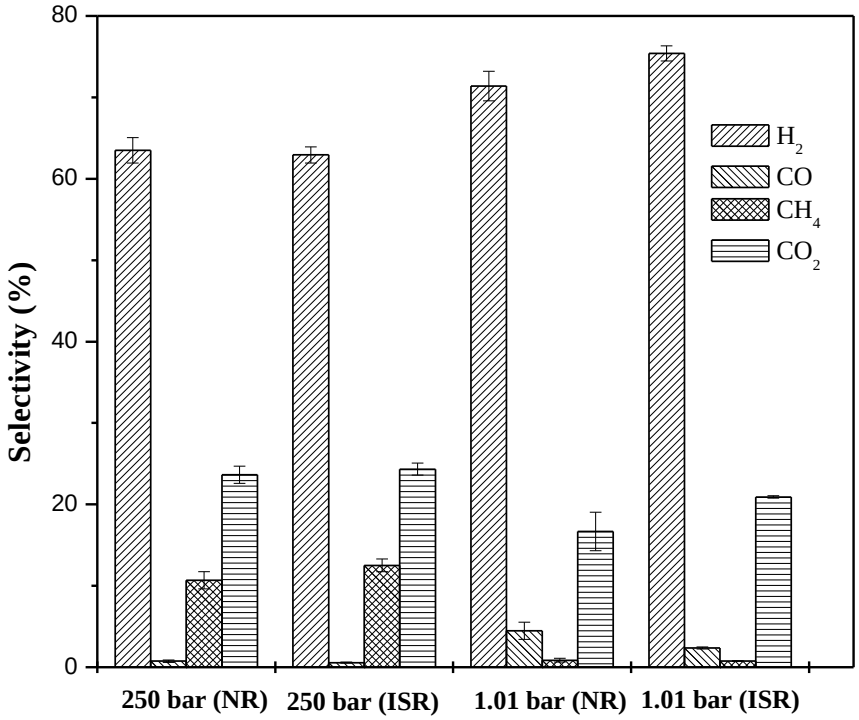

Figure 7-22: Product selectivities of the major products (H_2, CO, CH_4 and CO_2) over 10 wt.% Co/YSZ for different pressures and pre-treatments (5 wt.% ethanol, 1 g catalyst, 550°C, 1.88 g/min feed flowrate). Legend : NR- non reduced catalyst, ISR- In-situ reduced catalyst.

7.2.8 Accelerated "Self Reduction"

The previous results at 550°C have shown very little difference in terms of activity between reduced and non-reduced catalysts. It was proposed that the reason for this is the fast "self reduction" of the catalyst (CoO) by the hydrogen produced. It was also observed that below 550°C, this "self reduction" mechanism is significantly slower. A series of experiments was then proposed with non-reduced catalysts where the reaction first takes place at 550°C (for 3 hours) in order to accelerate the reduction of CoO to Co° and then run the reforming reaction at a desired temperature (e.g., 500 or 525°C). After this initial step at 550°C, the temperature was reduced to the desired temperature by slowly stepping down by 12.5°C with 10 minutes between each set point. This method was employed to avoid a sudden temperature decrease, which could have resulted in higher pressure fluctuations with the possibility of damaging the catalyst.

Figure 7-23 shows the result of the temperature change from 550°C to 500°C after 180 min at 550°C. In this figure, the only significant change observed is the ethanol conversion. The conversion shows a small increase at the beginning (from 90% (at 30 minute) to 99% (at 150 minute)), but drops back at 500°C to a conversion of about 85%. Compared to the result with in-situ and ex-situ reduction, the ethanol conversion is similar, around 85%, whereas it was only 30% with non-reduced catalyst at 500°C. This indicates that this accelerated "self-reduction" method does work. The product selectivities are almost constant during the whole experiment except for acetone. The selectivities of H_2, CO_2, and CH_4 are around 70%, 18% and 7%, respectively. Acetone selectivity indicates a small decrease at the beginning.

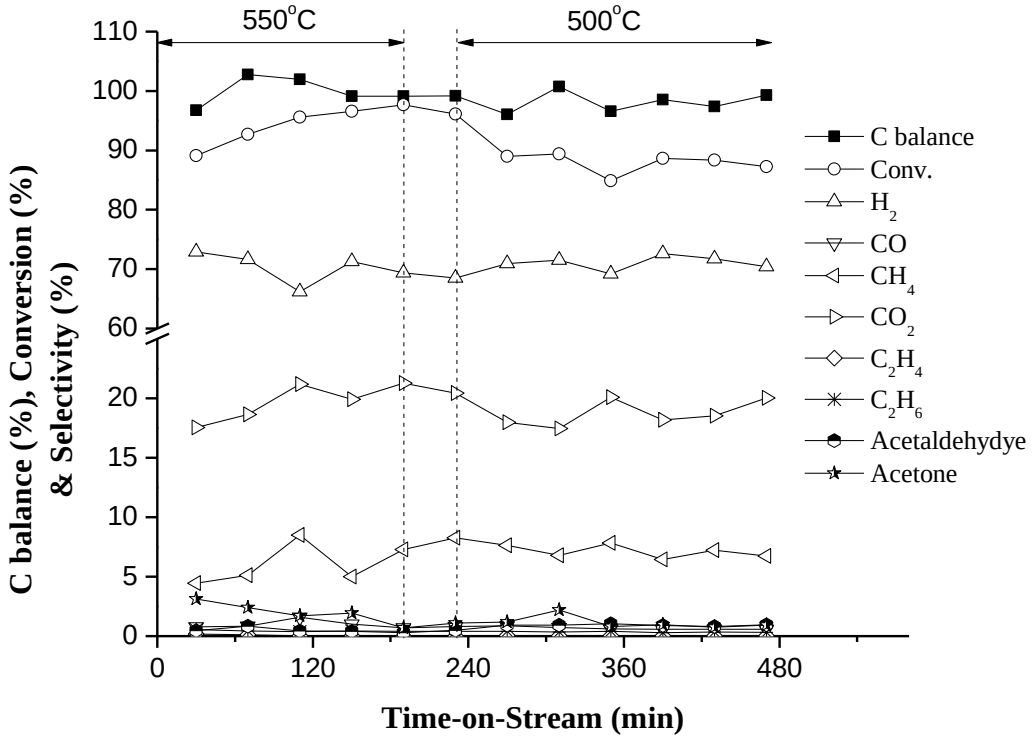

Figure 7-23: Temperature change 550°C (5 samples) to 500°C (7 samples). 250 bar, 5% wt., 1 g non reduced catalyst, 1.88 g/min)

The results of the temperature change from 550°C to 525°C are presented in Figure 7-24. Even after reducing the temperature to 525°C, the ethanol conversion continues to increase until reaching a plateau at ~100% for the rest of the experiment. Starting at 550°C and then lowering the temperature to 525°C allowed ethanol conversion to reach complete conversion even without pretreatment of the catalyst with H_2. However, the increase in conversion is accompanied by a slight decrease in H_2 selectivity, from 70% at 550°C down to 62% at 500°C after 240 minutes. Once again, the decrease in hydrogen is accompanied by an increase in CH_4 selectivity.

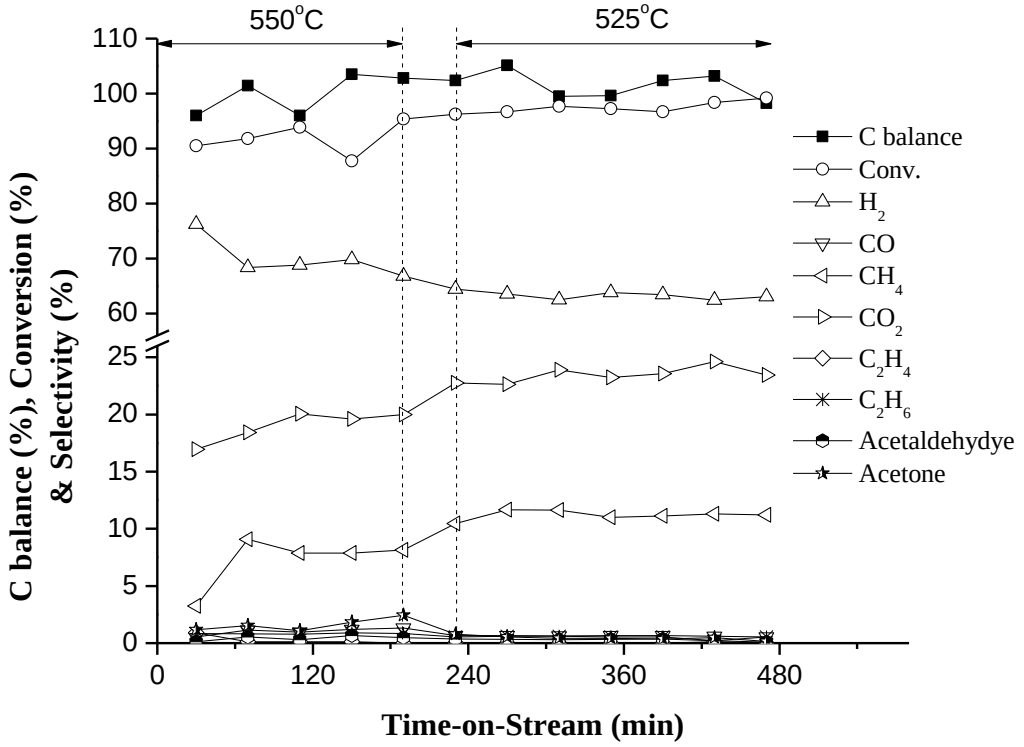

Figure 7-24: Temperature change 550°C (5 samples) to 525°C (7 samples). (250 bar, 5 wt.%, 1 g non reduced catalyst and 1.88 g/min feed).

7.2.9 Reaction Pathway

As in Chapter 6, before discussing reaction pathways, it is best to recall the possible reaction schemes, which are shown in Figure 7-25. In schemes 1 and 2, ethanol first undergoes dehydrogenation to form acetaldehyde and hydrogen. In scheme 1, acetaldehyde subsequently decomposes into CH_4 and CO. CH_4 can then be further reformed and CO can then react via the water-gas shift reaction. In scheme 2 acetaldehyde goes through a series of reactions involving lattice oxygen to form acetone, which in turn may be reformed. Finally, in Scheme 3 ethanol is first dehydrated to form C_2H_4, which is then hydrogenated to generate C_2H_6.

Scheme 1

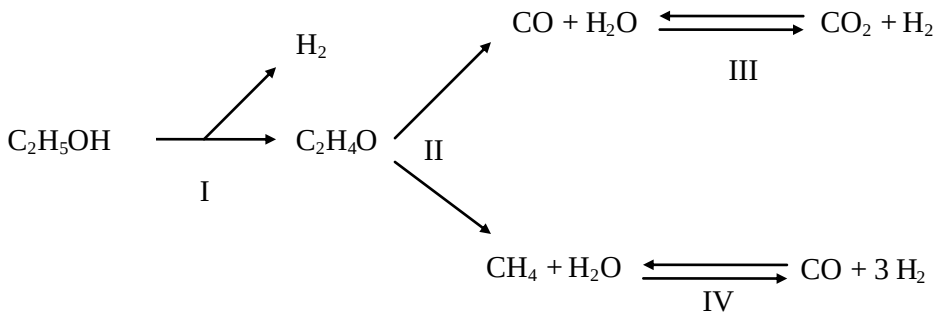

Scheme 2

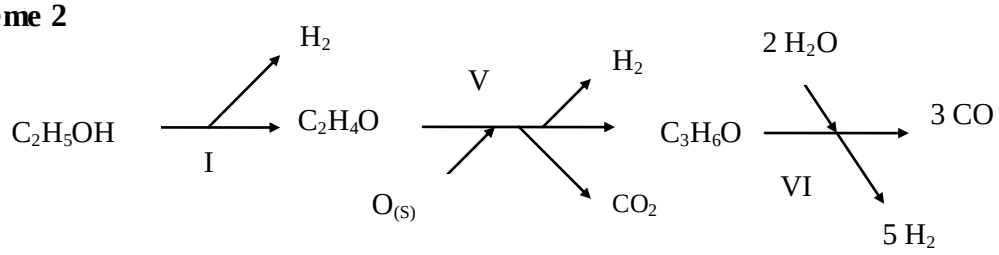

Scheme 3

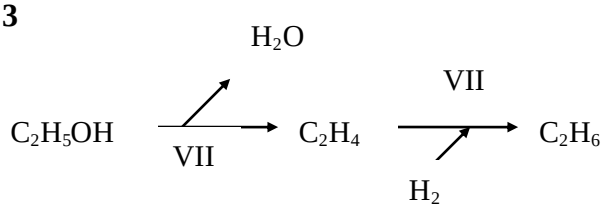

Reactions:
I – Ethanol dehydrogenation
II – Acetaldehyde decomposition
III – Water gas shift
IV – Methane reforming (the reverse being methanation reaction)
V – Acetaldehyde to Acetone
VI – Acetone reforming
VII – Ethanol dehydration
VIII – Ethylene hydrogenation

Figure 7-25: Most Probable Reaction Schemes.

To gain insight into reaction pathways, the selectivities of all detected species are presented, as a function of residence time, in Figure 7-26 to Figure 7-33.

Hydrogen selectivity is shown in Figure 7-26. For all temperatures, H_2 selectivity decreases with increasing residence time. This indicates that hydrogen that was produced in the early stage of the reaction is being consumed as the reaction proceeds. At 500 and 550°C, the H_2 selectivity decreases with residence time until it reaches a constant value of ~63%, at which point the conversion is nearly complete. At 550°C, the H_2 selectivity reaches 63% within 2 seconds, whereas it takes up to 4 seconds at 500°C. At 450°C the H_2 selectivity is much higher, but one should remember that the conversion was low, between 7% (after 2 seconds) and 25% (after 7 seconds). Another important observation is that the H_2 selectivity determined experimentally is much higher than that calculated from thermodynamics (21% at 450°C, 33% at 500°C and 44% at 550°C). This indicates that the reaction is far from reaching equilibrium.

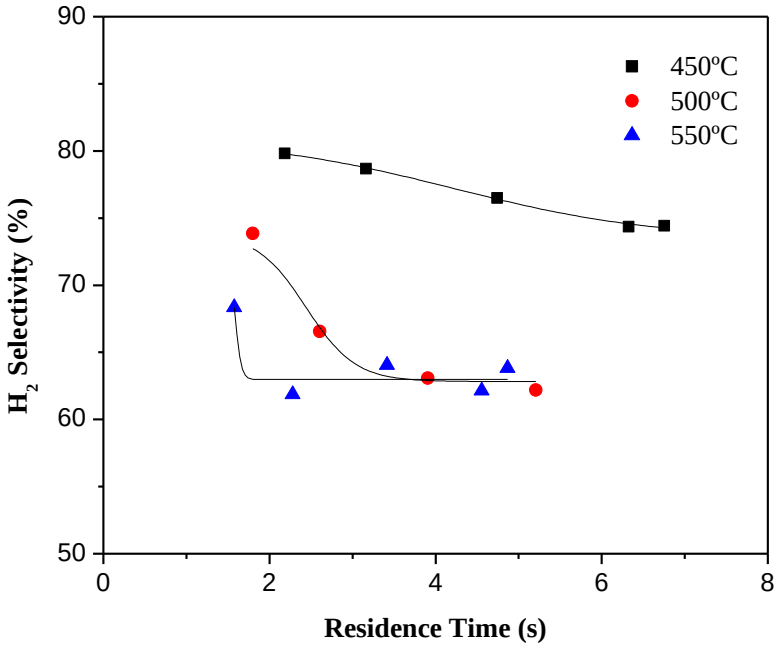

Figure 7-26: H_2 selectivity vs. residence time at 450, 500 and 550°C (250 bar, 5% wt. ethanol, 1 g non reduced catalyst and 1.88 g/min feed)

The thermodynamic calculations highlighted the strong correlation between the opposite trends for hydrogen and methane. Methane selectivity is shown in Figure 7-27. In the experiments, the trend for CH_4 is indeed the opposite to that of H_2: when H_2 selectivity decreases to reach a fixed value after 2 s at 550°C and 4s at 500°, the CH_4 selectivity is the exact opposite, i.e., CH_4 increases to a plateau after 2 s at 550°C and after 4 s at 500°C. In other words, when H_2 is being

consumed, CH_4 is being produced. This points to the importance of the methanation reaction, involving H_2 and CO to produce CH_4. Before developing any further the methanation route, let's first consider the source of hydrogen because Figure 7-26 clearly shows that hydrogen is being produced in higher amounts at the early stage of the reaction (low residence time).

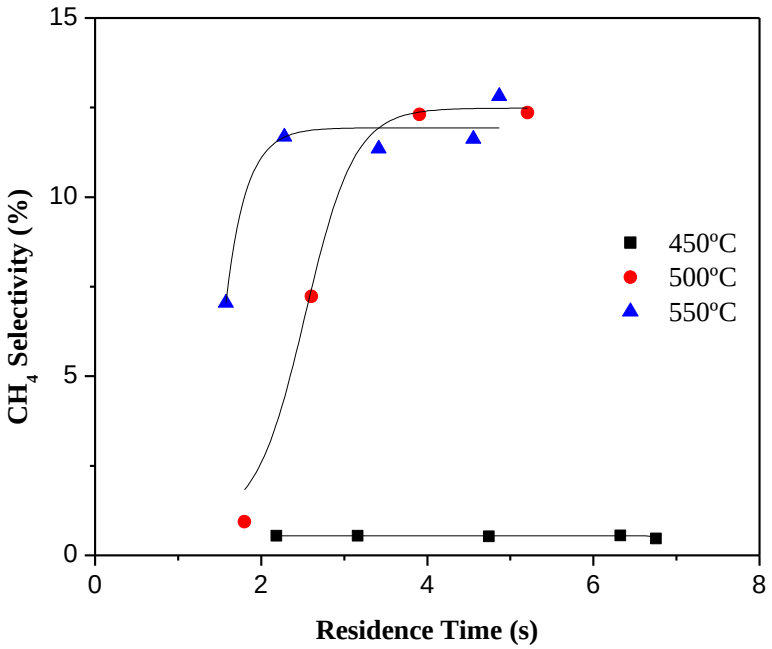

Figure 7-27: CH_4 selectivity vs. residence time at 450, 500 and 550°C (250 bar, 5% wt. ethanol, 1 g non reduced catalyst and 1.88 g/min feed)

From the reactions schemes shown in Figure 7-25, one of the most obvious pathways to generate hydrogen at the early stage of the reforming reaction is the dehydrogenation of ethanol to form acetaldehyde. The acetaldehyde selectivity vs. residence time is shown in Figure 7-28. This figure clearly shows a decrease in acetaldehyde selectivity when the residence time increases. In other words, acetaldehyde is first produced and then consumed as the reaction proceeds. As the temperature increases, the acetaldehyde selectivity decreases, which could be attributed to either a lower amount of acetaldehyde produced at high temperature and/or much faster consumption of acetaldehyde as the temperature increases. Lower amounts of acetaldehyde produced at higher temperatures mean that the reaction scheme would shift from the ethanol dehydrogenation (scheme 1 and 2) to ethanol dehydration (scheme 3). Considering that the selectivities of C_2H_4 and C_2H_6 are below 1% (see Figure 7-32 and Figure 7-33), we can safely disregard the possibility of a major shift from ethanol dehydrogenation to ethanol dehydration. We, therefore, conclude that the

decrease in acetaldehyde selectivity at high temperature is essentially due to a higher rate of acetaldehyde consumption. Acetaldehyde consumption can occur through two main routes: 1) decomposition to CH_4 and CO, and 2) reaction with lattice oxygen to form acetone.

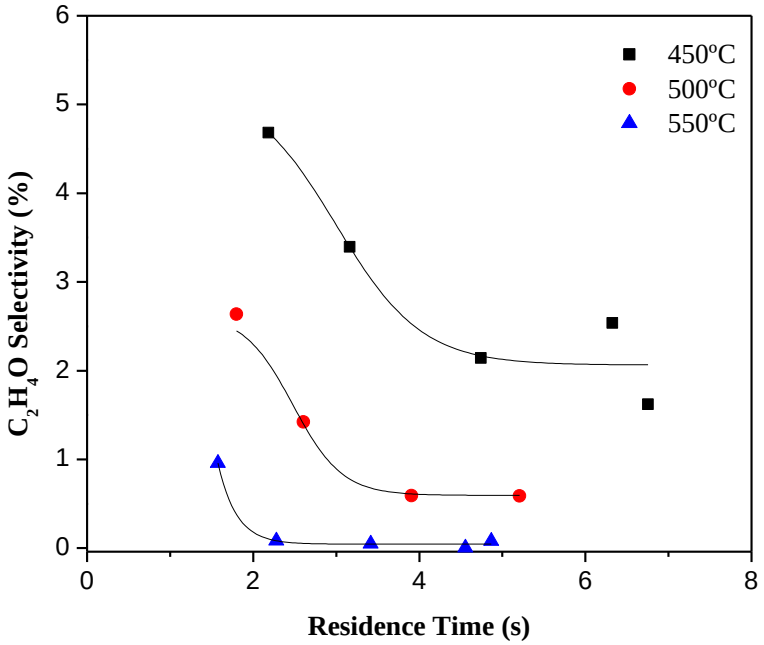

Figure 7-28: Acetaldehyde selectivity vs. residence time at 450, 500 and 550°C (250 bar, 5% wt. ethanol, 1 g non reduced catalyst and 1.88 g/min feed)

If we assume that acetaldehyde is mostly consumed via decomposition to CH_4 and CO, then we should pay particular attention to CH_4 and CO selectivities. At high temperatures we have seen that CH_4 increases (see Figure 7-27). In addition, CH_4 also increases with residence time, which is consistent with the disappearance of acetaldehyde when the residence time increases. For CO selectivity (refer to Figure 7-31) it is clear that CO selectivity is small (less than 1% and actually closer to 0.5% for steady values at 500 and 550°C). This suggests that CO is consumed significantly through the water-gas shift reaction and, indeed, CO_2 increases as the reaction proceeds.

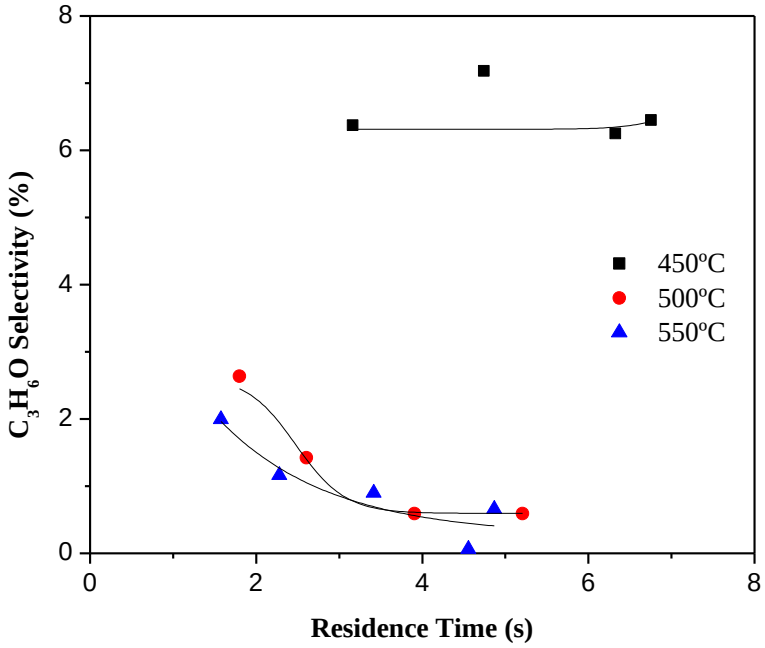

Figure 7-29: Acetone selectivity vs. residence time at 450, 500 and 550°C (250 bar, 5% wt. ethanol, 1 g non reduced catalyst and 1.88 g/min feed)

Another possible fate for acetaldehyde is its reaction with lattice oxygen on YSZ to form acetone. Acetone selectivity versus residence time is shown in Figure 7-29. At 450°C, the acetone selectivity remains constant at a value between 6 and 7%. At 500 and 550°C acetone selectivity decreases with residence time from 2-3% after 1.5 s down to 0.5% after 4 s. The disappearance of acetone could be attributed to acetone reforming, likely producing CO and H_2. In such a case, acetone can become an important source of hydrogen, as one mole of acetone can yield 5 moles of H_2 (in fact up to 8 moles of H_2 if CO is shifted to CO_2 and H_2). The relatively high value of acetone selectivity at 450°C suggests that in the early stage of the reforming reaction an important amount of acetone can be produced. As the residence time decreases, in particular at 500 and 550°C, the acetone selectivity increases, but, unfortunately, it was not possible to carry out experiments with residence time less than 1.5 s to verify how high the acetone selectivity can be at lower residence time. Small amounts of ethylene and ethane were also detected, indicating that the reaction pathway starting with ethanol dehydration (scheme 3) should not be disregarded, although this route is of minor importance compared to the dehydrogenation route. The ethylene and ethane selectivities are shown in Figure 7-32 and Figure 7-33, respectively. Ethylene selectivity quickly

decreases with residence, especially at higher temperature. Simultaneously, as ethylene decreases, ethane increases.

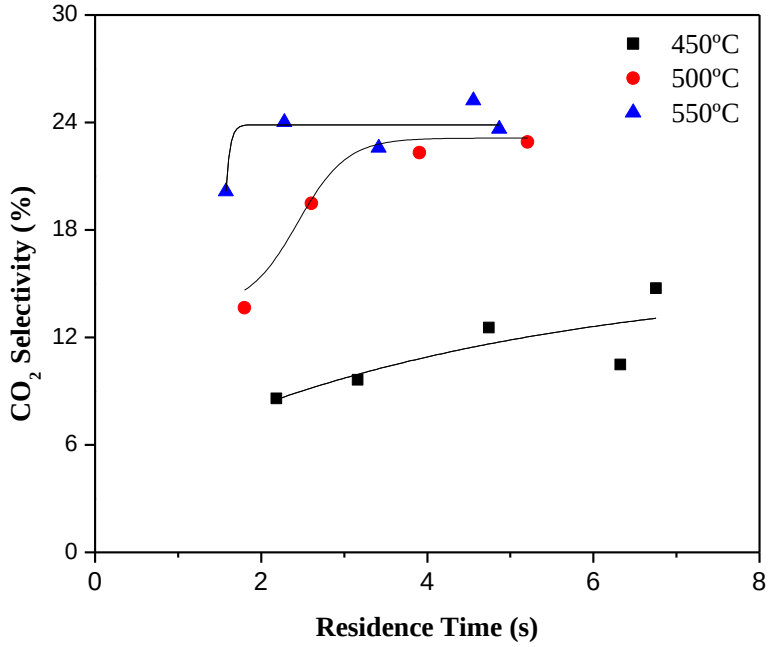

Figure 7-30: CO_2 selectivity vs. residence time at 450, 500 and 550°C (250 bar, 5% wt. ethanol, 1 g non reduced catalyst and 1.88 g/min feed)

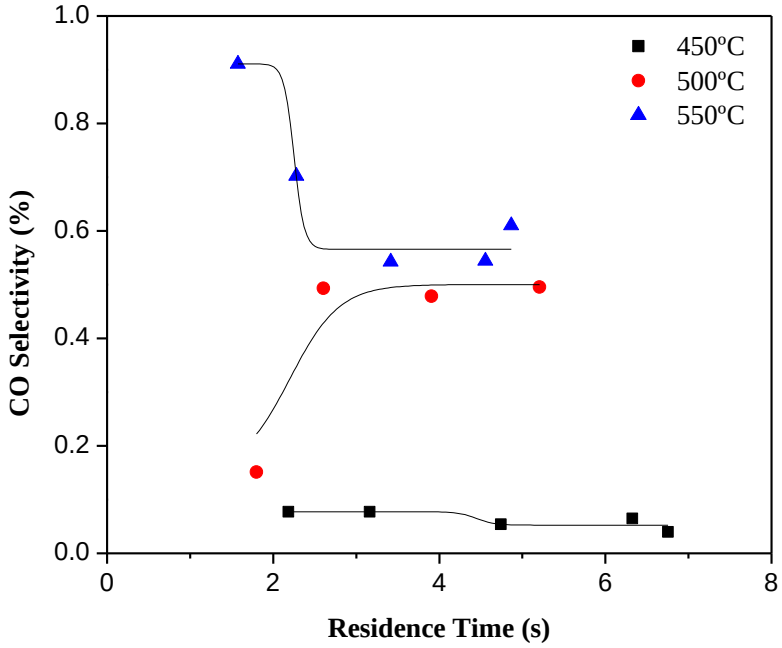

Figure 7-31: CO selectivity vs. residence time at 450, 500 and 550°C (250 bar, 5% wt. ethanol, 1 g non reduced catalyst and 1.88 g/min feed)

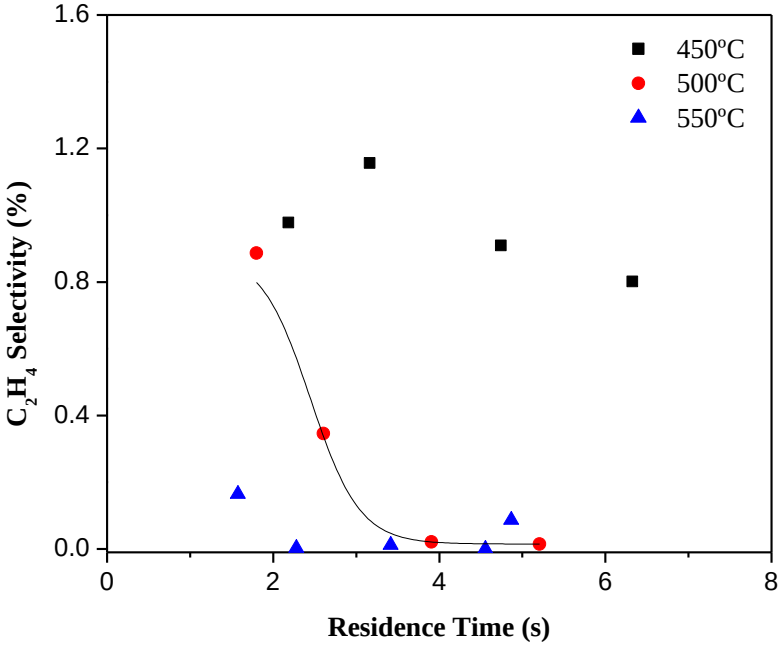

Figure 7-32: Ethylene selectivity vs. residence time at 450, 500 and 550°C (250 bar, 5% wt. ethanol, 1 g non reduced catalyst and 1.88 g/min feed)

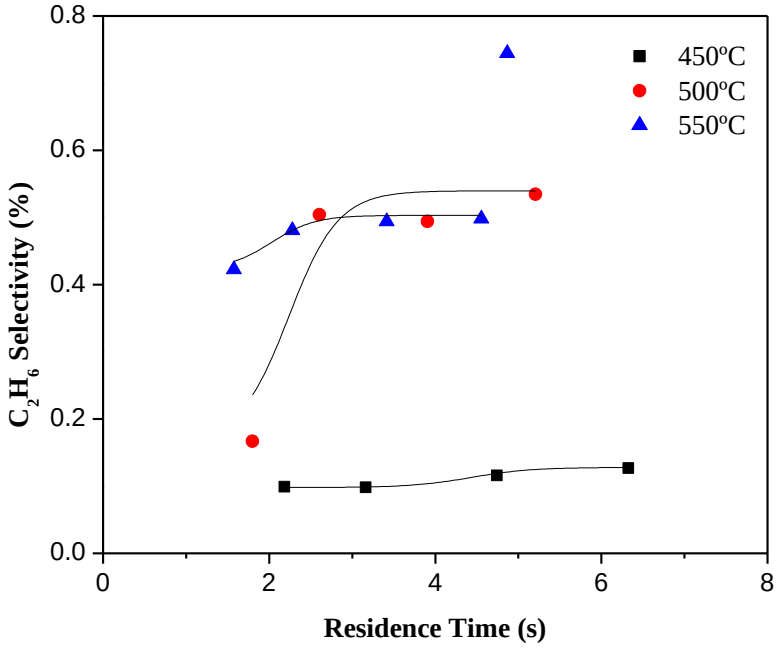

Figure 7-33: Ethane selectivity vs. residence time at 450, 500 and 550°C (250 bar, 5% wt. ethanol, 1 g non reduced catalyst and 1.88 g/min feed)

The results show the importance of the ethanol dehydrogenation route to acetaldehyde, but the relative importance of acetaldehyde decomposition and acetaldehyde reaction to acetone needs to be further examined. We have seen that the hydrogen selectivity obtained experimentally (63% at 500 and 550°C) is higher than that calculated at equilibrium (32% at 500°C and 42% at 550°C). Likewise, the observed CH_4 selectivity (12% at 500 and 550°C) is lower than the equilibrium one (41% at 500% and 30% at 550°C). If ethanol reforming follows primarily Scheme 1, assuming that CO is completely consumed (reasonable considering the very small CO selectivity observed), a simple material balance calculation shows that the only way to reconcile the observed selectivities of H_2, CH_4 and CO_2 at 500 or 550°C is for a fraction of the methane formed (in fact ~ 35%) to be reformed and for all the CO to be shifted to CO_2. The main problem with this is that H_2 would only be generated and not consumed, whereas CH_4 would be first produced and then consumed to some extent. This is contrary to the observed behaviour for H_2 and CH_4 (See Figure 7-26 and Figure 7-27). In addition, the notion that CH_4 might be consumed as the reaction proceeds is contrary to the fact that at equilibrium the CH_4 selectivity should be much higher than that observed. Therefore, Scheme 1 alone is not adequate to explain the experimental results.

We have seen that the decrease in H_2 selectivity as the reaction proceeds is accompanied by an increase in CH_4 selectivity and it was pointed out that this behaviour would be characteristic of the methanation reaction. This also means that CH_4 has to be generated after H_2 and CO have been produced. This is not possible based on Scheme 1 alone, but is possible according to Scheme 2 when acetone is being reformed. In fact, Scheme 2, followed by methanation, can explain well all trends observed experimentally:

- Acetaldehyde selectivity first increases and then decreases, indicative of ethanol dehydrogenation followed by acetaldehyde consumption to produce acetone.

- Hydrogen is rapidly produced initially from ethanol dehydrogenation, acetaldehyde reaction with lattice oxygen, and from acetone reforming, and is then consumed via methanation. Hence, the increase in H_2 at low residence time followed by a decrease in H_2 selectivity.

- CO is first produced from acetone reforming and then consumed by methanation and water-gas shift reaction. Since one mole of acetone would yield 3 moles of CO when reformed, and because the selectivity of CO is smaller than that of acetone, this means that either acetone reforming is slow or CO is consumed very rapidly. Because the selectivity of CH_4 is much higher than that of CO, even at lower residence time, and because CH_4 is generated from CO via methanation, then acetone reforming cannot be a slow reaction. One could argue that the CH_4 produced actually come from acetaldehyde decomposition, but then CO would be produced in similar molar amounts to CH_4. Because CO selectivity is small, CO would have to be then consumed rapidly via the water-gas shift reaction. In any case, everything points toward rapid consumption of CO. In addition, it is interesting to note that the thermodynamic calculations lead to CO and CO_2 selectivity of less than 0.5% and of 25%, respectively, which is very close to the value found experimentally. We can then conclude that the water-gas shift reaction is a fast reaction that rapidly reaches equilibrium.

- CH_4 is produced from methanation and would increase as the reaction proceeds. Because CO_2 is generated first from the reaction yielding acetone, before methanation occurs, there should be a delay between the appearance of CO_2 and CH_4. If CH_4 were

to be formed from acetaldehyde decomposition (Scheme 1), then CO, and thus CO_2 because of the fast shift reaction, should appear simultaneously. At 500°C and at the lowest residence time (1.5 s) the CO_2 selectivity is 13% when CH_4 selectivity is only ~1%. This delay between the appearance of methane and that of CO_2 further demonstrates that Scheme 2 is the primary route during ethanol reforming at 500°C. At 450°C, CH_4 selectivity remains less than 1% (even after 6 s residence time), whereas CO_2 selectivity goes up to ~12%. Combined with the fact that acetone selectivity at 450°C is up to 6%, this shows that acetaldehyde decomposition (at least at 450°C) occurs primarily via a reaction leading to acetone and not via acetaldehyde decomposition.

The above reasoning demonstrates that the acetone route (Scheme 2) is the main reaction pathway at 450 and 500°C. At 550°C, all trends are also in agreement with Scheme 2 being the main route during ethanol reforming, although it is difficult to assess to what extent acetaldehyde decomposition occurs. In addition, we have seen that a comparison between thermodynamic calculations and experimental data suggests that the water-gas shift reaction is fast and quickly approaches equilibrium. On the other hand, because methane selectivity is below its equilibrium value, it can be concluded that methanation is a comparatively slow reaction. The fact that the water-gas shift reaction is fast and methanation is slower is of important practical importance because if the reaction can be stopped before reaching equilibrium, a much higher hydrogen selectivity (and lower CH_4 selectivity) can be obtained. The importance of Scheme 2 is due to the presence of lattice oxygen capable of reacting with acetaldehyde. If this were not the case, then the reaction would not be able to go through the acetone route, and higher hydrogen yields than equilibrium at almost complete ethanol conversion would not be possible.

7.3 Summary

Several reaction parameters have been studied over Co/YSZ catalysts. XRD results have shown that the activity of ethanol reforming depends on the Co phase. It was found that ethanol reforming is favoured in the presence of the metallic phase of cobalt, Co°. Non reduced catalyst at 550°C resulted in complete ethanol conversion for residence time as short as 1.5 s, and only Co° phase was present after the experiment. The experiments carried out in this study have shown that non reduced fresh catalysts can be reduced as the reforming reaction proceeds by the hydrogen thus generated. This was termed “self reduction”. It was shown that conditions favouring higher

production of hydrogen, such as high Co loading, high mass of catalyst, high ethanol concentration or high temperature contributed to faster self-reduction of the catalyst, resulting in higher conversion. An important result is that, whether cobalt in the fresh catalyst is in the form of Co_3O_4 or Co°, after being exposed to supercritical water it will be either reduced or oxidized to end up being in CoO phase. It was therefore deemed that pre-treatment of the catalyst in hydrogen was not necessary.

Nonetheless, some experiments were carried out with a fully reduced fresh catalyst (either in-situ reduction or ex-situ reduction). At 550°C, reduced and non-reduced catalysts yield the same performance. At 500°C, the reduced catalyst yields higher activity than the non reduced one, but the method of reduction (ex-situ vs. in-situ has) did not matter. At 475°C, however, the reduction method results in very different conversions; the conversion with ex-situ reduced catalysts shows very little activity, comparable to that with the non reduced catalyst. But the in-situ reduction yielded considerable higher conversion, which we attributed to reduced metal sites on the reactor's wall capable of "igniting" ethanol reforming and generating hydrogen earlier on during the reaction.

In an attempt to accelerate reduction of the fresh catalyst without having to feed hydrogen, we proposed to first carry out the reaction at 550°C for a certain duration (e.g., 3 hours), as it was found that cobalt was fully reduced after such experiments. Then, the temperature was reduced to the desired reaction temperature (e.g., 500 or 525°C). This method was been shown to work, although the catalysts was found broken up in smaller particles, but this may have been caused by pressure fluctuations when reducing the temperature.

A comparison of catalyst performance at 550°C between atmospheric pressure and 250 bar showed higher conversion at high pressure, but somewhat lower hydrogen selectivity and higher methane selectivity.

Analysis of reaction pathways shows that ethanol reforming over Co/YSZ in SCW water mainly goes first through ethanol dehydrogenation to form the intermediate acetaldehyde. Acetaldehyde can then decompose to methane and CO or react with lattice oxygen on the YSZ surface to form acetone. Our results suggest that the route via acetone is the main route for Co/YSZ. It was also suggested that methanation is a relatively slow process, thus explaining the reason for obtaining hydrogen yields greater than the calculated equilibrium values.

Chapter 8

Conclusions and Recommendations

8.1 Conclusions

This work has shown the practicality of catalytic ethanol reforming in supercritical water. The catalytic activity of the Inconel-625 reactor was evaluated in terms of ethanol hydrolysis activity. Reactor plugging in the empty reactor occurred at temperatures above 575°C due to coking on the screen inside the reactor. Therefore, it was decided that the experiments with catalysts would not exceed 550°C. Even with the most favourable conditions of high temperature (550°C) and low flowrate (0.88 g/min), ethanol conversion in the empty reactor was below 25%.

Catalyst screening over two active metals, Ni and Co, supported on various supports (γ-Al_2O_3, α-Al_2O_3, ZrO_2 and YSZ) have been tested at 250 bar, 5 wt.% ethanol, 1.88 g/min feed flowarate, 10 wt.% metal loading, 1 g of non reduced catalyst, and temperatures range of 475 to 550°C. The presence of catalyst does increase the activity of ethanol reforming. However, the activity is highly influenced by the reducibility of the active metal. The results show that Ni is more active than Co regardless of the type of support. Since those experiments were carried out with non-reduced catalysts, we speculated that the higher performance of Ni was due to the smaller amount of hydrogen required to reduce Ni oxide than that to reduce Co oxide. Several experiments failed because of coking problems: Ni and Co supported on γ-Al_2O_3 above 500°C, and Co/α-Al_2O_3 above 525°C. The failure over γ-Al_2O_3 is due to its high selectivity toward ethylene, because of the highly acidic nature of γ-Al_2O_3. For α-Al_2O_3 support there was one failed experiment over Co/α-Al_2O_3 at 550°C. Ni and Co on zirconia-based catalysts are active, but zirconia is fragile, as evidenced by its tendency to break up into smaller particles. The catalyst supported on YSZ was stable and active for ethanol reforming in SCW. The activity of Ni and Co over YSZ is comparable, but Co is more selective toward H_2 production and less selective toward CH_4. Co/YSZ catalyst was therefore chosen for further study.

For Co/YSZ, several reaction parameters have been studied, such as feed low rate, mass of catalyst, residence time, Co loading, ethanol concentration, pressure and pre-treatment/reduction with H_2.

The XRD profile of Co/YSZ shows that the ethanol reforming activity depends on the Co phase. Cobalt has to be in Co° phase in order to become active for ethanol reforming. XRD analysis also showed that whether one starts with Co° or Co_3O_4, after exposure to supercritical water for 30 minutes, the cobalt was either oxidized or reduced to a CoO phase.

It was shown that at 550°C, non-reduced Co/YSZ can achieve performances comparable to reduced catalysts. This was attributed to rapid self-reduction as the reaction proceeds by the hydrogen formed during the reaction. Below 550°C, the non-reduced catalyst yielded lower conversions than the reduced one. At 500°C, in-situ and ex-situ reduction led to similar conversions and selectivities. The non-reduced catalyst at 500°C was much less active. At 475°C, the conversion with ex-situ reduction was low, comparable to that with non-reduced catalyst, but the in-situ reduction, yielded much higher conversion. This is probably due to reduced metal sites on the reactor's wall. A method was proposed and tested to accelerate self-reduction by first carrying out the reaction at 550°C to reduce cobalt to Co°, and then reduce the temperature to the desired reaction temperature. This method has worked, although there was problem of catalyst break-up, but it is believed that a better control of the pressure within the reactor while changing the temperature could resolve this issue.

Comparison of reduced or non reduced catalyst between the reaction at atmospheric pressure and supercritical pressure (250 bar), shows the advantages of SCW in terms of improved conversion, but at the expense of somewhat lower H_2 yield and higher CH_4 yield.

An important finding with Co/YSZ is that H_2 selectivity is much higher than the calculated value at equilibrium and conversely CH_4 selectivity is lower than what is expected at equilibrium.

Analysis of reaction pathways indicated that ethanol reforming over Co/YSZ first goes through ethanol dehydrogenation to form acetaldehyde. Then, because of the nature of YSZ, acetaldehyde reacted primarily with lattice oxygen to form acetone, which was subsequently reformed. This acetone route was found to be more important than acetaldehyde decomposition to CH_4 and CO. It was also found that over this catalyst the water-gas shift reaction is fast, faster than methanation. The ability of Co/YSZ to favour a reaction pathway with acetone intermediate, combined with slow methanation reaction allows for higher H_2 yield and lower CH_4 yield.

8.2 Recommendations

This work has shown the potential of Co/YSZ catalyst for ethanol reforming in SCW. Due to the properties of YSZ it is possible to obtain high hydrogen selectivity, actually higher than equilibrium selectivity if the reaction is stopped before complete methanation. Nonetheless, to assess the practicality of generating high-pressure, high-purity hydrogen from ethanol, there are a number of further studies that need to be done. These further studies can be divided into three categories:

1) Kinetics and catalyst development
2) Improvement in the SCW setup
3) Process development

Kinetics and Catalyst Development:

1. In this work the Co/YSZ was tested for a maximum duration of 8 hours. A much longer duration test are required to assess the long time stability of the catalyst. With our current apparatus, we are actually limited in duration by the volume of the ISCO pump (up to 25 hours for typical 2 g/min flowrate). Nonetheless, addition of a second ISCO pump would eliminate any limitation in time.

2. A detailed kinetic study must be done to quantify the various reaction rates and to confirm the reaction pathways. This will be particularly useful when optimizing the reactor, especially since the reaction is kinetically controlled. To do so, a number of experiments targeted at particular reactions must be carried out. For example, the methanation and water-gas shift reactions could be investigated by feeding various mixtures of CO, H_2 and CO_2 in supercritical water. Other reactions that must be further investigated are acetone reforming and reactions involving acetaldehyde. Again, such a study would require the purchase of a second ISCO pump.

3. More work should be done regarding catalyst preparation in order to render it tougher and more resistant to the supercritical water environment.

4. Fuels, other than ethanol should be investigated as well, for example glycerol, which is a byproduct from biodiesel production. Methanol could be another candidate.

Improvement in the SCW Setup

5. As mentioned previously, addition of another ISCO pump would eliminate limitation in the duration of the experiments. It will also allow for more flexibility in term of gas mixtures injection for kinetic studies.

6. One element of the current setup that has caused numerous problems is the back pressure regulator. A better control of pressure fluctuation would reduce the risk of catalyst damage. It will also allow for the use of higher ethanol concentration in the feed. Currently, when too much gas is produced the BPR has great difficulty to keep the pressure stable. One possibility to resolve this issue would be to have to two BPR's in parallel, therefore dividing by two the gas flow rate going through each BPR.

Process Development:

7. Study the means for hydrogen separation and purification. The AspenPlus simulations presented here has shown that 95% of CO_2 and 70% of methane can be removed in a flash unit simply by lowering the temperature to ambient temperature while keeping the pressure at 250 bar. This should be verified in actual experiments. For hydrogen purification at high pressure, pressure swing adsorption may be the technology of choice, but sorbent efficiency should be verified by operating at 250 bar, which eventually could lead to the development of a new sorbent.

8. Study overall process integration, including energy recovery to minimize heat losses. An economic evaluation of the entire process needs to be done.

References

Alberton, A. L., Souza, M. M.V.M. Schmal, M. (2007). Carbon formation and its influence on ethanol steam reforming over Ni/Al_2O_3 catalysts. *Catalysis Today*, 123, 1-4, 257-264.

Anikeev, V.I., Yermakova, A., Manion, J. and Hugh, R. (2004). Kinetics and thermodynamics of 2-Propanol dehydration in Supercritical Water. *J. of Supercritical Fluids*, **32**, 123-135.

Arita,T., Nakahara, K., Nagami, K. And Kajimoto O. (2003). Hydrogen Generation from Ethanol in Supercritical Water without Catalyst. *Tetrahedron Letters*, **44**, 1083-1086.

Armbruster, U., Martin, A., and Krepel, A. (2001a). Hydrolysis and Oxidative Decomposition of ethyl acetate in Sub- and Supercritical Water. *Applied Catalysis B: Environmental*, **31**, 263-273.

Armbruster, U., Martin, A. and Krepel, A. (2001b). Partial oxidation of propane in sub- and supercritical water. *The Journal of Supercritical Fluids*, **3,** 233-243.

Armor, J. N., (1999). The multiple roles for catalysis in the production of H_2. *Applied Catalysis A: General*, **176**, 159-176

Arnoldy, P. and Moulijn, J. A. (1985). Temperature-programmed reduction of CoO/Al_2O_3 catalysts. *Journal of Catalysis*, **1,** 38-54.

Aupretre, F., Descorme, C. and Duprez, D. (2002). Bio-ethanol Catalytic Steam Reforming over Supported Metal Catalysts. *Catalysis Communications*, **3**, 263-267.

Aupretre, F., Descorme, C., and Duprez, D. (2004). Hydrogen production for fuel cells from the catalytic ethanol steam reforming. *Topics in Catalysis*, **30**, 487-491.

Aupretre, F., Descorme, C., Duprez, D., Casanave, D., Uzio, D. (2005). Ethanol steam reforming over $Mg_xNi_{1-x}Al_2O_3$ spinel oxide-supported Rh Catalysts. *Journal of Catalysis*, **233**, 464-477.

Baiker, A. (1999) Supercritical Fluids in Heterogeneous Catalysis. *Chem. Rev*, **99**, 453-473.

Bañares, M. A. (1999). Supported metal oxide and other catalysts for ethane conversion: a review. *Catalysis Today*, **2,** 319-348.

Batista, M. S., Santos, R. K. S., Assaf, E. M., Assaf, J. M. and Ticianelli, E. A. (2004). High efficiency steam reforming of ethanol by cobalt-based catalysts. *Journal of Power Sources*, **1,** 27-32.

Batista, M. S., Santos, R. K. S., Assaf, E. M., Assaf, J. M. and Ticianelli, E. A. (2003). Characterization of the activity and stability of supported cobalt catalysts for the steam reforming of ethanol. *Journal of Power Sources*, **1,** 99-103

Bellido, J. D. A. and Assaf, E. M. (2008). Nickel catalysts supported on ZrO_2, Y_2O_3-stabilized ZrO_2 and CaO-stabilized ZrO_2 for the steam reforming of ethanol: Effect of the support and nickel load. *Journal of Power Sources*, **1,** 24-32.

Benito, M., Padilla, R., Rodríguez, L., Sanz, J. L. and Daza, L. (2007). Zirconia supported catalysts for bioethanol steam reforming: Effect of active phase and zirconia structure. *Journal of Power Sources*, **1,** 167-176.

Boero, M., Terakura, K., Ikeshoji, T., Liew, C.C. and Parrinello, M. (2001). Water at Supercritical Conditions: A first principles Study. *J. of Chemical Physics*. **115(5),** 2219-2227.

Boukis N., Diem V., Habicht W. and Dinjus E. (2003a). Methanol Reforming in Supercritical Water. *Ind. Eng. Chem. Res.*, **42**, 728-735.

Boukis N., Habicht, Franz, G., and Dinjus E. (2003b). Behavior of Ni-base alloy 625 in Methanol-Supercritical Water Systems. *Materials and Corrosion*, **54**, 326-330.

Boukis, N., Diem, V., Galla, U., and Dinjus, E. (2006). Methanol Reforming in Supercritical Water for Hydrogen Production. *Combust. Sci. and Tech.*, **178**, 467-485.

Breen J.P., Burch R. and Coleman, H.M. (2002). Metal-catalysed steam reforming of ethanol in the production of hydrogen for fuel cell applications. *Applied Catalysis B: Environmental*, **39**, 65-74.

Bröll, D., Kaul, C., Krämer, A., Krammer, P., Richter, T., Jung, M., Vogel, H. and Zehner, P. (1999). Chemistry in Supercritical Water. *Angew. Chem. Int. Ed.*, **38**, 2998-3014.

Busca, G. in Fierro, J.L.G (2006). Metal Oxides: Chemistry and Application. *Taylor and Francis Group*, Florida, USA.

Byrd, A. J., Pant, K. K., Gupta, R. B. (2007a). Hydrogen Production from Glucose Using Ru/Al_2O_3 Catalyst in Supercritical Water. *Ind. Eng. Chem. Res.*; 46(11); 3574-3579.

Byrd, A. J., Pant, K.K., Gupta, R. B. (2007b). Hydrogen Production from Ethanol by Reforming in Supercritical Water Using Ru/Al_2O_3 Catalyst. *Energy & Fuels* 21 3541-3547

Byrd, A. J., Pant, K. K., Gupta, R. B. (2008). Hydrogen production from glycerol by reforming in supercritical water over Ru/Al_2O_3 catalyst. *Fuel*, 87, 2956-2960.

Calvara, Y., Joussot-Dubien, C., Boissonnet, G., and Sarrade, S. (2005). Evaluation of biomass gasification in Supercritical Water Process for Hydrogen Production. *Energy Conversion and Management*, **46**, 615-631.

Cavallaro, S., Chiodo, V., Freni, S., Mondello, N. and Frusteri, F. (2003). Performance of Rh/Al_2O_3 catalyst in the steam reforming of ethanol: H_2 production for MCFC. *Applied Catalysis A: General*, **249**, 119-128.

Chang, F.W., Yang, H.C., Roselin, L.S. and Kuo, W.Y. (2006). Ethanol dehydrogenation over copper catalysts on rice husk ash prepared by ion exchange. *Applied Catalysis A: General* **304**, 30-39.

Chladek, P. (2007). *Catalytic Separation of Pure Hydrogen from Synthesis Gas by an Ethanol Dehydrogenation / Acetaldehyde Hydrogenation Loop*. PhD Thesis. University of Waterloo, Ontario, Canada.

Coleman, L.J. (2008). *Preparation, Characterization, and Evaluation of Mg-Al Oxide supported Nickel Catalysts for the Steam Reforming of Ethanol.* PhD Thesis. University of Waterloo, Ontario, Canada.

Comas J., Marino F., Laborde, M. and Amadeo, N. (2004). Bio-ethanol Steam Reforming on Ni/Al_2O_3 catalyst. *Chemical Engineering Journal*, **98**, 61-68.

de la Peña O'Shea,Víctor A., Homs,N., Pereira, E. B., Nafria, R. and Ramírez de la Piscina, Pilar. (2007). X-ray diffraction study of Co_3O_4 activation under ethanol steam-reforming. *Catalysis Today,* **1-2,** 148-152.

Denis, A., Grzegorczyk,W., Gac,W., and Machocki, A. (2008). Steam reforming of ethanol over Ni/support catalysts for generation of hydrogen for fuel cell applications. *Catalysis Today*, **137**, 2-4, 453-459

Diagne, C., Idriss, H. and Kiennemann, A. (2002). Hydrogen production by ethanol reforming over Rh/CeO_2-ZrO_2 catalysts. *Catalysis Communications*, **3**, 565-571.

Ding, Z. Y. Frisch, M. A, Li, L., and Gloyna, E. F. (1996). Catalytic Oxidation in Supercritical Water. Ind. Eng. Chem. Res., **35**, 3257-3279.

Ding, Z.Y., Aki, S.N.V.K, and Abraham, M.A. (1995). Catalytic Supercritical Water Oxidation: Phenol Conversion and Product Selectivity. *Environ. Sci. Technol.*, **29**, 2748-2753.

Ding, Z.Y., Li, D., Wade, D., and Gloyna., E.F. (1998). Supercritical Water Oxidation of NH_3 over a MnO_2/CeO_2 Catalyst. *Ind. Eng. Chem. Res.*, **37**, 1707-1716.

Dinjus, E. and Kruse, A. (2004). Hot Compressed Water-a Suitable and Sustainable Solvent and Reaction Medium? *J. Phys. Condens. Matter.*, 16, 1161-1169.

Dinjus, E., and Kruse, (2002) *A. Physico-Chemical Properties of Water at High Temperature and Pressure*: Application of Supercritical Water. In High Pressure Chemistry: Synthetic, Mechanistic, and Supercritical Applications edited by Rudi van Eldik, Frank-Gerrit Klärner. Weinheim : Wiley-VCH, Germany.

Diskin, A. M., Cunningham, R. H. and Ormerod, R. M. (1998). The oxidative chemistry of methane over supported nickel catalysts. *Catalysis Today,* **2-3,** 147-154.

Duan, S., and Senkan, S. (2005). Catalytic conversion of ethanol to hydrogen using combinatorial methods. *Ind. Eng. Chem. Res.* **44**, 6381-6386.

Duprez, D. (1992). Selective steam reforming of aromatic compounds on metal catalysts. *Applied Catalysis A: General,* **2,** 111-157.

Dybkjaer, L., (1995). Tubular reforming and Autothermal reforming of natural gas- An Overview of Available Processes. *Fuel Processing Technology*, **42**, 85-107.

Erdőhelyi, A., Raskó, J., Kecskés, T., Tóth, M., Dömök, M. and Baán, K. (2006). Hydrogen formation in ethanol reforming on supported noble metal catalysts. *Catalysis Today,* **3,** 367-376.

Elliott, D.C, Phelps, M.R., Sealock, L.J. Jr., and Baker, E.G. (1994). Chemical Processing in High-pressure Aqueous Environments. 4. Continuous-Flow reactor Process Development Experiments for Organics Destruction *Ind. Eng. Chem. Res.*,**33**, 566-574

Elliott, D.C, Sealock, L.J. Jr., and Baker, E.G. (1993). Chemical Processing in High-Pressure Aqueous Enviroments. 2. Development of Catalyst for Gasification. *Ind. Eng. Chem. Res.*, **32**, 1542-1548.

Fatsikostas, A.N. and Verykios, X.E. (2004). Reaction Network of Steam Reforming of Ethanol over Ni-based Catalysts. *Journal of Catalysis*, **225**, 439-452.

Fatsikostas, A.N., Kondarides, D.I. and Verykios, X. E. (2002) Production of hydrogen for fuel cell by reformation of biomass-derived ethanol. *Catalysis Today*, **75**, 145-155.

Finke, T., Gernsbeck, M., Eisele, U., (2008). Numerical modelling of the adsorption and thermal desorption of NH_3 on ZrO_2. *Thermochimica Acta,* **1-2,** 32-39.

Freni, S., (2001). Rh based catalysts for indirect reforming ethanol applications in molten carbonate fuel cells. *J. Power Sources*, **94**, 14-19

Freni, S., Cavallaro, S., Mondello, N., Spadaro, L. and Frusteri, F. (2003). Production of hydrogen for MC fuel cell by steam reforming of ethanol over MgO supported Ni and Co catalysts. *Catalysis Communications*, **4**, 259-268.

Freni, S., Mondello, N., Cavallaro, S., Cacciola, G., Parmon, V.N and Sobyanin, V.A. (2000). Hydrogen production by steam reforming of ethanol: A two step process. *React. Kinet. Catal. Lett.*, **71**, 143-152.

Freni, S., Cavallaro, S., Modello, N., Spadora, L., and Frusteri, F. (2002). Steam reforming of ethanol on Ni/MgO catalysts: H_2 production for MCFC. *Journal of Power Sources*, **108**, 53-57.

Frusteri, F., Freni, S., Chiodo, V., Spadora, L., Blasi, D., Bonura, G., Cavallaro, S. (2004c). Steam reforming of bio-ethanol on alkali-doped Ni/MgO catalysts: Hydrogen production for MC fuel cell. *Applied Catalysis A: General*, **270**, 1-7.

Frusteri, F., Freni S., Spadaro, L., Chiodo, V., Bonura, G., Donato, S., and Callaro, S. (2004a). H_2 Production for MC fuel Cell by steam reforming of ethanol over MgO supported Pd, Rh, Ni, and Co. *Catalysis Communications*, **5**, 611-615.

Frusteri, F., Freni, S., Spadaro, L., Chiodo, V., Bonura, G., Donato, S., and Callaro, S. (2004b). Potassium improved stability of Ni/MgO in the steam reforming of ethanol for the production of hydrogen for MCFC. *Journal of Power Sources*, **132**, 139-144.

Frusteri, F. and Freni, S. (2007) Bio-ethanol, a suitable fuel to produce hydrogen for a molten carbonate fuel cell. *Journal of Power Sources*, **173**, 1, 200-209.

Furusawa, T., Sato, T., Sugito, H., Miura, Y., Ishiyama, Y., Sato, M., Itoh, N.; Suzuki, N. (2007). Hydrogen production from the gasification of lignin with nickel catalysts in supercritical water. *International Journal of Hydrogen Energy*. **32**, 699-704

Gadhe, J.B. and Gupta, R.B. (2005). Hydrogen Production by Methanol Reforming in Supercritical Water: Suppression of Methane Formation. *Ind. Eng. Chem. Res.*, **44**, 4577-4585.

Galvita, V.V., Semin, G.L., Belyaev, V.D., Semikolenov, V.A., Tsiakaras, P. and Sobyanin, V.A. (2001). Synthesis Gas Production by Steam Reforming of Ethanol. *Applied Catalysis A: General*, **220**, 123-127.

Garcia, E. Y. and Laborde, M.A. (1991). Hydrogen Production by the Steam Reforming of Ethanol : Thermodynamic Analysis. Int. J. Hydrogen Energy, **16**, 307-312.

Galetti,A. E., Gomez, . F., Arrua,L. A., Marchi,A. J. and Abello,M. C. (2008). Study of CuCoZnAl oxide as catalyst for the hydrogen production from ethanol reforming. *Catalysis Communications*, **6,** 1201-1208.

Goula, M.A., Sotiria, Kontou, K., Tsiakaras, P. E., (2004). Hydrogen production by ethanol steam reforming over a commercial Pd/γ-Al_2O_3 catalyst. *Applied Catalysis B*: *Environment*, **49**, 135-144.

Grgicak, C.M., Green, R.G. and Giorgi, J.B (2006). Control of Microstructure Sinterability and Performance in Ni-YSZ, Cu-YSZ and Co-YSZ SOFC Anodes. *J. Mater. Chem.* 9, 885-897.

Habicht, W., Boukis, N., Franz, G., and Dinjus, E. (2003). Investigation of Nickel-Based Alloys Exposed to supercritical water envroments. *Microchimica Acta*, **145**, 52-62.

Haga., F., Nakajima, T., Yamashita, K., Mishima, S., (1997a). Nippon Kagaku Kaishi (*J. Chem. Soc. Japan*), **1**, 33.

Haga, F., Nakajima, T., Miya, H. and Mishima, S. (1997b). Catalytic Properties of supported Cobalt Catalyst for Steam Reforming of Ethanol. *Catalysis Letter*, **48**, 223-227.

Hao, X.H., Guo, L.J, Mao, X., Zhang, X.M. and Chen, X.J. (2003). Hydrogen Production from Glucose Used as a Model Compound of Biomass Gasified in Supercritical Water. *Int. J. of Hydrogen Energy*, **28(1)**, 55-64.

Haryanto, A., Fernando, S., Murali, N., and Adhikari, S. (2005). Current status of hydrogen Production Techniques by Steam Reforming of Ethanol: A Review. *Energy & Fuels*, **19**, 2098-2106.

Helling, R. K., and Tester, J. W. (1988). Oxidation of Simple Compounds and Mixtures in Supercritical Water: Carbon Monoxide, Ammonia and Ethanol. Environ. *Sci. Technol.*, **22(11),** 1319-1324.

Hilmen, A. M., Schanke, D., Hanssen, K. F. and Holmen, A. (1999). Study of the effect of water on alumina supported cobalt Fischer–Tropsch catalysts. *Applied Catalysis A: General,* **1-2,** 169-188

Hirth, T. and Franck, E.U. (1993). Oxidation and Hydrothermolysis of Hydrocarbons in Supercritical Water at High Pressure. *Ber. Bunsenges. Phys. Chem.*, **97(9),** 1091-1098.

Holgate, H. R., Meyer, J.C., and Tester, J.W. (1995). Glucose Hydrolysis and Oxidation in Supercritical Water. *AIChE*, **41**, 637-648.

Hong, G.T. and Spritzer, M.H., (2000). Supercritical water oxidation. Proceedings of the 2002 U.S. DOE Hydrogen Program Review, NREL/CP-610-32405.

Hosseinpour, N., Khodadadi, A. A., Mortazavi, Y. and Bazyari, A. (2009). Nano-ceria–zirconia promoter effects on enhanced coke combustion and oxidation of CO formed in regeneration of silica–alumina coked during cracking of triisopropylbenzene. *Applied Catalysis A: General,* **2,** 271-281.

Hsiao, W. W.W. (2003). *Hydrogen Production from Ethanol by Supercritical Water Partial Oxide*. McS Thesis. University of Waterloo, Ontario, Canada.

Idris, H. (2004). Ethanol Reactions over the Surfaces of Noble Metal/Cerium Oxide Catalysts. *Platinum Metal Rev.*, **48**, 105-115.

Innes, W.B, in: Anderson R.B (Ed.) (1968). *Experimental Methods in Catalytic Research, Academic Press, New York*, p. 44

Izumikazi, Y., Park, K.C, Tachibana, Y., Tomiyasu, H., and Fuji, Y. (2005). Organic Decomposition in Supercritical Water by an aid of Ruthenium (IV) Oxide as a Catalyst-Exploration of Biomass Resources for Hydrogen Production. *Progress in Nuclear Energy*, **47**, 544-552.

Jacobs, G., Keogh, R. A. and Davis, B. H. (2007). Steam reforming of ethanol over Pt/ceria with co-fed hydrogen. *Journal of Catalysis,* **2,** 326-337.

Jen, R. R.N, and Thomas R.N. (2002). Large scale hydrogen production. *Cattech*. **6**, 150-159.

Juan-Juan, J., Román-Martínez, M. C. and Illán-Gómez, M. J. (2004). Catalytic activity and characterization of Ni/Al_2O_3 and NiK/Al_2O_3 catalysts for CO_2 methane reforming. *Applied Catalysis A: General,* **2,** 169-174.

Kaddouri, A. and Mazzocchia, C. (2004). A study of the influence of the synthesis conditions upon the catalytic properties of Co/SiO_2 or Co/Al_2O_3 catalysts used for ethanol steam reforming. *Catalysis Communications,* **6,** 339-345.

Kingston, H.M., and Jassie, L.B. (1988). Introduction to Microwave Sample Preparation: Theory and Practice. ACS Proffessional Reference Book. Washington, USA.

Klouz, V., Fierro, V., Denton, P., Katz H., Lisse, J.P., Bouvot-Mauduit, S., and Mirodatos, C., (2002). Ethanol Reforming for Hydrogen Production in a Hybrid Electric Vechile: Process Optimisation. *J. Power Sources,* **105**, 26-34.

Krajnc, M. and Levec, J. (1997). Oxidation of Phenol over a Transition-Metal Oxide Catalyst in Supercritical Water. *Ind. Eng. Chem. Res.* **36**, 3439-3445.

Kritzer, P and Dinjus, E. (2001). An Assessment of Supercritical Water Oxidation (SCWO) Existing Problems, Possible Solutions and New Reactor Concepts. *Chemical Engineering Journal,* **83**, 207-214.

Kritzer, P. (2004). Corrosion in High-Temperature and Supercritical Water and Aqueous Solutions: A Review. *J. of Supercritical Fluids*, **29**, 1-29.

Kruse, A. and Dinjus, E. (2003). Hydrogen from Methane and Supercritical Water. *Angew. Chem. Int. Ed.*, **42(8)**, 909-911.

Kruse, A., Meier, D., Rimbrecht, P., and Schacht, M. (2000). Gasification of Pyrocatechol in Supercritical Water in the Presence of Potassium Hydroxide. *Ind. Eng. Chem. Res.*, **39**,4842-4848.

Kugai, J., Velu, S., and Song, C. (2005). Low-temperature reforming of ethanol over CeO_2-supported Ni-Rh bimetallic catalyst for hydrogen production. *Catalysis letter*, **101**, 255-264.

Lee, D. S. (1996). Heterogeneous oxidation kinetics of acetic acid in supercritical water. *Environ.Sci.Technol.*, 3487-3492.

Lee, H.C., Son, S.H., Hwang, K.Y., and Lee, C.H. (2006). Surface Chemical Analysis on the Corrosion of Alloys in the Supercritical Water Oxidation of Halogenated Hydrocarbon. *Ind. Eng. Chem. Res.* **45**, 3412-3419.

Lee I. G., Kim M. S., and Ihm, S. K. (2002). Gasification of Glucose in Supercritical Water. *Ind. Eng. Chem. Res.*, **41**, 1182-1188.

Lin, H. and Chen, Y. (2004). The mechanism of reduction of cobalt by hydrogen. *Mater. Chem. Phys.*, **1,** 171-175.

Liberatori, J. W. C., Ribeiro, R. U., Zanchet, D., Noronha, F. B. and Bueno, J. M. C. (2007). Steam reforming of ethanol on supported nickel catalysts. *Applied Catalysis A: General*, **2,** 197-204.

Liguras, D.K., Kondarides, D.I., Verykios, X.E. (2003). Production of hydrogen for fuel cells by steam reforming of ethanol over supported noble metal catalysts. *Applied Catalysis B: Enviromental*, **43**, 345-354.

Lin, K. and Wang, H. P. (2000). Supercritical Water Oxidation of 2-Chlorophenol Catalyzed by Cu^{2+} Cations and Copper Oxide Clusters. *Environ. Sci. Technol.*, **22,** 4849-4854.

Llorca, J., Homs, N., Sales J, and Piscina, P.R. (2002). Efficient Production of Hydrogen over Supported Cobalt Catalysts from Ethanol Steam Reforming. *Journal of Catalysis*, **209,** 306–317.

Llorca, J., Homs, N., Sales, J., Feirro, J.L.G. and Piscina, P.R. (2004). Effect of sodium addition on the performance of Co-ZnO based catalyst for hydrogen production from bioethanol. *Journal of Catalysis*, **222**, 470-480.

Lu, Y.J., Guo, L.J., Ji, C.M., Zhang, X.M., Hao, X.H., and Yan, Q.H. (2005). Hydrogen Production by Biomass Gasification in Supercritical Water. A Parametric Study. *International Journal of Hydrogen Energy*, **31**, 822-831.

Mariño, F., Boveri, M., Baronetti, G. and Laborde, M. (2001). Hydrogen production from steam reforming of bioethanol using Cu/Ni/K/γ-Al_2O_3 catalysts. Effect of Ni. *International Journal of Hydrogen Energy,* **7,** 665-668.

Mariño, F. J., Cerrella, E. G., Duhalde, S., Jobbagy, M. and Laborde, M. A. (1998). Hydrogen from steam reforming of ethanol. Characterization and performance of copper-nickel supported catalysts. *International Journal of Hydrogen Energy*, **12,** 1095-1101.

Mariño, F., Boveri, M., Baronetti,G. and Laborde, M. (2001). Hydrogen production from steam reforming of bioethanol using Cu/Ni/K/γ-Al_2O_3 catalysts. Effect of Ni. *International Journal of Hydrogen Energy*, **7,** 665-668.

Mariño, F., Baronetti, G., Jobbagy, M. and Laborde, M. (2003). Cu-Ni-K/γ-Al_2O_3 supported catalysts for ethanol steam reforming: Formation of hydrotalcite-type compounds as a result of metal–support interaction. *Applied Catalysis A: General*, **1,** 41-54.

Martin, A., Armbruster U., Schneider M., Radnik, J. and Pohl, M.M. (2002). Structural Transformation of an Alumina-supported MnO_2-CuO Oxidation Catalyst by Hydrothermal Impact of Sub- and Supecritical Water. *J. Mater. Chem.*, **12**, 639-645.

Matsumura Y., Xu X. and Antal M.J. (1997). Gasification Characteristics of an Activated Carbon in Supercritical Water. *Carbon*, **35(6)** ,819-824.

Matsumura, Y., Minowa, T., Potic, B., Kersten, S.R.A., Prins, W., Swaaij W.P.M., Beld, B.V., Elliot, D.C., Neueschwander, G.G., Kruse, A., Antal, M.A. (2005). Review, Biomass Gasification in Near- and Supercritical Water: Status and Prospects. *Biomass and Bioenergy*, **29**, 269-292.

Milton, D.B., Yoon, J.H., Latanision, R.M. (2000). Overview of Corrosion phenomena in SCWO systems for Hazardous Waste Destruction, Corros. Eng., **49**, 130-141.

Molina, R. and Poncelet, G. (1998). α-Alumina-Supported Nickel Catalysts Prepared from Nickel Acetylacetonate: A TPR Study. *Journal of Catalysis*, **2,** 257-267.

Morgenstern, D. A. and Fornango, J. P.,(2005). Low Temperature Reforming of Ethanol over Copper-Plated Raney Nickel: A New Route to Sustainable Hydrogen for Transportation. *Energy & Fuels*, **19**, 1708-1716.

Nakajima, T., Tanabe, K., Yamaguchi, T., Matsuzaki, I. and Mishima, S. (1989). Conversion of ethanol to acetone over zinc oxide—calcium oxide catalyst optimization of catalyst preparation and reaction conditions and deduction of reaction mechanism. *Applied Catalysis*, **3,** 237-248.

Navarro, R. M., Álvarez-Galván, M. C., Sánchez-Sánchez, M. C., Rosa, F. and Fierro, J. L. G. (2005). Production of hydrogen by oxidative reforming of ethanol over Pt catalysts supported on Al2O3 modified with Ce and La. *Applied Catalysis B: Environmental*, **4,** 229-241.

Ni, M., Leung, D.Y.C and Leung M.K.H. (2007). A review on reforming bio-ethanol for hydrogen production. *International Journal Hydrogen Energy*, **32**, 15, 3238-3247.

Nishiguchi, T., Matsumoto, T., Kanai, H., Utani, K., Matsumura, Y., Shen, W.J., Imamura, S. (2005). Catalytic steam reforming of ethanol to produce hydrogen and acetone. A*pplied Catalysis A: General*, **279**, 273-277.

Nunoura, T., Lee, G., Matsumura, Y., and Yamamoto (2003). Reaction Engineering Model for Supercritical Water Oxidation of Phenol Catalyzed by Activated Carbon. *Ind. Eng. Chem. Res.*, **42**, 3522-3531.

Osada, M., Sato, T., Watanabe, M., Adschiri, T., and Arai, K. (2004). Low-Temperature Catalytic Gasification of Lignin and Cellulose with a Ruthenium Catalyst in Supercritical Water. *Energy & Fuels*, **18**, 327-333.

Osada, M., Sato, O., Watanabe, M., Arai, K and Shirai, M. (2006). Water density effect on lignin gasification over supported noble metal catalysts in supercritical water, *Energy & Fuels*, **20**, 930-935.

Panasyuk, G.P., Danchevskaya, M.N, Belan V.N., Voroshilov, I.L., and Ivakin, Y.D. (2004). Phenomenology of corundum Crystal formation in Supercritical Water Fluid. *J. Phys. Condens. Matter.*, **16**, 1215-1221.

Parmaliana, A., Arena, F., Frusteri, F and Giordano. F (1990). Temperature-programmed Reduction Study of NiO-MgO Interactions in Magnesia-supported Ni Catalyts and NiO-MgO Physical Mixture. *J. Chem. Soc. Faraday Trans.*, **86**, 14, 2663-2669.

Pinkwart, K., Bayha, T., Lutter, W., and Krausa, M. (2004). Gasification of Diesel oil in Supercritical Water for Fuel Cell. *Journal of Power Sources*, **136**, 211-214.

Profeti, L. P. R., Ticianelli, E. A. and Assaf, E. M. (2008). Production of hydrogen by ethanol steam reforming on Co/Al2O3 catalysts: Effect of addition of small quantities of noble metals. *Journal of Power Sources*, **1,** 482-489.

Ramayya, S., Brittain, A., DeAlmeida, C., Mok, W., and Antal, J. (1987). Acid Catalyzed Dehydration of Alcohols in Supercritical Water. *Fuel*, **66**, 1364-1371.

Resini, C., Concepción H. D. ,M., Presto,S., Alemany,L. J., Riani,P., Marazza,R., Ramis,G., Busca,G. (2008). Yttria-stabilized zirconia (YSZ) Supported Ni–Co Alloys (Precursor of SOFC Anodes) as Catalysts for the Steam Reforming of Ethanol. *International Journal of Hydrogen Energy*, **33**, 14, 3728-3735

Rice, S. F., Steeper, R.R., and Aiken, J.D. (1998). Water Density Effects on Homogeneous Water-Gas Shift Reaction Kinetics. *J. Phys. Chem. A.*, **102**, 2673-2678.

Richardson, J. T. and Vernon, L. W. (1958). The Magnetic Properties of the Cobalt Oxide–Alumina System. *J.Phys.Chem.*, **10,** 1153-1157.

Ritter, A., Ebner, A.D., Wang, J. and Zidan, R. (2003). Implementing a hydrogen economy. *Materials Today*, **6**, 18-23.

Sánchez-Sánchez, M.C., Navarro, R.M., & Fierro, J.L.G. (2007). Ethanol steam reforming over Ni / $M_x O_y$-$Al_2 O_3$ (M = Ce, La, Zr and Mg) catalysts: Influence of support on the hydrogen. *International Journal Hydrogen Energy*, 32, 10-11

Sato, T., Kurosawa, S., Smith R.L., Adschiri, T., and Arai K. (2004). Water Gas Shift Reaction kinetics under Noncatalytic Conditions in Supercritical Water. *J. of Supercritical Fluids*, **29**, 113-119.

Savage, P. E. (1999). Organic Chemical Reactions in Supercritical Water. *Chem. Rev.*, **99**, 603-621.

Savage, P.E., Gopalan, S., Mizan, T. I., Martino, C. J., and Brock, E. E. (1995). Reactions at Supercritical Conditions: Applications and Fundamentals. *AIChE J.*, **41**, 1723-1778.

Schanzenbächer, J., Taylor, J.D., and Tester, J.W. (2002) Ethanol Oxidation and Hydrolysis Rates in Supercritical Water", *J. of Supercritical Fluids*, **22**, 139-147.

Schmieder, H., Abeln, J., Boukis, N., Dinjus, E., Kruse, A., Kluth M., Petrich, G., Sadri, E., Schacht, M. (2000). Hydrothermal gasification of biomass and organic wastes. *J. Supercritical Fluids*; **17**, 145-153.

Shaw, R.W., Brill, T.B., Clifford, A.A., Eckert, C.A., and Franck, E.U. (1991). Supercritical Water a Medium for Chemistry. *Chem. Eng. News*, **69**, 26-39.

Shibasaki, Y., Kamimori, T., Kadokawa J.C., Hatano, B. and Tagaya, H. (2003). Decomposition Reaction of Plastic Model Compounds in Sub- and Supercritical Water. *Polymer Degradation and Stability*, Article in Press.

Sheng, P. Y., Chiu, W. W., Yee, A., Morrison, S. J. and Idriss, H. (2007). Hydrogen production from ethanol over bimetallic Rh-M/CeO2 (M = Pd or Pt). *Catalysis Today,* **3-4,** 313-321.

Sinag, A., Krunse, A., and Rathert, J. (2004). Influence of the Heating Rate and the Type of Catalyst on the Formation of Key Intermediates and on the Generation of Gases During Hydropyrolysis of Glucose in Supercritical Water in a Batch Reactor. *Ind. Eng. Chem. Res.*, **43,** 502-508.

Song, H., Zhang, L., Watson, R. B., Braden, D. and Ozkan, U. S. (2007). Investigation of bio-ethanol steam reforming over cobalt-based catalysts. *Catalysis Today,* **3-4,** 346-354.

Srinivas, D., Satyanarayana, C.V.V., Potdar, H.S., and Ratnasamy, P. (2003). Structural studies on NiO-CeO_2-ZrO_2 catalysts for steam reforming of ethanol. *Applied Catalysis A: General*, **246**, 323-334.

Sirijaruphan, A., HorvÃ¡th, A., Goodwin, J. G. and Oukaci, R. (2003). Cobalt Aluminate Formation in Alumina-Supported Cobalt Catalysts: Effects of Cobalt Reduction State and Water Vapor. *Catalysis Letters*, **1,** 89-94.

Sun, J., Qiu, X.P., Wu, F., and Zhu, W.T. (2005). H_2 from steam reforming of ethanol at low temperature over Ni/Y_2O_3, Ni/La_2O_3 and Ni/Al_2O_3 catalysts for fuel-cell application. *Int. J. Hydrogen Energy*, **30**, 437-445.

Tang, C., Wang, C. and Chien, S. (2008). Characterization of cobalt oxides studied by FT-IR, Raman, TPR and TG-MS. *Thermochimica Acta,* **1-2,** 68-73.

Takahashi H., Hisaoka S., and Nitta T. (2002). Ethanol Oxidation Reactions Catalyzed by Water Molecules: $CH_3CH_2OH + nH_2O \rightarrow CH_3CHO + H_2 + nH_2O$ (n = 0,1,2). *Chem. Phys. Lett.*, 3**63**, 80-86.

Taylor, J. D., Herdman, C. M., Wu, B. C., Wally, K., Rice, S. F. (2003). Hydrogen Production in a Compact Supercritical Water Reformer. *Int. J. Hydrogen Energy*, **28**, 1171-1178.

Tomita, K., and Oshima, Y. (2004). Stability of Manganese Oxide in Catalytic Supercritical Water Oxidation of Phenol. *Ind. Eng. Chem. Res.*, **43**, 7740-7743.

Tomita, K., Koda, S., and Oshima Y. (2002). Catalytic Hydration of Propylene with MoO3/Al2O3 in Supercritical Water. *Ind. Eng. Chem. Res.*, **41**, 3341-3344.

Triantafillidis, C. S., Vlessidis, A. G. and Evmiridis, N. P. (2000). Dealuminated H−Y Zeolites: Influence of the Degree and the Type of Dealumination Method on the Structural and Acidic Characteristics of H−Y Zeolites. *Ind Eng Chem Res*, **2,** 307-319.

Tu,Y.-J. and Chen,Y.-W. (1998). Effects of alkaline-earth oxide additives on silica-supported copper catalysts in ethanol dehydrogenation. *Industrial and Engineering Chemistry Research* **37**, 2618-2622.

Tuti, S. and Pepe, F. (2008). On the Catalytic Activity of Cobalt Oxide for the Steam Reforming of Ethanol. *Catalysis Letters*, **1,** 196-203.

Vaidya, P. D. and Rodrigues, A. E. (2006). Insight into steam reforming of ethanol to produce hydrogen for fuel cells. *Chemical Engineering Journal*, **1,** 39-49.

Vizcaíno, A. J., Arena, P., Baronetti, G. (2008). Ethanol steam reforming on Ni/Al_2O_3 catalysts: Effect of Mg addition. *International Journal of Hydrogen Energy*, **13,** 3489-3492

Wang, J. and Takarada, T. (2001). Role of Calcium Hydroxide in Supercritical Water Gasification of Low-Rank Coal. *Energy & Fuels*, **15**, 356-362.

Watanabe , M., Inomata, H., Smith, R.L and Arai, K. (2001). Catalytic Decarboxylation of Acetic Acid with Zirconia Catalyst in Supercritical Water. *Applied Catalysis A: General*, **219**, 149-156.

Watanabe, M., Inomata H. and Arai, K. (2002). Catalytic Hydrogen Generation from Biomass (glucose and cellulose) with ZrO_2 in Supercritical Water. *Biomass and Bioenergy*, **22**, 405-410.

Watanabe, M, Osada, M., Inomata, H., Arai, K., and Kruse, A. (2003b). Acidity and Basicity of Metal oxide Catalyst for Formaldehyde Reaction in Supercritical Water at 673 K. *Applied Catalyst A: General*, **245**, 333-341.

Watanabe, M., Lida, T., Aizawa, Y., Ura, H., Inomata, H., and Arai, K. (2003a). Conversion of some small organic compounds with metal oxides in supercritical water at 673 K. *Green Chemistry*, **5**, 539-544.

Weingartner, H. and Franck, E.U. (2005). Supercritical Water as a Solvent. *Angew. Chem. Int. Ed.*, **44**, 2622-2692.

Xu, X. and Antal, M.J. (1998). Gasification of Sewage Sludge and other Biomass for Hydrogen Production in Supercritical Water. *Enviromental Progress*, **17**, 215-220.

Xu, X., Almeida D., and Antal M.J. (1991). Mechanism and Kinetics of the Acid-Catalyzed Formation of Ethene and Diether from Ethanol in Supercritical. *Ind. Eng. Chem. Res.*, **30**, 1478-1485.

Xu, X., Matsumura Y., Stenberg J. and Antal M.J. (1996). Carbon-Catalyzed Gasification of Organic Feedstocks in Supercritical Water. *Ind. Eng. Chem. Res.*, **35**, 2522-2530.

Yang, Y., Ma, J. and Wu, F. (2006). Production of hydrogen by steam reforming of ethanol over a Ni/ZnO catalyst. *International Journal of Hydrogen Energy,* **7,** 877-882.

Xu, Bo-Qing, Yamaguchi, T and Tanabe, K. (1988). Acid-base Bifunctional behaviour of ZrO_2 in Dual Adsorption of CO_2 and NH_3. *Chemistry Letters,* 1663-1666.

Yoshida, T. and Oshima Y. (2004). Partial Oxidate and Catalytic Biomass Gasification in Supercritical Water: A promising Flow Reactor System. *Ind. Eng. Chem. Res.*, **43**, 4097-4104.

Yu, D., Aihara M. and Antal M.J. (1993). Hydrogen Production by Steam Reforming Glucose in Supercritical Water. *Energy & Fuels*, **7**, 574-577.

Yu, J and Savage P.E. (2001). Catalyst activity, stability, and transformation during oxidation in supercritical water. *Applied Catalysis B: Environmental*, **31**, 123-132.

Yu, J. and Savage, P.E. (2000) Kinetics of Catalytic Supercritical Water Oxidation of Phenol over TiO_2. *Environ. Sci. Technol.*, **34**, 3191-3198.

Zafeiratos, S. and Kennou, S. (2003). The interaction of ultrathin nickel films with yttria-stabilized zirconia (1 0 0). *Surf Sci*, 402-408.

Zhang, J., Chen, J., Ren, J. and Sun, Y. (2003). Chemical treatment of γ-Al_2O_3 and its influence on the properties of Co-based catalysts for Fischer–Tropsch synthesis. *Applied Catalysis A: General*, **1,** 121-133.

Appendix A:
Microwave Digestion Procedure

Prior to perform the catalyst digestion, the microwave power level can be checked using the following procedure (Obtained from ASTM D5513: Standard Practice for Microwave Digestion of Industrial Furnace Feedstreams and Waste for Trace Element Analysis). Although the equipment manufacturers specify general power output ratings for microwave digestion units, it is important to verify the actual power output of a specific unit. It is recommended that this microwave power check procedure be performed regularly.

Power Check Procedure at 100 % Instrument Power:

1. Program the instrument for 4-min time and 100 % power.
2. Transfer 2000 ± 2 mL of room temperature (19 to 25°C) water into a 2-L polypropylene beaker.
3. Measure and record the initial water temperature (*T*i) to the nearest 0.1°C.
4. Place the beaker in the right front corner of the instrument cavity (as you face the front of the instrument). This position closely approximates the position of a digestion vessel during processing.
5. Heat the water for the programmed time.
6. When the heating cycle is complete, immediately remove the beaker from the cavity, thoroughly stir the water to ensure even heat distribution, and measure the final temperature (T_f) to the nearest 0.1°C.
7. Calculate the delivered power in accordance with the following equations:

$$\boldsymbol{Power}\,(\boldsymbol{watt}) = \Delta \boldsymbol{T}\,(^{\circ}\boldsymbol{C}) \times 35\,(\boldsymbol{watt} / {}^{\circ}\boldsymbol{C})$$

where:

$$\Delta \boldsymbol{T} = \boldsymbol{T}_f - \boldsymbol{T}_i$$

$$\boldsymbol{W} \quad {}^{\circ}\boldsymbol{C} \quad = \frac{\boldsymbol{K} \times \boldsymbol{C}_P \times \boldsymbol{M}}{\boldsymbol{t}}$$

where:

W = watts,

K = 4.2, the factor for converting thermo-chemical calories/s to joules to watts.

C_p = 1.0, the heat capacity for water, cal/g.°C,

M = mass of water, g (1 mL H_2O = 1 g), and

t = time, s.

If the calculated power is not within the specifications of the unit, do a second test. The resulting power versus power level is shown in the figure below.

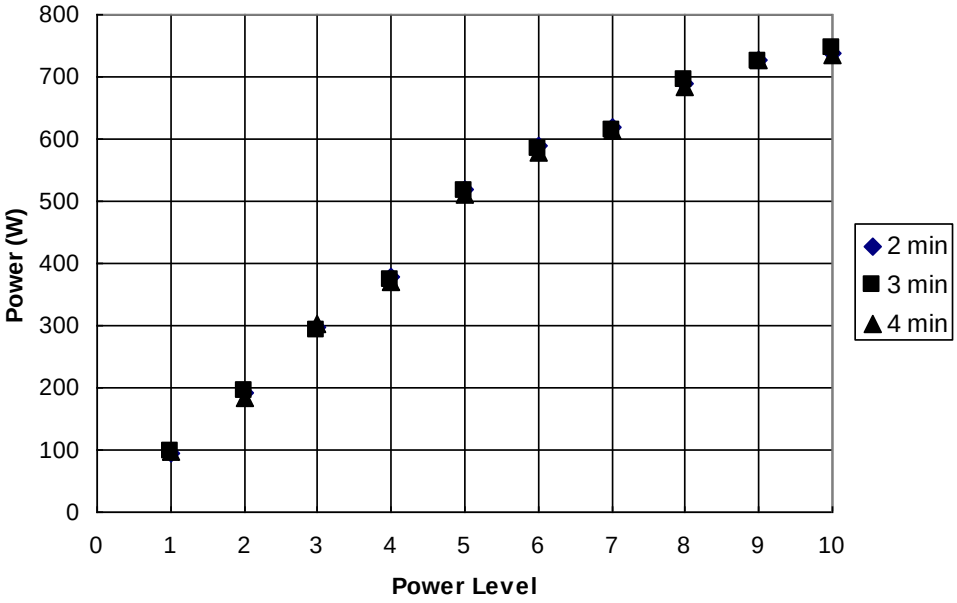

The Power delivered vs the setting power level of the commercial microwave (Panasonic model Inverter NN-S533, 1200W®)

Microwave Digestion Procedure

1. Crush the catalyst sample into fine powder and filter using 100 mesh sieve.
2. Weigh 50 mg sample and place in the 23-mL Teflon container of a Parr Digestion bomb
3. Add the appropriate acid mixture (see Chapter 3 for mixture composition)
4. Replace the cap of the container, place it inside the housing of the bomb digester (Parr Vessel) and close the cap screw tightly.
5. Place the bomb in the microwave. Heat it up at 400W (power level 4) for 2 min, wait for 1 min and then heat up again for another 1 min at power level 4. Unplug the microwave immediately after.
6. Wait for 30 min to let the sample cool down inside the microwave cavity and then immerse into a cold water bath for at least one hour for further cooling.
7. Pour the sample into a 100 mL volumetric flask and dilute it with demineralized water until filling up the 100 mL flask.
8. Pour the diluted mixture into a 250 mL High Density Polyethylene (HDPE) bottle and store it until ICP is available.
9. For the ICP-AES, prepared at least 5 known standard solution of metal (10, 20, 50, 80 and 100 ppm).
10. Prior to the ICP analysis, the mixture must be further diluted in demineralized water 100 times (0.5 mL of the mixture + 5 mL of demineralized).

Appendix B

Calibration Charts (GC)-Gas calibration (N_2, H_2, CO_2, CH_4, CO, C_2H_4, C_2H_6)

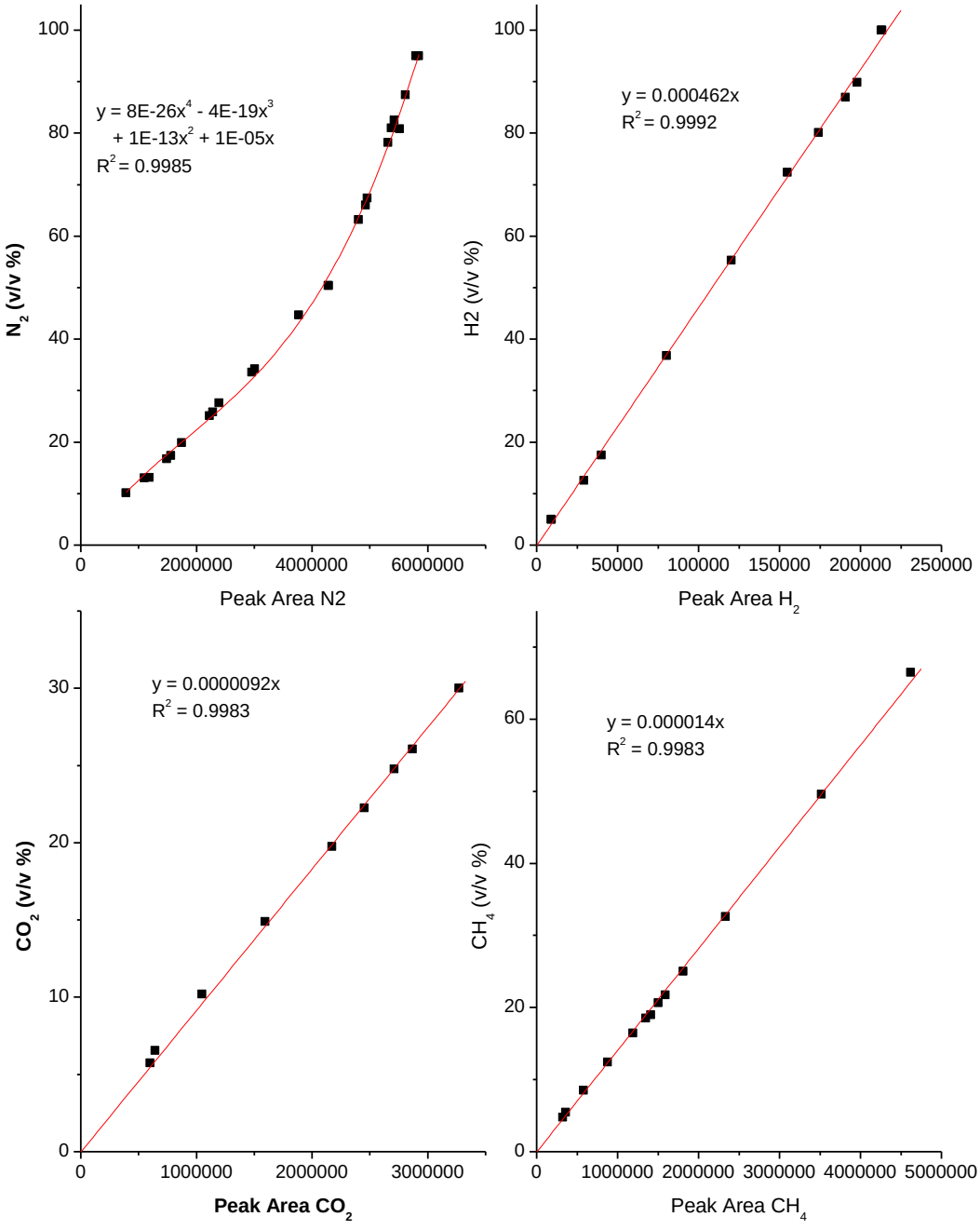

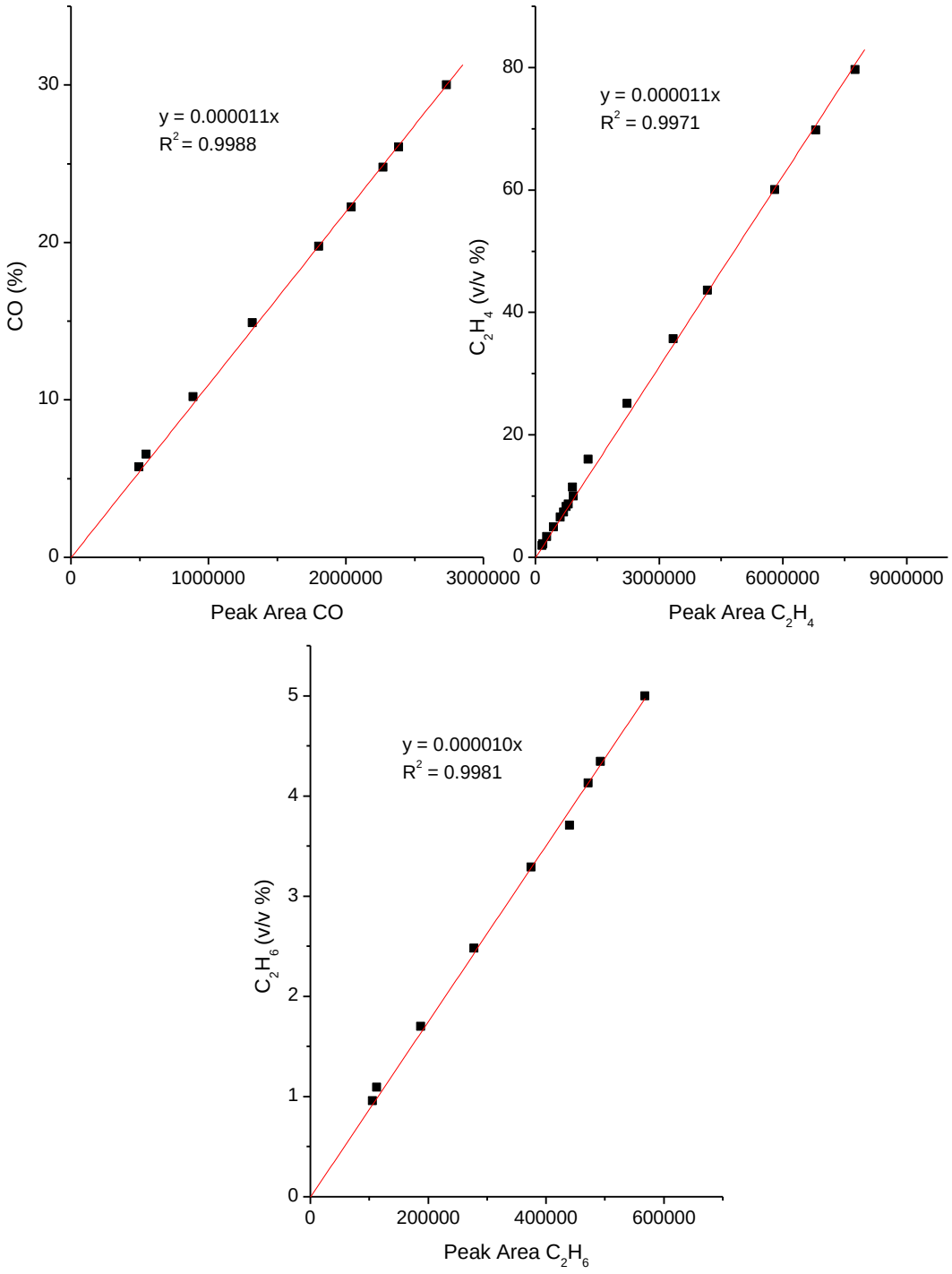
y = 0.000011x
R2 = 0.9988
CO (%)
Peak Area CO
0
10
20
30
0
1000000
2000000
3000000
y = 0.000011x
R2 = 0.9971
C2H4 (v/v %)
Peak Area C2H4
0
20
40
60
80
0
3000000
6000000
9000000
y = 0.000010x
R2 = 0.9981
C2H6 (v/v %)
Peak Area C2H6
0
1
2
3
4
5
0
200000
400000
600000

Liquid calibration (Ethanol, Acetaldehyde, Acetone and Diethyl-Ether)

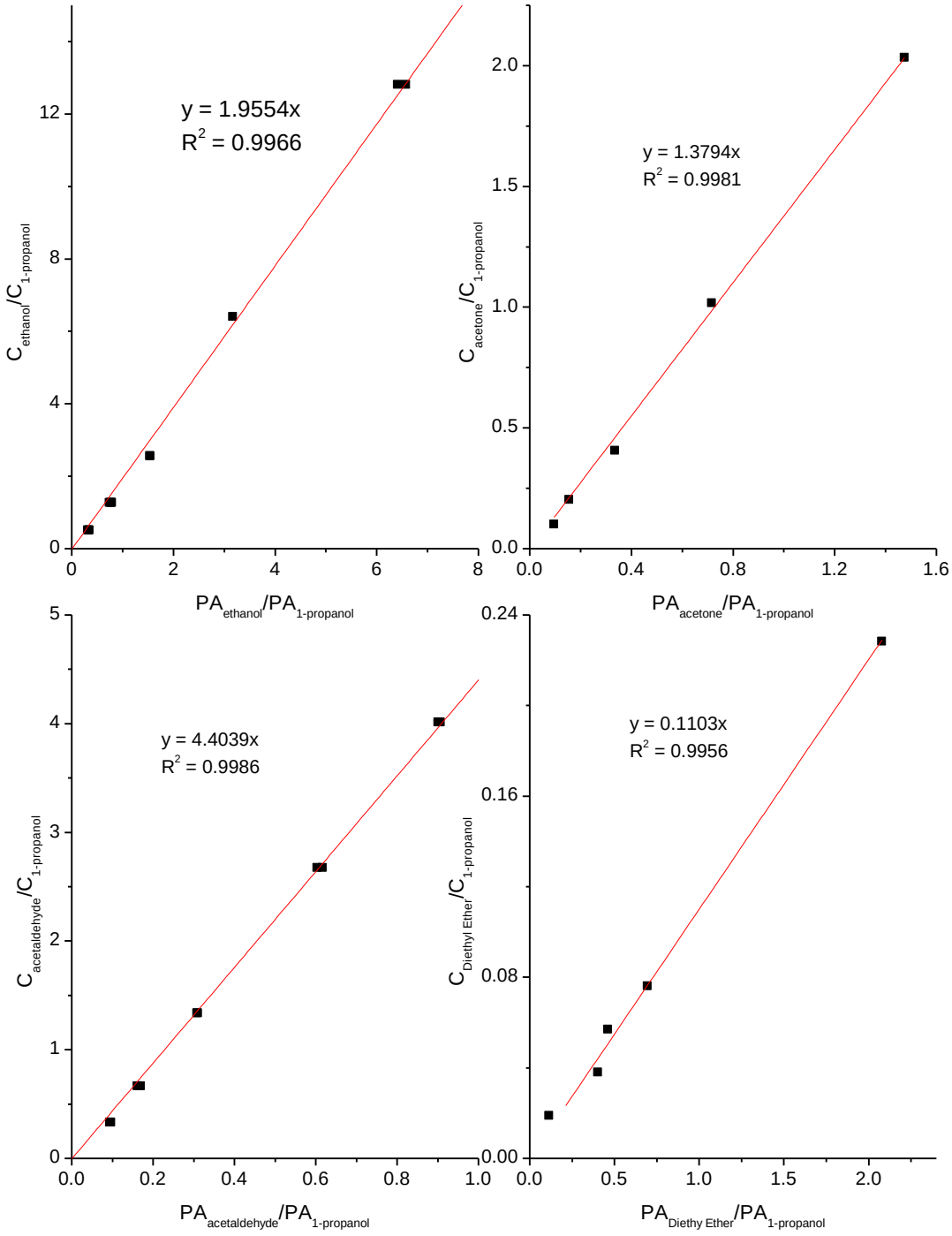

Appendix C
Supercritical Water Operating Procedure

Step 1: Prior to beginning experiment

I. Turn on the water bath containing 30 % (v/v) ethylene glycol/water and set the temperature at 7ºC. Lower temperature is important to condense all vapours, especially for acetaldehyde, which possesses the lowest boiling point of 21°C.

II. Warm up GC-1 (gas analysis) and GC-2 (liquid analysis).

III. Every joint of the reactor must be greased (use cupper base grease, (JetLube SS-30, recommended)) properly before being tightened. The larger nut must be tightened to at least 110 lb.ft (maximum 140 lb.ft), whereas the smaller joints are tightened to 45 lb.ft.

Step 2: Experimental procedure

I. Prior to increase the temperature, flow N_2 gas at least 20 mL/min pass through the reactor to avoid any possible change for the catalyst, especially the reduced catalyst.

II. Turn on the furnace and set the experimental temperature (**Warning: do not exceed 600°C unless adjust lowering the alarms for maximum working pressure)**. The default alarm (BPR and pump) is 350 bar for reaction temperatures below 600°C.

III. Access the ICM software and close valve #1.

IV. Set pump 1 (water) flow rate at 3 g/min (above critical pressure of water, 221 bar) for the rapid filling of the liquid gas separator in order to remove any residual gas in the separator.

V. Place a beaker at the gas product outlet. Once the water dips into the beaker, decrease the water flowrate to the desired flowrate and wait for a few minutes to remove any small particles.

VI. Turn on gas N_2 and drain liquid to the lowest level (leave some) and then turn off N_2.

VII. Set the back pressure regulator using the handheld palm, to the experimental value [**Warning: do not exceed 300 bar].**

VIII. Using ICM, set flow rate for the water pump 1, and the pre-heater at 200 °C.

IX. Start will a lower pressure, by adjusting the BPR's needle. The starting pressure depend on the amount of the total gas product, higher gas product requires lower starting pressure. This is an important step to reduce pressure fluctuation. The starting pressure is not necessary the same as the set pressure.

X. Once the pressure is stable, turn on pump 2 (ethanol water feed). Set at 1 g/min for a rapid filling and set to the desired flowrate once the pressure achieves half of the starting pressure.

XI. Wait until pressure stabilizes (expect to wait for at least 30 minute after the ethanol was fed, one hour being not uncommon) and adjust the needle until it achieves the experimental conditions.

XII. Gas product is analyzed using online HP 5890 series II GC (TCD)

XIII. At same time, collect liquid product and analyze using HP 5890 series II GC (FID)

Step 3: Shut down procedure

I. Once the last sample is collected, turn off pump 2 (ethanol pump). Let pump 1 running for additional 20 minutes.

II. Turn off pump 1.

III. Set the temperature of the furnace to 25^{o}C.

IV. Turn off the pre-heater using ICM software.

V. Decrease the pressure gradually using the back pressure regulator until it reaches atmospheric pressure.

VI. Open valve 3 slowly **[never open valve 3 fully at once; by doing that it will damage the heating and cooling system]**

VII. Flow nitrogen at 10 mL/min overnight to cool down the system and dry the catalyst.

Appendix D
Sample calculation

Calculation around the gas liquid separator

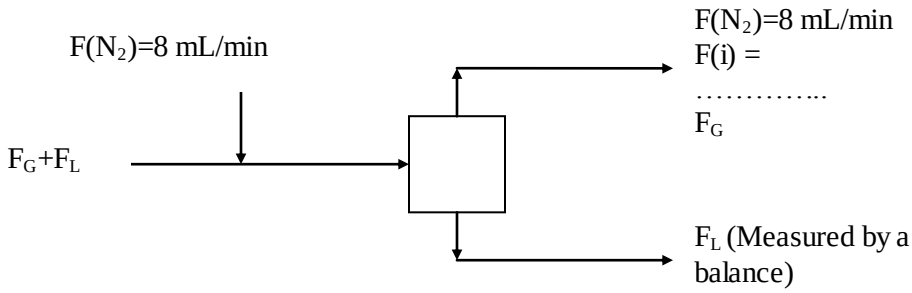

For gas calculation:

Gas composition of species i is calculated from the peak area of species i according to the gas calibration as shown in.

$$\left.\begin{aligned} y_{N_2} &= 8\times10^{-26}PA_i^4 - 4\times10^{-19}PA_i^3 + 1\times10^{-5}PA \\ y_{H_2} &= 5\times10^{-4}PA_i \\ y_{CO_2} &= 9.2\times10^{-6}PA_i \\ y_{CO} &= 1\times10^{-5}PA_i \\ y_{CH_4} &= 1\times10^{-5}PA_i \\ y_{C_2H_4} &= 1\times10^{-5}PA_i \\ y_{C_2H_6} &= 1\times10^{-5}PA_i \end{aligned}\right\} \qquad \text{(A- 1)}$$

where: PA_i is peak area of species i obtained from GC(TCD).

Calculation of total gas product around the gas liquid separator,

$$F_G = \frac{F_{N_2}}{y_{N_2}}\text{, or } \quad F_G = \frac{8}{y_{N_2}}\ \text{(mL/min)}\ \textbf{or}\ \ F_G = \frac{0.000328}{y_{N_2}}\ \text{(mol/min)} \qquad \text{(A- 2)}$$

where F_{N2} is set at 8 mL/min @ 3.28×10^{-4} mol/min (using PV=nRT) and y_{N_2} is calculated from gas calibration. However, total gas flowrate was also measured using a bubble flow meter,

measured gas is averaged of 10 times, usually around 5 min. The flow rate of each species is calculated according

$$F_i = \frac{F_G}{y_i} \tag{A- 3}$$

In term of molar flowrate (combination of equation A-2 and A-3)

$$F_i = \frac{0.000328}{y_i \times y_{N_2}} \text{ (mol/min)} \tag{A- 4}$$

For the liquid calculation:

The concentration of species i,

$$Concentration_i = \frac{Concentration_{1-propanol}}{RRF_i} \times \frac{Peak\ Area_i}{Peak\ Area_{1-propanol}} \tag{A- 5}$$

where, concentration of 1-propanol is set 1 v/v %, (~0.13369 mol/L). From the result of concentration, the molar flowrate can be calculated if the volume flowrate is known using equation (A-6)

$$F_{i(L)} = Conc._i \left(\frac{\text{mol}}{\text{L}}\right) \times F_L \left(\frac{\text{g}}{\text{min}}\right) \times \frac{1}{\rho}\left(\frac{\text{mL}}{\text{g}}\right) \tag{A- 6}$$

where, $Conc._i$ is the concentration of species i calculated from equation (A-5), F_L is the total liquid flowrate (record by a balance) and ρ is density of fluid. Since, the concentration of ethanol is used in the experiment is small, the density of the liquid phase at the outlet is assumed to be the density of water, 1 g/mL. Molar flowrate of ethanol inlet is calculated using equation (A-6) as well.

RRFs for the liquid product species, see calibration chart

Species	**RRF**
Ethanol	1.9554
Acetaldehyde	4.4039
Acetone	1.3794
Diethyl Ether	0.1103

The carbon in each species can be calculated according to:

$$F_i(C) = F_i \times n_i \qquad \textbf{(A- 7)}$$

where, n_i is the number of carbon cointaining in the hydrocarbon (e.g, n_{C2H5OH}=2 of atom carbon). And, the carbon balance is calculated using equation (A-8);

$$\textbf{\textit{Carbon balance}} \quad : C_T = \frac{\sum_i C_{outlet}}{\sum_i C_{inlet}} = \frac{\sum_i C_{outlet(gas)} + \sum_i C_{outlet(liq.)}}{2F_{ethanol(inlet)}} \times 100 \qquad \text{(A- 8)}$$

The ethanol conversion, and product selectivity is calculated using equation (A-9) and (A-10), respectively.

$$\textbf{Ethanol conversion, } \mathbf{X_{EtoH}}\textbf{:} \quad X_{EtoH} = \frac{F_{EtOH,in} - F_{EtOH,out}}{F_{EtOH,in}} \qquad \text{(A- 9)}$$

where, $F_{EtOH,in}$ and $F_{EtOH,out}$ are the feed and outlet molar flow rate of ethanol with unit of mol/min, respectively.

$$\textbf{Product selectivity:} \quad S_i(\%) = \frac{F_i}{\sum_{i=n} F_i} \times 100 \qquad \text{(A- 10)}$$

where, F_i is the molar gas flow rate of product i, and $\sum_{i=n} F_i$ is the total molar flowrate of the product.

95% confidence interval

To show the result in term of the mean/average with 95% confidence interval

($\bar{X} \pm$ error (95% conf. interval) , to calculate the 95% confidence interval,

$$95\% \, confindence \, \text{int} \, erval = t(0.05, dF) \times \frac{Stdev}{\sqrt{N}} \qquad \text{(A- 11)}$$

$$\textbf{Standard deviation:} \quad Stdev = \frac{N \sum X^2 - \left(\sum X\right)^2}{N(dF)} \qquad \text{(A- 12)}$$

$$\textbf{Degree of Freedom:} \quad dF = N - 1 \qquad \text{(A- 13)}$$

Example of the catalyst performance calculation for the 10 wt.% Co/YSZ at 550°C, 250 bar, 1.88 g/min feed flowrate,

Peak Area from the GC-1 (TCD)

	Peak Area (from GC)						
Time (min)	**H_2**	**N_2**	**CO**	**CH_4**	**CO_2**	**C_2H_4**	**C_2H_6**
30	84840	403828	30046	189882	1148554	42723	66028
70	117314	314577	62650	755189	2116580	1531	80553
110	113624	317329	60992	921147	2260717	852	49815
150	112173	283781	53553	920189	2489284	254	45688
190	121988	273295	70999	985076	2158854	0	41802
230	108653	270499	61677	1006012	2168042	235	46910
270	110293	284634	86340	1018185	2285874	156	58805

The calculation of each gas composition including N_2 from equation (A-1)

	y_i (mol/mol%) **Gas composition Including N_2**						
Time (min)	**H_2**	**N_2**	**CO**	**CH_4**	**CO_2**	**C_2H_4**	**C_2H_6**
30	42.42	4.03	0.30	1.90	10.71	0.43	0.59
70	58.66	3.14	0.63	7.55	18.98	0.02	0.72
110	56.81	3.17	0.61	9.21	20.18	0.01	0.45
150	56.09	2.84	0.54	9.20	22.10	0.00	0.41
190	60.99	2.73	0.71	9.85	19.33	0.00	0.38
230	54.33	2.70	0.62	10.06	19.41	0.00	0.42
270	55.15	2.85	0.86	10.18	20.40	0.00	0.53

Comparison between the measured gas flowrate (using bubble flowmeter) and the calculation (calculated value) using equation (A-2)

Measured (mL/min)	**Calculated (mL/min)**	**Calculated F_G (mol/min)**
180	198	0.0081
205	254	0.0104
230	252	0.0103
275	282	0.0116
298	293	0.0120
290	296	0.0121
294	281	0.0115

The molar flowrate of each gas calculated equation (A-4)

		Flowrate (mol/min)				$\sum F_{i(Gas)}$
H_2	**CO**	**CH_4**	**CO_2**	**C_2H_4**	**C_2H_6**	**(mol/min)**
0.001755	1.24E-05	7.86E-05	0.000443	1.77E-05	2.46E-05	0.002331
0.006119	6.54E-05	0.000788	0.00198	1.6E-06	7.56E-05	0.00903
0.005876	6.31E-05	0.000953	0.002088	8.81E-07	4.64E-05	0.009026
0.006484	6.19E-05	0.001064	0.002555	2.94E-07	4.75E-05	0.010212
0.007598	8.84E-05	0.001227	0.002408	0	4.69E-05	0.011369
0.006588	7.48E-05	0.001244	0.002557	2.85E-07	5.12E-05	0.010515
0.006587	0.000103	0.001216	0.002436	1.86E-07	6.32E-05	0.010406

The carbon of each species containing carbon in the gas phase calculated using equation (A-7)

Carbon out (gas) (mol/min)					
CO	**CH_4**	**CO_2**	**C_2H_4**	**C_2H_6**	$\sum C_{out(Gas)}$
1.24E-05	7.86E-05	0.000443	3.53E-05	4.92E-05	0.000619
6.54E-05	0.000788	0.00198	3.19E-06	0.000151	0.002988
6.31E-05	0.000953	0.002088	1.76E-06	9.27E-05	0.003198
6.19E-05	0.001064	0.002555	5.87E-07	9.51E-05	0.003776
8.84E-05	0.001227	0.002408	0	9.37E-05	0.003818
7.48E-05	0.001244	0.002557	5.7E-07	0.000102	0.003979
0.000103	0.001216	0.002436	3.73E-07	0.000126	0.003882

For Liquid phase analysis

Peak Area from the GC-2(FID)

	Peak Area (from GC)				
Time (min)	**Acetal**	**Acetone**	**Diethy**	**EtOH**	**1-Prop**
30	1158	29323	234	10227	28939
70	1367	252508	519	7342	192840
110	718	76580	359	2544	104690
150	1772	100212	517	13699	240114
190	1789	48831	21	5147	129620
230	1037	47838	111	3198	143546
270	1752	62092	0	5660	172495

The result of molar flowrate of each species as shown in Table below, total liquid flowrate is measured from the ScotPro balance. The concentration and the molar flowrate of each species is calculated from equation (A-5) and (A-6).

F(LP)out	**Concentration (mol/L)**				**Flowrate (mol/min)**				$\sum F_{(Liq)}$
(g/min)	**Acetal.**	**acetone**	**Diethyl**	**Ethanol**	**Acetal.**	**Acetone**	**Diethyl**	**Ethanol**	mol/min
1.7382	0.0241	0.1855	0.0001	0.0924	0.0000	0.0003	0.0000	0.0002	0.00036
1.6064	0.0043	0.2397	0.0000	0.0100	0.0000	0.0004	0.0000	0.0000	0.00039
1.7873	0.0041	0.1339	0.0001	0.0064	0.0000	0.0002	0.0000	0.0000	0.00025
1.7091	0.0044	0.0764	0.0000	0.0149	0.0000	0.0001	0.0000	0.0000	0.00014
1.6091	0.0083	0.0690	0.0000	0.0104	0.0000	0.0001	0.0000	0.0000	0.00012
1.6018	0.0044	0.0610	0.0000	0.0058	0.0000	0.0001	0.0000	0.0000	0.00010
1.6018	0.0061	0.0659	0.0000	0.0086	0.0000	0.0001	0.0000	0.0000	0.00012

Molar ethanol inlet is calculated using equation (A-5) and (A-6):

PAethanol	PAprop	PAet/Papro	Cethanol in	Fethanol in
724166	171501	4.2225	1.103835	0.002021

Carbon in the liquid phase is calculated using equation (A-6);

Carbon out (liquid)				$\sum C_{out(Liq)}$
Acetal	**Acetone**	**Diethy**	**Ethanol**	
8.38E-05	0.000967	8.29E-07	0.000321	0.001373
1.37E-05	0.001155	2.55E-07	3.2E-05	0.001201
1.48E-05	0.000718	3.62E-07	2.27E-05	0.000756
1.52E-05	0.000392	2.17E-07	5.1E-05	0.000458
2.68E-05	0.000333	1.54E-08	3.34E-05	0.000393
1.39E-05	0.000293	7.31E-08	1.87E-05	0.000326
1.96E-05	0.000317	0	2.75E-05	0.000364

Total carbon from the inlet and outlet can be calculated from data above as

$\sum_i C_{Ethanol}$ (mol/min)	$\sum_i C_{out(Liq)} + \sum_i C_{out(Gas)}$ (mol/min)	$\sum F_i$ (Mol/min)
0.00404	0.00259	0.00495
0.00412	0.00419	0.00942
0.00404	0.00395	0.00927
0.00408	0.00423	0.01035
0.00400	0.00407	0.01108
0.00406	0.00408	0.01039
0.00408	0.00411	0.01016

The conversion, carbon balance and product selectivity are calculated using equation (A-8), (A-9) and (A-10), respectively, as shown below.

Conv. (%)	**C balance (%)**	**Selectivity (mole%)**								
		H_2	**CO**	**CH_4**	**CO_2**	**C_2H_4**	**C_2H_6**	**Acetal.**	**Acetone**	**Diethyl**
91.63	64.07	69.73	0.49	3.12	17.61	0.70	0.98	0.85	6.51	0.00
99.10	101.59	64.95	0.69	8.36	21.01	0.02	0.80	0.07	4.09	0.00
99.42	97.80	63.36	0.68	10.27	22.51	0.01	0.50	0.08	2.58	0.00
98.65	103.70	62.64	0.60	10.28	24.68	0.00	0.46	0.07	1.26	0.00
99.06	101.72	66.08	0.77	10.67	20.95	0.00	0.41	0.12	1.00	0.00
99.47	100.36	63.39	0.72	11.74	22.65	0.00	0.49	0.07	0.94	0.00

To calculate the 95% confidence interval, the calculation were done according to equation (A-11) to (A-13), considering 5 sample (neglect the first data)

			Selectivity (%)								
	Conv. (%)	**C bal. (%)**	**H_2**	**CO**	**CH_4**	**CO_2**	**C_2H_4**	**C_2H_6**	**C_2H_4O**	**C_3H_6O**	**Diethyl**
Average	**99.14**	**101.03**	**64.09**	**0.69**	**10.26**	**22.36**	**0.01**	**0.53**	**0.08**	**1.97**	**0.00**
Stdev	0.33	2.17	1.40	0.06	1.22	1.53	0.01	0.16	0.02	1.36	0.00
N	5	5	5	5	5	5	5	5	5	5	5
dF	4	4	4	4	4	4	4	4	4	4	4
Tinv(0.05,dF)	2.78	2.78	2.78	2.78	2.78	2.78	2.78	2.78	2.78	2.78	2.78
95% confidence interval	**0.41**	**2.69**	**1.74**	**0.08**	**1.52**	**1.89**	**0.01**	**0.19**	**0.03**	**1.68**	**0.00**

Appendix E

Statistics, example One Way ANOVA calculation

One-way ANOVA for the empty reactor at the different pressure, calculated using OriginPro 8.0)

Descriptive Statistics

	Sample Size	Mean	Standard Deviation	SE of Mean
A	5	8.23836	1.2641	0.56532
B	6	8.50873	1.24787	0.50944
C	5	9.29372	1.92459	0.8607

One Way ANOVA

	DF	Sum of Squares	Mean Square	F Value
Model	2	3.03275	1.51638	0.6799
Error	13	28.99378	2.23029	
Total	15	32.02653		

Null Hypothesis: The means of the levels are equal

Alternative Hypothesis: The means of one and more levels are different

At the 0.05 level, the population means are not significantly different.

Means Comparisons: Turkeys Test

	MeanDiff	SEM	q Value	Prob	Alpha	Sig	LCL	UCL
Level2 Level1	0.27037	0.90431	0.42282	0.9521	0.05	0	-2.11738	2.65812
Level3 Level1	1.05536	0.94452	1.58018	0.5207	0.05	0	-1.43856	3.54929
Level3 Level2	0.78499	0.90431	1.22762	0.66896	0.05	0	-1.60276	3.17274

Sig equals 1 indicates that the means difference is significant at the 0.05 level.

Sig equals 0 indicates that the means difference is significant at the 0.05 level

	DF	Sum of Squares	Mean Square	F Value	Prob>F
Model	2	1.13375	0.56688	1.01019	0.39103
Error	13	7.29505	0.56116		

At the 0.05 level, the population variations are not significantly different.

Appendix F

Experiment with support only

This section presents the experimental result for the experiment with the support material only (without active metal). The support of α-Al_2O_3 and ZrO_2 were studied at one temperature only, 525°C and 500°C, respectively. However, YSZ were studied at four different temperature, from 475 to 550°C.

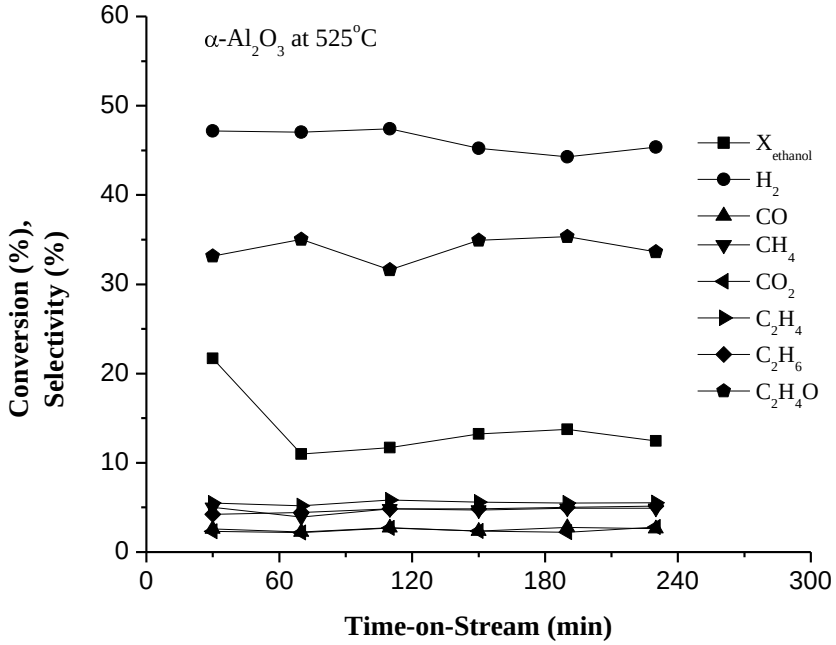

Figure F-1: Ethanol conversion and product selectivities over α-Al_2O_3 support at 525°C (250 bar, 5 wt. % ethanol, and 1.88 g/min feed flowrate)

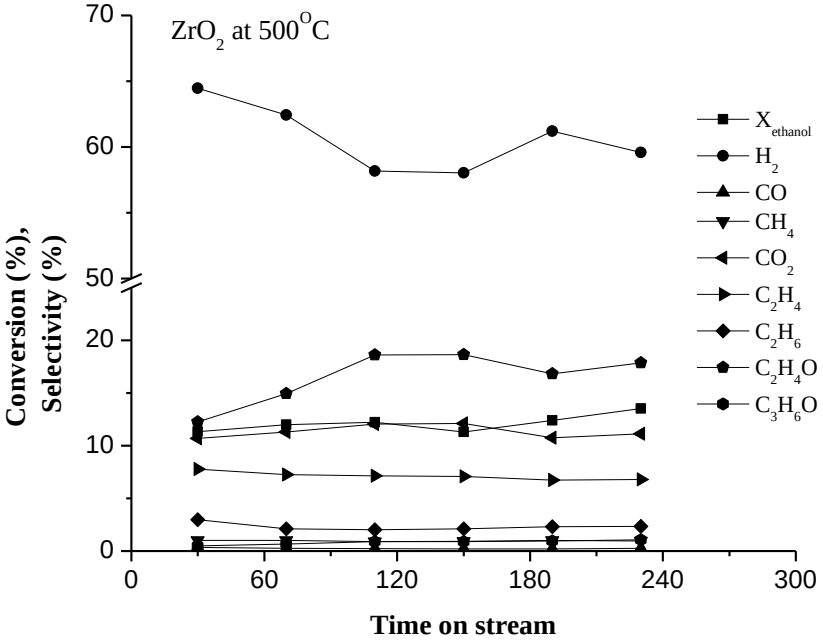

Figure F-2: Ethanol conversion and product selectivities vs time-on-stream over ZrO_2 support at 500°C (250 bar, 5 wt. % ethanol, and 1.88 g/min feed flowrate)

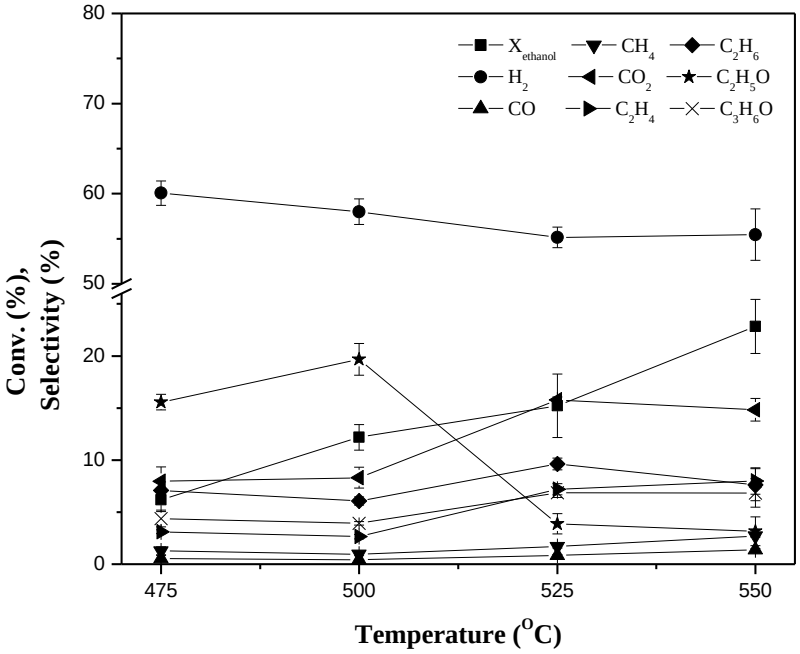

Figure F-3: Ethanol conversion and product selectivities over YSZ support at different temperature (250 bar, 5 wt. % ethanol, and 1.88 g/min feed flowrate, 1 g of YSZ)

Appendix G

Other data used in the calculation

Density of Water in Supercritical Conditions.

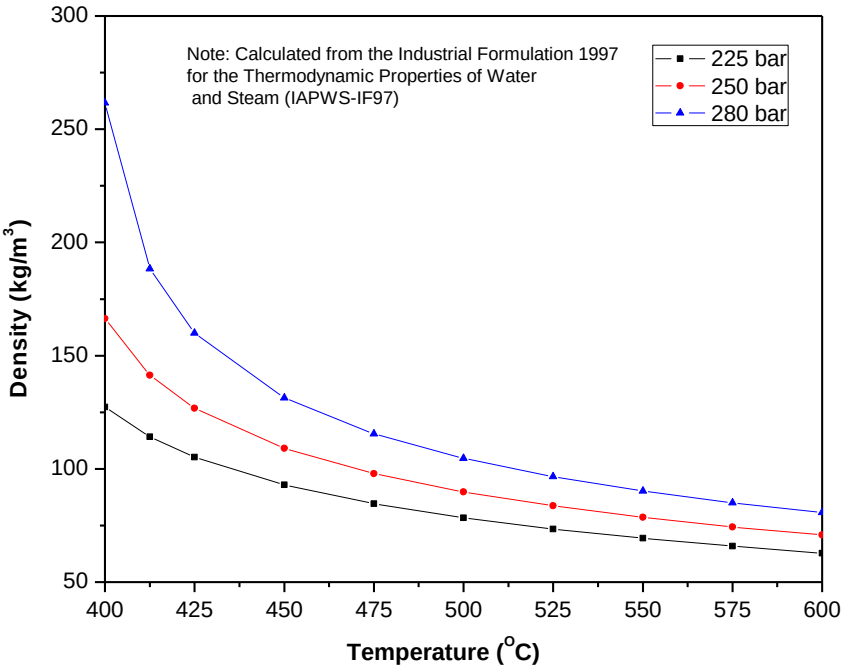

Figure A6-1: Density of SCW at the temperatures range from 400 to 600°C for 225, 250 and 280 bar